The Inhibition of Carboxypeptidase A and Angiotensin Converting Enzyme by Target Enzyme-Activated Inhibitors and N-Acylhydrazones

by

Christopher Michael Lanthier

A thesis
presented to the University of Waterloo
in fulfilment of the
thesis requirement for the degree of
Doctor of Philosophy
in
Chemistry

Waterloo, Ontario, Canada, 1996

The University of Waterloo requires the signatures of all persons using or photocopying this thesis. Please sign below, and give address and date.

The Inhibition of Carboxypeptidase A and Angiotensin Converting Enzyme by Target Enzyme-Activated Inhibitors and N-Acylhydrazones

Zinc metallo-peptidases such as carboxypeptidase A (CPA), angiotensin converting enzyme (ACE), matrix metalloenzymes and enkephalinase, play important roles in human biology and are therefore of interest in fundamental and practical research. In each of these enzymes a Zn^{2+} ion, which is catalytically essential, is bound in the active site. Among the most effective inhibitors for these enzymes are compounds designed to bind competitively to the active site through strong metal-inhibitor interactions. The use of metal binding inhibitors as therapeutic agents against specific enzymes may suffer from the problem of undesirable side affects resulting from non-specific interactions with other metalloenzymes (e.g., Captopril for inhibition of ACE). Incorporation of the metal binding moiety within a substrate analogue such that the metal binding group will be released only upon interaction with the target enzyme may be a solution. In this study it has been found that thioester substrate analogues can act as mechanism-based inhibitors of carboxypeptidase A and angiotensin converting enzyme. Enzymatic hydrolysis of the thioester group releases a free thiol inhibitor which binds tightly to the active site through a strong Zn^{2+}-sulfur interaction and non-covalent interactions with the active site region.

The thioester (S)-2-(S-benzoylthio)-3-phenylpropanoic acid (**50**) was designed as a mechanism-based inhibitor of CPA, where the CPA-catalyzed hydrolysis would result in the release of thiol inhibitor (S)-2-mercapto-3-phenylpropanoic acid (**35**). Examination of the potency of **35** as an inhibitor of the peptidase activity of CPA has revealed that it is a much more potent inhibitor (K_i=12.6 nM) than previously reported (K_i=1.2 μM) and that previous studies had likely examined inhibition by the disulfide formed by an unusually facile air oxidation of **35**.

The hydrolysis of **50** by CPA was found to proceed with burst kinetics at room temperature. The pre-steady state phase of the process was accompanied by a burst of proton release and a lag in thiol release. The similarity of the kinetic parameters found for CPA-catalyzed hydrolysis of **50** and those found for hydrolysis of O-benzoyl-(S)-phenyllactate suggest that the rate limiting step in each case may involve the release of benzoate. A molecular mechanism consistent with these observations is proposed.

The thioester **50** has been shown to be an effective time-dependent inhibitor of the peptidase activity of CPA thus demonstrating the feasibility of target enzyme-activated inhibition by a latent metal binding agent. Similarly, CBZ-Phe-Ψ[CO-S]-Ala-Phe (**86**) has been synthesized and shown to be an effective enzyme-activated inhibitor of the dipeptidase activity of ACE.

In addition, N-acylhydrazones, which are known metal binding agents currently being explored as potential therapeutic agents in several areas including as potential anti-HIV agents through inhibition of HIV-1 reverse transcriptase (RT), have been studied as potential inhibitors of ACE and CPA. Although none of these compounds was found to be an effective inhibitor of ACE, one such compound, N-(4-*t*-butylbenzoyl)-2-hydroxy-1-naphthaldehyde hydrazone (**NAH306**), which is a potent inhibitor of RT, was found to inhibit CPA. The discovery that this compound inhibits CPA, not by removal of the active site metal ion, but by binding to the enzyme in a mixed uncompetitive-competitive mode has led to the proposal of a molecular mechanism involving binding to the S_1 and S_2 subsites of free CPA as well as to the binary complex of CPA with phenylalanine, the hydrolysis product of the peptidase substrate hippuryl-L-phenylalanine.

Acknowledgements

I would like to thank Dr. Gary Dmitrienko for his expertise and guidance throughout my graduate studies, and for his assistance in the writing of this thesis.

I would like to thank my wife Lydia, for her understanding and support during these busy times, and for helping to type this thesis.

I would also like to thank the members Dr. Dmitrienko's laboratory for their helpful discussions and assistance during my research studies. Special thanks to Dr. Stefanie Seidel and Dr. Ron Fletcher for their immense knowledge in biochemical analysis and enzyme assays, to Dr. Sam Mithani for sharing his knowledge of organic chemistry and to Matt Brown for his humour and entertaining pranks in the lab. Finally, I would like thank Dr. N. J. Taylor for determinating the x-ray crystal structure of **NAH306** which was used in our molecular modeling studies.

To Lydia

Table of Contents

List of Figures

List of Figures (continued)

List of Figures (continued)

List of Figures (continued)

List of Figures (continued)

List of Figures (continued)

List of Schemes

List of Schemes (continued)

List of Schemes (continued)

List of Tables

Abbreviations

ACE	angiotensin converting enzyme
ar	aryl
BOC	*tert*-butoxycarbonyl
br	broad
bp	boiling point
Bn	benzyl
°C	degrees Celsius
calcd	calculated
CBZ	benzyloxycarbonyl
CI	chemical ionization
CPA	carboxypeptidase A
δ	chemical shift in parts per million from TMS
d	doublet
dansyl	5-dimethylaminonaphthalene-1-sulfonyl
DCC	N,N-dicyclohexylcarbodiimide
DMF	dimethylformamide
DMSO	dimethyl suloxide
EDTA	ethylenediaminetetraacetic acid
ee	enantiomeric excess
FAPGG	2-furanacryloyl-L-phenylalaninylglycylglycin
h	hour(s)
HP	hippuryl-L-phenylalanine
HRMS	high resolution mass spectrum
Hz	hertz
IR	infrared
J	coupling constant
m	multiplet
min	minute(s)
mol	moles
mp	melting point
MS	mass spectrum
NAH	N-Acylhydrazone

Abbreviations (contined)

q	quartet
RT	reverse transcriptase
rt	room temperature
s	singlet
S_N2	bimolecular nucleophilic substitution
t	triplet
TFA	trifluoroacetic acid
UV	ultraviolet

Chapter 1:

1.0 Zinc Metalloenzymes

Among the transition and group II elements, zinc is second only to iron in terms of abundance in biological systems. Zinc is essential to many enzymes, some of which are useful therapeutic targets, such as angiotensin converting enzyme (ACE)[1], aminopeptidase[2], matrix metalloenzymes[3,4] and enkephalinase[5], all of which utilize zinc (Zn^{2+}) in a catalytic role.

The research to be described in this thesis is aimed at the exploration of new strategies for improvement of the specificity of inhibitors of zinc dependent hydrolytic enzymes in general. In particular, the studies described herein have employed bovine carboxypeptidase A (CPA) and ACE as test beds for a new specific inhibitor strategy. As a consequence, it is appropriate that this introductory chapter be devoted to an overview of the current state of knowledge concerning the structure and mechanism of action of CPA and ACE, and of current inhibition strategies which are outlined below.

1.1 Carboxypeptidase A Structure and Mechanism

As a result of the vast structural and mechanistic knowledge of carboxypeptidase A (CPA), this enzyme is a useful model system for gaining insight into the mechanism and inhibition of other zinc metalloenzymes. CPA has been the subject of detailed studies of substrates and inhibitors, as well as of site-directed mutagenesis experiments and x-ray crystallographic analyses.[6]

Carboxypeptidase A (CPA, EC. 3.4.17.1) is a zinc metalloexopeptidase which cleaves single residues from the C-terminus of peptides through amide bond hydrolysis (Scheme 1).[7] CPA also possesses esterase activity[8] for related ester

substrates (Scheme 1). The zinc cation (Zn^{2+}) is situated in the active site of CPA and plays an essential role in substrate binding and hydrolysis. CPA preferentially hydrolyses peptides with C-terminal aromatic or branched aliphatic groups.[9] At least five C-terminal residues of the substrate influence K_m and, to a lesser extent, also influence k_{cat}.[10]

Scheme 1

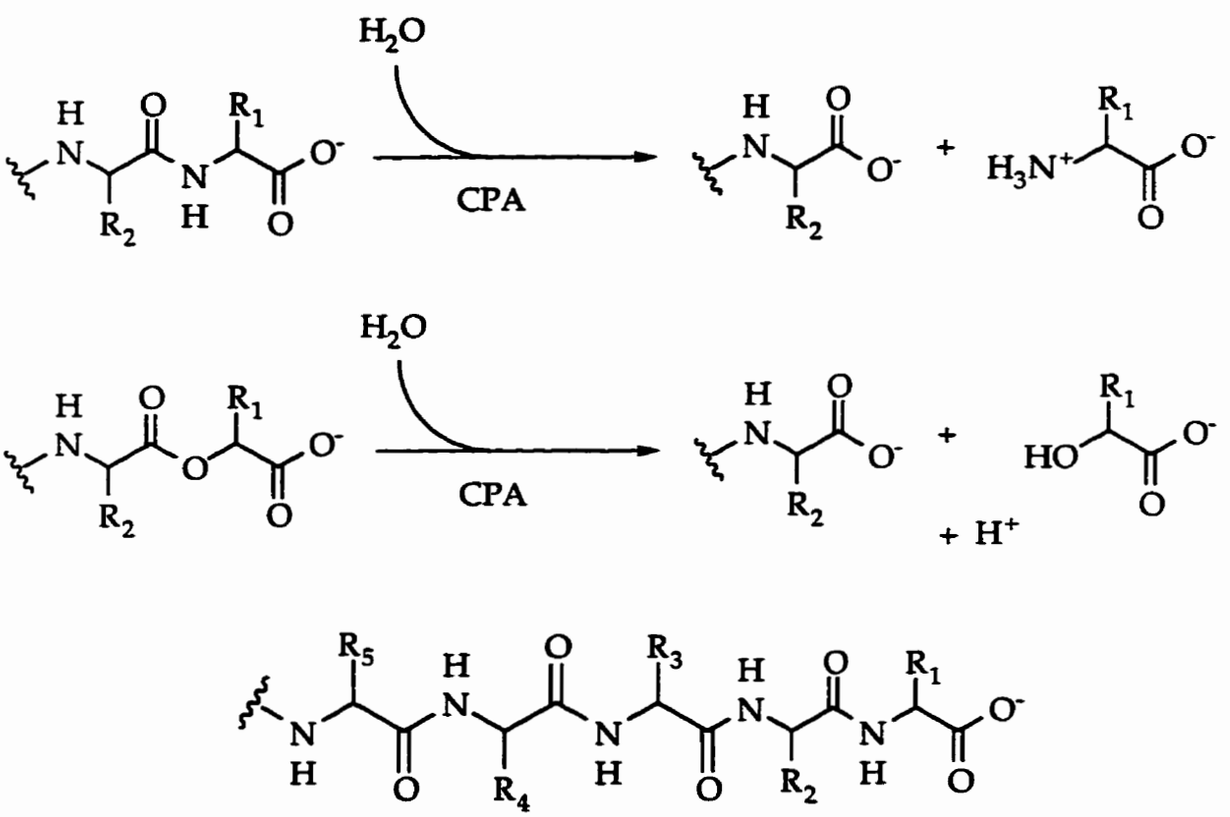

Ester substrates generally bind more tightly and are hydrolyzed more rapidly than peptide substrates.[11,12] Amide substrates as simple as N-acyl dipeptides, as well as their ester substrate analogues, have been shown to be hydrolyzed quite rapidly by CPA.[12] N-Acyl ester and amide single amino acid substrates, also known as "non-specific substrates", have also been shown to be hydrolyzed by CPA.[7,13,14,15,16,17,18,19] In particular, trans-cinnamoyl-β-L-phenyllactate and its N-acyl para-substituted

derivatives have been shown to be hydrolyzed by CPA quite efficiently as compared with other non-specific substrates.[20]

"Non-specific substrate"

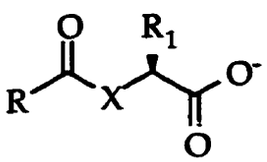

X=NH or O

R=alkyl or aryl group

trans-cinnamoyl-β-L-phenyllactate

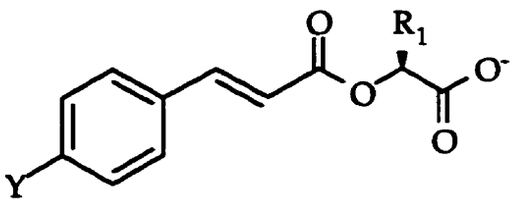

Y=H, Cl, NO_2, CN, OMe

Thionesters [RC(S)OR] and thioamides [RC(S)NHR][21,22] have been also shown to be hydrolyzed by CPA, with K_m values comparable to their ester and amide analogues. Thionester substrate hydrolyses normally exhibit k_{cat} values comparable to those for ester hydrolysis, whereas for thioamide substrate hydrolysis k_{cat} values are much smaller than those associated with the corresponding amide substrates. Thioester [RC(O)SR] substrates have received relatively little attention. The only published reports in this area are associated with the hydrolysis of S-(trans-cinnamoyl)-α-mercapto-phenylpropionic acid (**1**).[20,23] A detailed discussion of thioester hydrolysis by CPA will be presented later in Chapter 2.

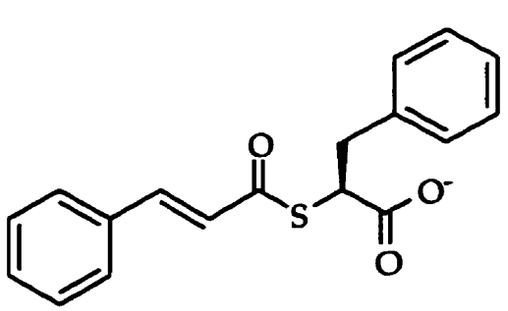

1

1.2 Structure of Carboxypeptidase A

The structure of CPA has been well studied by of single crystal x-ray diffraction.[24,25,26,27,28,29,30] Lipscomb and coworkers have revealed that CPA is about 30% helix, and contains a pleated β-sheet twisted by 120° from top to bottom, containing both parallel and anti-parallel pairs of extended chains. About 15% of CPA is involved in β-sheet hydrogen bonding . The β-sheet separates the enzyme into two regions of helices. There are only two cysteine residues (Cys-138, Cys-161) and in the structure of CPA, which are joined by a disulfide bond on the exterior of the enzyme.

Figure 1

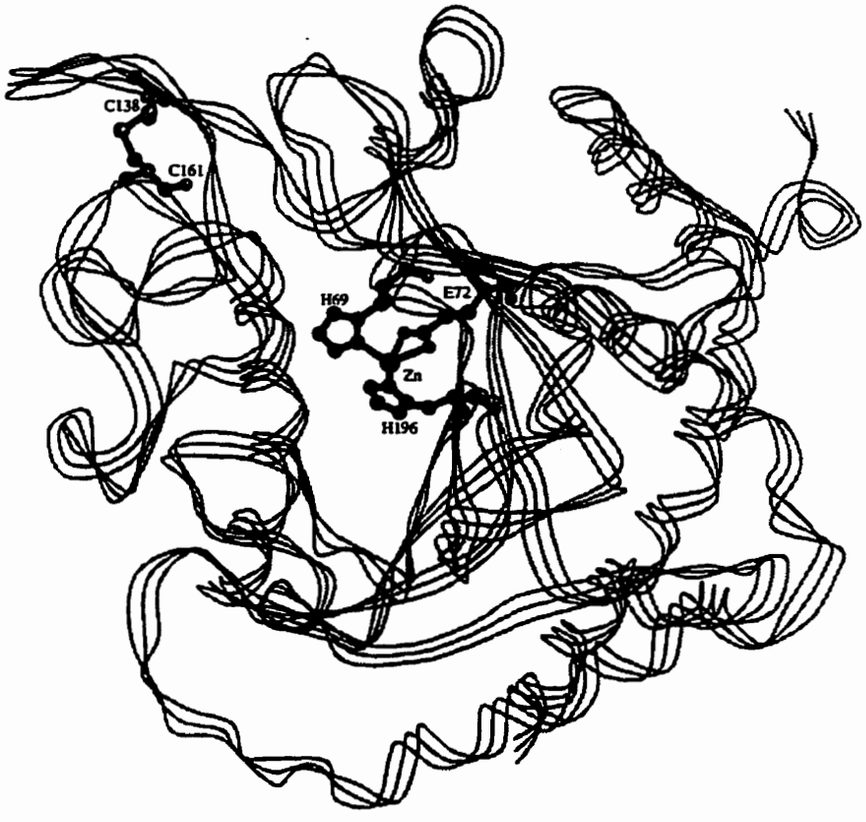

The CPA active site, in its native state, contains one Zn^{2+} atom, which is coordinated to His-69 (involved in a type I turn), His-196 (involved in an α-helix), Glu-72 (involved in a type III turn), and a water molecule in a distorted tetrahedral configuration (Figure 1).[24] Peptidase and esterase activities still remain after Zn^{2+} has been replaced by Co^{2+}, Ni^{2+}, Mn^{2+}, and Fe^{2+}, whereas no activity exists for apoCPA and Cu^{2+} substituted CPA.[31,32] Esterase activity also remains upon substitution of Zn^{2+} by Hg^{2+} or Cd^{2+}, but the peptidase activity is lost. The crystal structure of CPA bound to the inhibitor Gly-Tyr which hydrolyzes very slowly suggests which residues might be involved in substrate binding (Figure 2).[24,33]

Figure 2

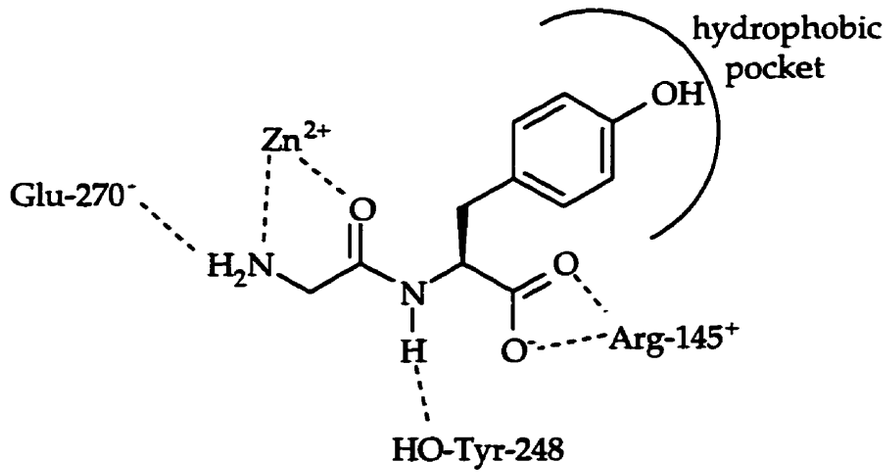

The binding site for polypeptide substrates in protease enzymes such as CPA consists of subsites for the binding of individual residues (Figure 3). Within the CPA active site there is an S_1' subsite, consisting of a hydrophobic pocket which interacts with the side chain of the C-terminal amino acid of the peptide substrate, an arginine residue (Arg-145) which interacts electrostatically with the C-terminal carboxylate group, and a zinc ion which likely binds the scissile amide or ester carbonyl group

oxygen (where H_2O has been replaced by the carbonyl oxygen of the substrate). The guanidino group of Arg-127 and the hydroxyl group of Tyr-248 are involved in substrate-enzyme binding interactions to a lesser extent. The hydrophobic pocket is lined with the side groups of Tyr-248, Leu-203, Gly-253, Ile-255, Ala-250 and Thr-268.

Figure 3

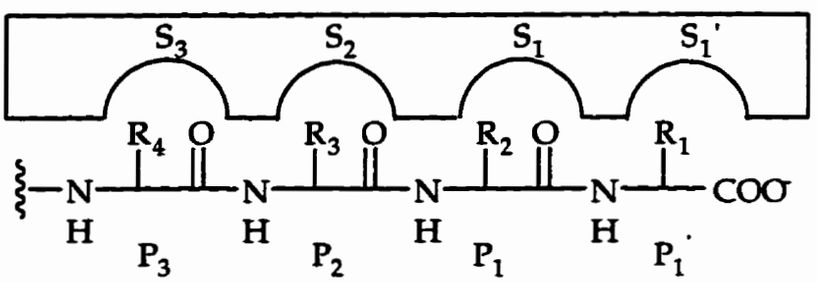

Upon binding Gly-Tyr, CPA undergoes a conformational change involving Tyr-248 which helps form the hydrophobic pocket. The side chain of Tyr-248 rotates by 120° about the Cα-Cβ bond and some limited motion of the peptide backbone, occurs to allow the aromatic group of Tyr-248 to fold over the C-terminal side chain of the peptide substrate. The phenolic OH of Tyr-248 moves 12 Å in this conformational change. This folded conformation is observed in all other CPA-inhibitor/substrate complexes studied by x-ray crystallography.[34,35,36,37]

A second possible binding site adjacent to the active site involves residues Arg-71, Tyr-198, and Phe-279.[24] Residues Arg-71, Tyr-198, and Phe-279 along with Ser-197 and Ile-247 have been suggested to be involved in the S_1, S_2 and S_3 binding subsites.[30,36] Arg-127 has been considered to be involved in the S_1 binding subsite[30] or in pre-catalytic binding interactions with the terminal carboxylate of the substrate.[38]

Bunting and coworkers[13,14] have studied the kinetics of CPA catalyzed hydrolysis of substrates in the presence of a variety of inhibitors to investigate various sites of interaction within the active site of CPA. It was concluded that there were two carboxylate binding regions (thought to be Arg-145 and Arg-127), and two hydrophobic binding regions. In addition, Bunting, using various carboxylate inhibitors, concluded that specific ester substrates (e.g. hippuryl esters), non-specific ester substrates and peptides all bind differently. The specific esters (2) were ester analogues of N-acyl-dipeptides, and the non-specific esters (3) were ester analogues of N-acylated amino acids. From these studies, Bunting suggested that peptides may have an additional binding site on CPA separate from that of specific esters.

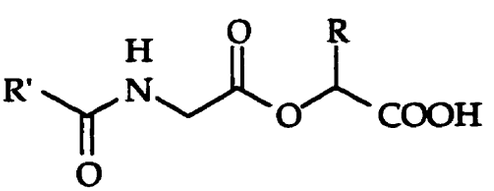

2

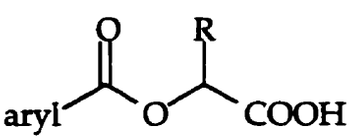

3

More recently, using further crystallographic studies of CPA complexed with an ester analogue, indoleacetate, and other CPA inhibitors, Lipscomb[26] proposed that the S_1' subsite was the catalytic site for both esters and peptides, and that peptides bind initially to S_2 (Tyr-198, Phe-279, Arg-71) prior to entry into the S_1' subsite, whereas ester substrates bind directly to the S_1' subsite. Lipscomb and coworkers discovered, by x-ray crystallographic analysis, that indoleacetate binds to the S_1'-subsite. Since indoleacetate is a competitive inhibitor of esterase activity they reasoned that ester substrates also bind directly in S_1'. On the other hand, indoleacetate is observed to act as a non-competitive inhibitor of peptidase activity. It was argued that, if the peptide substrate normally bound to the S_1'-subsite directly, indoleacetate, which binds to the S_1'-subsite also should be a competitive inhibitor as

observed for inhibition of esterase activity. The observed non-competitive inhibition could be explained if the binding of indoleacetate to the S_1'-subsite does not prevent the binding of the peptide substrate to a second site (presumably S_2), but does prevent the rate limiting entry of the peptide into the S_1'-subsite.

1.3 Mechanism of Carboxypeptidase A

The active site Zn^{2+} and residues Glu-270, Arg-127, and Tyr-248 have all been considered to be involved in catalysis.[24,34,35] The mechanism of peptide and ester hydrolysis by CPA is still the subject of debate even though CPA is one of the more well studied zinc metalloenzymes. Lipscomb[24,28] first proposed the two major theories regarding the mechanism for peptide/ester hydrolysis, the so-called "general base" and "anhydride" mechanisms. In the general base mechanism (Scheme 2), the carbonyl oxygen of the scissile bond of the substrate displaces the Zn^{2+} bound water molecule. This type of interaction was observed in the Gly-Tyr bound CPA crystal structure.[24] The Zn^{2+} is proposed to act as a Lewis acid, polarizing the carbonyl group, and the Glu-270 carboxylate acts as a general base, promoting the addition of water to the scissile amide bond. The amine is then released from the tetrahedral intermediate yielding the zinc bound carboxylate which then dissociates to complete the reaction. Glu-270 is suggested to be involved in proton-transfers as well as promotion of nucleophilic attack of the water molecule.[39] The structurally similar Zn^{2+}-peptidase thermolysin is also considered to utilize a glutamate residue (Glu-143) in a similar general base induced attack of a water molecule on the substrate.[40]

The side chain of Tyr-248 was originally considered to be involved in proton-transfers during hydrolysis[41], but this possibility has been discounted on the basis of the results of site-directed mutagenesis studies.[42,43] By replacing Tyr-248 with Phe, Hilbert demonstrated that Tyr-248 is involved in substrate binding (increase in K_m

values), but not catalysis (with little change in k_{cat} values) for esterase and peptidase activity. The difference in the presence of the hydroxyl group when comparing substrate binding of wild type CPA and the Phe-248 mutant suggests a role for the phenolic OH in simple hydrogen bonding to substrates.

Scheme 2

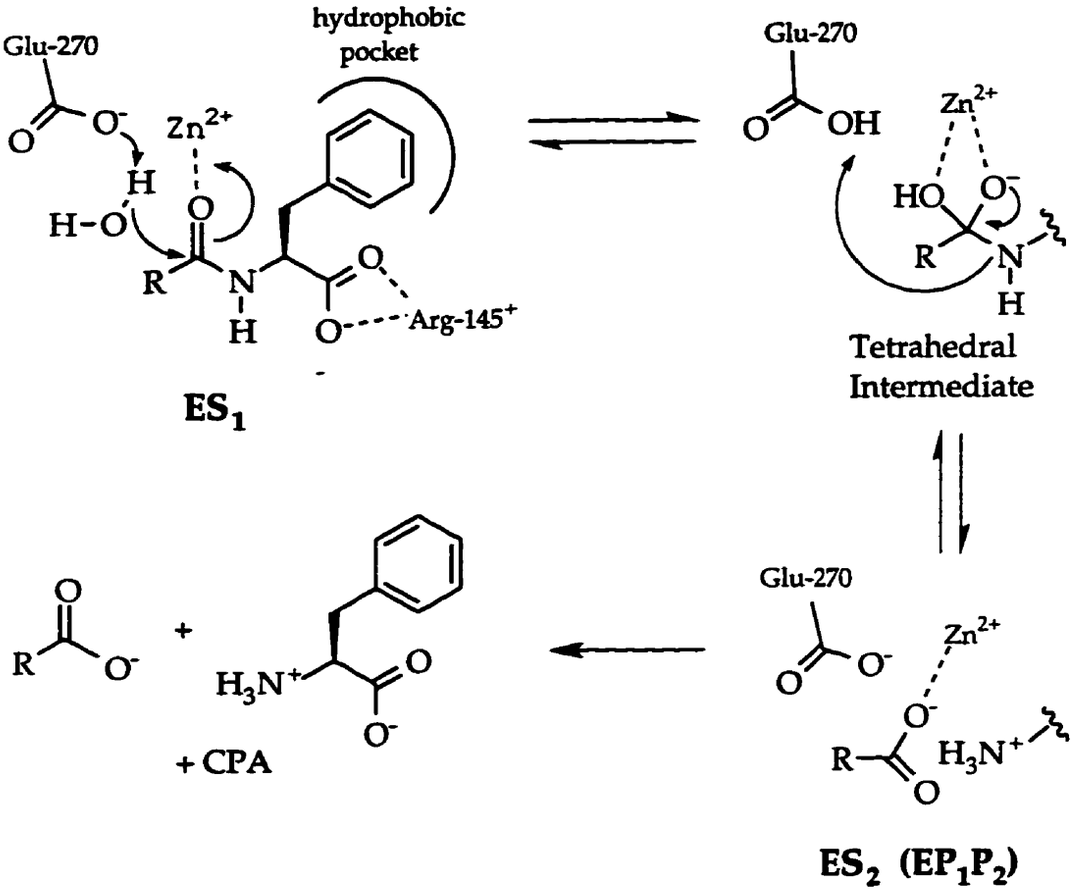

The proposed anhydride mechanism (Scheme 3) involves binding of the substrate without displacement of the Zn^{2+} bound water molecule. In addition Glu-270 acts as a nucleophile on the scissile carbonyl bond, forming an acyl-enzyme intermediate.[44,45] The mixed anhydride is then cleaved by the Zn^{2+} bound water/hydroxide.

Scheme 3

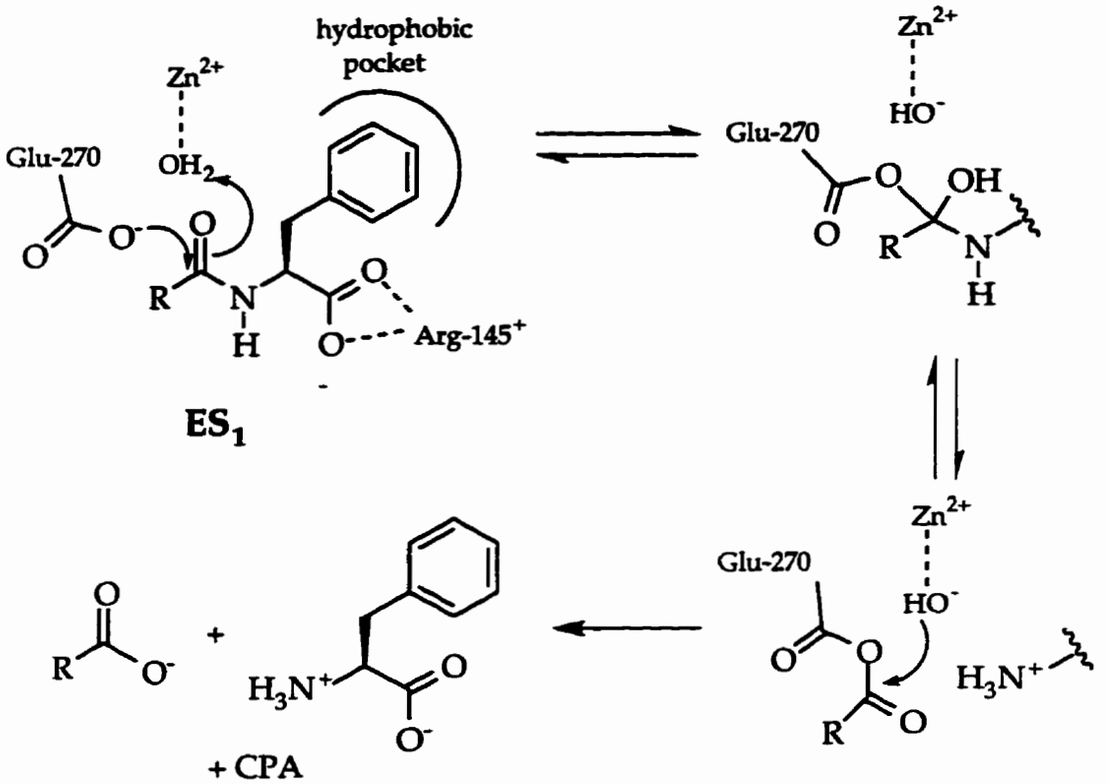

Another variation of the anhydride mechanism includes the possibility of a Zn^{2+} bound water being displaced by the scissile carbonyl oxygen (Scheme 4). Nucleophilic attack by the side-chain carboxylate of Glu-270 would produce a Zn^{2+} bound tetrahedral intermediate, which would then collapse to give the acyl enzyme (mixed anhydride).[46]

Scheme 4

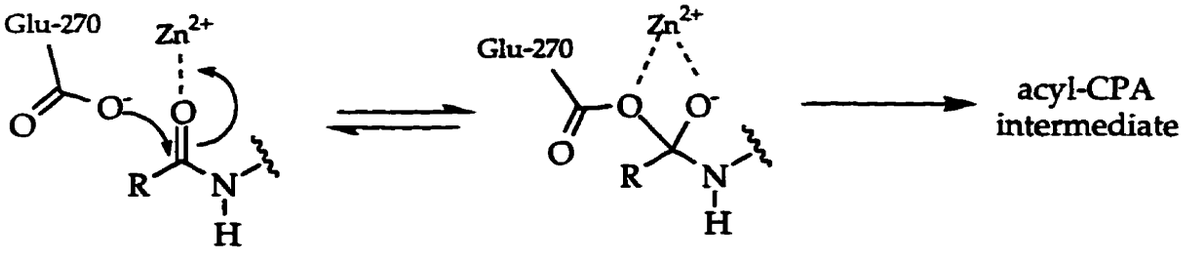

Breslow et al. provided the first evidence to support the general base theory.[47,48] Breslow et al. studied ^{18}O exchange (using ^{18}O-enriched substrates) during reverse hydrolysis reactions by incubating CPA with various isotope labeled products (Scheme 5). Even though the hydrolyses of both peptides and esters are exothermic, there is a low rate of synthesis that may allow for exchange to occur.

Scheme 5

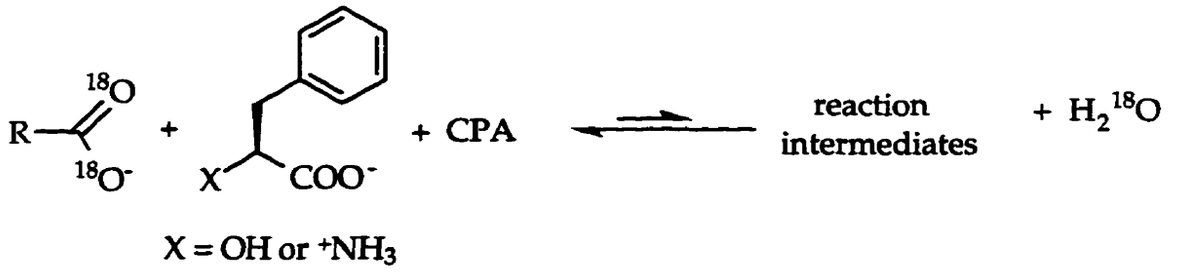

It was reasoned that, if the hydrolysis of peptides and esters does proceed through an anhydride mechanism, the incubation of ^{18}O-labeled acid (N-benzoylglycine) and the enzyme should result in some exchange of ^{18}O with the H_2O solvent. No exchange was observed. Breslow offered a possible explanation in that the water molecule produced during the condensation may remain bound in the

active site (perhaps bound to the Zn^{2+} atom), and may be used in the hydrolysis of the mixed anhydride. This would explain the lack of ^{18}O-exchange with the medium.

Scheme 6

To evaluate the possibility of general-base catalysis, Breslow incubated the enzyme with L-Phe and the ^{18}O-labeled acid N-benzoylglycine. In this case, if the general-base mechanism were to hold true for peptidase activity, exchange of ^{18}O with the water solvent would be expected. Breslow did observe a positive result for this experiment. On the other hand, the incubation of β-phenyllactate, ^{18}O-labeled N-benzoylglycine and the enzyme resulted in no exchange of ^{18}O with the water solvent. Breslow suggested that if the hydrolysis of both peptides and esters did occur via the anhydride mechanism, the hydrolysis of the acyl-enzyme intermediate, formed by peptide hydrolysis through the anhydride mechanism, and its resynthesis might be strongly catalyzed by enzyme-bound amino acids (Figure 4). The hydrolysis of the acyl-enzyme intermediate might be expected to be catalyzed much less effectively by enzyme-bound hydroxy acids as a result of the low basicity of the HO-group, resulting in a lack of ^{18}O-exchange. Breslow, however, went on to show that phenylalanine was more likely to be involved as a component and not a cocatalyst. When L-Phe, ^{18}O-labeled N-benzoylglycine and CPA were incubated, the rates of ^{18}O-exchange were similar to those calculated if L-Phe was regarded as a resynthesis component.

Figure 4

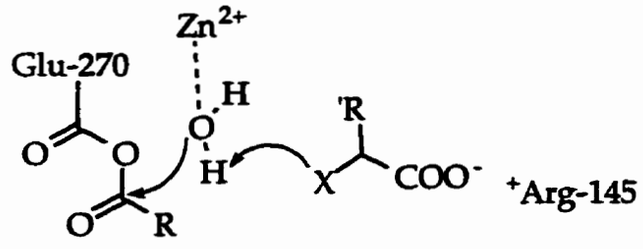

Other work by Breslow[47] involving peptide and ester hydrolysis in the presence of methanol (5 M) showed no incorporation of methanol into hydrolysis products (ester formation). This contrasted with other known peptidases that involve acyl-enzyme intermediates during hydrolysis such as α-chymotrypsin and trypsin, where methanol incorporation is observed. The lack of incorporation may suggest the need for both of the protons on the attacking water to be removed during the course of hydrolysis, which would only occur in the general base mechanism. Breslow has suggested the general base mechanism for at least peptide hydrolysis on the basis of the results of his experiments and Lipscomb's early x-ray data[24] showing that peptide substrates bind via carboxyl oxygen-Zn^{2+} interaction and the lack of a Zn^{2+} bound water in the substrate-enzyme complex.

The key evidence put forward in support of the anhydride mechanism involves the hydrolysis of unusual ester substrates by CPA.[44,45,49,50] Makinen and coworkers[44,45] studied the hydrolysis of O-(trans-p-chlorocinnamoyl)-L-β-phenyllactate (**4**) at subzero temperatures.

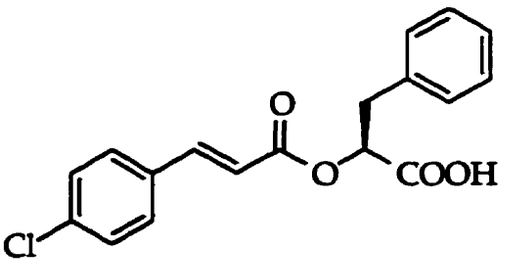

4

Hydrolysis of this unusual ester substrate was shown to be biphasic, with an initial faster step, followed by a slow rate determining step and release of hydrolysis products. Makinen was able to isolate an intermediate at -60° using gel filtration.[49] This species was suggested to be an acyl-enzyme intermediate, which was considered to be the Glu-270-mixed anhydride formed through the anhydride mechanism. The apparent acyl-CPA species was stable for 90 minutes at -60°, and broke down spontaneously when warmed to 0°. Makinen went on to study the pH dependence of the equilibrium between Zn^{2+} bound water and the zinc bound hydroxide using Co^{2+}-substituted CPA. It was later suggested that the anhydride intermediate and a water molecule remain chelated to the Zn^{2+} ion to form a pentacoordinated metal ion (In this experiment, Makinen considers the Glu-72 carboxylate double oxygen ligand interaction to be equivalent only to a monooxygen donor ligand).[51,52] The Zn^{2+} bound water molecule then attacks the anhydride (Scheme 7).

Scheme 7

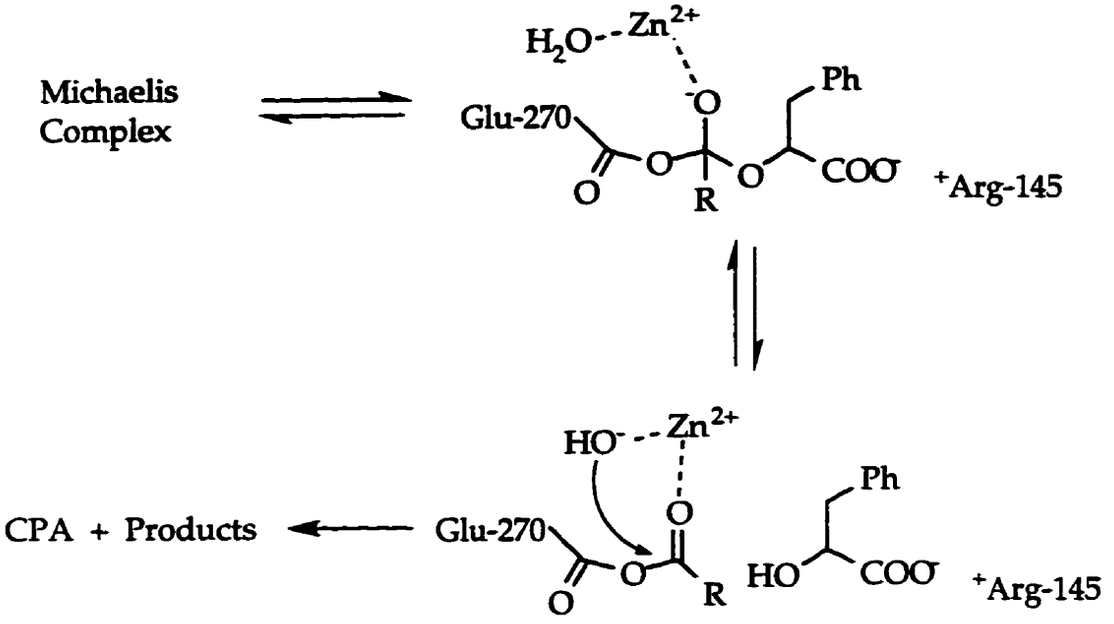

Suh and coworkers,[53] using two different substrates (**5** and **6**) with the same acyl group, demonstrated that the rate-determining steps are kinetically very similar for both substrates and suggested that the same acyl-enzyme intermediate exists in both cases. Attempts at trapping the putative acyl-enzyme intermediates, however, using hydroxylamine as an external nucleophile were unsuccessful.

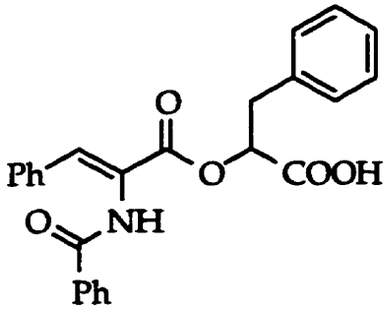

5

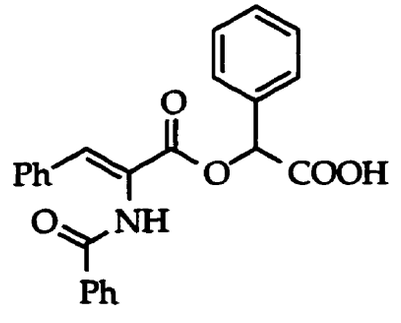

6

More recently, Kaiser[54] has shown the lack of anhydride characteristics in the so-called acyl-enzyme intermediate formed between CPA and Makinen's O-(trans-p-chlorocinnamoyl)-L-β-phenyllactate (**4**) using resonance Raman cryospectroscopy. Lipscomb and Christianson,[40] in a later review, agreed with Kaiser's findings, stating that the isolated apparent acyl-enzyme intermediate was likely a tight complex between the enzyme and the hydrolysis products, held together in part, by the lack of proper diffusion at subzero temperatures. The breakdown of the complex upon warming to 0°, would then not involve hydrolysis of a mixed anhydride, but merely diffusion of the products from the active site.

Makinen argued in return that Kaiser's lack of spectral evidence for the acyl enzyme was probably due to the inadequate mixing of the viscous solvents at low temperatures.[51]

Later, further Raman spectroscopic studies did show some evidence of a possible anhydride intermediate during the hydrolysis of ester substrate **7** by CPA.[55] Weak but reproducible peaks observed in the 1720-1800 cm^{-1} region were very similar to those observed during analysis of $ZnCl_2$ complexed with the mixed anhydride between p-dimethylaminobenzoic and acetic acid.

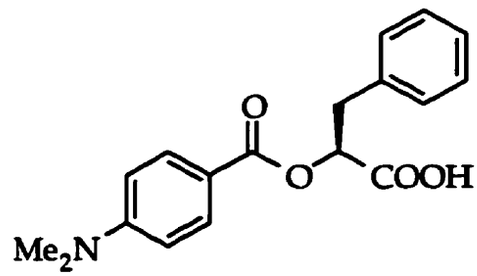

7

It would seem that, since spectroscopic evidence supporting and discounting the existence of the putative acyl-enzyme intermediate, has been reported, the acyl enzyme hypothesis remains to be established unambiguously for the CPA.

Vallee and coworkers have conducted extensive studies of the hydrolysis of peptides and esters by CPA using cryoenzymology.[56,57,58,59] Using low temperatures with Zn^{2+} and Co^{2+}-CPA, Vallee was able to trap intermediates (ES_2 in Scheme 8), which are distinct from the initial enzyme-substrate complex (ES_1). These trapped ES_2 intermediates were studied using UV/visible spectroscopy, electron paramagnetic resonance (EPR), CD and MCD, and fluorescence spectroscopy (using N-dansyl-substrates) (Scheme 8).

Scheme 8

$$E + S \underset{}{\overset{K_s}{\rightleftharpoons}} ES_1 \underset{k_{-2}}{\overset{k_2}{\rightleftharpoons}} ES_2 \xrightarrow{k_3} E + P_1 + P_2$$

-where ES_2 is EP_1P_2 for ester hydrolysis

Vallee concluded that peptides and esters are hydrolyzed via similar pathways in which the rate-determining steps differ. With peptide substrates, ES_2, which is the predominant intermediate, was found to be the CPA-bound substrate, and for ester hydrolysis the intermediate was found to be a complex between the enzyme and products (EP_1P_2). Thus, it appears that during peptide hydrolysis, the enzyme first binds the substrate weakly to form ES_1 which is converted rapidly into a second CPA-substrate complex, ES_2. This is followed by the rate-determining hydrolysis of the amide bond, and rapid release of the products. Ester substrate hydrolysis, on the other hand, also involves formation of an initial enzyme-substrate complex, ES_1, but this is followed by rapid hydrolysis to form the EP_1P_2 intermediate. Dissociation of the enzyme and products is argued to be the rate determining step. No acyl-enzyme intermediates were observed spectrophotometrically for any of the many N-acyl di- and tri- peptides and depsipeptides studied. All attempts to trap anhydride

intermediates chemically were unsuccessful. Based on this work, Vallee has argued strongly that both esters and amides are hydrolyzed via similar water-promoted general base mechanisms.

It has been pointed out that the difference in the nature of the rate determining steps for ester versus amide hydrolysis may be related to the fact that alcohols bind more tightly to the active site than the corresponding amino acids. For example, L-β-phenyllactate binds more tightly than L-phenylalanine with K_i's of 0.13 mM and 5.5 mM respectively.[60] The structure of L-β-phenyllactate bound to the CPA active site has been determined by x-ray crystallographic studies.[61] In this structure L-β-phenyllactate is bound into the active site in the same orientation as are substrates, with the enzyme in the closed conformation and with the phenyl group of L-β-phenyllactate in the hydrophobic pocket of S_1' defined by the side chains of Tyr-248, Leu-203, Gly-253, Ile-255, Ala-250 and Thr-268, and with the favourable interaction of the carboxylate with Arg-145 (Figure 5). There is also an additional interaction between the OH group and Zn^{2+} through a water bridge.

Figure 5

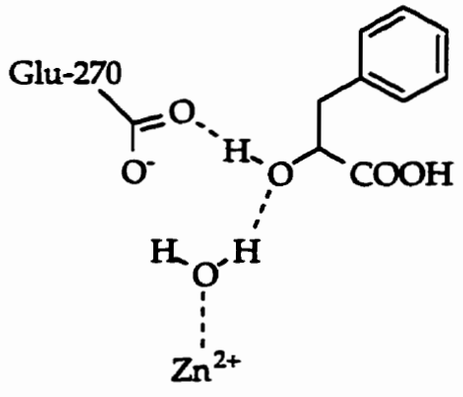

It was suggested by Mangani[61] that during release of ester hydrolysis products, P_2 (the acid product) may be released from the EP_1P_2 complex to be replaced by a water

molecule binding to the Zn^{2+} ion and stabilizing the EP_1 complex (see Figure 5) which is now slower to dissociate. This extra interaction does not take place with the protonated amine produced during peptide hydrolysis. Crystallographic studies of CPA-L-Phe binding showed L-phenylalanine bound in the same manner, but with the protonated amine interacting with Glu-270,[62] rather than with Zn^{2+} via a water bridge.

Perhaps the strongest evidence supporting the general base theory is the binding of transition-state analogues such as ketone[63,64,65] and aldehyde hydrates[66,67], sulfodiimines[68], phosphonates[69] and phosphoramidate[70,71] inhibitors to CPA. These inhibitors bind to the active site Zn^{2+}, imitating the tetrahedral intermediate (or the transition-state involved in its formation) that occurs during general base hydrolysis.

The racemic mixture of the fluorinated inhibitor 2-benzyl-4-oxo-5,5,5-trifluoropentanoic acid **8** was shown to bind to CPA in this manner (K_i=0.2 μM).[72] The trifluoromethyl group promotes hydration of the carbonyl to mimic the tetrahedral hydrolysis intermediate (Scheme 9).[37]

Scheme 9

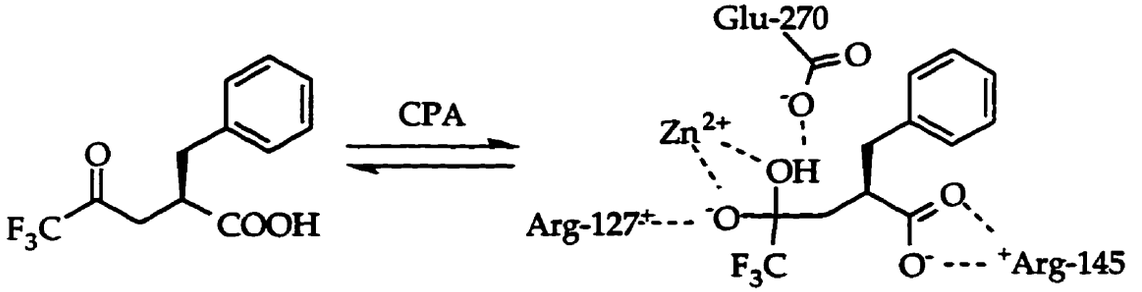

8

Both Glu-270 and Arg-127 were found to form stabilizing contacts with the inhibitor as shown in Scheme 9. ^{19}F-NMR studies have shown the CPA bound hydrate to be

the monoanion form, similar to the hypothetical tetrahedral intermediate of the general base mechanism.[73]

Ketonic substrate analogues **9** and **10** were found to bind to CPA in similar hydrated forms.[64,65] Again Arg-127 and Glu-270 were found to be involved in stabilization of the complex (Figure 6).

Figure 6

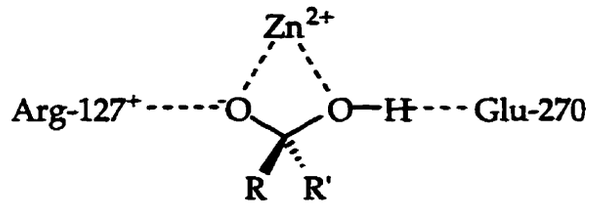

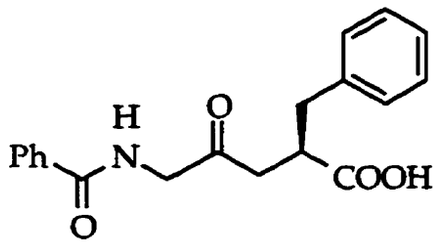

9

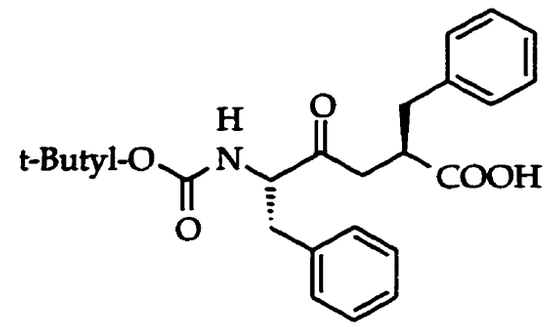

10

An interesting observation concerning the ketonic inhibitors **9** and **10** is that the hydrated species is unfavourable in aqueous solution (<0.2%). The enzyme either has selected the gem-diol, as it is continuously formed in solution through equilibrium, or has facilitated hydration through promoted water attack on the carbonyl group of the inhibitor.

These crystallographic studies not only give strong evidence in favour of the general base theory, but also suggest roles for Glu-270 and Arg-127 in transition-state stabilization in peptide and ester hydrolysis. Further studies into the catalytic

involvement of Arg-127 in the formation of the oxyanion hole were conducted using site-directed mutagenesis. Arg-127 to Lys, Met and Ala substitutions were found to cause little effect on substrate binding (K_m) but to decrease k_{cat} greatly for both esterase and peptidase activity.[74] It appears that once Glu-270 promotes attack by the water molecule on the carbonyl group of the substrate it remains in interaction with the transition-state, while Arg-127 now stabilizes the newly formed negative charge on the carbonyl oxygen.

More recently, crystallographic studies of sulfodiimine (**11**), phosphoramidate (**12**) and phosphonate (**13**) inhibitors complexed with CPA have also led to similar conclusions supporting the general base theory.[68,70,71,75]

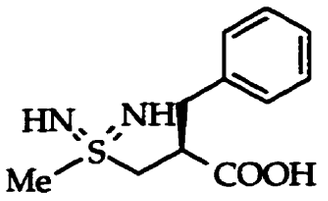

11

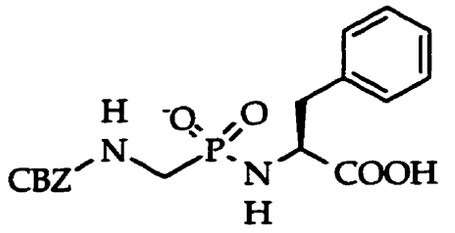

12

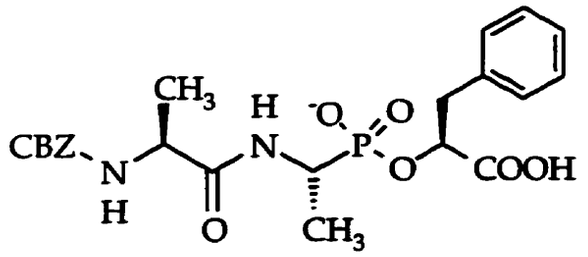

13

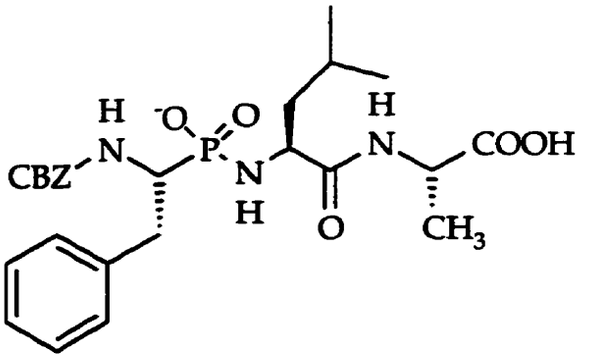

14

These compounds all appear to act as transition-state analogue inhibitors as a consequence of the tetrahedral geometry at the metal binding moiety which mimics the tetrahedral transition-state of ester and peptide hydrolysis. The crystal structure

of CPA and phosphonate **13** shows again the Zn^{2+}, Arg-127, and Glu-270 stabilization of the transition-state analogue (Figure 7).[69] Phosphonate inhibitor **13** is one of the tightest binding inhibitors of CPA with a reported K_i of 3 pM.[76] Glu-270 is thought to be protonated in order to interact with the anionic oxygen of the phosphonate group. Similar results were observed for the binding of tight binding transition-state phosphinyl inhibitors to the Zn^{2+} endopeptidase thermolysin (TLN).[77,78] Thermolysin, for which the general base mechanism is firmly accepted for peptide hydrolysis, has an active site similar to that of CPA.[79] Catalysis by thermolysin is thought to involve a water-promoted attack on the scissile amide carbonyl, which is polarized by enzyme bound Zn^{2+}. The addition of water is promoted by Glu-143 and His-231 which helps to stabilize the transition-state in the same way that Arg-127 does for CPA (Figure 7). Crystal structures of thermolysin and the tight-binding phosphoramidate inhibitor **14** (K_i=0.068 nM) demonstrated these interactions.[80]

Figure 7

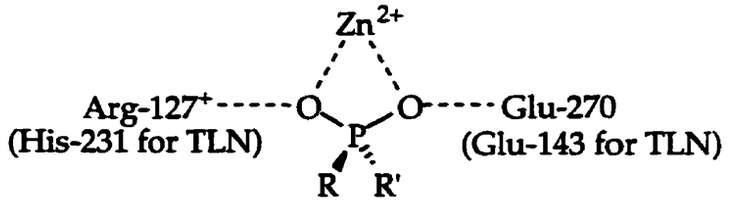

The strong similarities between phosphonates and the actual transition-state during amide hydrolysis was further established by Bartlett's extensive phosphonate inhibitor studies. By measuring the inhibition of fourteen tri- and tetrapeptide derivatives, Bartlett demonstrated a strong correlation between K_i values of the inhibitors and the K_m/k_{cat} values of the corresponding amide substrates.[76] Further

work was done involving wild-type and the Lys-127, Met-127 and Ala-127 mutants with more phosphonate inhibitors and their peptide substrates to further establish this relationship as well as the need for stabilization of the transition-state analogue complexes and transition-states by Arg-127.[81] These studies closely paralleled earlier studies by Bartlett comparing phosphoramidate inhibitors (K_i) for thermolysin with corresponding peptide substrates (K_m/k_{cat}) which gave a similar correlation.[82]

In light of the results of crystallographic studies of CPA with the transition-state analogues, Lipscomb[40,64] has offered a modified version of his original general base mechanism for peptide hydrolysis (Scheme 10).[24] In this revised version, the amide (or ester) carbonyl does not displace the Zn^{2+} bound water molecule found in the native enzyme but actually shares zinc coordination with the Zn^{2+} bound water. Some studies have suggested that the attacking water molecule and the scissile carbonyl oxygen are both coordinated to the active site Zn^{2+} prior to catalysis.[74,83,84,85,86] The scissile carbonyl is polarized by both Arg-127 and Zn^{2+}. The Zn^{2+} bound water is converted to Zn^{2+} bound hydroxide through deprotonation by Glu-270. The hydroxide then can attack the scissile carbonyl to give a transition-state intermediate, in which the hydroxyl is stabilized by the newly protonated Glu-270 and Zn^{2+}, and the generated oxyanion is stabilized by both and Zn^{2+} and Arg-127. Collapse of the intermediate involves transfer of a proton from Glu-270 to the newly formed amino group. This modification is applicable also to the general base mechanism associated with thermolysin catalyzed hydrolysis.[79,87]

Scheme 10

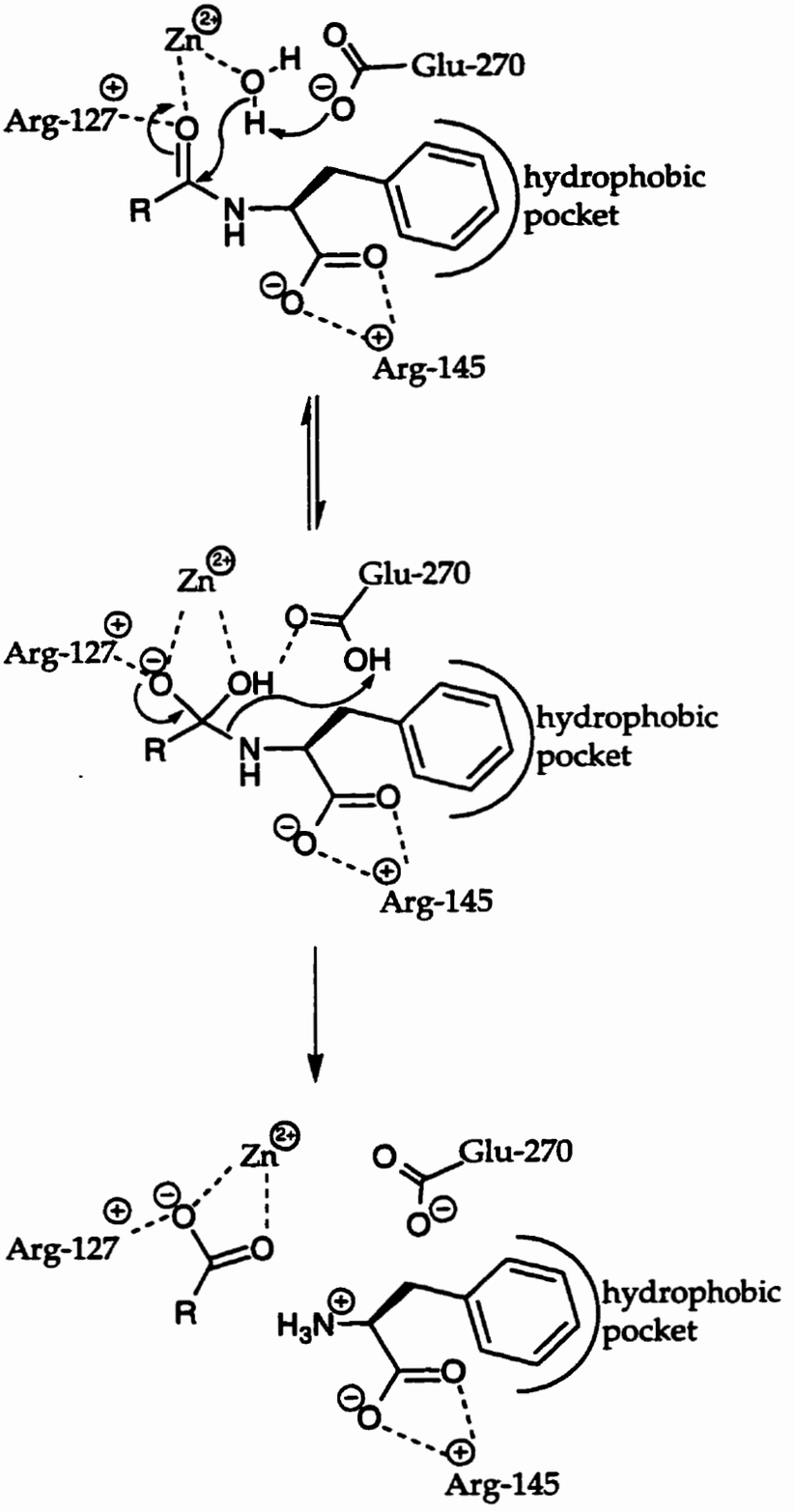
Zn
Glu-270
Arg-127
hydrophobic pocket
Arg-145
Zn
Glu-270
Arg-127
hydrophobic pocket
Arg-145
Zn
Glu-270
Arg-127
hydrophobic pocket
Arg-145

1.4 Angiotensin Converting Enzyme (ACE)

Angiotensin converting enzyme (ACE, EC 3.4.15.1), although structurally much less well understood than CPA, is an important pharmaceutical target and has been subject to many inhibition studies as a consequence of its important role in blood pressure regulation. ACE is a Zn^{2+}-exopeptidase which cleaves dipeptides from the C-terminal end of peptide chains three residues and longer. The two most important natural substrates of ACE are the decapeptide angiotensin I and the nonapeptide bradykinin.[88,89] The product of cleavage of angiotensin I is the octapeptide angiotensin II, which is one of the most potent vasoconstrictive agents known. As a result, ACE is an attractive target for hypertension therapy since inhibition of ACE prevents angiotensin II release. The angiotensin system and its interrelationships with the kallikrein-kinin system have been reviewed by Peach (Figure 8).[90]

ACE is a membrane bound glycosylated enzyme which is found in vascular endothelial cells of organs such as lungs and kidneys.[91] ACE is composed of a single polypeptide chain of approximately 837 residues with a molecular weight in the range of 130,000-140,000, depending on the degree of glycosylation. Each mole of protein contains one mole of Zn^{2+}.[92,93] Loss of the active site Zn^{2+} completely inactivates ACE and activity can be restored only with Zn^{2+}, Co^{2+} or Mn^{2+}.[92,94]

The Zn^{2+}-enzyme interaction was found to be weaker in ACE than in either CPA or thermolysin, with the log of the stability constant ($\log K_E$) of 10.5, 11.3 and 8.6 for CPA, thermolysin and ACE respectively.[95] This characteristic suggests a different steric arrangement of Zn^{2+} ligands in ACE, or possibly a different number or nature of ligands in ACE as compared to the Zn^{2+} binding pocket containing two histidyl ligands and one glutamyl ligand found in both CPA and thermolysin.[92]

Figure 8: Overview of the Renin-Angiotensin System and Reactions Catalyzed by ACE

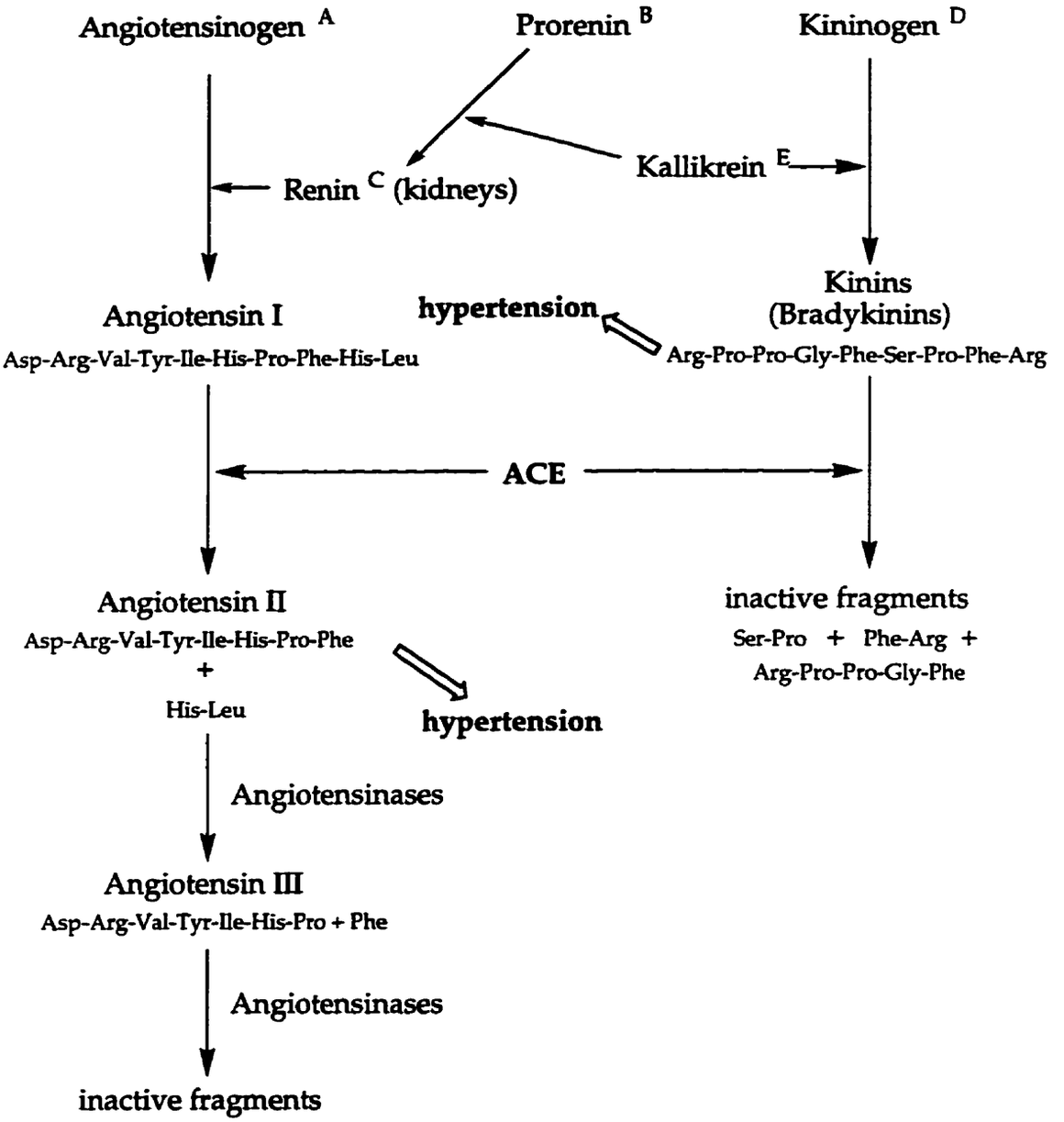

A - a blood glycoprotein

B - Inactive renin precursor found in kidneys, brain and plasma (MW=43,000-56,000)

C - Found in kidneys (MW=40,000)

D - Large precursor to bradykinin (MW=50,000)

E - Found in plasma

The metal ion was suggested to be bound in the active site possibly to a single carboxylate from the side chain of an aspartyl or glutamyl residue.[1] Co^{2+}-substituted ACE does show a lower symmetry metal-ligand environment than that found in CPA or thermolysin.[96] Cysteine was excluded as a possible ligand because of the lack of characteristic sulfur-Co^{2+} charge transfer bands in the MCD spectrum.

The formation of complexes between metal-binding ACE inhibitors such as enalaprilat (**15**) or captopril (**16**) and Co^{2+}-ACE results in an alteration of the metal-ligand environment from one of low symmetry to one of tetrahedral geometry. By contrast, upon binding of thiol inhibitors, Co^{2+}-CPA and Co^{2+}-thermolysin retain the irregular tetrahedral geometry about Co^{2+} as the metal bound water is displaced by the tight binding sulfur atom.[97] Phosphinyl inhibitors have been shown to convert the Co^{2+} atom of CPA and thermolysin from a pentacoordinated environment to a hexacoordinated environment,[98] as mentioned earlier.

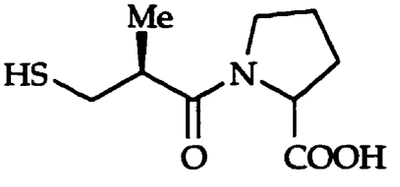

15

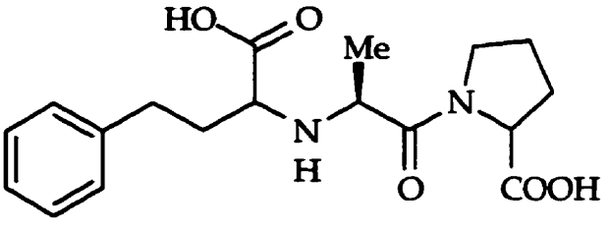

16

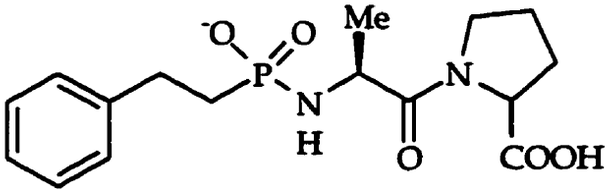

17

Unlike the situation with CPA, ACE activity involves a much broader range of substrate specificity. The natural substrates angiotensin I and bradykinin have the C-

terminal ends -Phe-His-Leu and -Pro-Phe-Arg respectively. A review of the diversity of ACE substrates is given in by Cushman and Ondetti.[99] ACE was found to be selective for substrates with antepenultimate, penultimate, and C-terminal residues with the L-configuration.[100,101] ACE hydrolyzes peptides as short as N-acyl tripeptides, and shows no activity with N-acyl dipeptides.[102] Tripeptides with a free N-terminal amino group act as inhibitors and are hydrolyzed quite slowly, parallel to the interactions between dipeptides and CPA. ACE cannot hydrolyze substrates with C-terminal Asp or Glu residues, or a penultimate Pro residue such as in angiotensin II.[103,104] Interestingly, unlike substrates with a C-terminal Glu or Asp, which bind weakly to the ACE active site,[103] substrates with a C-terminal Pro do in fact bind tightly to the ACE active site.[101,103] A C-terminal proline is found in many tight binding inhibitors of ACE, such as captopril (**15**), enalaprilat (**16**) and **17**. Additional studies have shown that, in terms of binding specificity, the relative importance of the P_1 (antepenultimate), P_1' (penultimate) and P_2' (C-terminal) positions is $P_2' > P_1' > P_1$. The reverse is observed for substrate specificity where $P_1 > P_1' > P_2'$.[101]

The concentration of chloride ions in solution has also been found to affect the activity of ACE. It has been suggested that chloride ions induce a conformational change in ACE that may differentially alter the binding affinity for different substrates.[105] Riordan and coworkers,[106,107] using extensive kinetic studies, demonstrated that there are three classes of substrate on the basis of Cl^- activation. The classes differ in the effect that Cl^- has on the rate of hydrolysis, and, importantly, the order in which Cl^- and the substrate bind to the active site.

Class I substrates such as furanacryloyl-Phe-Gly-Gly essentially require the presence of Cl^- for hydrolysis and as an important activator.[106,108] Increases in Cl^- concentration were shown to decrease K_m values, with a K'_A of 80 mM, but had no affect on k_{cat} values, where the chloride binding constant (K'_A) represents the Cl^- concentration at which k_{cat}/K_m is half-maximal. Class I substrates in general have

been found to possess K'_A values ranging 80-150 mM. The Cl^- ion is required to bind before the substrate binds to the active site, prior to hydrolysis (Scheme 11).

Scheme 11

$$E + Cl^- \rightleftharpoons E\text{-}Cl^- + S \rightleftharpoons E\text{-}Cl^-\text{-}S \longrightarrow E\text{-}Cl^- + P$$

Class II and III substrates also show an activation by Cl^-, but to a lesser extent as compared to Class I substrates, where Class III substrates display a greater activation by Cl^- than do Class II substrates. Unlike the Class I substrates, Class II and III substrates do not show absolute dependence on Cl^-. Both K_m and k_{cat} values are affected by Cl^- concentrations, with K'_A values of 3-5 mM and 18-30 mM for classes II and III respectively. In the hydrolysis of these substrates, ACE can bind Cl^- in the free enzyme (**E**) or **ES** state (Scheme 12). Stopped-flow radiationless energy-transfer kinetics were used to show that the ACE-Cl^--substrate complex with the class III substrate dansyl-Lys-Phe-Ala-Arg consisted of two species.[109] There is an initial $E{\cdot}Cl^-{\cdot}S_1$ complex, followed by a $E{\cdot}Cl^-{\cdot}S_2$ complex in which the substrate is bound more tightly to the active site (Scheme 12). This two-step mechanism was found for the binding of slow-tight-binding inhibitors enalaprilat and captopril as well (see discussion in Section 1.5).

Class II substrates consist of compounds with arginine or lysine in the C-terminal or penultimate position, whereas Class I and III substrates possess no clear distinguishing features, except that all class III substrates have a penultimate alanine residue. The chloride ion concentration is observed to affect the binding of inhibitors as well.[107] Other anions such as Br^-, phosphates and sulfates have also been shown to bind to ACE and to affect activity.[110]

Scheme 12

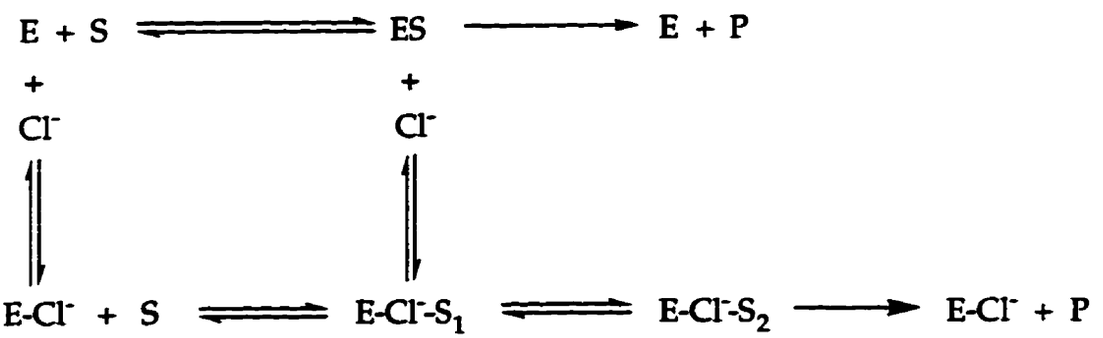

ACE also possesses esterase activity.[100] N-Acyl tripeptides and their ester analogues (N-acyl-P_1-O-P_1'-P_2') were found to have very similar K_m values, but k_{cat} values for ester substrate hydrolysis were found to be 5 to 33 times lower than those for the corresponding amide substrates. Studies of the pH profile, Cl^- effect, inhibition and chemical modification of ACE reveal no mechanistic differences between esterase and peptidase activity.

Although a crystal structure has never been determined for ACE, the enzyme is considered to contain one CPA-like active site per protein molecule. Like CPA and thermolysin, ACE contains a single Zn^{2+}, Arg, Tyr^{111} and $Glu^{111,112,113}$ at the active site. The hypothesis concerning the involvement of these residues in catalysis is based on chemical modification studies. The rates of irreversible chemical modifications were diminished in the presence of reversible ACE competitive inhibitors. These experiments parallel chemical modification studies conducted with CPA.[111]

The proposed general base mechanism for ACE (Figure 9) is similar to that for CPA and thermolysin.[92,113] Again, an Arg residue is involved in binding the C-terminal carboxylate. There are binding pockets S_1', S_2' and S_1 for binding substrate side groups. The Tyr residue is thought to be involved in hydrogen bonding to the

scissile amide hydrogen and may possibly aid in formation of the S_1' binding pocket paralleling the proposed function of Tyr-248 in CPA. The active site Zn^{2+} and glutamyl residue are suggested to be involved in a water promoted attack on the scissile amide bond. On the basis of substrate specificity studies, the active site was proposed to be an extended linear trench that can accommodate a polypeptide with perhaps as many as 10 residues.[114]

Figure 9

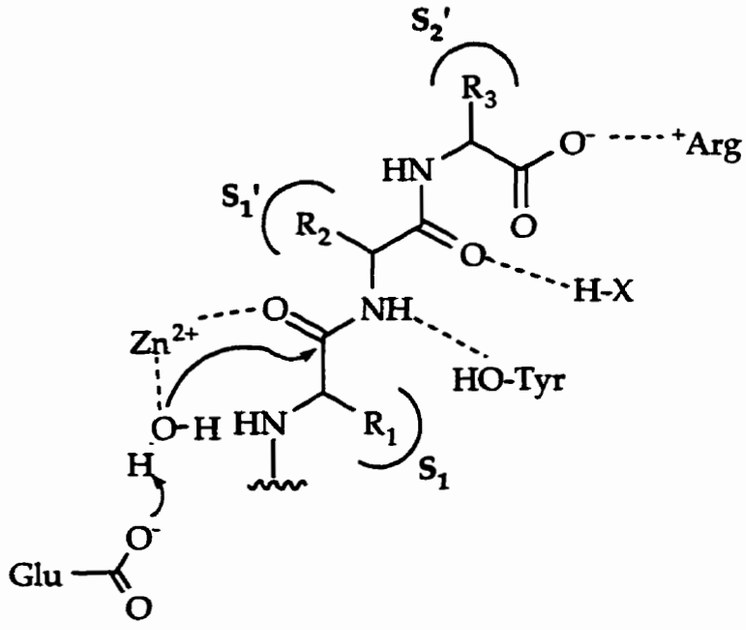

During the hydrolysis, a Zn^{2+} stabilized tetrahedral intermediate is proposed to be formed. The existence of this suggested transition-state is supported by the tight binding of transition-state analogues, similar to those which inhibit CPA and thermolysin. The carboxylate of Enalaprilat was suggested to bind the active site Zn^{2+} in a transition state-like geometry for general base hydrolysis (Figure 10). Spectrophotometric and MCD analyses of Co^{2+}-ACE complexed to enalaprilat indicate a strong interaction between the Co^{2+} atom and the carboxylate of the

inhibitor,[96] but whether the binding involves a mono or dioxygen-Co^{2+} interaction has not been resolved. Enalaprilat (K_i of 0.06 nM)[115,116] also contains the characteristic tight binding proline C-terminal residue.

Figure 10

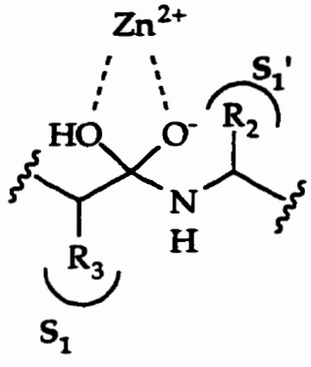

Hydrolysis Transition-State

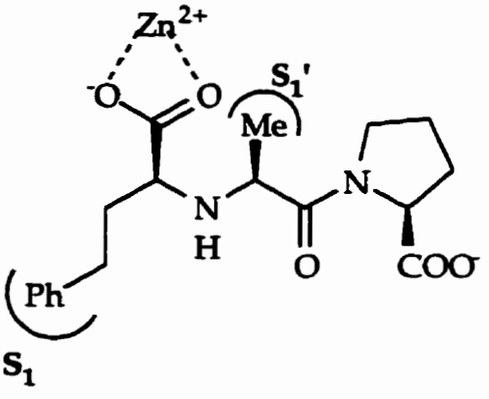

ACE-Enalaprilat Complex

Transition-state analogues **17** and **18** (K_i = 0.5 nM and 1.4 nM respectively)[117] as well as other phosphoramidates are thought to inhibit ACE by mimicking the tetrahedral transition-state in the same way that transition-state analogues strongly inhibit CPA (Figure 11).

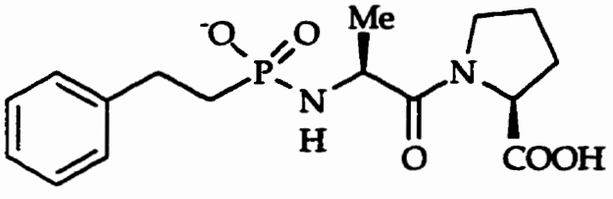

17

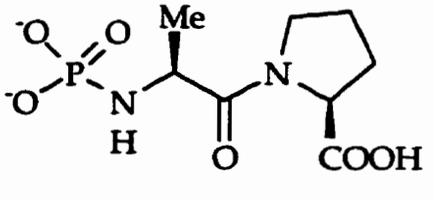

18

Figure 11

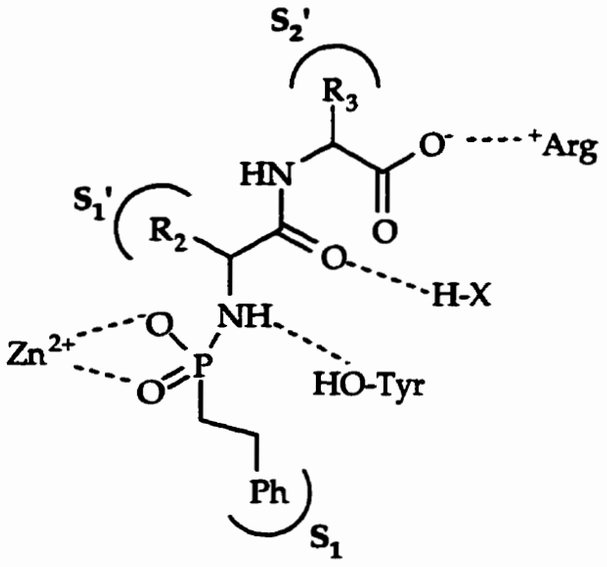

Chemical modification studies indicate the importance not only of active site Glu, Arg and Tyr residues, but also of a Lys residue.[111,118] This is unlike the situation with CPA where there is no evidence suggesting any catalytic involvement of a Lys residue. Methylation of a single Lys residue increases K_m values for substrate binding with no effect on k_{cat}.[118] ACE was partially protected from methylation by the addition of either competitive inhibitors or Cl^-, suggesting the catalytic Lys was located at or near the active site. Interestingly, however, the addition of Cl^- and a competitive inhibitor together caused a strong synergism in protection from methylation.

The Lys residue is thought to be involved in the anion activated substrate binding mechanism. Furthermore, the species involved in the anion activation mechanism was determined to have a pK of 9.4,[119] consistent with a positively charged lysyl residue in a hydrophobic microenvironment and/or near an active site Zn^{2+}. These environments would stabilize the unionized form of the ε-amino group

of lysine, reducing the pK_a value (pK_a of a lysyl ε-amino group is usually 10.3). Similarly, α-amylase utilizes a lysyl residue for Cl^- binding for Cl^- activation, and with a pK reduced to 9.1.[120]

The Lys-Cl^- interaction is thought to induce conformational change, adapting the active site for certain substrates.[118] Excess Cl^- levels, however, were found to inhibit ACE by binding to low-affinity inhibitory sites in both an uncompetitive and a competitive mode.[119]

Later, Cl^- was found to lower K_m values for the binding of substrates to thermolysin as well,[121] in a non-essential mechanism. The Cl^- ion is thought to interact with Arg-203 to help stabilize the thermolysin-substrate complex. Arg-203 is involved in a salt bridge with Asp-170, which hydrogen bonds to His-142, one of the Zn^{2+} ligands. By competing with Asp-170 for Arg-203, Cl^- can alter active site conformation, optimizing substrate binding. This is in contrast to the effect of excess Cl^- on CPA activity. Cl^- competitively inhibits the binding of the substrate to the CPA active site by binding to Arg-145.[122,123] A substrate C-terminal carboxylate binding group such as Arg-145 for CPA does not exist for thermolysin, explaining the difference in Cl^- effects between CPA and thermolysin.

1.5 Inhibitors of CPA and ACE

CPA and ACE have been subjected to extensive inhibition studies in the past. This reflects the substantial fundamental and therapeutic importance of these enzymes. Reversible inhibitors for CPA and ACE have been the main focus for inactivation studies. Although irreversible inhibition of these metalloenzymes has been much less studied, there are some mechanistically interesting examples. For example, 2-benzyl-3-iodopropanoic acid (**19**) has been reported to irreversibly inactivate CPA in a time-dependent manner by S_N2 displacement of the iodide by Glu-270 or Tyr-248 with an observed k_{inact} of $0.078 min^{-1}$.[124] This inactivation reaction is thought to be catalyzed by a weak but favourable interaction between the active site Zn^{2+} and the iodide of **19** (Figure 12).

In addition, Kim and coworkers have found that the epoxide inhibitor **20** and thioepoxide inhibitor **21** inactivate CPA irreversibly by a similar mechanism.[125,126,127] X-ray crystallographic studies have shown that these inhibitors inactivate CPA irreversibly through a covalent bond formation between the inhibitor and the active site Glu-270 (Figure 12).[127] Again, this covalent bond formation is thought to be catalyzed by the interaction between the active site Zn^{2+} and the electrophilic moiety of the inhibitor. Surprisingly, however, the x-ray structure of the CPA-**20** covalent complex revealed that it is the D-form (in respect to substrate configuration) that is covalently attached to the Glu-270. This was unusual considering that the catalytic activity of CPA is highly specific for the L-configuration when binding transition-state analogues of substrates.[68,69,70,71] Kim,[127] using modeling studies, has proposed that as a consequence of the unusual geometry of the epoxide-containing substrate analogue **20**, the D-form (2S,3R) actually binds in the active site in an orientation slightly more favourable for nucleophilic attack by the Glu-270 carboxylate. The observed K_i and k_{inact} values for the inactivation by **20** (2S,3R) were 86 μM and 1.59 min^{-1} respectively.

The enantiomer (2R,3S) was observed to be a slightly less effective inactivator with K_i and k_{inact} values of 155 μM and 1.11 min^{-1} respectively. The thioepoxide derivative **21** (2S,3R), which was designed to take advantage of the strong affinity between Zn^{2+} and sulfur, was no more effective as an inactivator, with K_i and k_{inact} values of 94 μM and 1.31 min^{-1} respectively.[126]

Figure 12

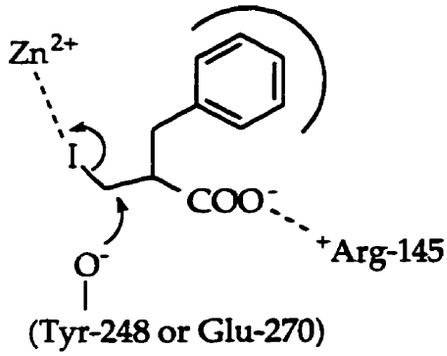

CPA-**19** complex

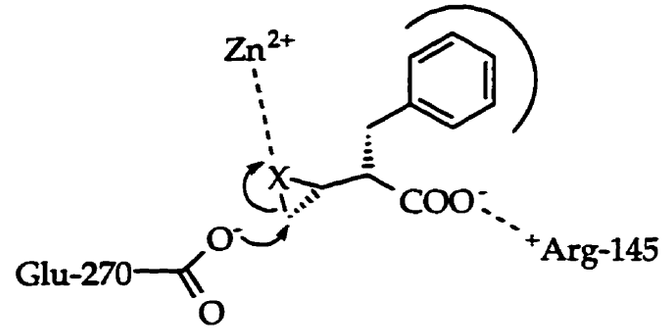

CPA complexed with
20: X=O
21: X=S

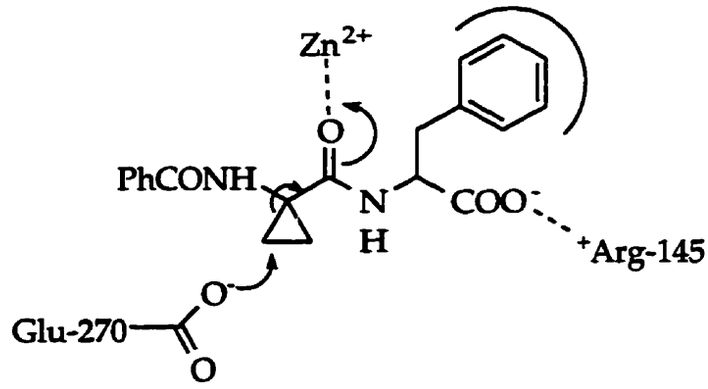

CPA-**22** complex

The Glu-270 side-chain carboxylate is also proposed to participate in nucleophilic ring opening of the cyclopropane ring of the irreversible inactivator **22** (Figure 12).[128,129]

As mentioned earlier, the investigations into the reversible class of inhibitors for CPA and ACE have been extensive. Many of the inhibitors investigated earlier were actually substrates themselves. CPA was found to bind tightly to dipeptides,[7] which were hydrolyzed only slowly. ACE was found to interact with tripeptides in the same fashion.[130] Crystal structures of CPA with the dipeptide Gly-Tyr helped resolve the interactions leading to this tight binding affect. As shown in Figure 2 (Section 1.2), Gly-Tyr binds to the active site with interactions considered normal for substrate-CPA complexes, with an additional interaction between the amino group of Gly-Tyr and Zn^{2+} and Glu-270 which interferes with catalysis.[33] A similar interaction may also occur with ACE complexed with free amino tripeptides.

Other inhibiting substrates include the C-terminal proline substrates for ACE. The snake poison BPP_{5a} (**23**) from *Bothops jararaca*,[131] with a K_i of 50 nM, is one of the more potent examples. It acts as a tight-binding mixed inhibitor which is also hydrolyzed slowly in the absence of Cl^- and not at all in presence of Cl^-. Extensive studies have been conducted to find the optimal tight-binding sequence for these C-terminal proline peptides.[99] The C-terminal proline, penultimate alanine, and antepenultimate phenylalanine or tryptophan residues were found to be the most effective as in BPP_{5a}. These structural features allow for the tightest enzyme substrate interactions but also cause hydrolysis to be unfavourable. The Ala-Pro C-terminal is also found in other types of the strongest inhibitors of ACE.

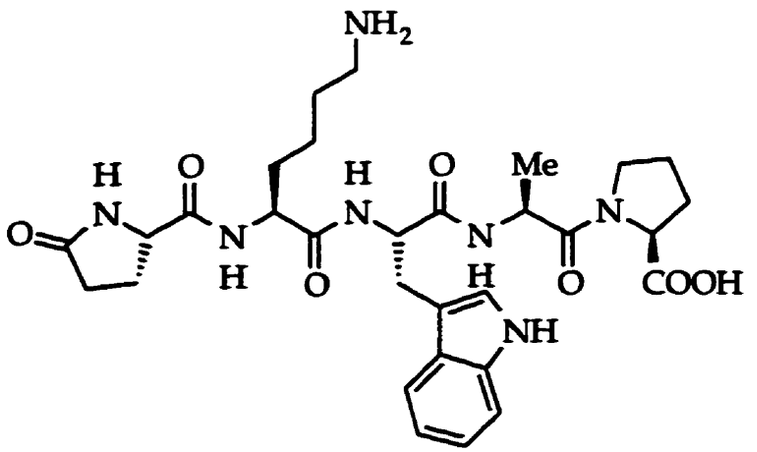

23

Compounds designed as substrate analogues which are incapable of undergoing hydrolysis, such as the ketonic CPA substrate analogue **24** and the ACE substrate analogue **25** (IC_{50} 26 μM),[132,133] are known to be good enzyme inhibitors. With the C-terminal phenylalanine substructure of **24** and the C-terminal -Phe-Ala-Pro substructure of **25**, both inhibitors utilize the optimal structural characteristics to increase binding.

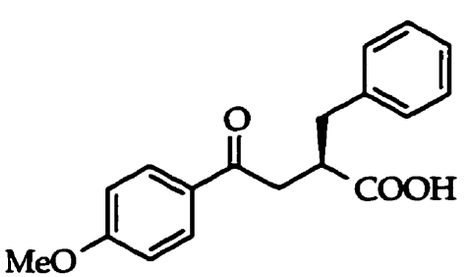

24

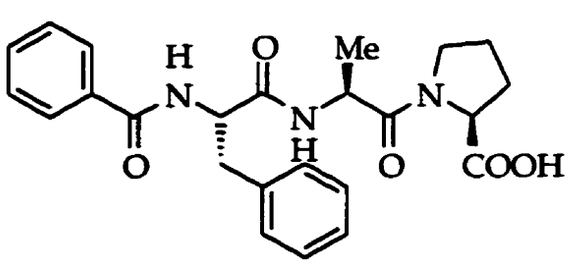

25

CPA not only binds **24** in the same orientation as it does normal substrates,[26,30,134] but also catalyzes enolate formation by stabilizing the negatively charged oxygen using Zn^{2+} (Figure 13).[133] Deuterium labeled **24** was used to demonstrate a stereoselective removal of the H_a (Pro-R) hydrogen, suggested to be

abstracted by Glu-270.[133] A crystal structure of CPA complexed with **24** shows a Zn^{2+}-carbonyl oxygen interaction and the side-chain carboxylate of Glu-270 within interaction range of H_a.[134]

Figure 13

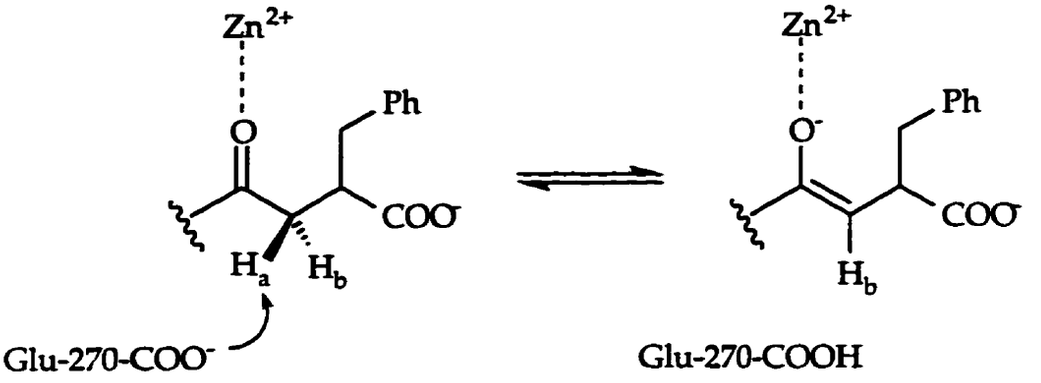

Other ketonic inhibitors of CPA along with certain aldehyde inhibitors have been shown to inhibit CPA as transition-state analogues. As mentioned in Section 1.3, **8**, **9** and **10** along with **26** and **27** were found to bind CPA in the hydrated form (Figure 6).[17,35,37,64,65,66,67,73]

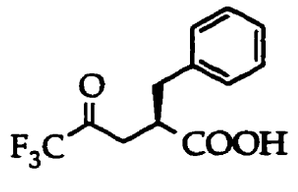

8

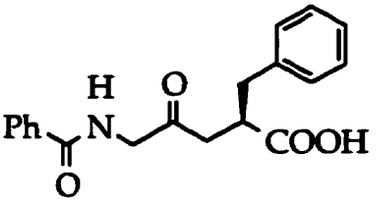

9

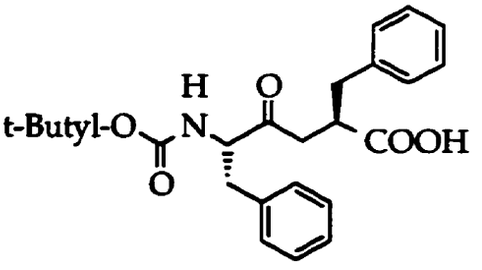

10

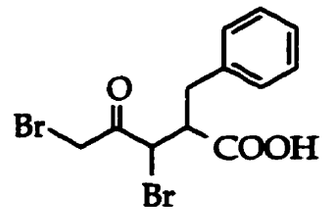

26

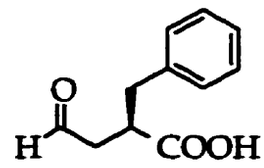

27

The halogenated inhibitors **8** and **26** were originally designed to help favour the hydrated form. Ketone inhibitors **9** and **10** were found to bind with CPA solely in the hydrated state, even though hydration for these ketones is normally unfavourable (less than 0.2% in solution).[64,65] These experiments show the importance of the transition-state geometry for designing better binding inhibitors. Interestingly, ketonic inhibitor **24** was shown not to be hydrated when complexed with CPA, possibly because of inadequate enzyme-inhibitor interactions due to steric effects between the acyl benzoyl group and the active site.[64] The Phe-279 side chain phenyl group in the S_1 subsite and the methoxybenzoyl group of **24** are thought to be involved in unfavourable interactions. These phenomena may also explain the poor substrate qualities of N-benzoyl-L-phenylalanine.[7]

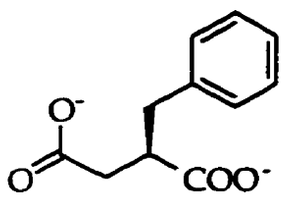

28

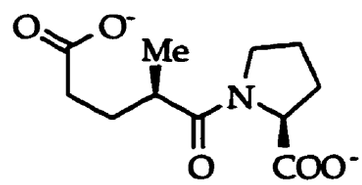

29

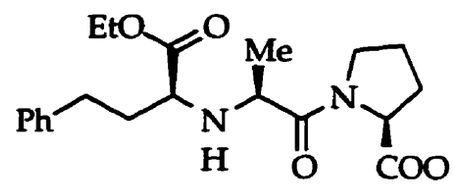

30

Another class of transition-state analogues well known to inhibit CPA and ACE is comprised of the dicarboxylates. L-Benzylsuccinic acid (**28**) with K_i 0.45 μM was originally designed by Wolfenden[60,135] to mimic the two products of hydrolysis

(Figure 14). Wolfenden proposed that the post-hydrolytic CPA-product complex involves both the acid and amine products bound to the active site, with the newly formed carboxylate chelated to the active site Zn^{2+}. A molecule such as **28** which incorporates two carboxylate groups so positioned as to mimic the carboxylates of the two products can be considered to be a bi-product analogue which might be expected, on the basis of entropy arguments, to bind more tightly than the two normal product molecules.[136] Benzyl succinate has also been classified as a transition-state analogue as a result of the strong inhibition observed which is usually characteristic of transition-state analogues.[136] Crystallographic studies have shown that the second carboxylate does bind to the Zn^{2+} in a bidentate fashion,[137] compatible with either bi-product or transition-state analogue binding. The dicarboxylate **29** which possesses the same byproduct design but the standard tight-binding ACE substrate/inhibitor structure was found to be a modest inhibitor with a IC_{50} of 0.8 μM.[138]

Figure 14

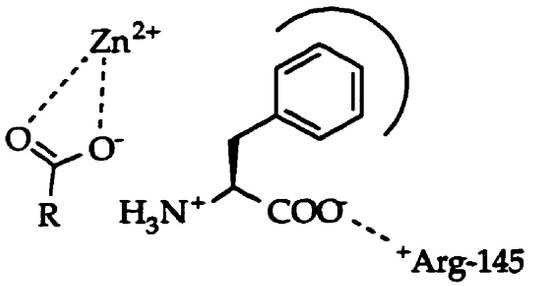

CPA complexed with hydrolysis products

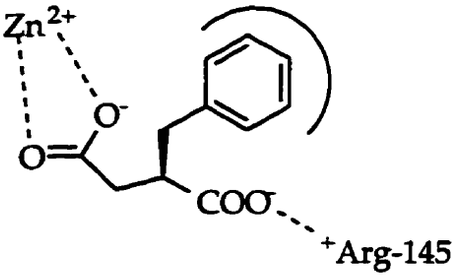

CPA complexed with **28**

Enalaprilat (**16**)[115], which is a slow-binding inhibitor,[116,139] is an example of a strong dicarboxylate ACE inhibitor with a K_i of 0.06 nM. Enalaprilat as well as many other dicarboxylate inhibitors[115] were designed as transition-state analogues (Figure 10). Visible absorption and MCD spectroscopy have been employed to study the

interaction of enalaprilat with Co^{2+}-ACE. It was concluded that the complex involved interaction between the active site Zn^{2+} and the carboxylate moiety of the inhibition possibly in a transition-state geometry.[96] Enalaprilat is used extensively for therapeutic purposes as an antihypertension agent. The drug form clinically used is the ethyl ester enalapril (**30**), a prodrug which is hydrolyzed *in vivo* to release the carboxylate.[115,138]

The tightest binding group of inhibitors for these enzymes is the organophosphorus class of transition-state analogues. As mentioned in Section 1.3, Bartlett and coworkers have developed many analogues for both thermolysin and CPA, which, to date, are the most potent inhibitors for these enzymes.[76,80,81,82,140,141,142] These inhibitors were shown to bind in a manner imitating the tetrahedral transition-state (Figure 7).[36,70,71,75,78,98,143] The two main types of organophosphorus CPA inhibitors are the phosphonates (**31**) and the phosphonamidates (**32**).

Figure 15

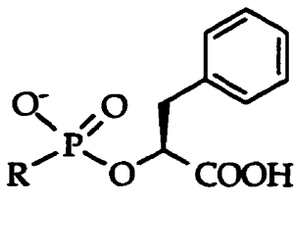

31

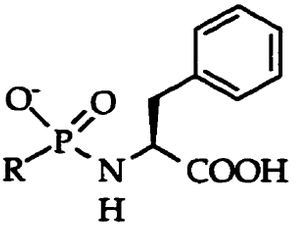

32

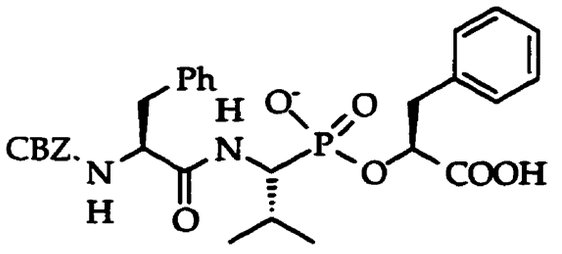

33

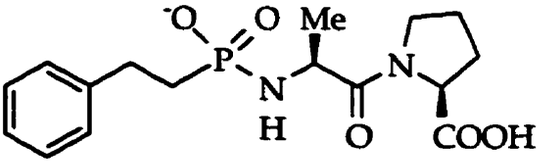

17

Using the basic phosphinyl-phenylalanine structure and varying the R groups (Figure 15) to imitate various N-carbobenzoyl di- and tri-peptides, Bartlett demonstrated the importance of the P_2 and P_1 groups for inhibitor binding (refer to Figure 3 for P group classification). With CBZ-Ala-Ala- and CBZ-Phe-Ala- as R groups on the phosphonate structure **31**, these inhibitors were found to possess K_i values of 1 pM and 3 pM respectively, demonstrating the importance of a P_2 phenylalanine.[76] With a phosphonate analogue of valine as the P_1 group in **33**, the K_i drops to 11 fM.[141] This compound is the tightest binding inhibitor reported to date for CPA, underlining the importance of hydrophobic interactions in the CPA S_1 and S_2 subsites. X-ray crystallographic studies of **33** complexed to CPA have shown the valine side chain to be inserted into the S_1 subsite pocket which is formed by Ser-197, Tyr-198, Ile-247, Tyr-248 and Glu-270.[36] Subsite S_2-inhibitor interactions were found to involve a hydrophobic interaction between Tyr-198 and Tyr-248 with P_2 phenylalanine side chain. Another important geometric observation for this complex was the aromatic-aromatic edge-to-face interactions between the P_1' phenyl group of the inhibitor and the Tyr-248 phenyl group, involving the slightly positively charged edge of one phenyl ring and the slightly negatively charged face of the other phenyl ring. This weak polar interaction affords more stabilization than found in face-to-face phenyl ring interactions which involve only Van der Waals forces and which are observed in other inhibitor-CPA complexes studied by x-ray crystallography.

Figure 16

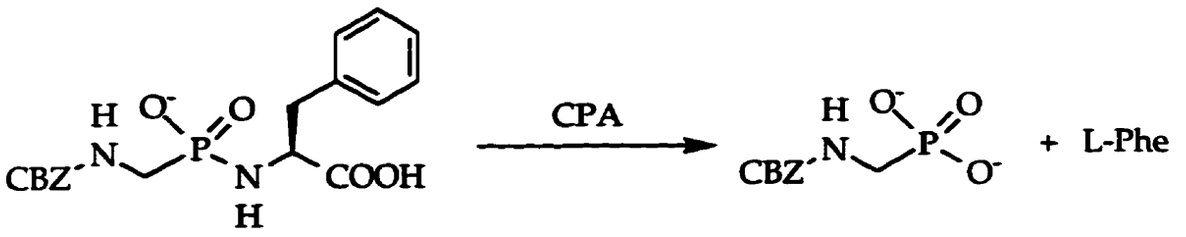

12

The original analysis of phosphonamidate **12** (K_i 90 nM) by Bartlett provided no evidence of hydrolysis of the phosphonamidate bond.[142] Later x-ray crystallographic studies of the complex of CPA with **12** revealed, however, that the inhibitor was bound to the CPA active site in the hydrolyzed form.[70] The L-phenylalanine product bound into the S_1' subsite, and the phosphonic acid product bound in the S_2 and S_1 subsites, with the phosphonate oxygens coordinated to the active site Zn^{2+}, in a product analogue geometry (Figure 16).

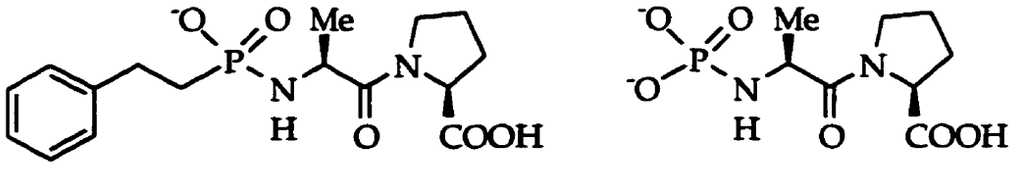

17 **18**

Phosphonamidate transition-state analogues **17** and **18** have also been studied as inhibitors of ACE.[117] Compound **17** with a K_i of 0.5 nM is a phosphonamidate with the enalaprilat (**16**) structural features. The organophosphorus ACE inhibitors were found to be less effective than their dicarboxylate analogues, unlike the situation with CPA and thermolysin for which the organophosphorus inhibitors are especially effective.

With all of the many types of inhibitors found for CPA and ACE, the tighter binding classes usually involve a substrate or transition-state structure with a metal binding moiety which coordinates to the active site Zn^{2+}. Other metal-binding inhibitors include simple metal chelators, such as 2,2'-dipyridyl and *o*-phenanthroline which inhibit CPA.[95] These compounds inhibit activity by removing the metal ion from the active site. ACE is known to be inhibited by EDTA and *o*-phenanthroline by the same mechanism.[144] This mode of inhibition is easily verified by regenerating enzyme activity by the addition of excess metal ion. EDTA and other highly charged metal chelators inhibit CPA slowly, due to the lack of active site penetration because of unfavourable interactions between the hydrophilic chelator and hydrophobic CPA active site.

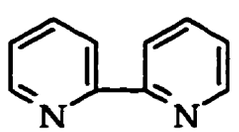

2,2'-dipyridyl

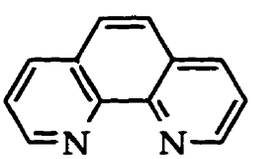

o-phenanthroline

Other classes of inhibitors that involve a strong Zn^{2+}-metal binding interaction are mercapto and hydroxamate inhibitors. Mercaptans such as cysteine, mercaptoacetic acid and mercaptoethanol also inhibit CPA by metal ion removal.[95] Thiol inhibitors such as those in Figure 17, on the other hand, have been shown to inhibit CPA by classical reversible competitive inhibition. These types of inhibitors were found to inhibit by binding Zn^{2+} in the CPA active site without removing the metal ion. Electronic absorption, CD, MCD and EPR spectroscopy using Co^{2+}-CPA are consistent with d-d transitions from the Co^{2+}-sulfur interaction.[97,145] ^{113}Cd-NMR analysis of ^{113}Cd-CPA also demonstrated that thiol-type inhibitors such as mercaptoacetic acid and **34** remain in the active site bound to the metal.[146] Although

mercaptoacetic acid was shown to be capable of removing the active site Zn^{2+} if allowed to incubate with the enzyme for 3 days,[95] its main mode of inhibition is considered to be simple competitive binding.[97]

Figure 17

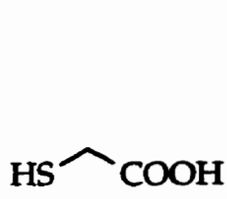

mercaptoacetic acid

K_i=9.0 μM (CPA)

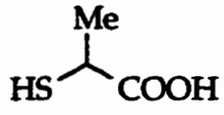

34

K_i=5.1 μM (CPA)
K_i=8.6 μM (ACE)

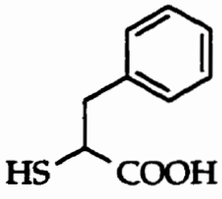

35

K_i=1.2 μM (CPA)

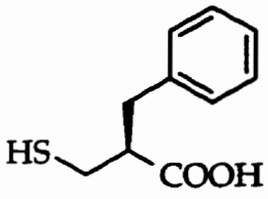

36

K_i=7.8 nM (CPA)

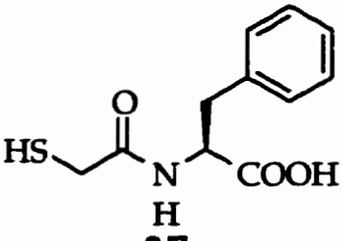

37

K_i=5.0 μM (CPA)
K_i=75 nM (ACE)

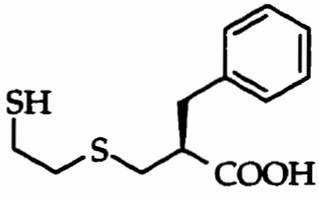

38

K_i=4.2 μM (CPA)

Vallee[97] has stated that compounds which 1) incorporate a metal-binding agent and 2) which are analogues of the substrate or transition-state may be potent and selective inhibitors. Inhibitors **35**[97], **36**[147], **37**[97] and **38**[148] all of which possess the phenylalanine substructure with thiol group, all are good inhibitors. The importance of the phenylalanine-like structure for good inhibition[97] is indicated by the lower potency of mercaptoacetic and mercaptopropanoic acid (**34**). The tight-binding inhibitor 2-benzyl-3-mercaptopropanoic acid (**36**), the most potent of the thiol-CPA

inhibitors with a K_i of 7.8 nM for the L-enantiomer,[149] is thought to represent the optimal binding geometry[147] (Figure 18). The free thiol is situated in the inhibitor for easy binding to the Zn^{2+} atom and the rest of the inhibitor fits into the active site in the substrate binding configuration.

Figure 18

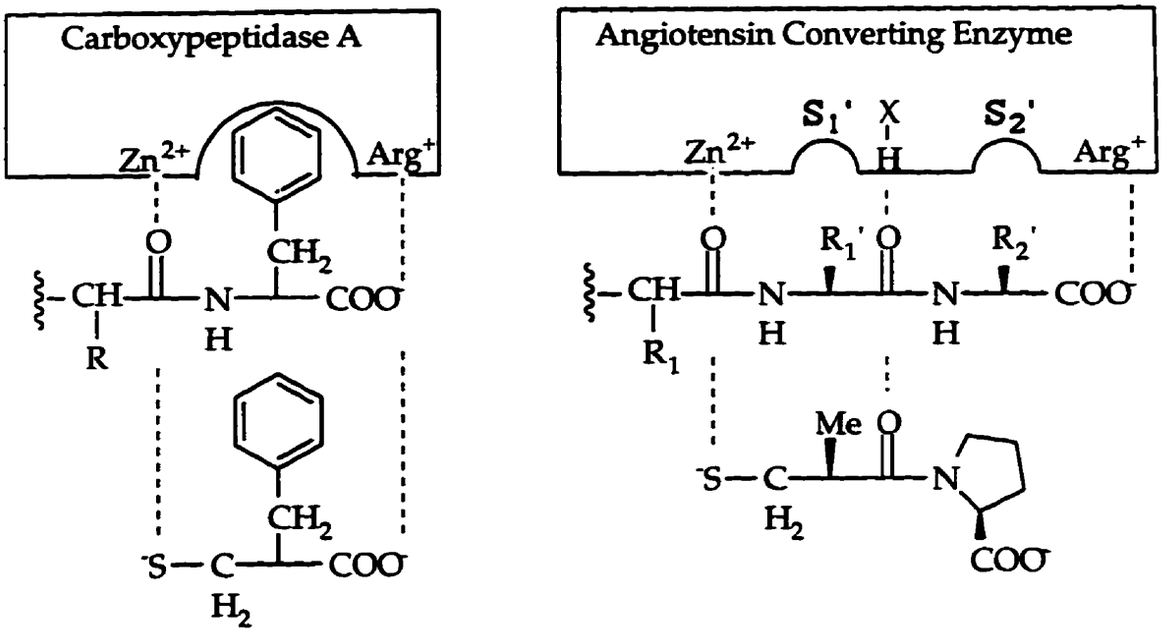

36 **39**

More recently Kim[150,151] has used various para-aromatic substituted analogues and phenyl-to-cyclohexyl and -naphthyl substituted analogues of **36** to estimate the dimensions of the hydrophobic pocket of the S_1' subsite of CPA. It was concluded that the subsite was approximately 3.5 Å x 7.1 Å in size.

2-Mercapto-3-phenylpropanoic acid (**35**), which lacks the methylene bridge between the α-carbon and the mercapto group found in **36**, was observed to have a higher K_i. The large difference in K_i values observed for thiols **35** and **36** was thought to result from an inadequate distance between the phenylalanine substructure and the

metal binding thiol group of **35**.[148] Captopril (**39**), a tight-binding mercapto inhibitor of ACE developed by Cushman and Ondetti,[152] exhibits a K_i of 1.7 nM. Captopril has been shown to bind ACE through the expected metal-thiol interaction on the basis of visible absorption and MCD spectroscopy with Co^{2+}-ACE.[96] Captopril possesses the -Ala-Pro substructure found in other tight-binding ACE inhibitors such as enalaprilat (**16**) and BPP_{5a} (**23**). Cushman demonstrated that upon removal of the methylene bridge to the SH group to give **40**, the IC_{50} was increased from 0.023 μM to 1.1 μM[152] emphasizing again that appropriate placement of the thiol group seems very important in optimizing binding. Upon removal of the methyl group of captopril to give a -Gly-Pro derivative (**41**) the IC_{50} increases to 0.20 μM. Adding another methylene group spacer to **41** to give **42** decreases inhibition again with an IC_{50} of 2.4 μM.[152] By substituting the Pro residue on **41** with other amino acids, Cushman showed that Phe, Arg and Ala analogues of captopril are also reasonably good inhibitors with IC_{50}'s of 0.43, 0.65 and 0.85 μM respectively.[152] Inhibitor **40** displays a higher IC_{50} value than captopril (**39**) as a consequence of the shortened structure. Replacing the C-terminal proline with the larger aromatic residue Trp (**44**) on the other hand, gives a more potent inhibitor **44** (IC_{50} of 0.08 μM).[153] ACE inhibitor **37** which has a "shortened" structure was shown to be a fairly potent inhibitor with a K_i of 75 nM presumably as a consequence of the C-terminal phenylalanine group.[97] Other mercapto inhibitors of ACE have been investigated and reviewed by Cushman and Ondetti.[99] Potent substrate analogue mercaptan inhibitors for thermolysin have also been investigated.[154]

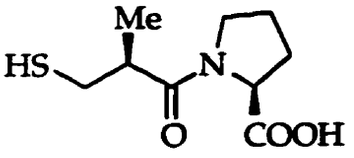

39

K_i=1.7 nM (ACE)

IC_{50}=0.023 μM (ACE)

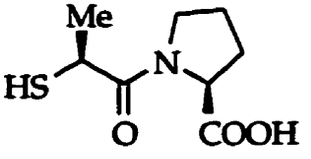

40

IC_{50}=1.1 μM (ACE)

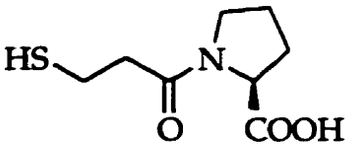

41

IC_{50}=0.20 μM (ACE)

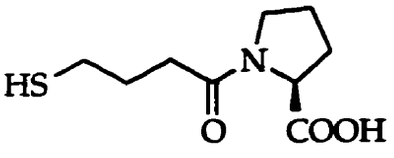

42

IC_{50}=9.7 μM (ACE)

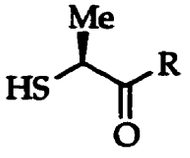

43 R=Cys, IC_{50}=8.0 μM (ACE)

44 R=Trp, IC_{50}=0.08 μM (ACE)

Hydroxamate substrate analogue inhibitors are thought to bind metalloenzymes with the same metal-binding mechanism as observed with thiol inhibitors. The hydroxamate functionality, which has a high affinity for Zn^{2+}, strongly chelates it in the enzyme-substrate type complex. ACE is inhibited by hydroxamic acids **45**[99] and idrapril (**46**)[155], with IC_{50} values of 610 nM and 470 pM respectively. Hydroxamic acids are thought to chelate the Zn^{2+} active site atom through the carbonyl oxygen and negatively charged deprotonated hydroxyl oxygen.[156] This type of Zn^{2+}-hydroxamic acid bidentate complex (Scheme 13) was observed for the binding of hydroxamic acid substrate analogues to thermolysin using x-ray crystallography.[87]

Scheme 13

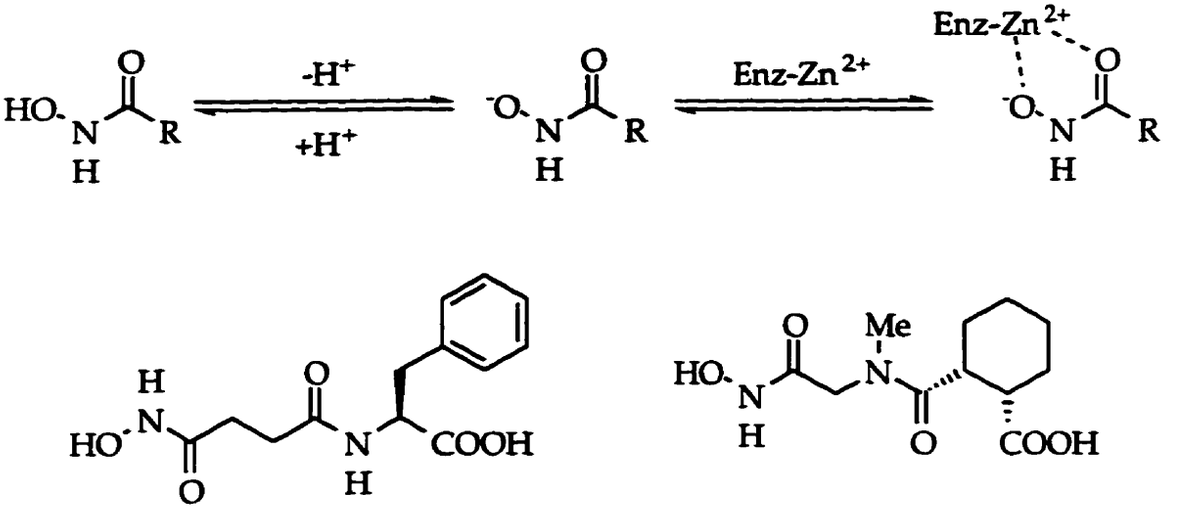

45 **46**

The ACE inhibitors captopril (**39**) and enalaprilat (**16**) are both used clinically in hypertension therapy. The inhibition of ACE by these inhibitors requires the presence of Cl^- in solution, similar to the binding of many of the substrates.[107] More detailed kinetic analysis of these inhibitors showed that they were actually slow-tight-binding competitive inhibitors,[107,116] for which there is an initial EI complex between ACE and the inhibitor followed by slow isomerization to a tighter EI' complex (Scheme 14). Captopril, in particular, was observed to be a better inhibitor (K_{iapp}=0.33 nM) than originally observed by Cushman (K_i=1.7 nM) when the tight binding phenomenon is taken into account in the kinetic analysis.[152] The Cl^- anion is thought to be involved in the stabilization of the EI' complex.[107]

Scheme 14

$$E + I \underset{}{\overset{K_i}{\rightleftharpoons}} EI \overset{K_i'}{\rightleftharpoons} EI'$$

Captopril K_i=47 nM
K_i'=0.33 nM

Enalaprilat K_i=9.2 nM
K_i'=0.05 nM

The use of mercapto compounds such as captopril for therapeutic purposes is sometimes accompanied by side-affects such as rashes and loss of taste.[157] The free SH group of the inhibitor is thought to cause many of the side-effects as a consequence its high affinity for Zn^{2+} which results in binding to other Zn^{2+}-metalloenzymes. Another free thiol inhibitor, thiorphan, (Figure 19) which targets the Zn^{2+}-peptidase enkephalinase, has been shown to possess significant inhibitory activity against other Zn^{2+}-dependent enzymes such as ACE (K_i of 150 nM) and leucine aminopeptidase (K_i > 10 μM).[158]

Figure 19

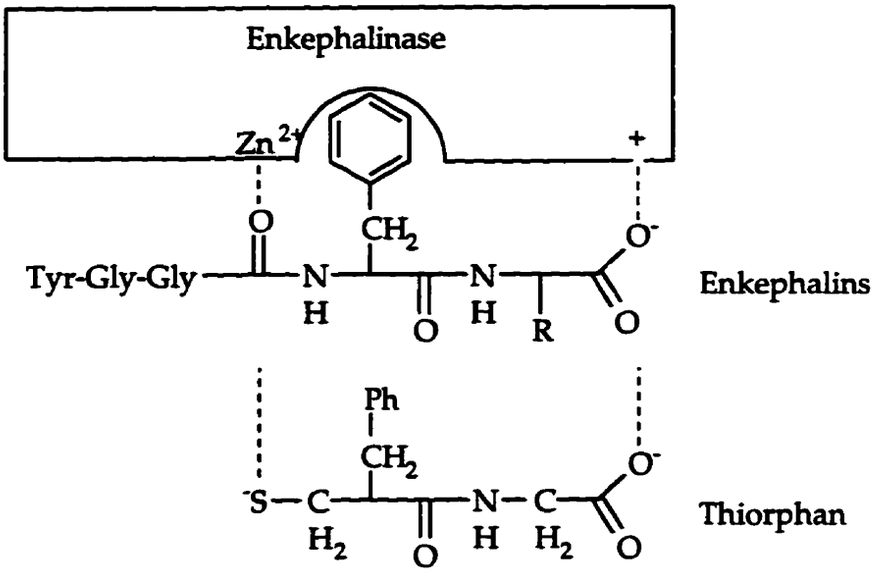

Thus, given that side effects are observed for such metal-binding compounds, there is room for improvement of specificity to avoid such interactions with enzymes other the target enzyme. Possible strategies for introducing additional specificity by relying on enzyme activation to release the metal binding agent are described below in Chapter 2.

Chapter 2:
Results and Discussion

2.0.1 Mechanism-Based Inhibition of Carboxypeptidase A by Thioester Substrate Analogues

Compounds that inhibit Zn^{2+}-proteases through metal-binding, usually do so through diffusion into the active site of the enzyme, followed by interaction between a ligand on the inhibitor (X) and the metal ion (Scheme 15).

Scheme 15

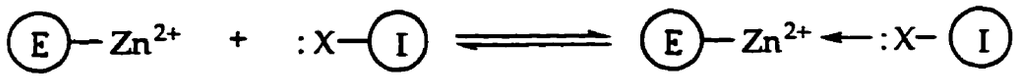

As indicated in Section 1.5, therapeutic use of these types of compounds sometimes leads to toxicity when the metal-binding group (X) binds and inhibits important metalloenzymes other than the target enzyme.[157,158] Thus, there is a need for strategies to increase the specificity of such enzyme inhibitors.

One strategy for creating highly specific enzyme inhibitors is based on the so-called "suicide substrate" or "Trojan horse" concept. In such an approach, the inhibitor is designed to possess a functionality capable of inhibiting the enzyme. However, this functionality is present in a modified or latent form which is activated through the catalytic action of the target enzyme.[159] One example of this type of inhibition is found with the halo enol lactones,[160,161,162] which are considered to inactivate α-chymotrypsin through formation of two covalent bonds. Halo enol lactones, such as **47**, are thought to undergo a nucleophilic attack by the catalytic Ser-195, which leads to ring opening and protonation (Scheme 16). The α-halide is then susceptible to

displacement by attack from a nucleophile, His-57 in this case, within the active site of the enzyme. Carbon-14 labeled halo enol lactone **48** was used to show that α-chymotrypsin inactivated by **48** contained one molecule of the inhibitor covalently bound to the enzyme.

Scheme 16

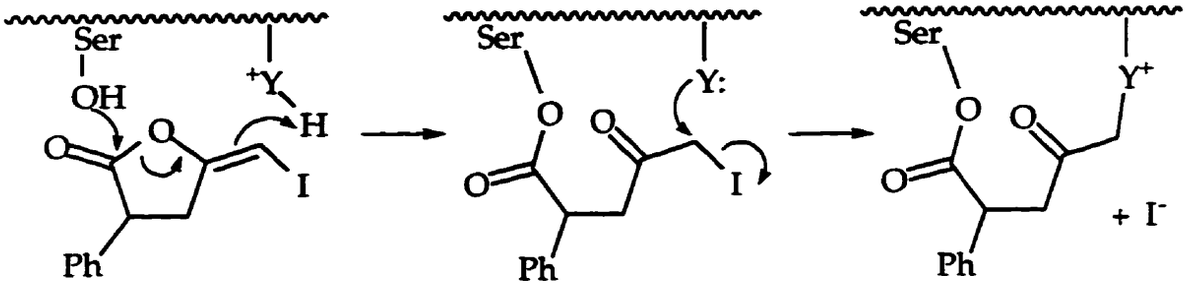

47

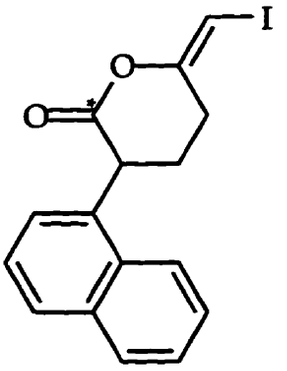

48

In most cases, suicide substrate inhibitors such as halo enol lactones are designed to release an electrophilic site to react with some nucleophilic amino acid side chain functionality in the active site of the target protein. In the present case, the target functionality in the active site is an electrophilic metal ion and, as a result, the appropriate functionality to be masked and subsequently released from the inhibitor

by the enzyme is a nucleophilic species capable of acting as a ligand to the metal ion. The concept is illustrated in Scheme 17.

Scheme 17

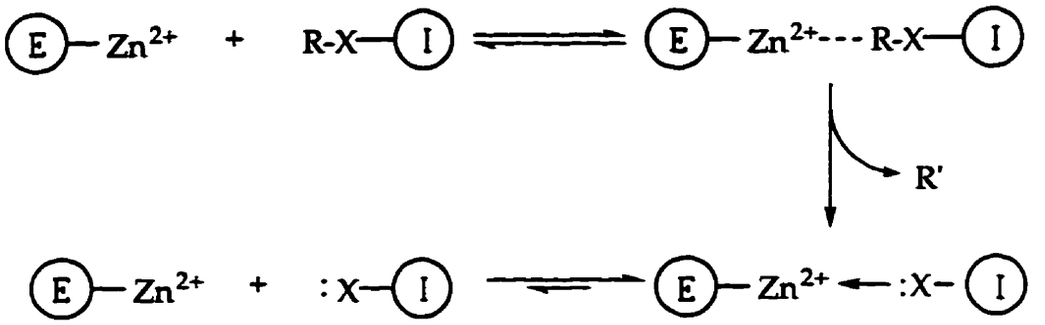

The principal interest in this class of mechanism-based inhibitors is related to the possibility of an increase in the specificity of the inhibition. As mentioned previously, captopril at higher doses causes side-effects because of the general metal-binding ability of free thiols.[157] As outlined in Section 1.5, mercapto compounds are known to inhibit Zn^{2+} containing enzymes through a strong Zn^{2+}-sulfur binding.[95] In the present strategy, it is intended that specificity be increased by designing molecules which are not themselves metal binding agents but which incorporate a latent metal ion binding site which is released by the catalytic activity of the target enzyme.

Thioester substrate analogues which release known free-thiol inhibitors upon hydrolysis are proposed as potential examples of this type of inhibitor. These compounds are designed such that the target enzyme will hydrolyze the thioester bond in essentially the same way amide and ester bonds are cleaved in natural peptide substrates and in synthetic ester substrates respectively. The X group in Scheme 17 would then be the free-thiol functionality (Scheme 18). An efficient thioester inhibitor of this type must meet two essential criteria: 1) the thioester

linkage must be recognized as a substrate by the target enzyme; and 2) the thiol released must be a good inhibitor.

Scheme 18

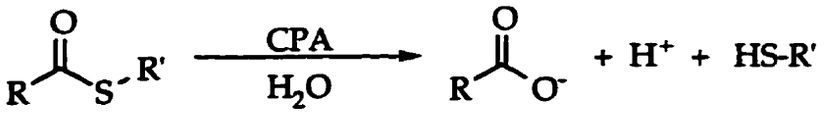

The first thioester analogues tested for this purpose were studied in this laboratory by MacKinnon,[163] who examined various S-acyl-2-benzyl-3-mercaptopropionic acid analogues (**49**) targeting CPA (Scheme 19). Hydrolysis of any of these would lead to the release of thiol **36** which is known as a tight-binding inhibitor (K_i 7.8 nM).[147]

Scheme 19

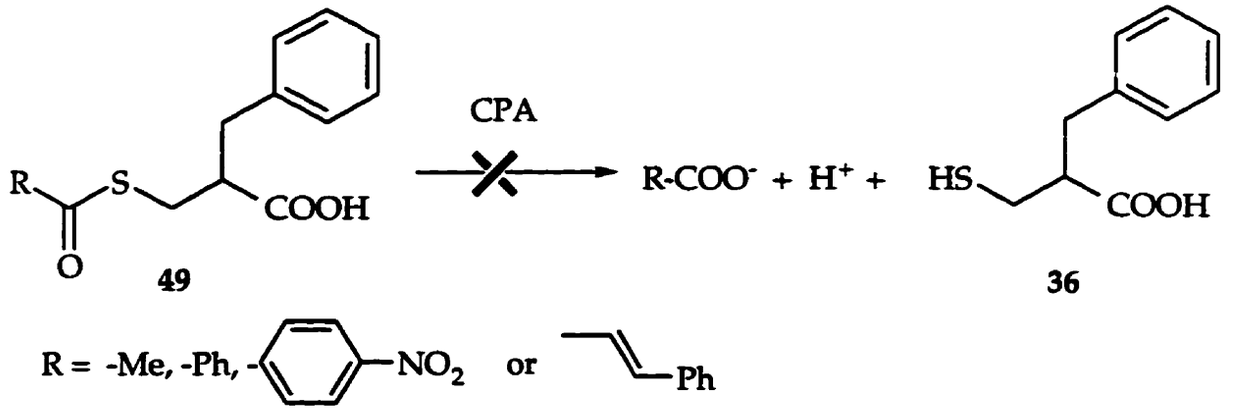

No hydrolysis was observed for these analogues. The extra methylene group between the α-carbon and the S atom was thought to be responsible for the lack of substrate recognition. Thioesters such as **49** satisfy the second criterion listed above, in that the

product of hydrolysis is an excellent inhibitor, but do not meet the first criterion in that **49** is not recognized as a substrate.

A better choice to satisfy the first criterion is thioester **50**, which is closer in structure to natural amide and ester substrates. The closer structurally similarity to normal substrates may increase the likelihood of the inhibitor being recognized as a hydrolyzable substrate (Figure 20). On the other hand, thioester **50** represents a compromise with respect to the second criterion, in that the released thiol product **35**[97] has been reported to be a much weaker inhibitor than **36**[147] (K_i 1.2 μM for **35** vs K_i 7.8 nM for **36**). MacKinnon conducted preliminary qualitative experiments in this laboratory with **50** which indicated that CPA was inhibited when incubated with racemic **50**.[163]

Figure 20

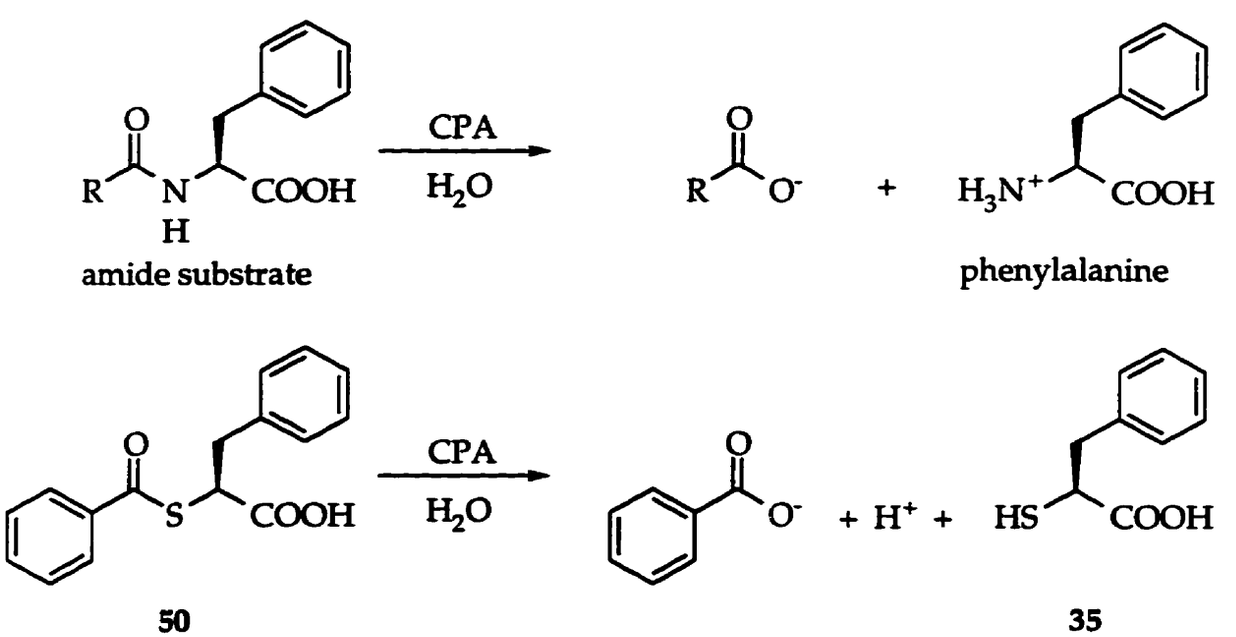

2.0.2 Synthesis of Thioester Substrates of CPA and Related Compounds

In order to investigate the nature of the inhibition of CPA by the proposed thioester substrate, (S)-**50** was required. In addition, comparison of the hydrolysis of **50** and the oxygen ester derivative **51** by CPA required the synthesis of (S)-**51**.

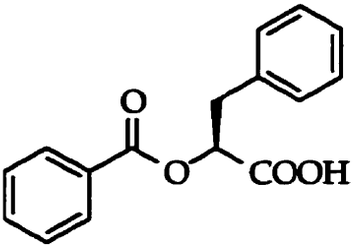

51

Racemic thioester **50** was originally prepared from (R,S)-phenylalanine by MacKinnon[163] through the steps outlined in Scheme 20. This method was adequate for the synthesis of racemic **50**, but inappropriate for the synthesis of (S)-**50** since the 18 hour acidic hydrolysis in the last step of the pathway was expected to result in substantial racemization.

In the present study, the asymmetric synthesis of (S)-**50** was pursued via a modified scheme which did not involve a harsh acid or alkaline hydrolysis step in order to generate the free acid form (Scheme 21). The first step involves the conversion of (R)-phenylalanine to the α-bromo acid derivative (R)-**52** with retention of configuration.[164] This step is thought to involve a diazonium intermediate which is converted to an α-lactone intermediate with inversion of configuration through an intramolecular nucleophilic attack (Scheme 22).[165] Nucleophilic ring opening of the α-lactone by bromide also occurs with inversion so that the final product is produced through a double inversion sequence resulting in overall retention of configuration.

Scheme 20

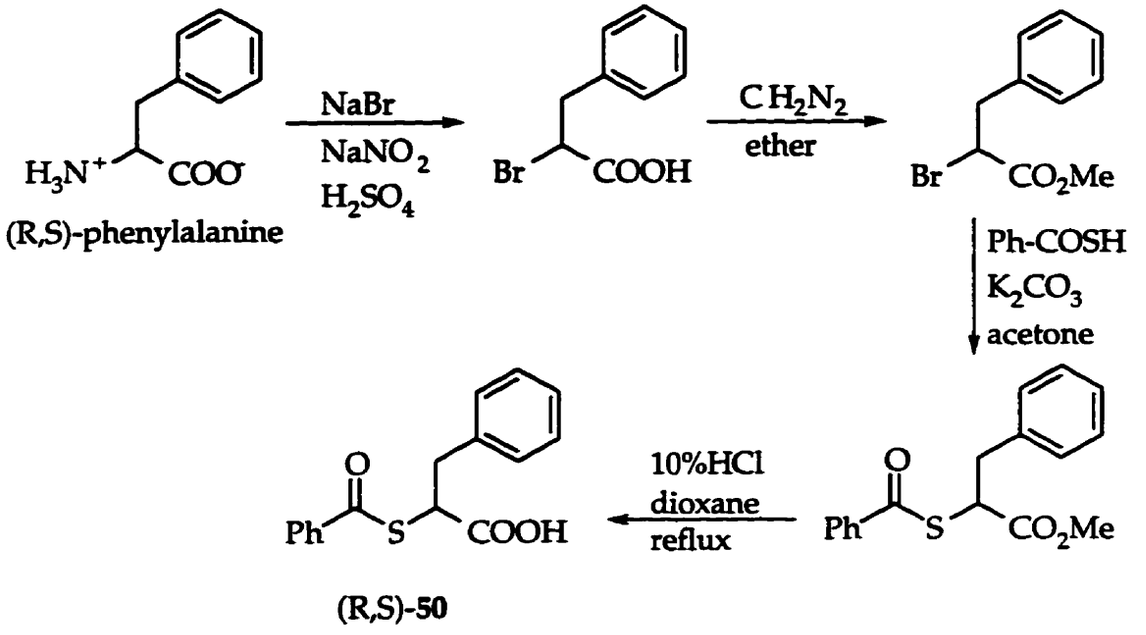

Scheme 21

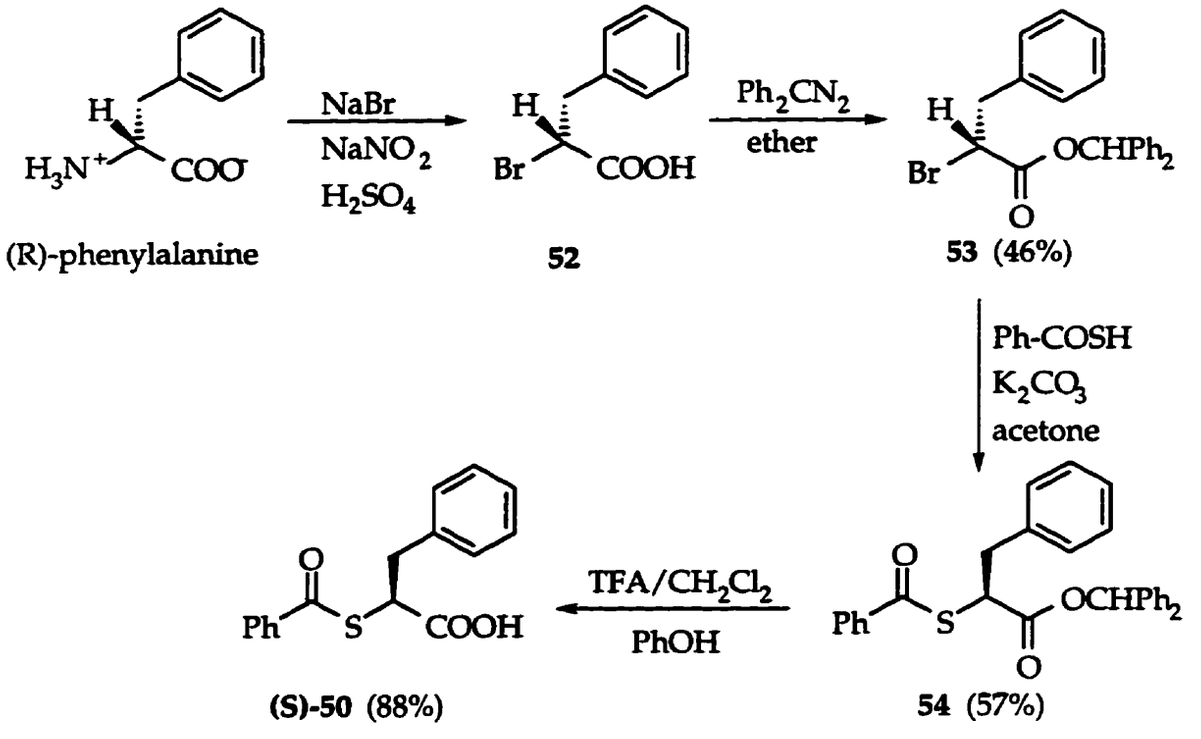

The carboxylic acid functionality was protected by formation of the benzhydryl ester **(R)-53** with a yield of 46% by reacting the acid **52** with diphenyldiazomethane which was prepared from benzophenone hydrazone.[166]

Scheme 22

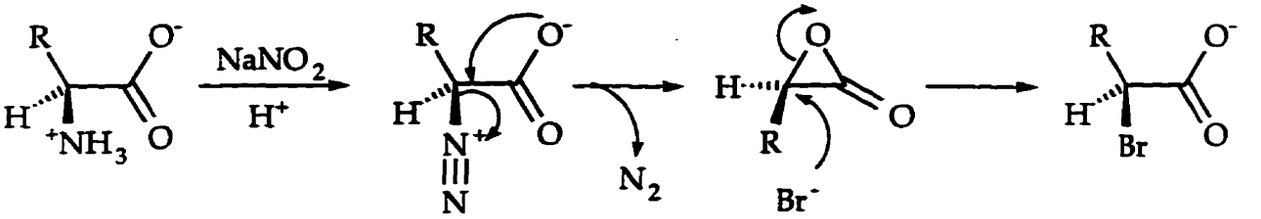

The thioester (S)-**54** was prepared in a yield of 57%, by reacting the bromide **53** with potassium thiobenzoate in acetone. This process is an S_N2 displacement and, hence, is expected to result in inversion of configuration. The benzhydryl group was then removed using trifluoroacetic acid (TFA) and phenol to give (S)-**50** in a yield of 88%.

The enantiomer (R)-**50**, was also synthesized using the same synthetic route described for (S)-**50**, but using (S)-phenylalanine as a precursor.

The enantiomeric purity of (S)-**50** was measured to be 95% through chiral salt formation using the chiral amine α-(S)-methylbenzylamine (Figure 21). The thioesters (S)-**50** and (R)-**50** were separately reacted with α-(S)-methylbenzylamine to form the (S,S) and (R,S)-chiral salts respectively. A sufficient difference in the ^1H NMR chemical shifts in benzene-d_6 was observed for the methine hydrogen at C-2 of the diastereomeric salts at 500 MHz to allow for estimates of the enantiomeric purities of the chiral thioester.

Figure 21

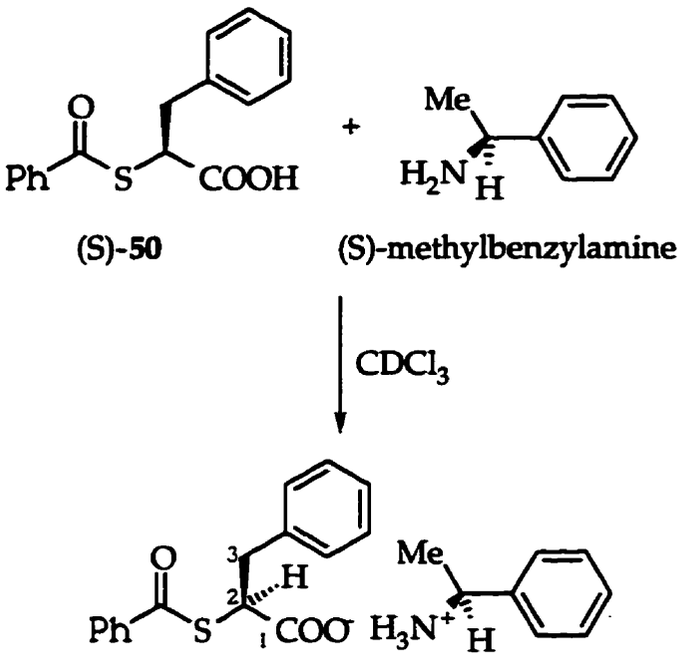

(S)-**50** (S)-methylbenzylamine

(S,S)-chiral salt

55

The ^{1}H-NMR signal for the methine proton of the (S,S) salt, **55**, was observed as a doublet of doublets (J_{AX}=7.5 Hz, J_{BX}=7.3 Hz) at 4.78 ppm and the corresponding signal for the (S,R) salt was observed as a doublet of doublets (J_{AX}=7.0 Hz, J_{BX}=7.0 Hz) at 4.69 ppm. In the NMR spectrum of the (S,S) salt, the minor component (the (R,S) salt) gave rise to a signal at 4.69 ppm. The ratio of (S,S) to (R,S) salt, measured by integration of the C-2 methine signals, was found to be 17.3:1. From this ratio , the sample of **50** prepared from (R)-Phe was estimated to contain 95% of the (S)-enantiomer (90% **ee**). Similar analysis of the (R,S) salt resulted in the estimate that 97% of the sample prepared from (S)-Phe was (R)-**50** (94% **ee**).

The commercial sample of (R)-phenylalanine was reported by the manufacturer to contain 98.8% of the R enantiomer (97.6% **ee**). Thus the synthetic route above resulted in a small but measurable degree of racemization. The higher

optical purity observed with the product derived from (S)-Phe may have resulted from a higher optical purity of the starting amino acid.

The oxygen ester derivative **51** (Scheme 23) was prepared by a route similar to that used in the synthesis of (S)-**50**. The benzoyl ester **56** was prepared by reacting **53** with sodium benzoate in DMF. This step took 6 hours of stirring at room temperature to go to completion. This is substantially longer than the similar step in the synthesis of (S)-**50** in which **53** is reacted with potassium thiobenzoate (Scheme 21) in only 30 min. The benzhydryl group was then cleaved using TFA and phenol.

Scheme 23

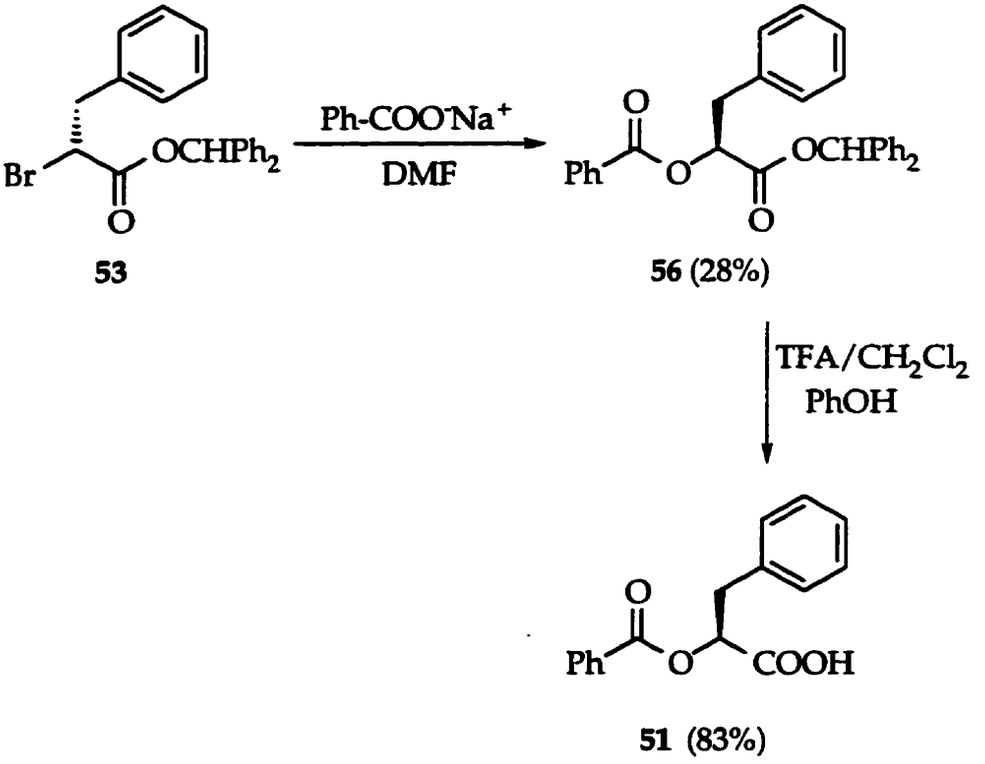

53 **56** (28%) **51** (83%)

The enantiomeric purity of **51** was estimated using a similar routine as for the analysis of (S)-**50**. The chiral salts (S,S) and (S,R) were prepared by mixing equimolar amounts of **51** and α-(S)-methylbenzylamine or α-(R)-methylbenzylamine in $CDCl_3$. Again, ^{1}H-NMR analysis at 500 MHz on a Bruker AMX-500 of the individual chiral

salts, as well as a 50:50 mixture of the salts, revealed the differences in chemical shifts between the two chiral salts. Only the chemical shifts of the methine hydrogen differed enough for accurate integration measurements (with shifts of 5.17 and 5.13 ppm for (S,S) and (R,S)-chiral salts respectively). Analysis of the integration allowed for an estimate that 77% of the sample was the S-configuration. Therefore, the enantiomeric purity was estimated to be only 54% **ee** from this analysis.

There is a substantial difference in the enantiomeric purities of (S)-**50** and **51** (90% **ee** and 54% **ee** respectively). This difference is believed to be due to the difference of reaction times and of solvent used during the coupling of **53** with potassium thiobenzoate (Scheme 21) or sodium benzoate (Scheme 23). The longer reaction time required for the bromide displacement using benzoate as the nucleophile is a reflection of the weaker nucleophilicity of benzoate in comparison with thiobenzoate (though benzoate ($pK_a = 4.20$)[167b] is known to be a stronger base than thiobenzoate ($pK_a = 2.48$)[167b]). During the course of the reaction bromide ions which have been displaced by benzoate to form **51**, may act as a nucleophile in the presence of a polar aprotic solvent (DMF) and attack the R enantiomer **53** (the starting material) to generate the S enantiomer of **53**. This racemization was aided by the extended time required for all of **53** (both enantiomers) to react with benzoate.

The thiol **35** was first synthesized in racemic form by Rovazzoni and coworkers[169] from benzaldehyde and rhodanine as shown in Scheme 24.

Vallee,[97] who first studied the inhibition qualities of **35** against Zn^{2+}-metalloenzymes, prepared it by coupling (±)-2-bromo-3-phenylpropanic acid and sodium thiobenzoate to give (±)-**50**, followed by hydrolysis to give racemic **35**.

The acid hydrolysis of an S-acyl bond in thioester is usually 8-30 times slower than that of the corresponding oxygen ester.[170] The differences in rates are lower with aryl as opposed to aliphatic acyl groups. The rates of hydrolysis under alkaline conditions, on the other hand, differ only slightly between thiol and oxygen esters.

Amino acids and peptides, however, are known to undergo substantial racemization under alkaline conditions.[171] Under acidic conditions, the rate of epimerization is usually lower, but it was felt that the prolonged hydrolysis required to cleave a thioester group using aqueous acid was likely to cause racemization.

Scheme 24

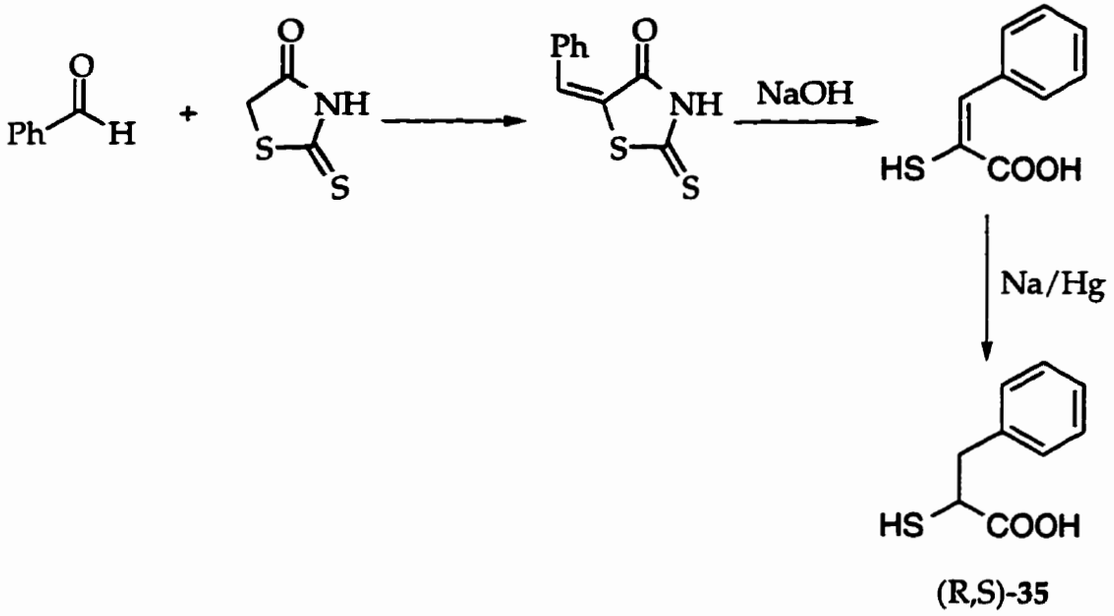

(R,S)-35

Figure 22

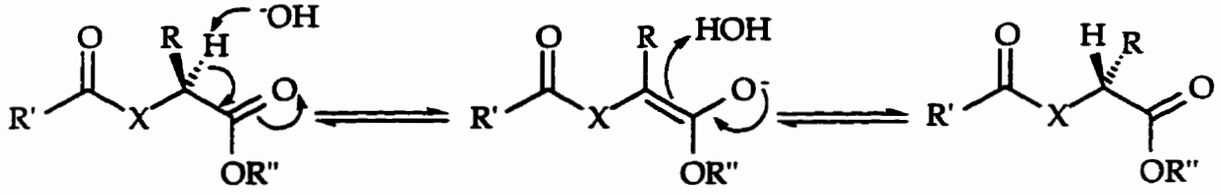

X = S, O, or NH

All of the approaches to (S)-35 explored in this study were designed in such a way as to avoid harsh basic or acidic conditions to minimize racemization. All of our

synthetic routes to (S)-**35** made use of (R)-**53**, generated as an intermediate in our preparation of (S)-**42**, as a precursor. Compound (R)-**53** was reacted with various thiol nucleophiles that were subsequently targeted for deprotection to generate the free thiol. The xanthates were first explored for this purpose. Potassium tert-butyl xanthate (**58**), which was prepared from coupling carbon disulfide and tert-butoxide (Scheme 25),[172] was proposed to displace the bromide of (R)-**53** in a S_N2 reaction to give the xanthate **59**.

Scheme 25

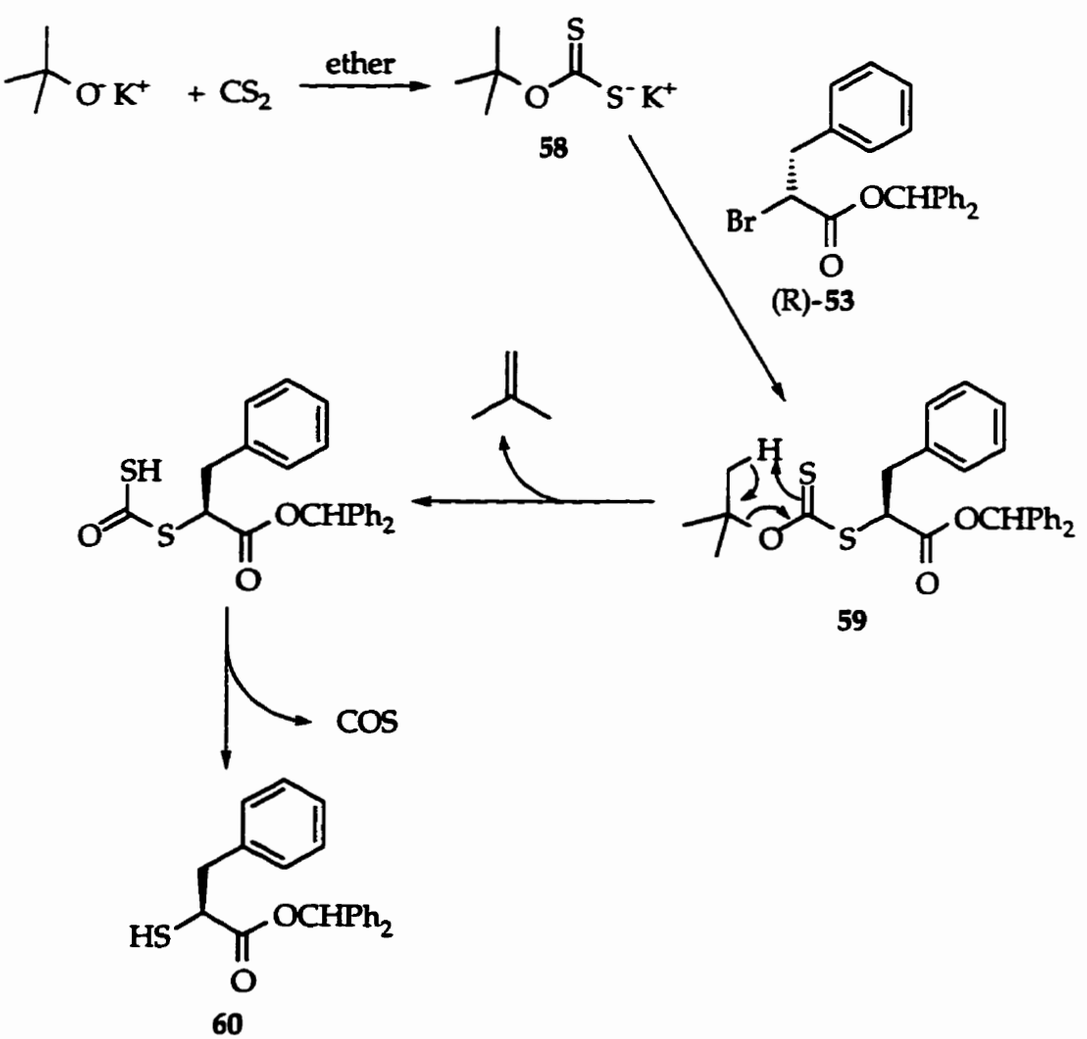

The free-thiol (**60**) might then be generated through a thermal β-elimination reaction,[172,173] or possibly at low temperatures with the aid of trifluoroacetic acid in a procedure similar to that used in the cleavage of N-^{t}BOC groups.

In practice, coupling of **58** with (R)-**53**, was not facile suggesting that **58** was a poor nucleophile. Complete displacement of the bromide took 3 days in acetone at room temperature, and 5 hours in DMF at 85-88°C. NMR analysis showed a 2:1 mixture of sulfide **61** and the free thiol **60** from the acetone reaction, and **60** as the only product from the reaction in DMF.

Scheme 26

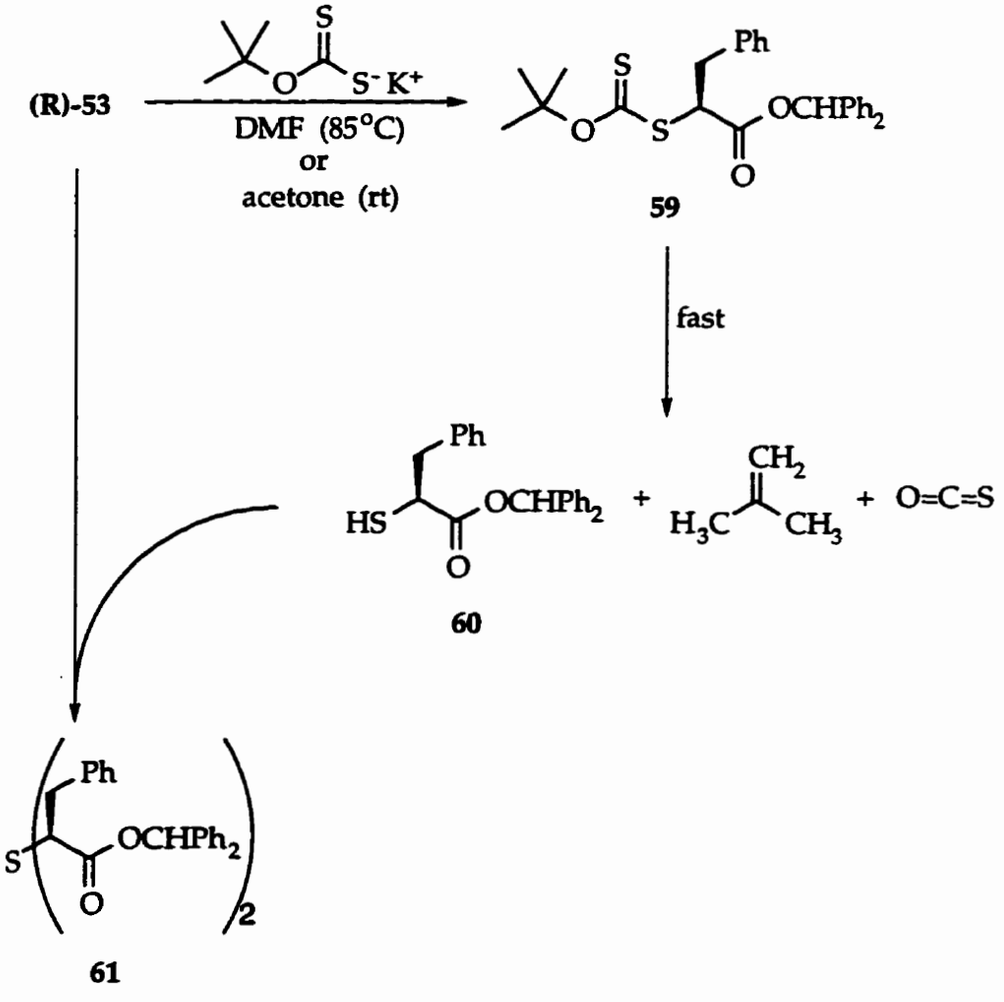

It would appear that decomposition of **59** through elimination was faster than S_N2 displacement of the Br^- anion of **53**. The thiol generated *in situ* can then compete with the xanthate salt as a nucleophile, attacking **53** to give the sulfide **61**. *t*-Butylxanthates have been reported to be rather unstable compared to other xanthates.[172] Attention was then turned to the use of other xanthates as nucleophiles.

The potassium benzyl xanthate salt **62** was prepared by coupling benzyl alcohol with CS_2 and was then used to displace Br^- in (R)-**53** to give **63**.

Scheme 27

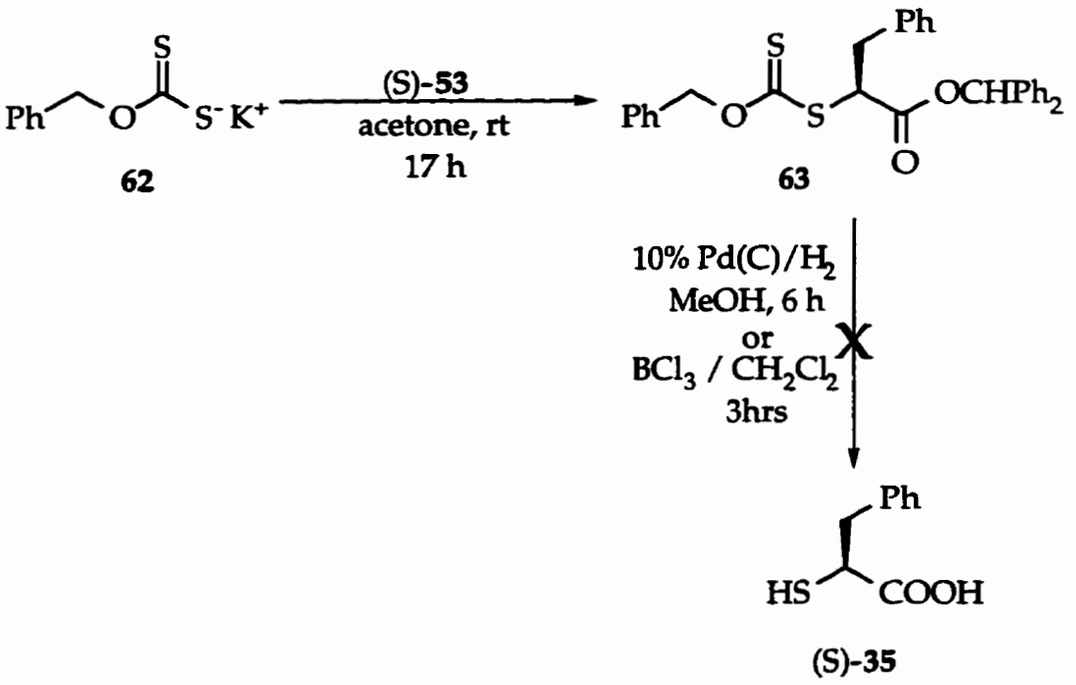

Xanthate **63** resembles benzyl carbonates (with C=S instead of C=O) which are used to protect alcohols.[174] Compound **63** was found to be much more stable than **59**, presumably because of the lack of a hydrogen on the carbon β to the O-alkyl group which then prevents the decomposition found with **59** (Scheme 25). Compound **63** was purified and then subjected to different chemical decomposition attempts to

break down the xanthate to liberate the free thiol group giving **60** or **35**. Hydrogenation, which is commonly used to deprotect benzyl carbonates to give an alcohol group,[174] was explored with **63**. Hydrogenation using 10% Pd(C) in methanol and acetic acid under 30 psi H_2 resulted in some cleavage of the benzhydryl ester group but left the benzyl xanthate group intact. The lack of hydrogenation was assumed to result from poisoning of the Pd catalyst by sulfur, but increasing the catalyst to substrate ratio to 1:1 (w/w) did not improve the result.

Since boron trihalides are known to cleave benzyl carbonates as well as other amine protecting groups,[175] the benzyl thiocarbonate **63** was treated with BCl_3 in CH_2Cl_2 but was found to be unreactive.

These difficulties led us to explore other nucleophiles for introduction of the thiol group. Benzhydryl thioethers have been used as a means of protecting cysteine side-chain mercapto group during peptide synthesis.[176] This group has been cleaved using TFA/phenol to regenerate the free-thiol. We reasoned that the sulfur atom could be introduced by nucleophilic attack of thiobenzhydrol **64** on the bromide **53** to give the thioether **65**, followed by reaction with TFA to yield the desired thiol under mild conditions (Scheme 28). Thiobenzhydrol (**64**) was prepared by reaction of benzhydrol with Lawesson's reagent (LR) in toluene at reflux for 30 min.[177]

The thioether **65** was obtained in a 92% yield upon reaction of **64** with K_2CO_3 in acetone followed by addition of the bromide **53**. Cleavage of the benzhydryl thioether (**65**) required a longer reaction time than benzhydryl ester cleavage in order for complete reaction at room temperature. Benzhydryl ester cleavage in **54** to give (S)-**35** (Scheme 21) required only 30 min and gave a yield of 88%. TFA cleavage of **65** required 18 hours and gave a yield of 31% of (S)-**35**.

Scheme 28

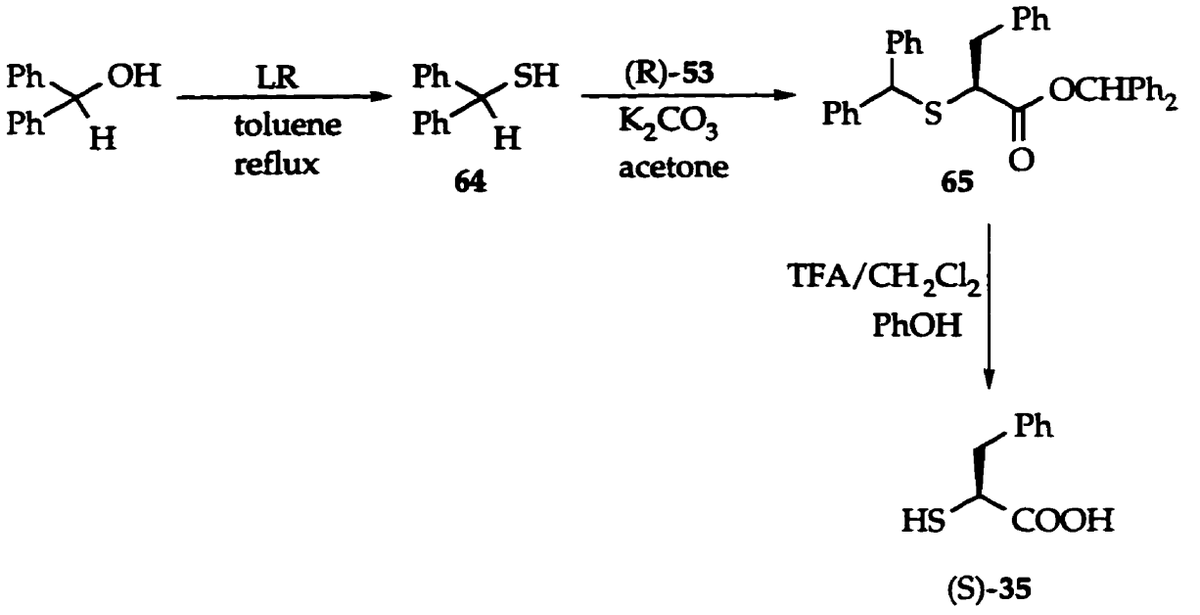

The optical purity of (S)-**35** was estimated by coupling the (S)-**35** methyl ester derivative (**69**) with (S)-(+)-Mosher's chloride [(S)-(+)-α-methoxy-(trifluoromethyl)phenylacetyl chloride,[178] **100**, to give the (S,S)- thioester **66** (Scheme 29).

The mercapto compound **69** was prepared using the same conditions used for the preparation of (S)-**35**, except for the use of diazomethane in place of diphenyldiazomethane. The methyl ester remained intact during the benzhydryl thioether cleavage step, to give **69**.

Scheme 29

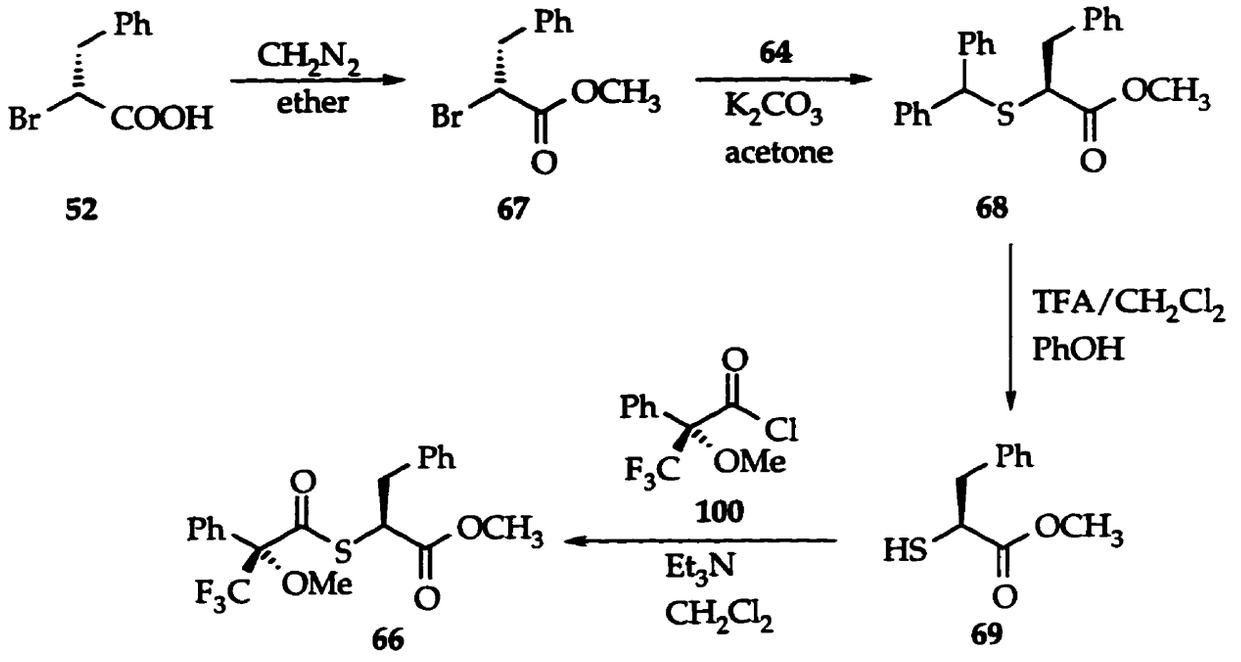

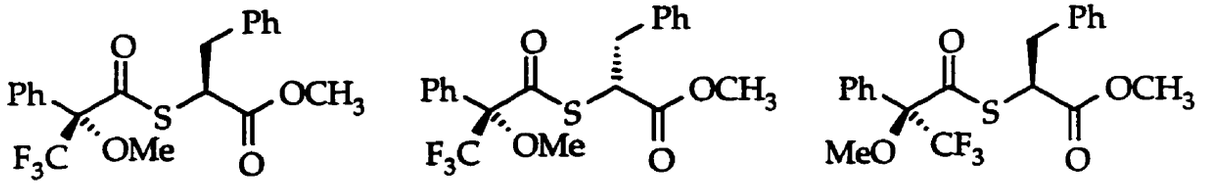

66

(S,S)

70a

(S,R)

71

(R,S)

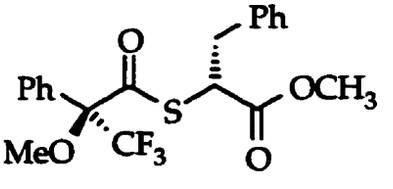

70b

(R,R)

The formation of the enantiomeric impurity ((R)-configuration) during synthesis of **69**, would result in the presence of **70a** as a contaminant in the sample of **66**. Thioester **70a** which is a diastereomer of **66** can be distinguished from **66** using NMR. ^{1}H-NMR analysis revealed the ratio of 0.947:0.053 for diastereomers **66:70a**. This value was determined by comparison of integration differences between proton peaks of the two diastereomers. From this observed ratio, the sample of **69** was determined to contain 94.7% of the (S)-enantiomer and 5.3% of the (R)-enantiomer. The Mosher's acid (Aldrich) that was used to synthesize **100** was reported by Aldrich to have an optical purity ranging 99.0% to 99.3%. The presence of 0.35% to 0.5% (S)-Mosher's chloride in the reagent **100** would cause a small underestimation of the optical purity for **69**.

The thiol was also reacted with racemic (R,S)-Mosher's chloride to generate a 1:1 mixture of the R,S and S,S isomers **71** and **66**, containing a small amount of a 1:1 mixture of the S,R and R,R isomers **70a** and **70b** for the purpose of signal identification in the NMR analysis.

It can be concluded from these experiments that 94.7% of the free-thiol **35** was that of the (S)-configuration, which corresponds to an **ee** of 89.4% (Scheme 28). The initial precursor, (R)-phenylalanine (Aldrich), was reported by Aldrich to have an **ee** of 97.6%.

2.1.1 The Kinetic Analysis of the Hydrolysis of Thioester (S)-50 by Carboxypeptidase A

Since the hydrolysis of the thiolester (S)-**50** was an essential component of the present inhibition strategy, it was appropriate to examine the function of (S)-**50** as a substrate before exploring the inhibitory potency of the thioester. In preparation for studies of the kinetics of thioester hydrolysis, the spectroscopic characteristics of (S)-**50** and the expected hydrolysis products were determined. In the initial analysis of the ultraviolet spectrum of **50**, in 25 mM Tris buffer containing 10% ethanol (v/v) to solubilize the thioester, two absorbance bands with maxima at 241.2 nm and 272.2 nm were observed (Figure 23). The effects of treatment of (S)-**50** with CPA on these spectroscopic features were then studied. Bovine carboxypeptidase A_α was employed with 10% ethanol (v/v) as cosolvent, 25 mM Tris (Tris (hydroxymethyl) aminomethane-HCl) at pH 7.5 and in 0.5 M NaCl maintained at 25°C. Figure 24 (Curve A) shows the spectrum of (S)-**50** (87 μM) in the presence of CPA (1.54 μM) immediately after mixing. After incubation of this solution for 24 hours, UV analysis yielded the spectrum shown in Figure 24 (Curve B). The decrease in absorbance at 273 nm ($\Delta\varepsilon_{273}$ of 6930 $M^{-1}cm^{-1}$) was consistent with the hydrolysis of the thioester as suggested by comparison of the extinction coefficient of the thioester with those of the expected products, benzoate (476 $M^{-1}cm^{-1}$) and the thiol **35** (1405 $M^{-1}cm^{-1}$).

Figure 23: UV absorption spectrum of (S)-**50** (87 μM) in 25 mM Tris, 0.5 M NaCl, pH 7.5, containing 10% EtOH (v/v), at 25°C.

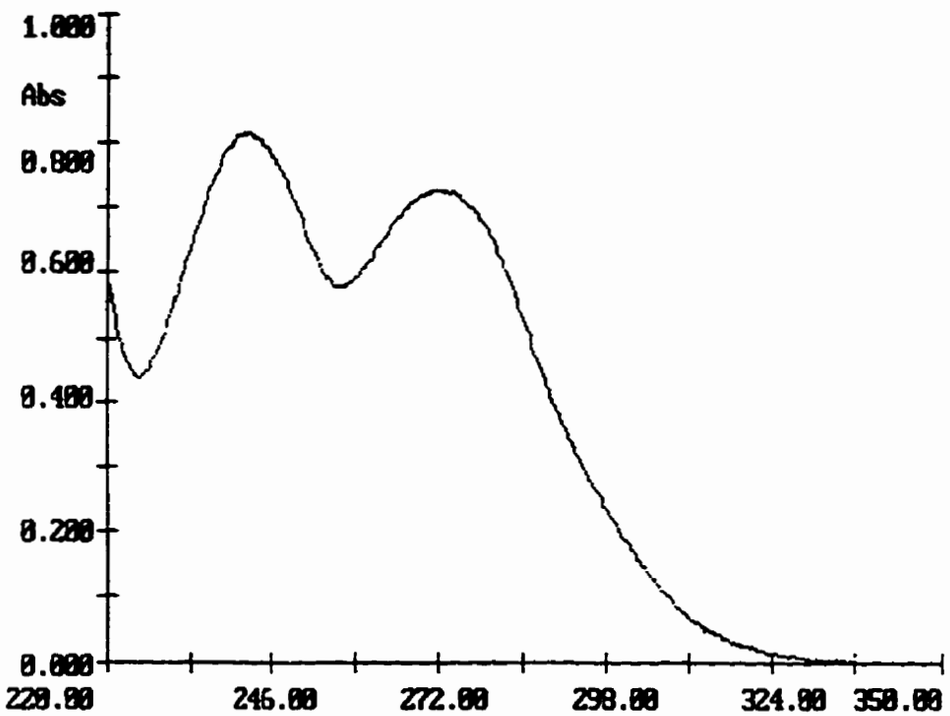

Figure 24: UV absorption spectrum of (S)-50 (87 µM) and CPA (450 nM) immediately after mixing (Curve A); after 30 hours incubation (Curve B). Analysis in 25 mM Tris, 0.5 M NaCl, pH 7.5, containing 10% EtOH (v/v), at 25°C.

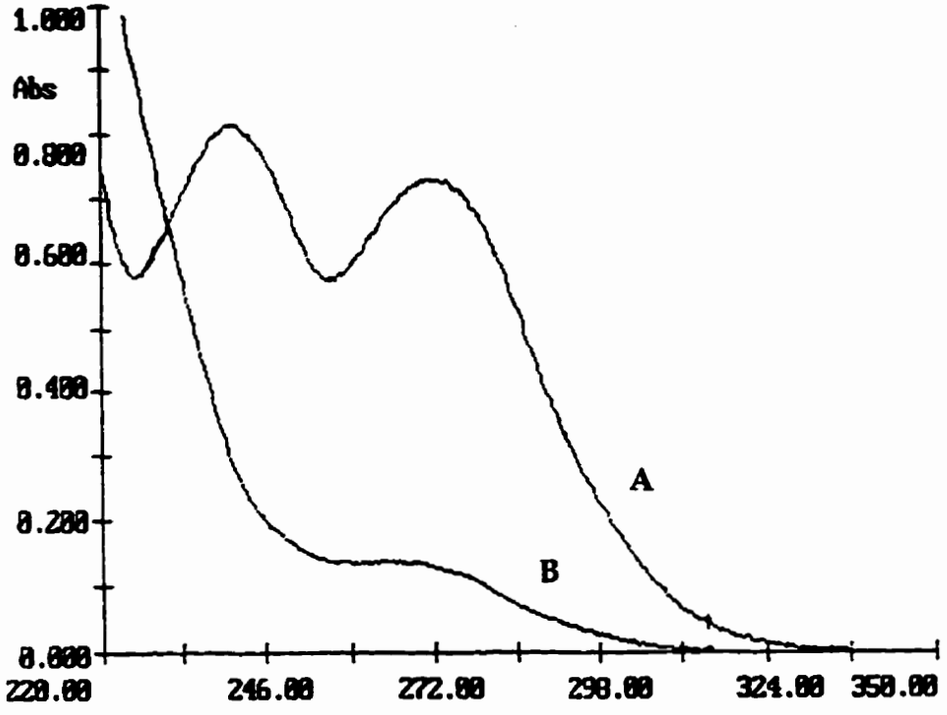

Further confirmation that the process being monitored at 273 nm was indeed the hydrolysis of the thioester was sought by isolation and identification of the products. To this end, the products of the CPA catalyzed reaction were extracted from solution after acidification and were characterized by TLC comparison with authentic samples and by high resolution mass spectrometric analysis (HRMS). It was found that the products obtained were benzoate and the disulfide **73** rather than the thiol **35**. The absence of the thiol was suspected since treatment of the CPA treated solution of (S)-**50** gave a negative test for thiols with DTNB (5,5'-dithiobis(2-nitrobenzoic acid))[179] which normally releases TNB, observable at 412 nm, upon reaction with a free thiol (Figure 25).

Figure 25

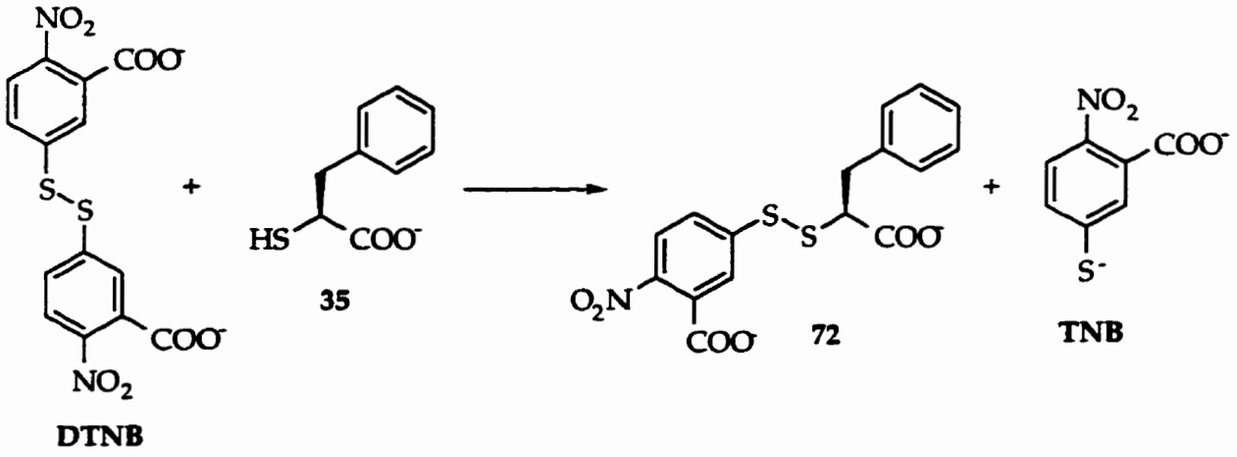

The overall process observed was then that shown in Scheme 30. This raised questions concerning the validity of the $\Delta\varepsilon_{273}$ value to be used to monitor thioester hydrolysis since differences in thiol/disulfide ratio in the product at different times during analysis might affect the observed absorbance. It was found, however, that the difference in absorbance at 273 nm for the thiol (ε_{273}=1405 $M^{-1}cm^{-1}$) and the

authentic disulfide (ε_{273}=3030 $M^{-1}cm^{-1}$) was sufficiently small that the effect of the oxidation process on the measured absorbance would be negligible.

Scheme 30

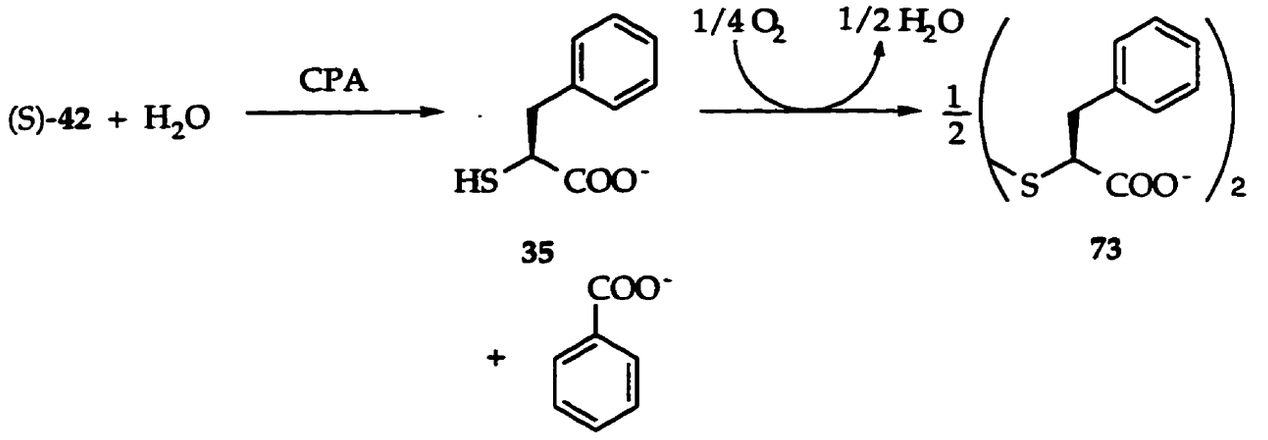

When the CPA catalyzed hydrolysis of (S)-**50** was first monitored at 273 nm, it became clear that the hydrolysis process was worthy of more detailed examination than originally planned. Particularly interesting was the observation that the progress curves for this catalytic process were clearly biphasic, the first part consisting of a burst phase lasting on the order of 20 to 55 s at +25°C, and a steady state phase. An example of such a progress curve is shown in Figure 26. Although this burst phenomenon was qualitatively similar to the bursts observed in pre-steady state analyses of the CPA catalyzed hydrolysis of various peptides and depsipeptides reported by Vallee and coworkers,[56,57,58,59,180] the pre-steady state burst for the thioester was observed at +25°C over a period of tens of seconds whereas that for the peptides and depsipeptides reported earlier the burst was observed only at subzero temperatures (-20°C) and on a much shorter time scale (400 milliseconds).

Figure 26: Progress curve of (S)-**50** (14.5 μM) hydrolysis by CPA (1.5 μM), with v_o of 36.3 nM/s for the burst and v_s of 6.3 nM/s for steady state, at 273 nm, 25°C, pH 7.5.

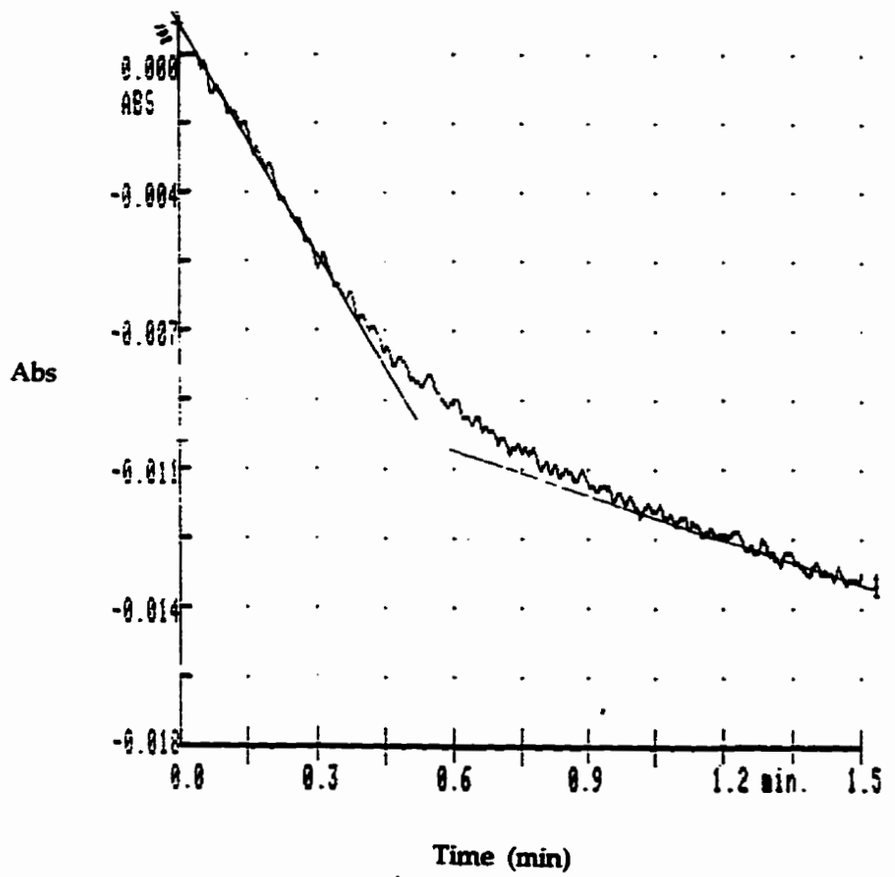

The fact that the burst phase involved a decrease in absorbance at 273 nm, strongly suggested that the pre-steady state burst is associated with hydrolysis, or at least cleavage, of the thioester linkage. Vallee and coworkers[56,57,58,59,180] have deduced that the hydrolysis of both peptides and depsipeptides can be described in terms of the following kinetic mechanism (Scheme 31 and Scheme 32):

Scheme 31

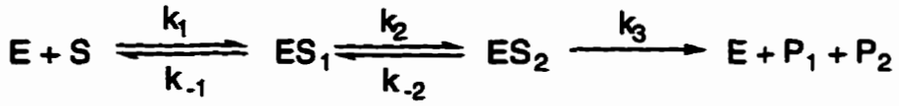

Scheme 32

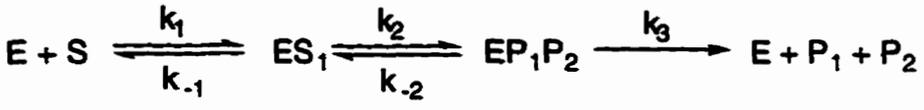

In each case, two intermediates are involved, and the pre-steady state burst is a measure of the formation of ES_2 with ES_1 formation occurring in a very rapid process which is not measurable on the time scale accessible by the experimental methods employed. In the case of peptide substrates, both ES_1 and ES_2 are believed to be complexes of the enzyme with the substrate and it is proposed that the hydrolysis occurs in the slow third step of the process. For depsipeptides, spectroscopic evidence suggests that the hydrolysis occurs in the burst phase in which ES_1 is converted to ES_2 so that ES_2 is better described as EP_1P_2 (Scheme 32). In this mechanism the hydrolytic step is proposed to be reversible and the slow step in the catalytic cycle is the release of products from the ES_2 (EP_1P_2) complex.

Thus, the thioester (S)-**50** appears to function as an ester-like substrate for CPA with hydrolysis occurring in the pre-steady state burst phase of the reaction. The fact that the burst observed for (S)-**50** was on a substantially slower time scale than those observed with the peptide and depsipeptides studies prompted us to probe further the nature of the processes involved in the pre-steady state hydrolysis of (S)-**50**. In particular, we speculated that for the hydrolysis of (S)-**50** the slow rate determining step likely involved release of the thiol which is known to have a strong affinity for the active site. As a result, we expected that the burst, associated with the hydrolytic

step, would be accompanied by a lag in release of the thiol. Furthermore, we were not certain whether the burst was associated with release of the carboxylic acid product or whether the acid was released subsequent to the release of the thiol.

As a result, experiments were designed to probe the order of release of products. In the present case, we reasoned that, if the benzoic acid product were released in a fast step after the hydrolytic step, then proton release should be observable on the time scale of the burst. In addition, the release of the thiol product 35 which was reasoned to occur during the slow rate-determining step, was studied through the use of DTNB. Details of these studies are presented below.

2.1.2 Kinetic Analysis of the Burst Phase of Thioester Hydrolysis

In principle, determination of the initial rates associated with the burst phase at various initial substrate concentrations could yield kinetic data suitable for fitting to a Michaelis-Menten model. Indeed when this was carried out the data shown graphically in Figure 27 were obtained and the kinetic parameters were found to be K_m=129±13 μM and k_{cat}=0.183±0.009 s^{-1}. It was recognized, however, that such an analysis was based on an assumption, the validity of which is difficult to test experimentally. The determination of $\Delta\varepsilon_{273}$ for the hydrolysis process is based on comparison of the free substrate and free products, which is perfectly valid for the steady state situation. In the pre-steady state analysis, however, one must consider that absorption at 273 nm will arise, in part, from enzyme-bound products as well as from products free in solution. Although it is reasonable to assume that the difference in extinction coefficient for the free and enzyme-bound products is not large, there was no direct method available to us to determine precisely how valid

this assumption was. Some verification of the validity of this assumption was obtained by analysis of the magnitude of the burst which is described in Section 2.1.4.

Figure 27: Pre-steady state relationship between (S)-50 concentration and initial rate in 25 mM Tris, 0.5 M NaCl, pH 7.5, containing 10% EtOH (v/v), at 25°C.

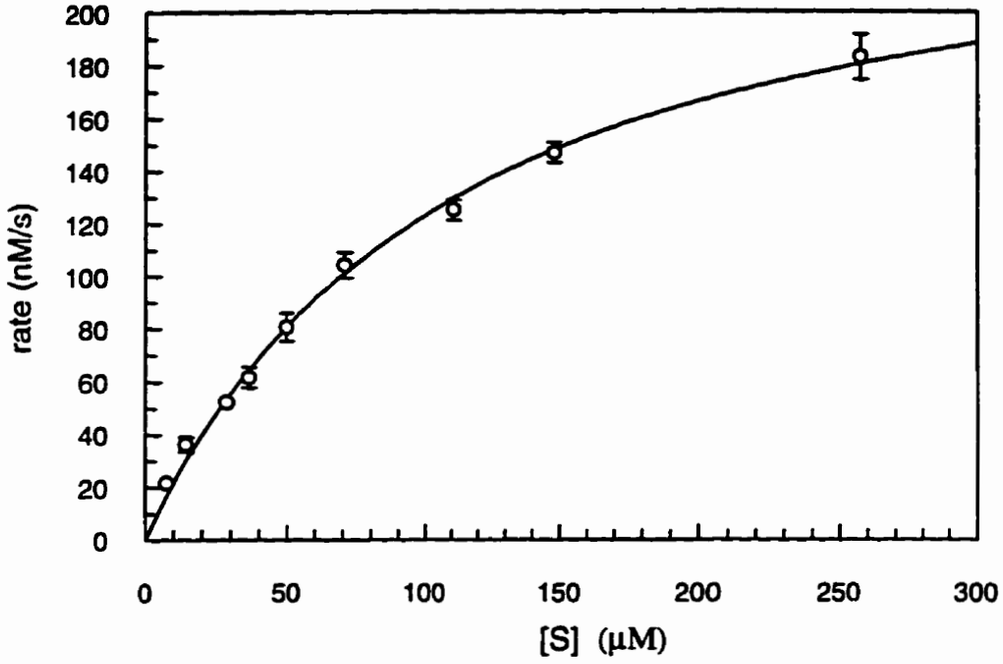

Each data point is the average of four or more separate determinations, shown with standard error bars. Error bars smaller than the symbols are not shown. For the mathematical determination of kinetic parameters, all determinations and not the means were included in the calculations.

2.1.3 Kinetic Analysis of the Steady State Phase of Thioester Hydrolysis

Measurement of the slopes of the linear portions of the steady state phases of progress curves for the CPA-catalyzed hydrolysis of (S)-50 yielded the kinetic data

displayed in Figure 28 which, when fitted to the Michaelis-Menten equation yielded K_m=16.8±1.8 μM and k_{cat}=(8.52±0.27)x10^{-3} s^{-1}.

Figure 28: Relationship between (S)-50 concentration and steady state rates in 25 mM Tris, 0.5 M NaCl, pH 7.5, 10% EtOH (v/v), at 25°C.

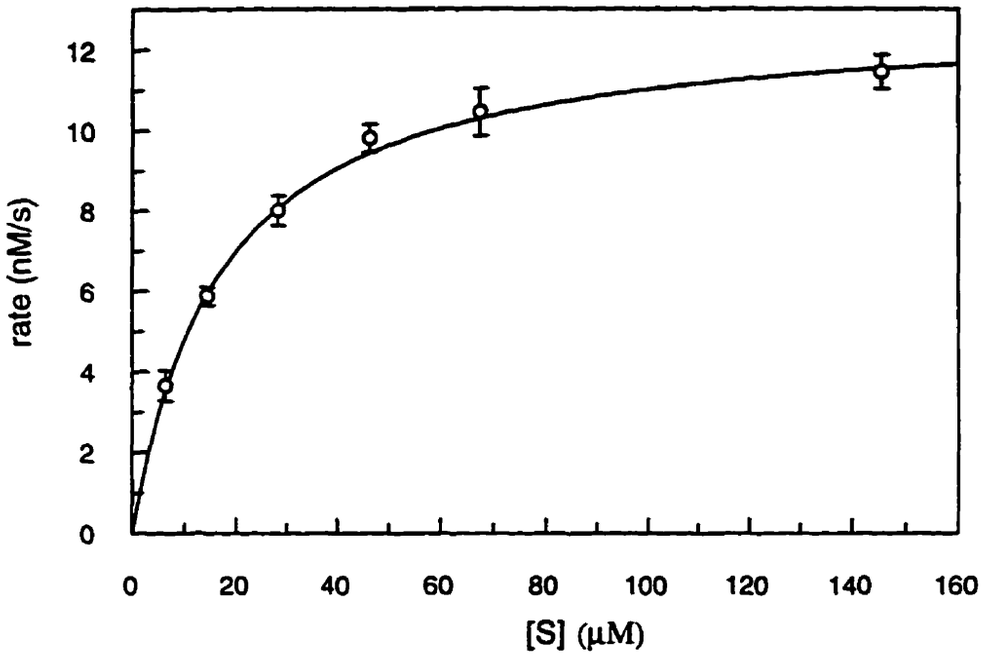

Each data point is the average of four or more separate determinations, shown with standard error bars. Error bars smaller than the symbols are not shown. For the mathematical determination of kinetic parameters, all determinations and not the means were included in the calculations.

The evaluation of the experimentally determined pre-steady state and steady state parameters led to the calculation of the kinetic constants k_2, k_{-2} and k_3 (shown in Scheme 32). The K_m and k_{cat} for this kinetic mechanism are shown below:

$$K_m = K_s (k_{-2} + k_3) / (k_2 + k_{-2} + k_3) \qquad (2.0)$$

$$k_{cat} = k_2 k_3 / (k_2 + k_{-2} + k_3) \qquad (2.1)$$

For the pre-steady state analysis of (S)-**50**, the observed k_{cat} is k_2 and the observed K_m is K_s. Therefore, using the values determined above for K_s and k_2 (129 μM and 0.183 s^{-1} respectively), k_{-2} and k_3 were then determined from the steady state data by fitting the data to the Michaelis-Menten equation:

$$v = \frac{E_o[S]\left(\frac{k_2 k_3}{k_2 + k_{-2} + k_3}\right)}{[S] + K_s \frac{k_{-2} + k_3}{k_2 + k_{-2} + k_3}} \qquad (2.2)$$

The rate constants k_{-2} and k_3 were calculated to be $(1.77\pm0.30)\times10^{-2}$ s^{-1} and $(9.80\pm0.46)\times10^{-3}$ s^{-1} respectively. The kinetic parameters observed for (S)-**50** hydrolysis are compared with those observed for dansyl-depsipeptides[180] in Table 1. The K_m and K_s for (S)-**50** hydrolysis are comparable to those of the depsipeptides, whereas the rate constants, k_{cat}, k_2, k_{-2} and k_3 are considerably lower for the thioester. It should be noted, however, that differences exist in the experimental conditions used to determine these parameters so that the comparison should not be considered to be precise. The pre-steady state analysis for the dansyl depsipeptides required stop-flow techniques and low temperatures (-20°C) in order to be observe the burst, which was observed within 400 msec. In comparison, the burst phase of the hydrolysis of the thioester (S)-**50** lasted much longer (20-55 s), and did not require any special techniques or low temperature analysis to be observable. The lower rate constants observed for thioester hydrolysis were thought to arise primarily from the molecular and geometric differences that exist between these substrates, namely a scissile thioester linkage for (S)-**50** as compared to a scissile ester linkage for the depsipeptides, although it was recognized that the differences in the acyl groups associated with the scissile bonds might contribute to the kinetic differences. The

dansyl-depsipeptides possess N-dansyl di or tri-peptide acyl groups which may be better representations of the natural substrate structure as compared to the benzoyl acyl group of the thioester (S)-**50**. A more detailed discussion of the possible mechanism of thioester hydrolysis and the effects of the benzoyl acyl group will be presented later in Section 2.1.7.

Table 1: Observed kinetic parameters for the hydrolysis of (S)-**50** and dansyl-depsipeptides.[180]

Substrate	K_m (μM)	K_s (μM)	k_{cat} (s^{-1})	k_2 (s^{-1})	k_{-2} (s^{-1})	k_3 (s^{-1})
(S)-**50** (a)	16.8	129	8.52×10^{-3}	0.183	0.0177	9.80×10^{-3}
Dns-$(Ala)_2$-OPhe (b)	1.6	129	0.062	53.3	0.50	0.062
Dns-Gly-Ala-OPhe (c)	5.6	75	0.14	15.6	0.66	0.15
Dns-$(Gly)_3$-OPhe (c)	22.3	164	3.13	32.6	1.41	3.61

(a) - observed at +25°C in 25 mM Tris, 0.5 M NaCl, pH 7.5, containing 10% EtOH (v/v)
(b) - observed at -10°C in 10 mM HEPES, 4.5 M NaCl, pH 7.5
(c) - observed at -20°C in 10 mM HEPES, 4.5 M NaCl, pH 7.5

2.1.4 Analysis of the Magnitude of the Burst

Back extrapolation of the linear steady state portion of the progress curve to zero time yields the magnitude of the burst represented by the so called π value defined as in Figure 29.[181] One of the best known examples of burst kinetics is that observed with the α-chymotrypsin catalyzed hydrolysis of esters.[181] In such cases, the pre-steady state phase is associated with acyl-enzyme formation and the rate-limiting process is deacylation as shown in Scheme 33.

Figure 29

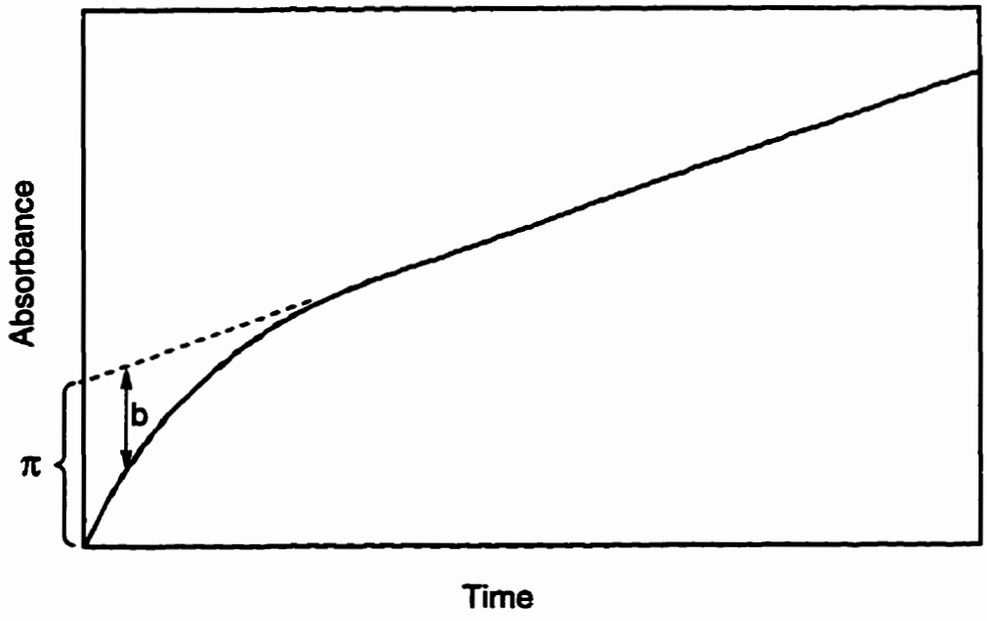

Scheme 33

$$E + S \underset{k_{-1}}{\overset{k_1}{\rightleftharpoons}} ES \xrightarrow{k_2} E\text{-acyl} \xrightarrow{k_3} E + P_2$$

$$ES \xrightarrow{k_2} P_1$$

For this example, Bender[181] has shown that the magnitude of the burst is related to the kinetic parameters and the enzyme concentration as shown below.

$$\pi = E_o \left(\frac{\frac{k_2}{k_2 + k_3}}{1 + K_m / S_o} \right)^2$$

For the CPA catalyzed hydrolysis of esters, the minimal kinetic mechanism, as deduced by Vallee and coworkers, is that shown in Scheme 32. In the case of the thioester (S)-**50**, the fact that the burst is associated with a decrease in absorbance at

273 nm is consistent with the assumption that thioester hydrolysis occurs in the burst phase which is the second step in Scheme 32. Unlike the situation with the chymotrypsin mechanism in which the burst is measured by observation of product release, the burst in the CPA mechanism, as defined by Scheme 32, involves formation of EP_1P_2 as well as free P_1 and P_2. Since the relationship of the experimentally determined π to the kinetic parameters associated with the mechanism shown in Scheme 32 had not been disclosed in the literature previously, a new mathematical derivation was necessary. This derivation, which is described in detail in Appendix A, results in the relationship expressed in equation 2.3.

$$\pi = E_o\left(\frac{k_2}{k_2 + k_{-2} + k_3}\right)\left(\frac{1}{1 + K_m/S_o}\right) \qquad (2.3)$$

Alternatively this expression can be reformulated, in terms of K_m and K_s only, by making use of the definition of K_m:

$$K_m = K_s\,(k_{-2} + k_3) \,/\, (k_2 + k_{-2} + k_3)$$

Thus,

$$\pi = E_o\left(\frac{1 - K_m/K_s}{1 + K_m/S_o}\right) \qquad (2.4)$$

Since K_m and K_s have been determined experimentally as described above, it is possible to calculate π based on the known value of E_o and S_o for a given experiment and also to measure π graphically from the progress curve. Thus, for an experiment in which S_o=76 μM and E_o=1.5 μM, the expected value of π is 1.09±0.04 μM. Experimental determination of the π value for three replicate experiments yielded a mean value of π=1.17±0.12 μM.

2.1.5 The Analysis of Thiol Release using DTNB

DTNB, which is used ordinarily for the quantitative measurement of mercaptans such as cysteine,[179] was used to react with **35** as the free thiol product was generated from thioester hydrolysis (Figure 25). Preliminary experiments involved the presence of DTNB (0.1 mM) in solution with CPA (1.5 μM) and (S)-**50** (9.6 μM to 178 μM), and any generation of TNB (ε_{412}=14160 $M^{-1}cm^{-1}$) from the reaction between DTNB and **35** was monitored at 412 nm. These experiments revealed that **35** was produced and trapped by DTNB, producing TNB and the disulfide **72** (Figure 25).

As shown in Figure 30, the progress curve has a lag-time prior to achievement of a steady state rate.

Figure 30: Progress curve of TNB generation using 9.62 μM (S)-**50**, 1.5 μM CPA, 0.1 mM DTNB, at 25°C, monitored at 412 nm.

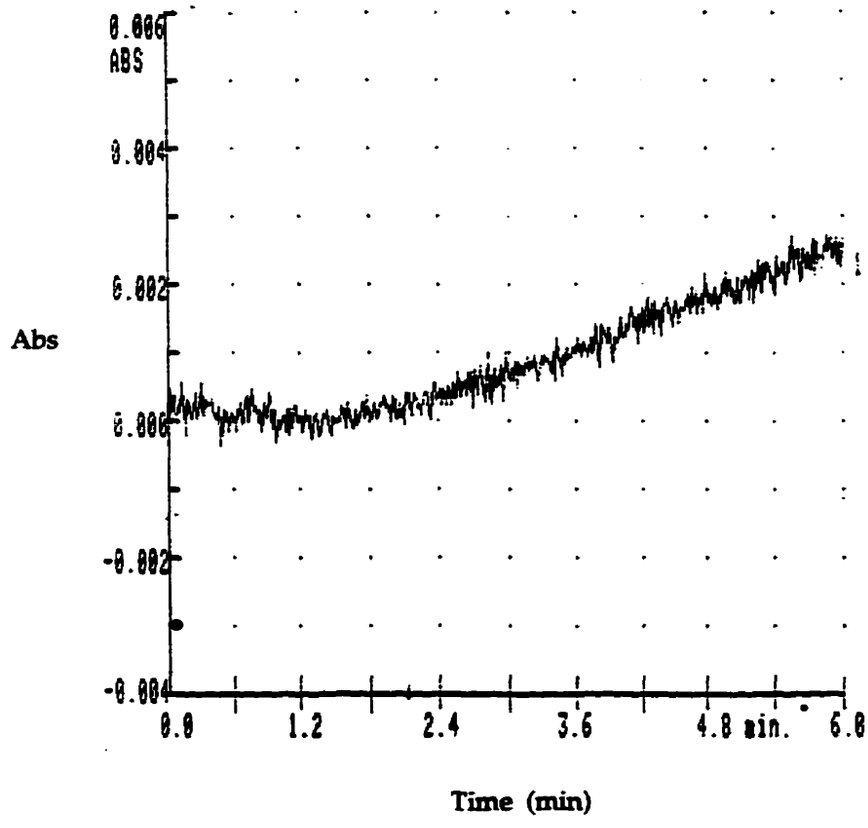

This lag-time varied from 15 to 75 s from time zero to the start of steady state, increasing in time with decreasing (S)-**50** concentration. These experiments confirmed our initial assumption that the free thiol product portion is released during the time-dependent slow step of thioester turnover (Scheme 32) and not in the pre-steady state burst phase. With increasing thioester concentration, the length in time of the burst decreased and the lag time decreased.

Another observation made was that the rate of TNB generation in the steady state phase was lower than the rate of thioester hydrolysis predicted from the kinetic parameters determined in the previous (S)-**50** hydrolysis studies monitored at 273 nm in the absence of DTNB. This difference was thought to be due to either or both of the following: 1) the inhibition of CPA activity by DTNB, slowing the rate of thioester hydrolysis and therefore slowing the generation of **35**; 2) a competition between trapping of **35** with DTNB and reaction of **35** with dissolved O_2 to yield the disulfide **73** (Scheme 34).

Scheme 34

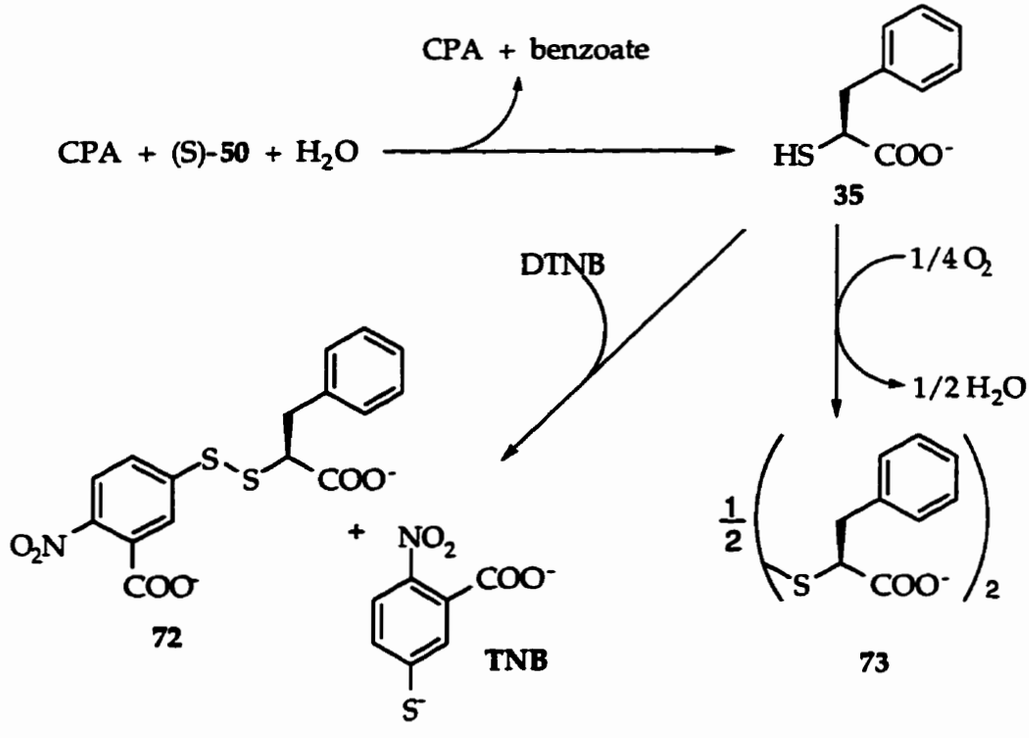

As a result, experiments were conducted to determine the effects of different DTNB concentrations on TNB generation at a constant concentration of CPA and (S)-50. The DTNB concentration was varied from 0.62 mM to 9.9 mM, with (S)-50 and CPA concentrations held constant at 168 μM and 3.2 μM respectively. As shown in Figure 31, the relationship between the steady state rate of TNB production and the DTNB concentration is parabolic, with a rate maximum at 4.9 mM DTNB. At lower DTNB concentrations, the lower rate of TNB production probably results from an insufficient concentration of DTNB in solution to trap the newly generated thiol product **35**. At these DTNB concentrations, oxidation of **35** by dissolved O_2 to form **73** becomes a substantial route of loss of **35**. At DTNB concentrations above 5.0 mM, the rate of TNB production decreases probably due to inhibition of CPA activity by DTNB.

Figure 31: Relationship between the rate of TNB generation and DTNB concentration at constant (S)-50 and CPA concentration of 168 μM and 3.12 μM respectively.

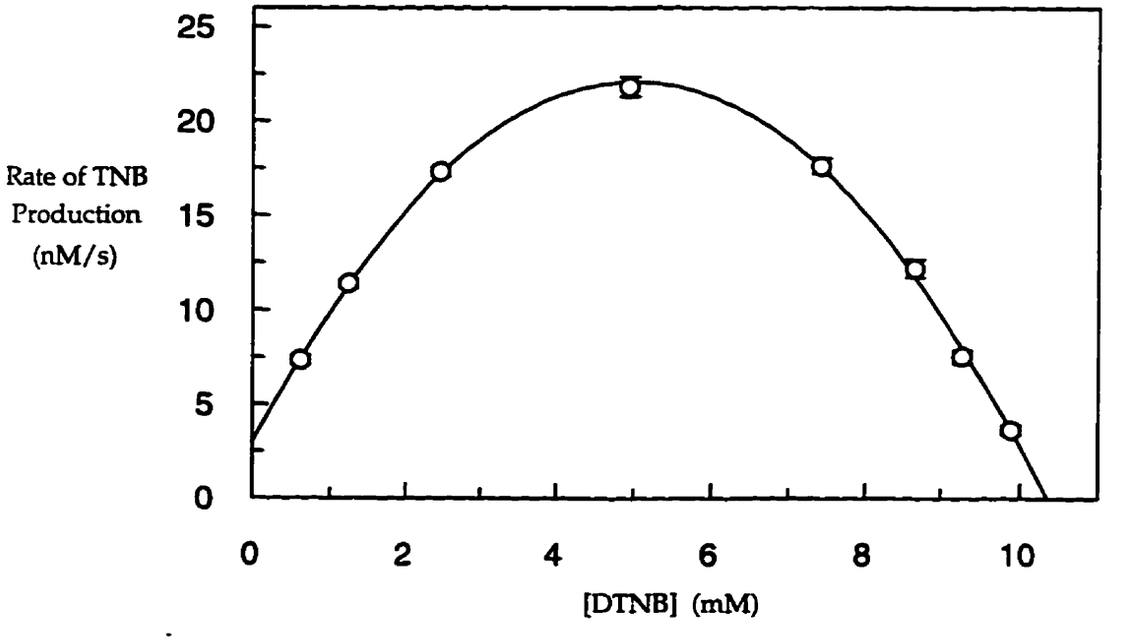

Each data point is the average of three separate determinations, shown with standard error bars. Error bars smaller than the symbols are not shown. For the graphical presentation, the data points were fitted to an order 2 polynomial equation.

In a separate experiment, DTNB was found to be a competitive inhibitor of CPA peptidase activity as well, with a K_i of 109±12 μM (Figure 32). The peptidase activity of CPA was monitored at 265 nm using the peptide substrate hippuryl-L-phenylalanine[182] in the presence of DTNB.

Figure 32: Inhibition of CPA-catalyzed hydrolysis of HP in the presence of DTNB. $[E]_o$=121 nM.

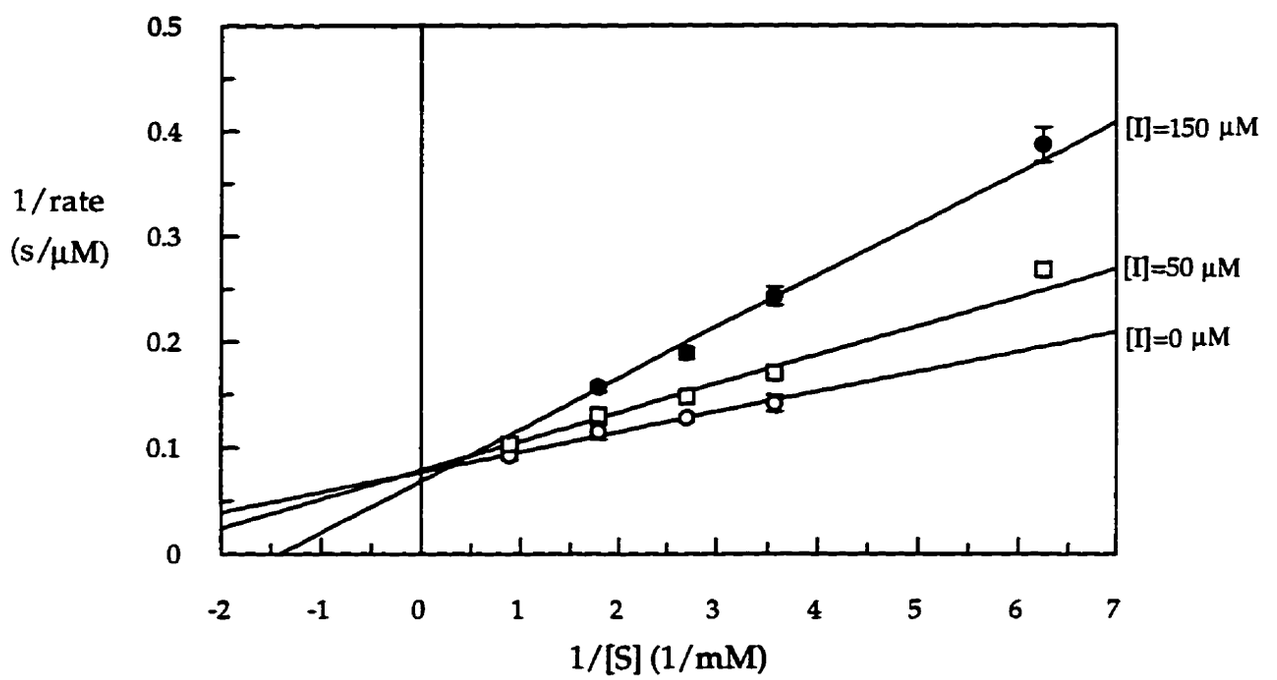

Each data point is the average of three or more separate determinations, shown with standard error bars. Error bars smaller than the symbols are not shown.

2.1.6 Analysis of Proton Release During CPA-Catalyzed Hydrolysis of (S)-50

Once the hydrolysis process had been shown to be accompanied by a lag in thiol release concomitant with the burst in thioester cleavage, attention turned to another question concerning the hydrolysis process which was of some interest in regard to the proposed inhibition of CPA by (S)-**50**; namely, the order of product release. Vallee and coworkers[56,57,58,59,180] had presented evidence, in their study of the pre-steady state kinetics of CPA catalyzed hydrolysis of depsipeptides, that the rapid hydrolytic step was a reversible process with k_{-2} in many cases being larger than k_3 (Scheme 32). This kinetic mechanism was contrasted with that observed with chymotrypsin in which product release occurs in the rapid burst phase creating the acyl-enzyme:

Scheme 35

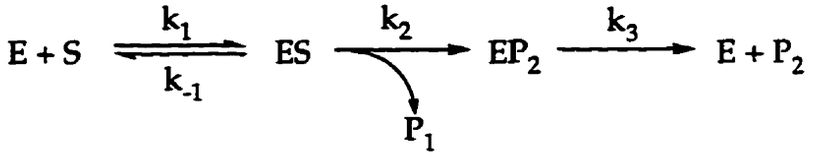

It has been pointed out that the rapid release of product during the burst phase of the chymotrypsin mechanism makes the burst step essentially irreversible since "k_{-2}" is dependent on $[P_1]$ which is effectively zero in the initial rate limit. In the present context of thioester hydrolysis, we reasoned that if release of the benzoic acid product occurred in the rapid phase of the hydrolytic process, proton release should occur during the burst phase of the reaction. As a result, experiments designed to

detect proton release during the course of hydrolysis of (S)-**50** were carried out. In particular, experiments in which a pH indicator serves as the buffer were employed.

Bromothymol blue (BTB) is a pH-indicator which indicates changes in the pH range of 6.2-7.6,[183] and possesses a pK_a of 7.2. In its deprotonated form, NaBTB (**74**), bromothymol blue gives a blue colour with a λ_{max} of 615 nm (Figure 33). When protonated, **74** gives **75**, which is a yellow coloured species with a λ_{max} at 420 nm. By using BTB and NaBTB as a buffering system in place of Tris, protons generated or consumed during the burst or steady state hydrolysis of (S)-**50** can be quantitatively measured at 420 nm and 615 nm. Preliminary experiments showed that the $\Delta\varepsilon_{615}$ value was 38600 $M^{-1}cm^{-1}$ for the conversion of NaBTB to BTB at 615 nm. Control experiments were conducted to verify the expected spectral change in the BTB/NaBTB system upon addition of a proton source (benzoic acid).

Figure 33

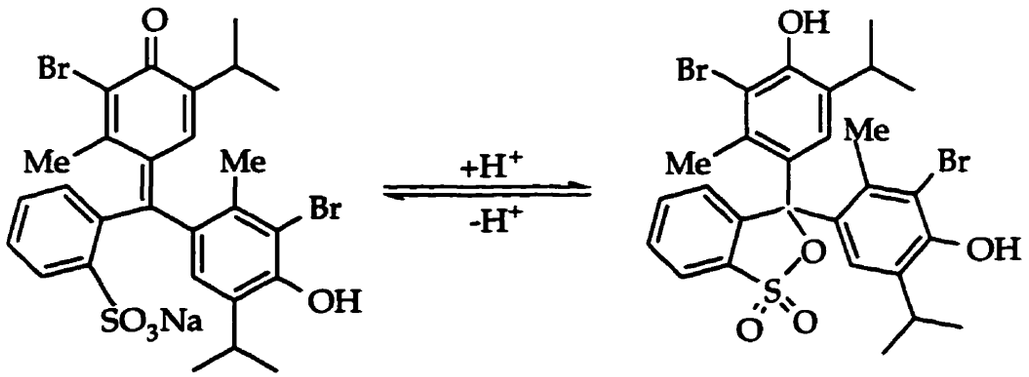

74, NaBTB
λ_{max}=615 nm

75, BTB
λ_{max}=420 nm

For the study of proton release, during hydrolysis, a solution of 0.181 mM BTB, 0.55 M NaCl and (S)-**50** predissolved in ethanol was titrated to pH 7.5 with NaOH. The solution which now contains BTB and NaBTB, is a blue-green colour. CPA (13.5 μM in 0.55 M NaCl) was added to aliquots of the BTB/NaBTB solution to give the

assay mixture with CPA at 1.35 μM, [BTB+NaBTB] at 145 μM, and (S)-**50** ranging from 10 μM to 26 μM in 10% EtOH (v/v). The assays were monitored at 615 nm where the initial absorbance was measured to be 1.95.

Preliminary results resembled the progress curves observed for (S)-**50** hydrolysis at 273 nm in Tris buffer. There was an initial burst followed by a slower steady state rate (Figure 34). These results indicate the release of H^+ during the fast step of the hydrolysis mechanism where the thioester bond is hydrolyzed.

During these assays, the burst and steady state rates were observed and measured within an absorbance difference of 0.174, which is a difference of 4.5 μM in BTB and NaBTB. If the reported pK_a of bromothymol blue (7.2) is assumed to be approximately valid in this case, the pH can be calculated to drop minimally from 7.50 to 7.44 during the course of the progress curve.

Controls were conducted in which CPA was added to a BTB/NaBTB solution at pH 7.5 in the absence of (S)-**50**. The progress curve revealed that there was no observable change in absorbance directly after addition that may cause the burst observed in the presence of (S)-**50**. These assays, with and without (S)-**50**, involved an initial strong absorbance of 1.95 at 615 nm because of the BTB concentration chosen for this assay. It was recognized that with strongly absorbing solutions deviations from the direct relationship between concentration and measured absorbance can arise. It was decided, however, that with the UV/visible spectrophotometer used in this study, the stray light value (0.02%) is sufficiently small to make the errors in concentration measurement arising from stray light effects, negligible. (See Appendix B for more details.)

Figure 34: The hydrolysis of (S)-**50** (26 μM) by CPA (1.35 μM) in BTB/NaBTB buffer (145 μM), monitored at λ=615 nm ($\Delta\varepsilon_{615}$ = 38600 $M^{-1}cm^{-1}$). Initial absorbance of 1.95 a.u. was suppressed.

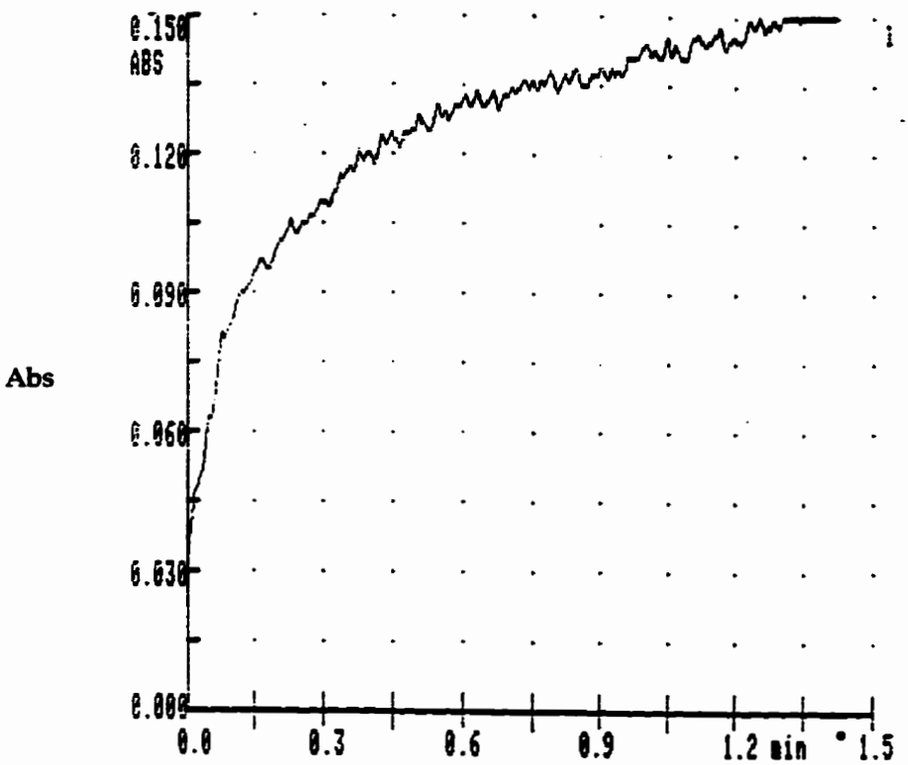

More detailed assays were conducted at (S)-**50** concentrations of 11 μM and 16 μM. Again, progress curves were found to show a similar result regarding the burst. The measured pre-steady state and steady state rates are listed in Table 2. Also listed in Table 2 are the observed burst and steady state rates of thioester hydrolysis at 273 nm in Tris buffer for the same (S)-**50** concentrations.

Thus, the rate of proton release in the burst phase of the catalytic process, in BTB/NaBTB buffered solution, is comparable to the rate of thioester cleavage as measured in Tris buffer; that is, one proton is released for each molecule of thioester hydrolyzed. In the steady state phase, however, the rate of proton release, in BTB/NaBTB buffer, is significantly lower than the hydrolysis rate in the Tris buffer. A plausible explanation for this observation is that k_3, which is related to product release, is significantly affected by the nature of the buffer (i.e. k_3 is smaller in BTB/NaBTB buffer as compared with Tris buffer) whereas k_2, which is related to the hydrolytic step is less sensitive to the nature of the buffer.

Table 2: Measured rate of release during burst and steady state hydrolysis of (S)-**50** in BTB/NABTB (145 μM) at 615 nm, as well as rates observed at 273 nm in Tris buffer, 25°C.

Portion of Progress Curve	[(S)-50]	[a]Rate of BTB formation monitored at 615 nm	[b]Rate of hydrolysis in Tris at 273 nm
Pre-steady state	11 μM	17±2 nM/s	21.6±2.3 nM/s
	16 μM	25±3 nM/s	30.3±3.1 nM/s
Steady state	11 μM	1.3±0.2 nM/s	5.1±0.4 nM/s
	16 μM	1.8±0.2 nM/s	6.2±0.4 nM/s

$\Delta\varepsilon_{615} = 38600\ M^{-1}cm^{-1}$, $E_o = 1.5\ \mu M$

[a] The above shown rates are the mean of two or more separate determinations, with ± standard error.

[b] The pre-steady state and steady state rates reported in Tris were not observed experimentally but calculated from presteady state parameters K_s=129±13 μM k_2=0.183±0.009 s^{-1}, and steady state parameters K_m=16.8±1.8 μM k_{cat}=(8.52±0.27)x10^{-3} s^{-1}.

This effect is also evident in the measured value of the magnitude of the burst in BTB/NaBTB buffer as compared to the value calculated on the basis of the kinetic parameters determined in Tris buffer. For the experiment with [(S)-50]=16 μM, the

$\pi_{observed}$=1.16±0.05 μM and $\pi_{calculated}$=0.65±0.07 μM, whereas for [(S)-**50**]=11 μM, the $\pi_{observed}$=1.41±0.15 μM and $\pi_{calculated}$=0.53±0.06 μM.

Since;

$$\pi = E_o\left(\frac{k_2}{k_2 + k_{-2} + k_3}\right)\left(\frac{1}{1 + K_m/S_o}\right) \qquad (2.3)$$

and $K_m = K_s\,(k_{-2} + k_3) \,/\, (k_2 + k_{-2} + k_3)$

therefore

$$\pi = E_o\left(\frac{k_2}{k_2 + k_{-2} + k_3}\right)\left(\frac{1}{1 + \dfrac{K_s\,(k_{-2} + k_3)}{S_o\,(k_2 + k_{-2} + k_3)}}\right)$$

$$= \frac{E_o\,k_2}{k_2 + k_{-2} + k_3 + (K_s/S_o)(k_{-2} + k_3)}$$

$$= \frac{E_o\,k_2}{k_2 + \left(1 + \dfrac{K_s}{S_o}\right)k_{-2} + \left(1 + \dfrac{K_s}{S_o}\right)k_3} \qquad (2.5)$$

Thus a decrease in k_3 is expected to result in an increase in π which is qualitatively consistent with the comparison of observed and calculated π values described above. It should be noted also that a decrease in k_{-2} might also contribute to an increase in π, but the available data does not give insight into the value of k_{-2} in BTB buffer. In any event, the release of a proton during the burst phase in the hydrolysis of (S)-**50** is firmly established.

One mechanistic interpretation of this observation is that the benzoic acid product is released in a rapid step following hydrolysis and then undergoes rapid

proton release. If this were so, however, the kinetic model which would describe the process is similar to that which fits the chymotrypsin catalyzed hydrolysis of esters. Namely, that shown below;

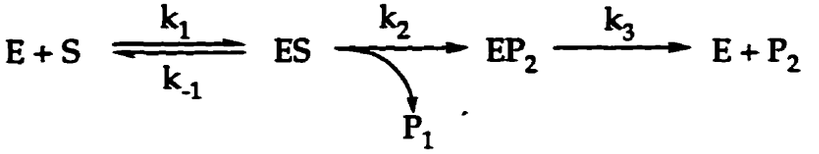

As indicated above, Vallee has pointed out that, for such a process, hydrolysis is effectively irreversible in the absence of added product since $[P_1]$ is essentially zero in the initial rate approximation. Thus for the steady state k_{cat} and K_m are defined by equation 2.6 and 2.7 respectively.

$$k_{cat} = (k_2\, k_3)/(k_2 + k_3) \qquad (2.6)$$

$$K_m = (K_s\, k_3)/(k_2 + k_3) \qquad (2.7)$$

For the present case, K_m=16.8±1.8 μM and k_{cat}=(8.52±0.27)x10^{-3} s^{-1}, and from the pre-steady state analysis K_s=129±13 μM and k_2=0.183±0.009 s^{-1}. From equation 2.6,

$$k_3 = (k_2\, k_{cat})/(k_2 - k_{cat}) = (8.96\pm0.70)\times10^{-3}\ s^{-1}$$

From equation 2.7 and this calculated value of k_3 it is possible to calculate the expected K_m as 6.02±0.82 μM. The poor agreement of this value with the observed K_m of 16.8±1.8 μM suggests that the data do not agree with a kinetic model involving rapid release of benzoate in the burst phase.

The alternative kinetic mechanism, as proposed by Vallee[180] (Scheme 32) is in better agreement with the observed kinetic parameters.

Scheme 32

$$E + S \underset{k_{-1}}{\overset{k_1}{\rightleftharpoons}} ES_1 \underset{k_{-2}}{\overset{k_2}{\rightleftharpoons}} EP_1P_2 \xrightarrow{k_3} E + P_1 + P_2$$

The K_m and k_{cat} expressions (equations 2.0 and 2.1) for Vallee's model were used to derive an expression for k_{-2} as a function K_s, k_2, k_{-2} and k_{cat}:

$$K_m = \frac{K_s\left[k_{-2} + \dfrac{k_{cat}\,(k_2 + k_{-2})}{k_2 - k_{cat}}\right]}{k_2 + k_{-2} + \dfrac{k_{cat}\,(k_2 + k_{-2})}{k_2 - k_{cat}}} = \frac{K_s\left(\dfrac{k_{-2}}{k_2 + k_{-2}} + \dfrac{k_{cat}}{k_2 - k_{cat}}\right)}{1 + \dfrac{k_{cat}}{k_2 - k_{cat}}} \qquad (2.8)$$

The expression contains the additional k_{-2} term, which is absent in the case of the expression derived for K_m using equations 2.6 and 2.7:

$$K_m = \frac{K_s\left[\dfrac{k_2\,k_{cat}}{k_2 - k_{cat}}\right]}{k_2 + \dfrac{k_2\,k_{cat}}{k_2 - k_{cat}}} = \frac{K_s\left(\dfrac{k_{cat}}{k_2 - k_{cat}}\right)}{1 + \dfrac{k_{cat}}{k_2 - k_{cat}}} \qquad (2.9)$$

The presence of that additional k_{-2} term may explain the higher K_m observed for the hydrolysis of (S)-**50**. This model proposed by Vallee should be further modified, however, for the present case in light of the observed release of a proton in the burst phase (Scheme 36).

Scheme 36

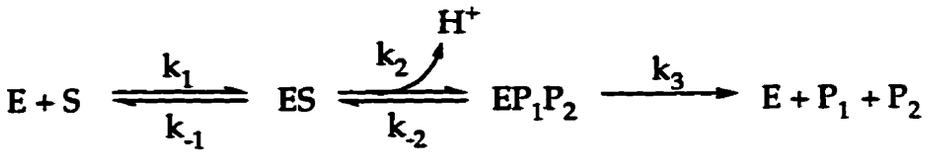

Thus, P_1 is now considered to be benzoate rather than benzoic acid and k_{-2} is actually a pH dependent pseudo first order rate constant better expressed as $k_{-2}=k_{-2}'[H^+]$. A molecular mechanism whereby proton release might be achieved in advance of benzoate release is suggested below in Section 2.1.7.

2.1.7 CPA Catalyzed Hydrolysis of O-Benzoyl Phenyllactate

The observation that the pre-steady state and steady state kinetic parameters for the CPA catalyzed hydrolysis of the thioester (S)-**50** differed very substantially from those observed for depsipeptides studied by Vallee and coworkers[180] raised questions about the structural features of (S)-**50** which were responsible for this behaviour (Table 1). In particular, it was of interest to determine whether the unusual kinetic behaviour was caused by the fact that (S)-**50** was a thioester or by the fact that the acyl group in (S)-**50** differed substantially from those in the depsipeptides studied by steady state and pre-steady state methods. As a result, a study of the hydrolysis of O-benzoyl phenyllactate **51** was undertaken. The hydrolysis of **51** was monitored by examination of the diminution in absorbance at 280 nm. As indicated in Table 3 below, the steady state kinetic parameters observed for **51** were found to be very similar to those observed for (S)-**50**.

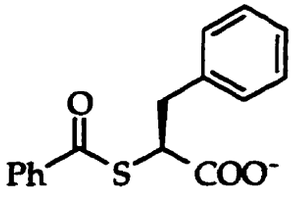

(S)-**50**

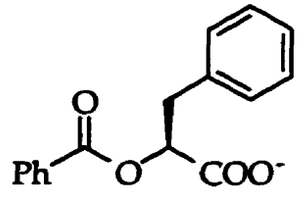

51

Table 3: Kinetic parameters for steady state hydrolysis of (S)-**50** and **51** in 25 mM Tris buffer, pH 7.5, containing 3.5% EtOH (v/v), at 25°C and for (S)-**50** hydrolysis in 25 mM Tris buffer, 0.5 M NaCl, pH 7.5, containing 10% EtOH (v/v), at 25°C.

Kinetic Parameters	**51** in 3.5% EtOH (v/v)	(S)-**50** in 3.5% EtOH (v/v)	(S)-**50** in 10% EtOH (v/v)
K_m	55±9 μM	61.8±7.0 μM	16.8±1.8 μM
k_{cat}	0.0226±0.0009 s^{-1}	0.0153±0.0006 s^{-1}	0.00852±0.00027 s^{-1}

The reported K_m and k_{cat} parameters for the hydrolysis of **51** have been corrected assuming that CPA is catalytically active only with the (S)-enantiomer of **51**.[184]

Since the $\Delta\varepsilon_{280}$ for this process was relatively low, it was not possible to observe a pre-steady state burst in these experiments. However, examination of proton release employing a bromothymol blue buffer, in the same manner as described for (S)-**50**, revealed that a burst of proton release did occur during hydrolysis of **51** on approximately the same time scale as observed with (S)-**50** at the same temperature of 25° (see Figure 35 and Table 4). In a parallel experiment, the rate of proton release for the hydrolysis of the fast hydrolyzing ester substrate hippurylphenyllactate[185] (**76**) was also monitored using bromothymol blue buffer. In this case, the rate of hydrolysis was considerably faster, as expected, and required a much lower enzyme concentration (7.2 nM) in order to observe proton release under these experimental conditions. During this experiment, it was not possible to detect the presence or absence of a pre-steady state burst, as a consequence of the low enzyme concentration used, as well as the relatively rapid rate of proton release for the hydrolysis of **76**.

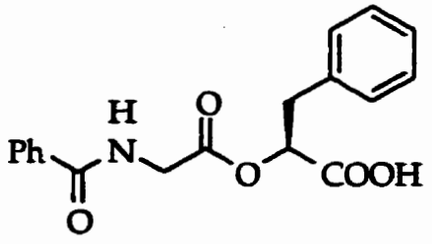

76

Figure 35: Proton release during the hydrolysis of 51 (50 μM) by CPA (1.44 μM) in bromothymol blue buffer (145 μM) at 25°C. ($\Delta\varepsilon_{615}$ = 38600 $M^{-1}cm^{-1}$)

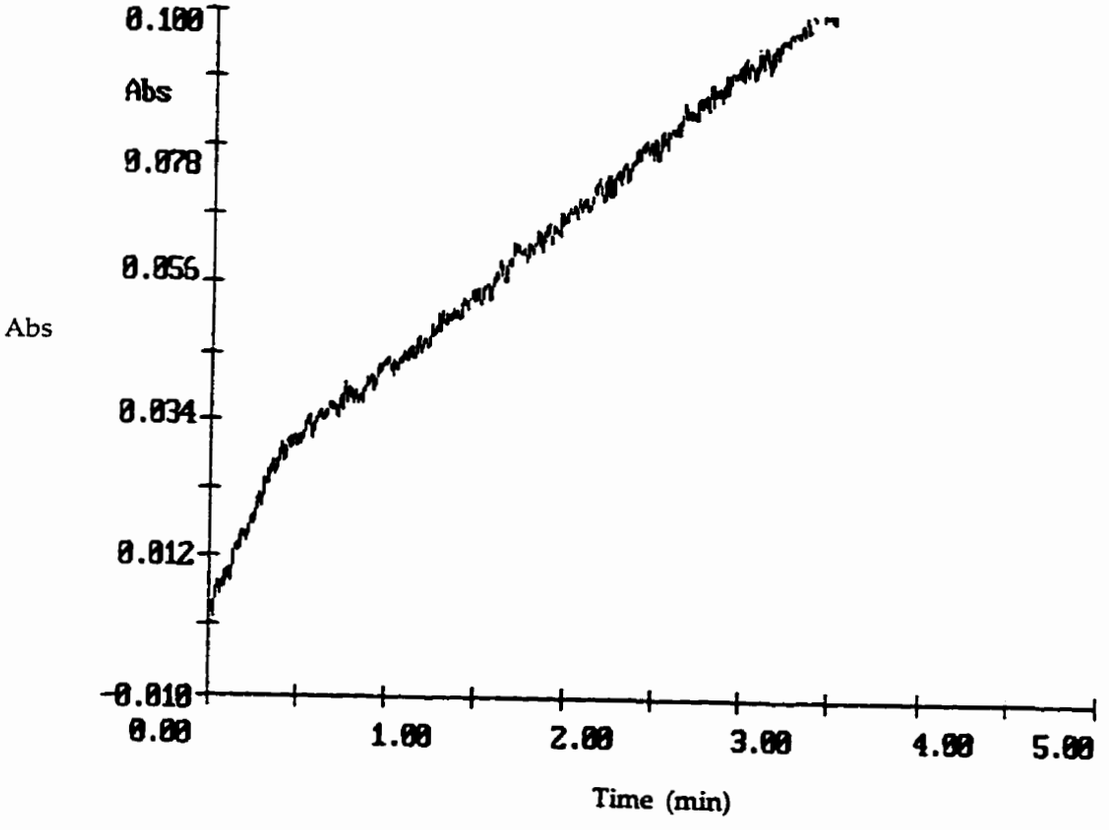

Table 4: Rate of H^+ release in bromothymol blue buffer (145 μM) and ester hydrolysis in Tris buffer (25 mM) for esters **51** and **76**, with ethanol content at 10% (v/v).

Ester substrate and conc.	[a] Pre-steady state rate of H^+ release in BTB/NaBTB buffer (615 nm)	[b] π (μM)	Steady state rate of H^+ release in BTB/NaBTB buffer (615 nm)	[c] Steady state rate ester release in Tris buffer
51				
38.5 μM	26.8±0.6 nM/s	0.43±0.02	10.2±0.2 nM/s	14.6±1.4 nM/s
123.2 μM	34.2±0.6 nM/s	0.48±0.10	19.4±0.6 nM/s	20.8±0.8 nM/s
76				
100 μM	-	-	0.24± 0.01μM/s	[d] 0.68± 0.09 μM/s
500 μM	-	-	0.30±0.01 μM/s	1.15± 0.08 μM/s

The enzyme concentrations used for assays with **51** and **76** were 1.44 μM and 7.2 nM respectively. The reported K_m and k_{cat} parameters for the hydrolysis of **51** and **76** have been corrected assuming that CPA is catalytically active with only the L-configuration of those esters.[184]

[a] The above shown rates are the means of three or more separate determinations, with ± standard error.

[b] The reported π values are the mean of three separate determinations ± standard error.

[c] The esters **51** and **76** were assayed at 280 nm and 265 nm respectively.

[d] The steady state rates reported for **76** hydrolysis in Tris buffer were not observed experimentally but were calculated from a K_m and k_{cat} of 104±24 μM and 193±12 s^{-1} (which were determined in from hydrolysis of **76** in 10% ethanol (v/v)).

As a result, it must be concluded that the kinetic parameters for both the pre-steady state and the steady state phases of the hydrolysis of the ester **51** are similar to those observed for the thioester (S)-**50**. The observation that k_{cat} values for the steady state in the hydrolysis of **51** and (S)-**50** were similar was surprising since it had been anticipated that release of the thiol **35**, which is a potent inhibitor of CPA (K_i=1.2 μM,[97] but see discussion in Section 2.2.7), would be much slower than release of the alcohol (β-phenyllactate) which is a weaker inhibitor (K_i=0.13 mM[60]).

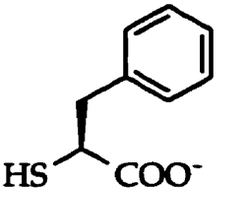

35

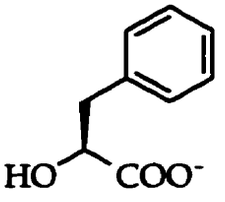

β-phenyllactate

These observations suggested that a more detailed consideration be given to the molecular events which are likely involved in product release in CPA catalyzed hydrolysis. As indicated in Chapter 1, much of the discussion of the mechanism of CPA catalyzed hydrolysis which appears in the literature is related to the debate concerning the acyl-enzyme (mixed anhydride) versus the direct zinc promoted hydration mechanisms. It is now widely accepted that the large body of experimental evidence available from structural, kinetic and spectroscopic studies can be best accounted for on the basis of the direct hydration process which has been summarized by Lipscomb[40,64] for amide hydrolysis as shown in Scheme 37 below. In this process, the catalytic steps include an essential water molecule (or hydroxide ion) bound to a zinc ion which bears three other ligands, two histidines and a glutamate. The substrate binds with interaction between the carbonyl group and Arg-127 which favours the hydration of the carbonyl group to yield a tetrahedral intermediate. In this process, the zinc ion is believed to become pentacoordinate as shown. Collapse of the zinc bound tetrahedral intermediate with concomitant proton transfers yields an intermediate in which the carboxylate group, derived from the acyl portion of the amide group, is bound to the zinc ion as one of the four ligands.

Scheme 37

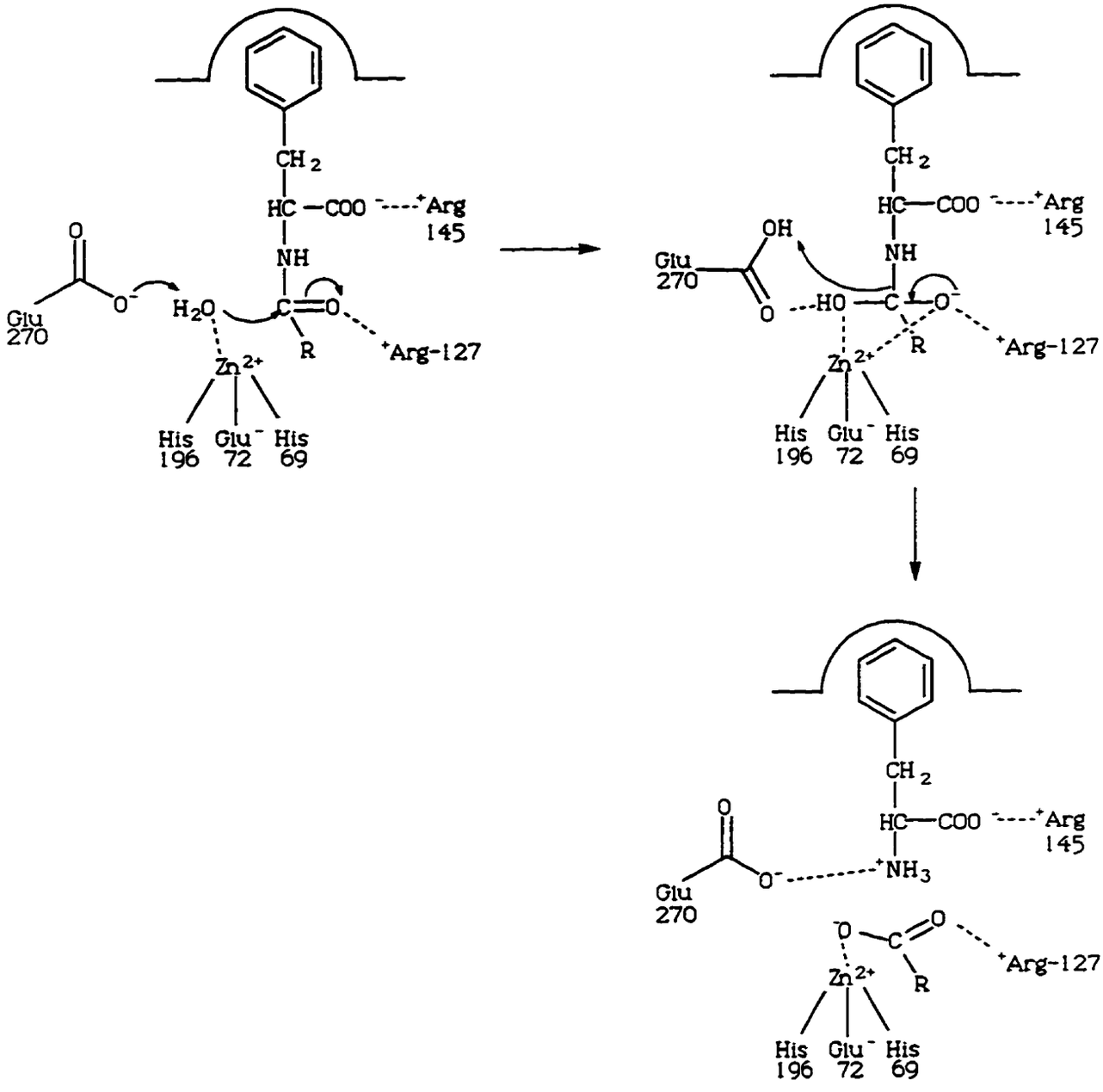
CH2
HC—COO
+Arg 145
NH
Glu 270
H2O
C=O
R
+Arg-127
Zn2+
His 196
Glu 72
His 69
OH
HO—C—O
NH3

A similar mechanism, illustrated in Scheme 38a, can be drawn for the hydrolysis of esters or thioesters. For the case of amides the processes shown in Scheme 37 represent all of the kinetically relevant catalytic steps since amide bond cleavage is believed to be rate-limiting. The molecular events which must occur in order to convert the intermediate product-bound enzyme into the catalytically active form may have not received attention since they are believed to occur rapidly following the hydrolytic-step and do not contribute to the observed rates of hydrolysis.

It has been shown for esters[12,56,57,58,59,180] and, in this study, for thioesters that the hydrolytic events shown in Scheme 38 and Scheme 39 occur in the rapid pre-steady state phase of the catalytic cycle and that product release is rate limiting. Little attention has been paid, however, to the possible details of the molecular events which must occur to convert the product-bound enzyme into its active form to complete the catalytic cycle, even though it is those events which determine the rate of such hydrolyses.

Scheme 38a

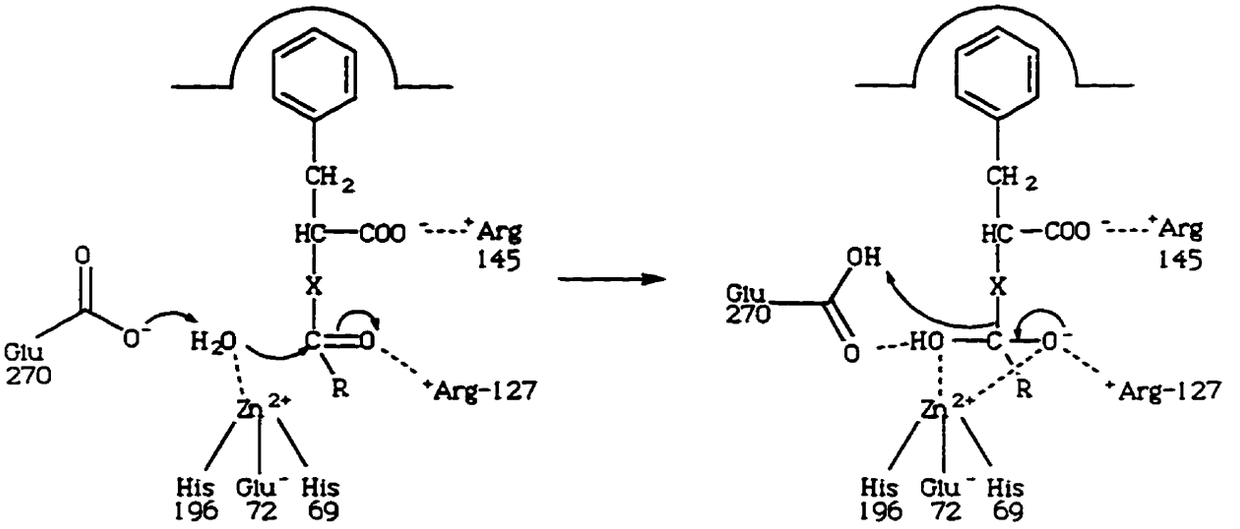

X = O or S

Continued in Scheme 38b

Scheme 38b

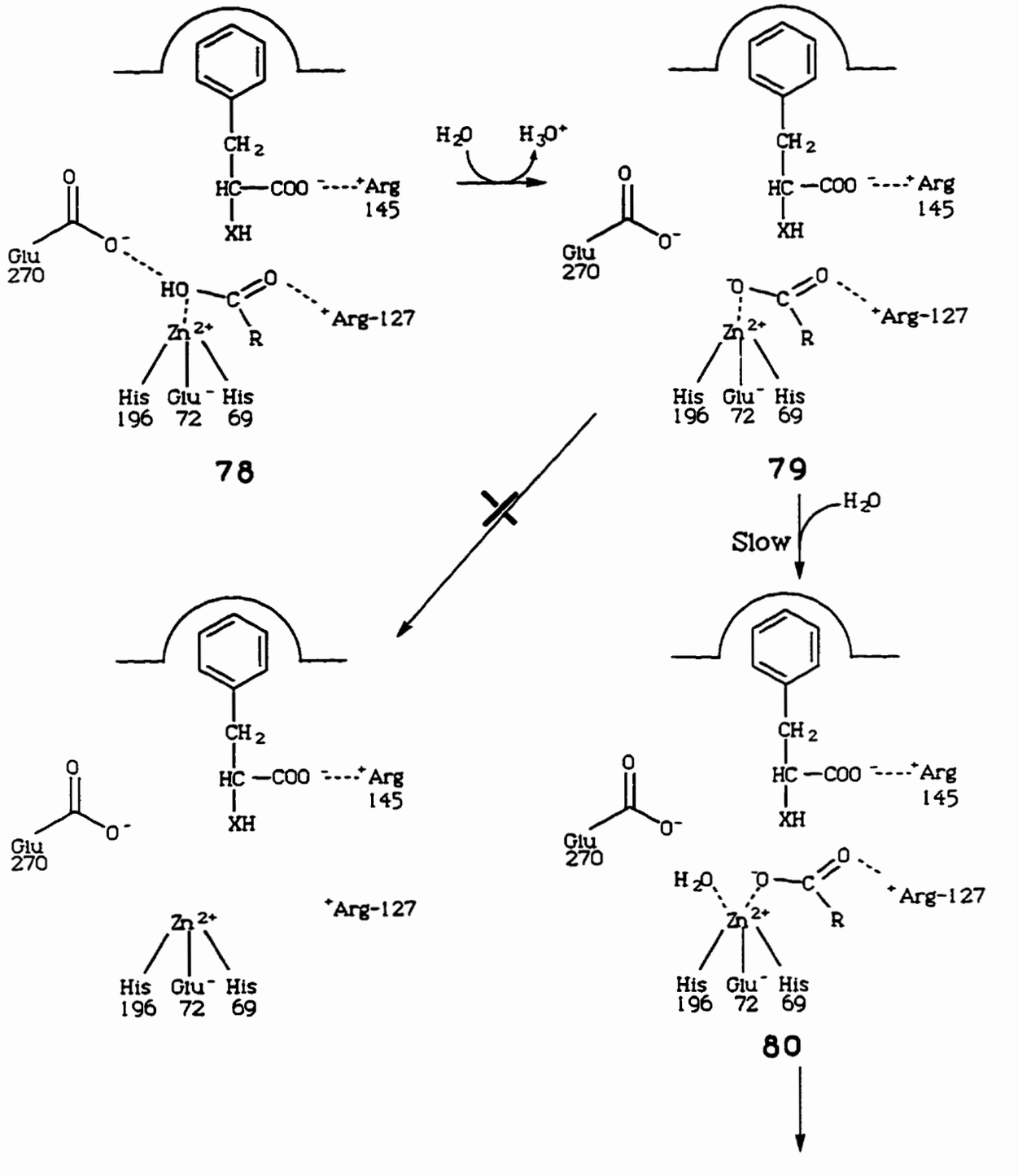

Continued in Scheme 38c

Scheme 38c

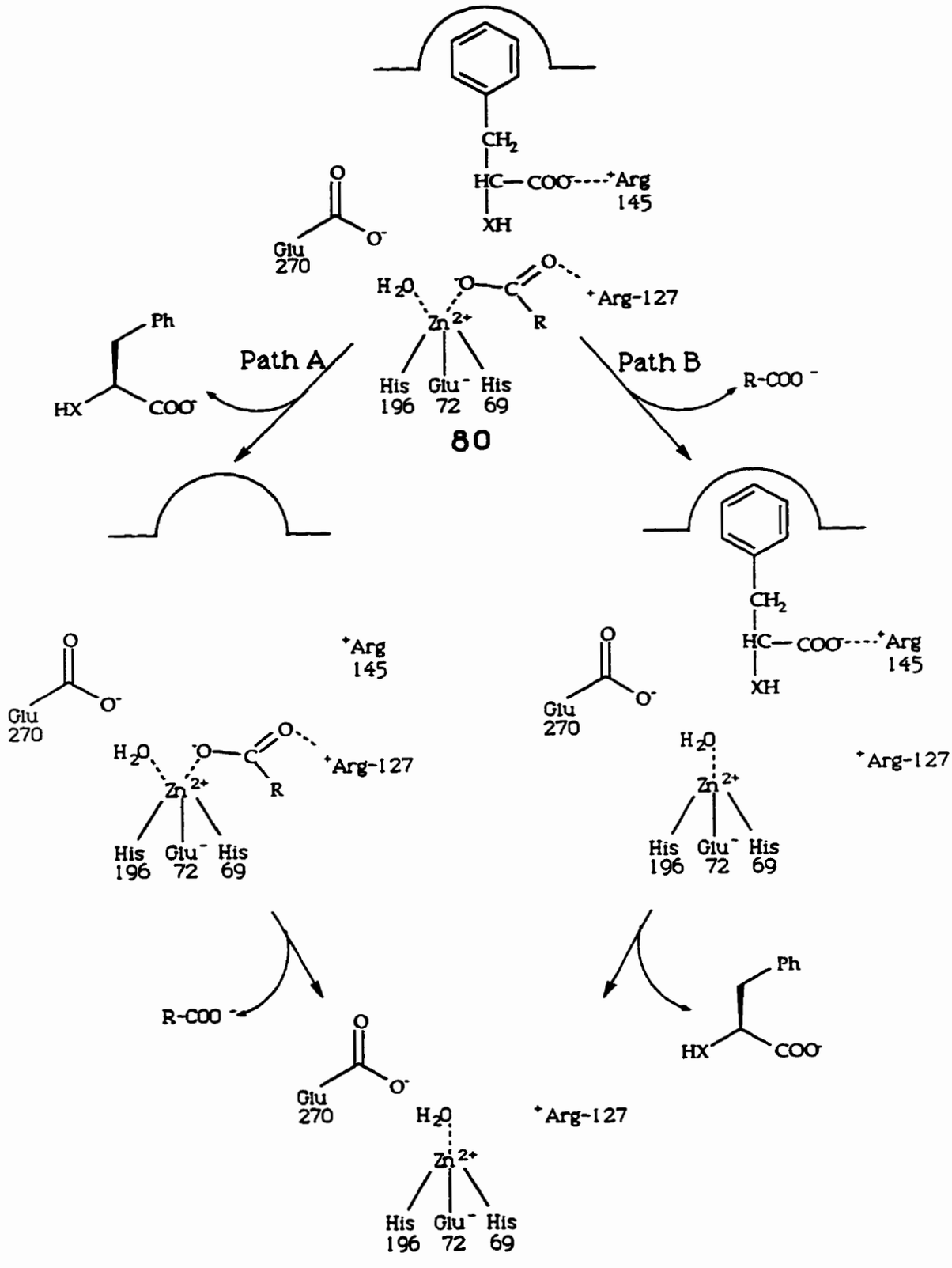
CH2
HC—COO----+Arg 145
XH
Glu 270
H2O
Zn2+
+Arg-127
R
Ph
HX
COO-
Path A
Path B
R-COO -
His 196
Glu- 72
His 69
80
Native CPA

Scheme 39

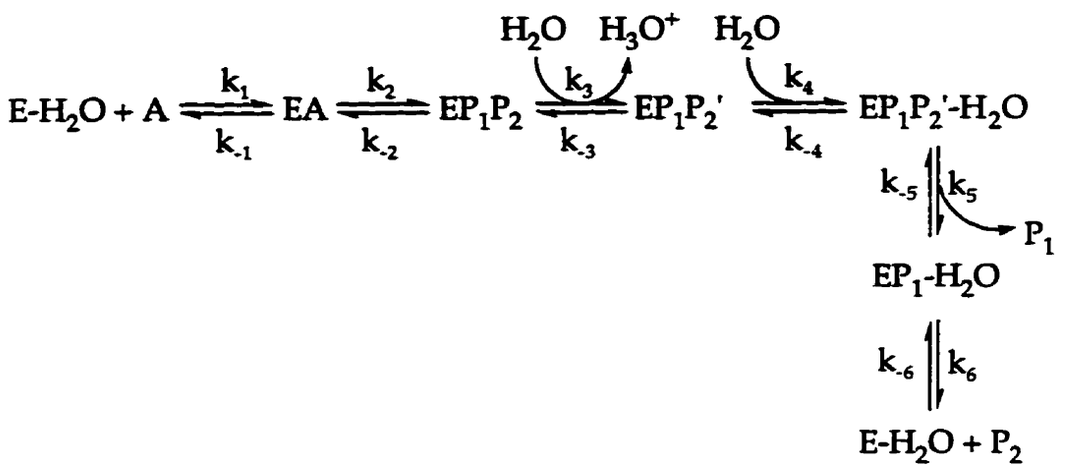

-where A is (S)-**50**

Shown in Scheme 38b and Scheme 38c is a hypothesis which considers the nature of the product release events. It is assumed that departure of the carboxylate ($RCOO^-$) cannot occur spontaneously from **79** to yield a tricoordinated zinc ion and that hydration to yield the pentacoordinated zinc species **80** is an obligatory step. This could be followed by departure of the carboxylate and alcohol or thiol products in an ordered (Path A or Path B) or random (Path A and Path B) sequence. In either case, the step in which the carboxylate is lost generates a tetracoordinate zinc ion bearing a water molecule as a ligand.

If it is accepted that Scheme 38 represents a reasonable approximation of the molecular events involved in product release, a rationalization of the kinetic characteristics of the CPA-catalyzed hydrolysis of (S)-**50** and **51** relative to those of depsipeptides studied by Vallee and coworkers becomes possible. For (S)-**50** and **51** the approach to steady state, determined by the magnitude of k_2, is slow relative to that observed for the depsipeptides. In this hydrolytic step, the carbonyl group of the

substrate undergoes hydration which generates a tetrahedral intermediate, bound to the zinc ion such that the metal ion is pentacoordinate.

Analysis of the x-ray crystallographic data concerning the binding of inhibitors to CPA suggests a possible explanation for the observation that such a step is disfavoured for (S)-**50** and **51**. Lipscomb and coworkers[26,30,33,64,65,134] have reported the three-dimensional structures for a number of substrate-like ketones known to inhibit CPA. The ketones **9**[64] and **10**[65], which exist in aqueous medium largely in the unhydrated form (<0.2% hydration), bind to the enzyme as the hydrates suggesting that the enzyme has catalyzed a hydration process to form the adducts observed. It has also been shown, however, that the ketone **24**,[26,30,64,134] which can be considered to be an analogue of a benzoyl ester substrate, binds to CPA in an unhydrated form. Although the tendency of **24** to undergo hydration may be disfavoured somewhat by the loss of conjugation between the aryl ring and the ketone carbonyl group upon reaction, it has been argued also that the formation of the hydrate may be disfavoured in the case of **24** because of steric conflicts between the bulky aryl group and active site amino acid residues upon formation of such an intermediate.[26,30,64,134]

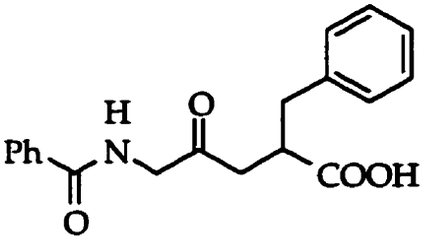

9

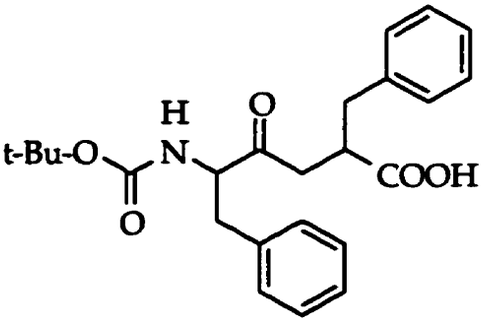

10

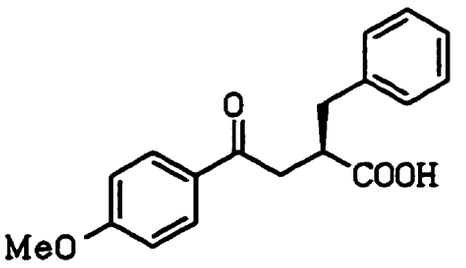

24

Thus, it is proposed that k_2 for the hydrolysis of (S)-**50** and **51** is small as a consequence of a combination of resonance and steric effects in the initial hydration process as suggested for the ketone **24**.[64]

In terms of rationalization of the slowness of the steady state process for (S)-**50** and **51**, analysis of the steps proposed in Scheme 38 becomes appropriate. It is suggested that the proposed obligatory formation of the hydrated pentacoordinated intermediate **80** (in Scheme 38) during product release plays a key role in determining the k_{cat} for the steady state in hydrolysis of (S)-**50** and **51**. In common with the initial hydrated intermediate **77** (in Scheme 38), the intermediate **80** incorporates a pentavalent zinc ion. It is reasonable to suggest that some of the same steric interactions which disfavour the formation of **77** when R=Ph are also present in **80** thus slowing down this essential stage of product release. It is also proposed that the remaining steps in the catalytic cycle with (S)-**50** and **51** are rapid relative to the rate of formation of **80**. This proposal explains the relative insensitivity of k_{cat} to the nature of the leaving group in the hydrolytic process since the interaction between the leaving group and the zinc ion is not strong in **80**.

It is the slow dissociation of the complex **80** that may also explain the observation of proton release during the pre-steady state hydrolysis of (S)-**50** and **51** using bromothymol blue buffer. After the collapse of the tetrahedral intermediate **77** to give the product bound complex **78**, a proton is generated that may be associated

with either the carboxylate of the acyl product, or the carboxylate of Glu-270. The dissociation of this proton appears to occur prior to the slow formation of the pentacoordinated complex **80**. In the case of other faster hydrolyzing substrates, a water molecule may readily enter the active site of the enzyme-products complex and coordinate to the zinc ion, displacing the acyl carboxylate group, initiating product release. In the case of (S)-**50** and **51** a water molecule entering the active site region of **78** may pick up the proton to form H_3O^+ and leave the active site, in preference to binding to the zinc ion to form the pentacoordinate zinc complex. Once the free proton has left complex **78**, an additional water molecule can enter the active site and initiate the slow rate limiting formation of **80**.

In terms of the possible rapid steps after formation of **80**, Path A seems more likely since Path B would yield a species which is similar to or identical to that produced by binding of the thiol (X=S) to free CPA. Since, as shown below in Section 2.2.7, the binding of **35** (X=S) is known to be very tight, it seems unlikely that the release of the leaving group from such an intermediate would be very rapid.

A similar analysis may explain the earlier observations by Suh and coworkers[53] which were suggested to support the concept of an acyl enzyme intermediate. Steady state kinetic analysis of the hydrolysis of the esters **5** and **6** led to the observation that the k_{cat} for the two esters were very similar, 0.46 s^{-1} and 0.28 s^{-1} respectively, even though the leaving groups, phenyllactate and mandelate, were different. This led to the proposal that a common intermediate, namely an acyl enzyme, was involved in the hydrolysis of each. The mechanism in Scheme 38 offers an alternative explanation if it is assumed that steric-interactions, arising from the acyl group, interfere in the formation of the intermediate **80** making this the rate determining step. The rate of the rate determining step is dependent more on the structure of the acyl component than on the structure of the leaving groups (phenyllactate versus mandelate).

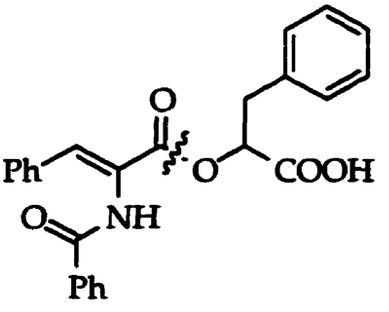

5

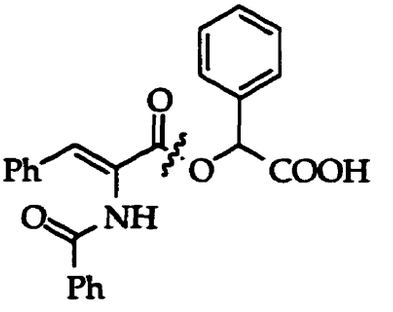

6

In the case of other esters such as the depsipeptides studied by Vallee and coworkers[180] it is possible that the formation of **80** may be rapid relative to the other steps of product release. Further studies of the influence of the leaving group structures on k_{cat} of the hydrolysis of depsipeptides might shed light on such mechanistic possibilities.

With respect to the thioester, which is of importance in the present study, it can be concluded that thiol release likely follows the rate limiting step in hydrolysis and hence does not influence reaction rate significantly. As a result, inhibition by (S)-**50** is expected to arise from binding of the product thiol to the free enzyme following completion of the catalytic-cycle rather than directly through the formation of a stable zinc bound intermediate during the catalytic-cycle. The details of inhibition of CPA by (S)-**50** are presented below. The following group of Sections (2.2.1 to 2.2.9) describe the investigative experiments and conclusions in which the thioester (S)-**50** was evaluated as an inhibitor to CPA.

2.2.1 Influence of Ethanol Content on CPA Activity

The fact that the solubility properties of (S)-**50** were such as to require the use of an organic cosolvent, ethanol, necessitated an analysis of the effect of ethanol on the kinetic parameters for the substrate to be used for kinetic analysis before appropriate assay condition for inhibition of CPA by (S)-**50** could be designed. Preliminary studies of CPA activity with the peptide substrate HP in a 10% EtOH (v/v) solution led to the observation that changes in co-solvent content affected K_m. At 10% (v/v) EtOH, HP hydrolysis was associated with a K_m of 0.13 mM. Hippuryl-L-phenylalanine (HP), which is convenient a substrate for estimating peptidase activity for CPA, differs in a number of ways from the thioester (S)-**50** as a substrate. HP is a much better substrate for CPA than is (S)-**50**. As a result, enzyme concentrations (60-130 nM) much lower than those used for the study of the hydrolysis of (S)-**50** (1.5 μM) and concentrations of HP in excess of 0.25 mM were required to measure initial rates for hydrolysis of HP to avoid substrate depletion. That is, higher enzyme concentration or lower substrate concentrations resulted in progress curves in which the linear region was too short to allow accurate and reproducible measurement of initial slopes. If peptidase activity for CPA was measured in a 10% (v/v) EtOH solution, the HP concentrations used would all lie well above the K_m for HP hydrolysis.

One potential solution to this dilemma was to lower the enzyme concentration and the substrate concentration to extend the linear portion of the progress curve while allowing for study of kinetic behaviour at substrate concentrations below as well as above K_m. In practice, however, this was not feasible since the relatively low absorbance change associated with HP hydrolysis ($\Delta\varepsilon_{265}$=137.7 $M^{-1}cm^{-1}$) required substantial turnover in order to measure the steady state rate accurately. For the HP

concentration range judged to be most appropriate for this study (0.25 mM to 1.3 mM) a K_m above 0.25 mM would be ideal for the substrate.

An analysis of HP hydrolysis by CPA at varying EtOH content was conducted to find an EtOH concentration at which the K_m for HP would be in an acceptable range. The kinetic parameters were estimated for HP hydrolysis, and are plotted against ethanol concentration in Figure 36. The K_m value was found to decrease considerably from 0% to 10% (v/v) ethanol, whereas k_{cat} was found to be relatively unaffected.

Figure 36: Relationship between ethanol content and observed K_m and k_{cat} values for HP hydrolysis. The parameters K_m and k_{cat} were estimated from rates measured at 0.44 mM and 1.76 mM HP (four or five determinations were conducted for each HP concentration). E_o=21 nM.

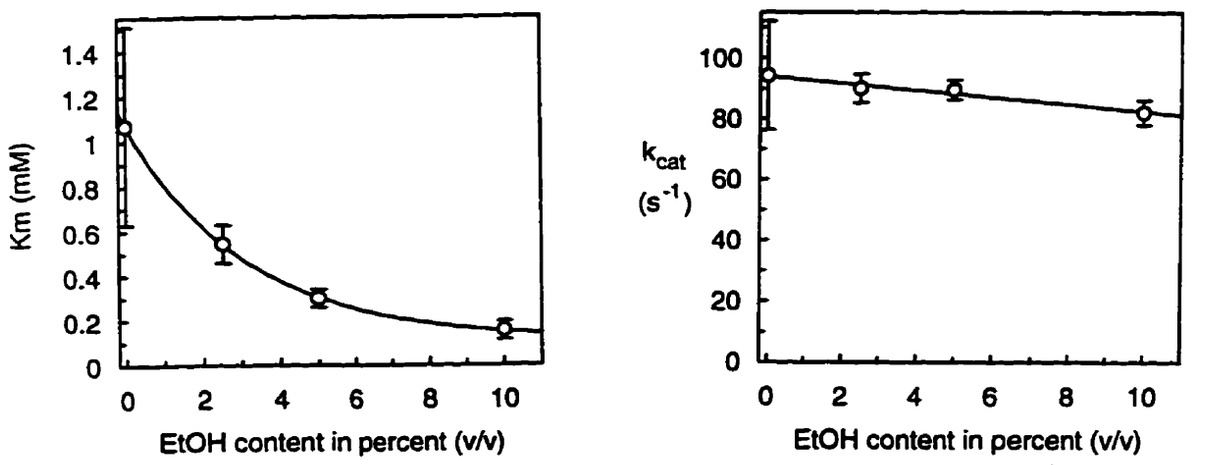

All deteminations at each ethanol content were used to calculate the K_m and k_{cat} parameters. Standard error bars indicate calculated standard errors. For graphical presentation, the ethanol content versus K_m data was fitted to a single exponential function, and ethanol content versus k_{cat} data was fitted to linear curve.

It was found that K_m of about 0.40 mM which was considered appropriate for our kinetic experiments, could be achieved at 3.5% (v/v) EtOH. A more detailed

determination of HP hydrolysis in 3.5% (v/v) ethanol led to a K_m and k_{cat} of 0.31±0.04 mM and 85.7±3.0 s^{-1} respectively.

With inhibition experiments now to be conducted in 3.5% (v/v) ethanol, it was of interest to analyze the hydrolysis of (S)-**50** in 3.5% (v/v) ethanol. The thioester (S)-**50** was observed to be soluble in 3.5% (v/v) EtOH at concentrations as high as 207 μM. The progress curves of (S)-**50** hydrolysis (Figure 37) revealed an initial burst followed by a steady-state region, as reported for the assays using 10% ethanol (v/v). The burst was observed on a somewhat shorter time scale under these conditions. At higher concentrations of (S)-**50**, the burst was too rapid to be totally observed on the progress curves. At these higher (S)-**50** concentrations, only the tail-end of the burst was observed, making the determination of the kinetic parameters for the burst step impossible without the use of stop-flow methods. Steady state kinetic analysis of the hydrolysis of (S)-**50** resulted in a K_m of 61.8±7.0 μM and a k_{cat} of (1.53±0.06)x10^{-2} s^{-1}.

It is also worth noting briefly that a burst is observable in the hydrolysis of (S)-**50** in the absence of ethanol ([(S)-**50**]=50 μM, [CPA]=1.1 μM, 25 mM Tris, 0.5 M NaCl, pH=7.5, 25°C) but the time scale is shorter such that a significant part of the burst occurs in the mixing time of the experiment.

Since ethanol is a nucleophilic solvent, the possibility that some incorporation of ethanol into the product (i.e.. formation of ethylbenzoate) in such CPA catalyzed reactions should be considered. However, Vallee and coworkers[180] and Breslow et al.[47] have clearly demonstrated that transesterification of esters or alcoholysis of amides is not catalyzed by CPA. In the present example, product analysis after CPA catalyzed hydrolysis of (S)-**50** in 10% ethanol (v/v) solution revealed that only the disulfide and benzoic acid were produced, as mentioned in Section 2.1.1.

Figure 37: Hydrolysis of (S)-**50** (40 μM) by CPA (1.34 μM) in 25 mM Tris, 0.5 M NaCl, pH of 7.5, 25°C, containing 3.5% EtOH (v/v).

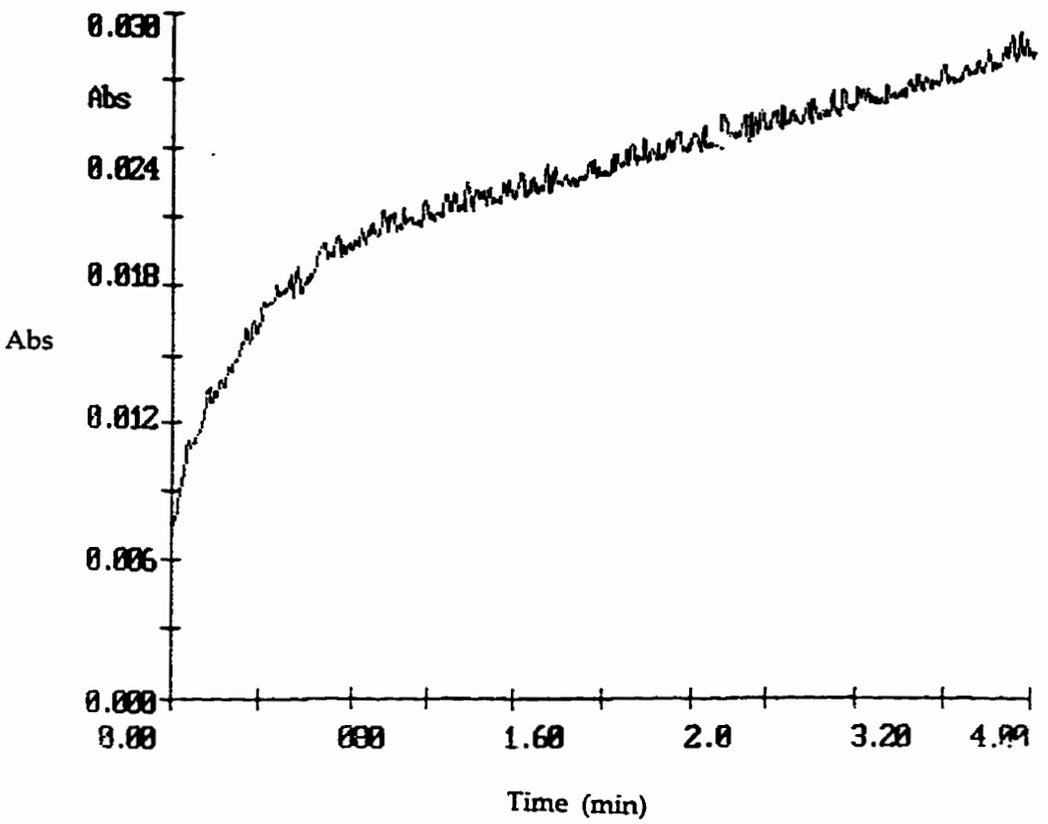

2.2.2 Thioester (S)-50 as a Competitive Substrate

Analysis of HP hydrolysis was monitored at 265 nm ($\Delta\varepsilon$=137.7 $M^{-1}cm^{-1}$) where hydrolysis of (S)-**50** can also be monitored. The $\Delta\varepsilon$ for (S)-**50** hydrolysis at 265 nm is 5070 $M^{-1}cm^{-1}$. Even though the extinction coefficient for (S)-**50** hydrolysis is greater than that of HP hydrolysis, the rate of hydrolysis for the substrate HP is much greater. The rate relationship between two competing substrates[186] at steady-state is normally expressed as follows:

$$\frac{\upsilon_A}{\upsilon_B} = \frac{(k_{cat}/K_m)_A[A]}{(k_{cat}/K_m)_B[B]} \qquad (2.10)$$

(see pg 232 for more details)

Since $\Delta A=(\Delta conc.)(\Delta\varepsilon)$, then:

$$\frac{\Delta A_A}{\Delta A_B} = \frac{(k_{cat}/K_m)_A[A]\Delta\varepsilon_A}{(k_{cat}/K_m)_B[B]\Delta\varepsilon_B} \qquad (2.11)$$

The lowest concentration of HP used during the assays was 160 μM, and the highest (S)-**50** concentration used was 132 μM. Under those conditions, the calculated $\Delta A_{HP}/\Delta A_{(S)\text{-}50}$ at steady-state, based on the measured K_m and k_{cat} for the two substrates, is 35, suggesting that any spectrophotometric change at 265 nm due to (S)-**50** hydrolysis is negligible.

During this analysis, (S)-**50** concentrations of 28.4 μM and 132 μM were used, with an enzyme concentration of 62 nM. CPA and the thioester (S)-**50** were allowed to incubate for 1 to 2 min prior to the addition of HP in order for the interactions between (S)-**50** and CPA to achieve a steady state. The resulting double-reciprocal

plot revealed a competitive relationship between the hydrolysis of HP and (S)-**50** (Figure 38).

Figure 38: Double-reciprocal plot of HP hydrolysis in the presence of (S)-50, 25 mM Tris, 0.5 M NaCl, pH of 7.5, 25°, containing 3.5% EtOH (v/v).

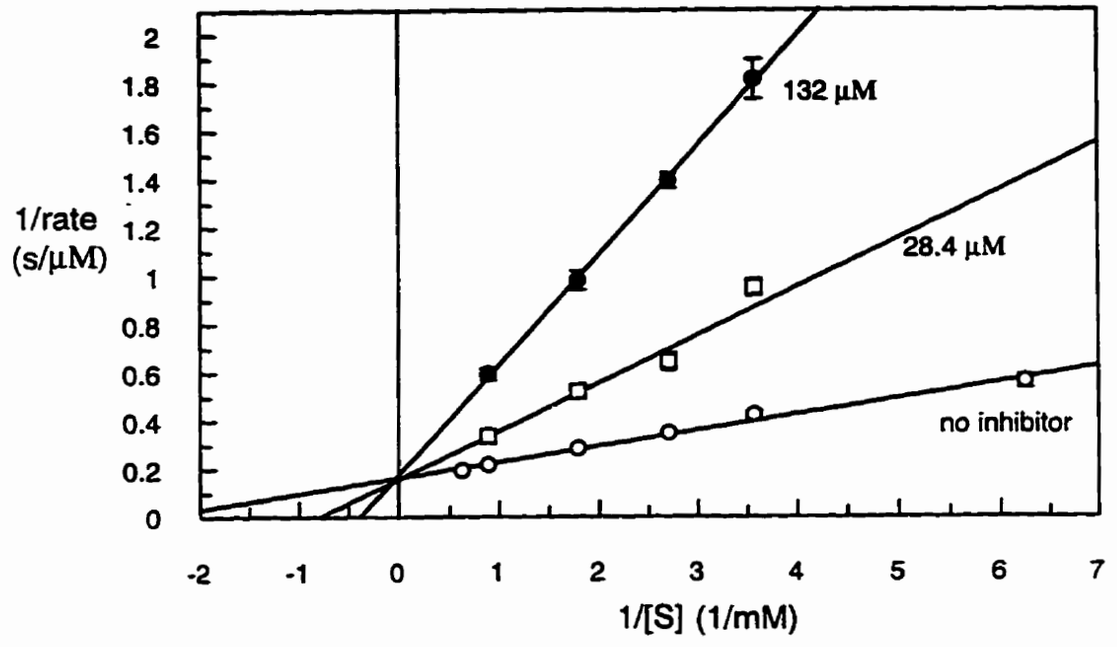

Each data point is the average of six or more separate determinations, shown with standard error bars. Error bars smaller than the symbols are not shown.

The initial rate kinetic relationship for competing substrates is similar to that for simple competitive inhibition:

$$v_A = \frac{E_o k_{cat}^{A}[A]}{[A] + K_m^{A}(1 + [B]/K_m^{B})} \qquad (2.12)$$

The calculated K_m^B from this assay was 18.9 μM, which is less than the actual steady-state K_m for hydrolysis of (S)-**50** in 3.5% ethanol (v/v) of 62.3 μM. This result suggested that significant product inhibition was being observed under these reaction conditions. For such a situation the appropriate rate expression is:

$$v_A = \frac{k_{cat}^A E_o [A]}{[A] + K_m^A \left(1 + \frac{[B]}{K_m^B} + \frac{[P]}{K_i^P}\right)} \qquad (2.13)$$

where P is the thiol product **35** and K_i^P is the inhibition constant for the thiol.

One interpretation of this observation was that under the reaction conditions employed, complete rapid oxidation of the thiol product **35** to the disulfide **73** was not occurring, unlike the situation observed in the study of hydrolysis of (S)-**50** which employed much higher enzyme concentrations. This possibility encouraged us to explore the inhibition of CPA by (S)-**50** under more controlled conditions which would disfavour oxidation of the thiol product. These experiments are described below.

2.2.3 Inhibition of Peptidase Activity by (S)-50 under O_2-Free Conditions Using Argon

It was decided that to evaluate (S)-**50** as a suicide substrate, experimental conditions employing an anaerobic environment to allow for the accumulation of the free thiol product **35** would be required. This was achieved by incubating (S)-**50** with CPA under Ar at 25°C. At different time intervals during the incubation, aliquots of the incubation mixture were withdrawn and tested for peptidase activity (using HP as substrate), and thiol content (using DTNB), as shown in Scheme 40. Therefore, the

loss in peptidase activity may now also be correlated to the accumulation of **35** as well.

Scheme 40

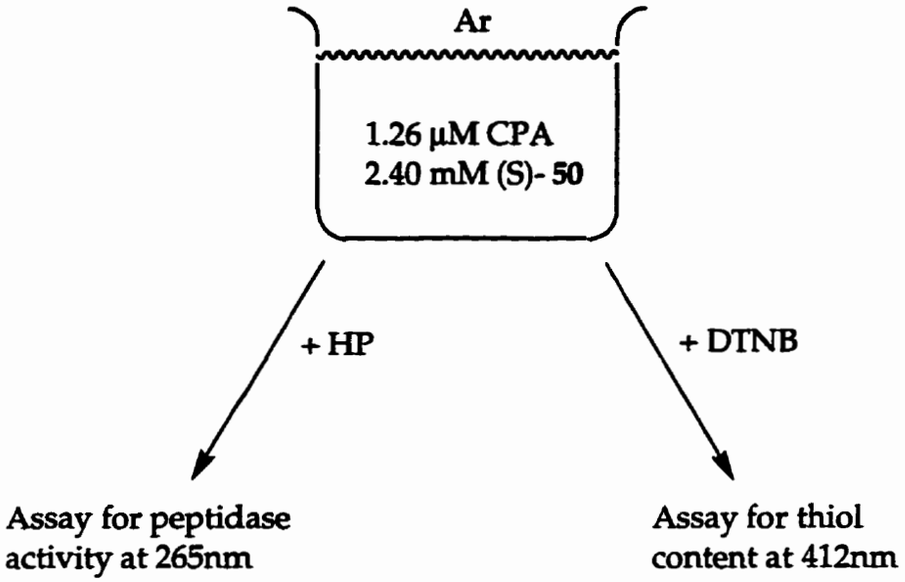

A detailed description of this experiment is given in the Experimental section. As shown in Figure 39, thiol content was observed to increase over time, indicating an accumulation of **35** in solution. Accompanying this build-up of **35** was the expected decrease in peptidase activity (Figure 39). Control experiments in which CPA was incubated under Ar in the absence of (S)-**50** with periodic testing of peptidase activity were also conducted. In addition, a control experiment in which (S)-**50** was incubated under Ar revealed that no hydrolysis occurred in the absence of CPA as indicated by testing with DTNB.

Figure 39: Measured thiol content† and peptidase activity* during incubation of CPA (1.26 μM) with (S)-**50** (2.4 mM), 25 mM Tris, 0.5 M NaCl, pH of 7.5, 25°C, 3.5% EtOH (v/v).

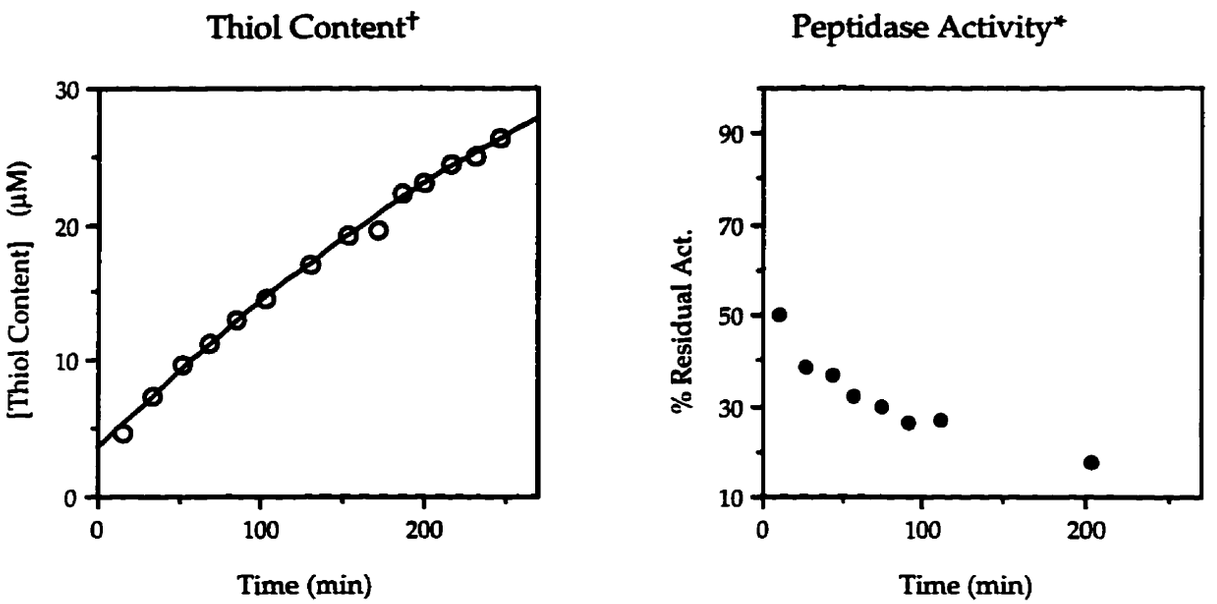

† Measured at 412 nm (ε_{412}=14160 $M^{-1}cm^{-1}$) after mixing 500 μL of incubation mixture with 500 μL of 0.4 mM DTNB, in 3.5% ethanol (v/v). The thiol content given represents the concentration in the reaction mixture prior to dilution.

* Measured at 265 nm (ε_{412}=137.7 $M^{-1}cm^{-1}$) after mixing 50 mL of incubation mixture with 950 mL of 0.99 mM HP, in 3.5% ethanol (v/v). Rate result reported as a percentage of observed rate in absence of (S)-**50**. The results given represents the activity observed in the peptidase assay mixture.
Since the reaction of the thiol with DTNB was not instantaneous, some thiol generation occurred during the DTNB analysis. Back-extrapolation of the linear apparent steady state portion of the time course of the DTNB reaction was carried out to estimate the amount of thiol present at time zero.

This experiment was useful in providing a direct correlation between the accumulation of **35** and the decrease in CPA activity. From this data it was possible to estimate the inhibitory potency of the free thiol **35**. The inhibition observed in this experiment is a combination of inhibition from (S)-**50** as a "competitive substrate", and from **35** as a product inhibitor. As indicated in Section 2.2.2, the appropriate rate expression for this system is that in equation 2.13:

$$\upsilon_A = \frac{k_{cat}^{A} E_o [A]}{[A] + K_m^{A}\left(1 + \frac{[B]}{K_m^{B}} + \frac{[P]}{K_i^{P}}\right)} \qquad (2.13)$$

This equation can be rewritten so that V/v vs. [P] can be plotted allowing the determination of K_i^P from the slope:

$$\frac{V}{\upsilon_A} = \frac{K_m^{A}}{K_i^{P}[A]}[P] + \frac{K_m^{A}}{[A]}\left(1 + \frac{[B]}{K_m^{B}}\right) + 1 \qquad (2.14)$$

-where: $V = E_o k_{cat}^{A}$
$slope = K_m^{A}/K_i^{P}[A]$

Since in the time course of this experiment only 26.3 μM of thiol was observed to be generated from a total initial concentration of thioester equal to 2400 μM, the assumption that [B]=2400 μM was judged to be valid. Using the known [A] (0.94 mM) and K_m^A (0.31 mM) for HP hydrolysis under these assay conditions, K_i^P was calculated to be 59 nM (Figure 40).

A K_i of 59 nM for **35** is considerably less than the K_i of 1.2 μM for the racemate of **35** reported by Vallee and coworkers.[97] This discrepancy raised questions about the value reported by Vallee. In our laboratory, the free thiol was thought to be easily oxidized in the presence of dissolved O_2, as a result of the absence of **35** and the presence of the disulfide **73** as a hydrolysis product. Further investigation of the susceptibility of **35** to oxidation was then conducted.

Figure 40: The relationship between measured thiol content and peptidase activity during the incubation of CPA (63 nM) with (S)-**50** (120 μM), 25 mM Tris, 0.5 M NaCl, pH of 7.5, 25°C, containing 3.5% EtOH (v/v). This relationship represents that observed in the peptidase assay mixtures. The thiol content ([P]) was determined by adjusting the thiol content observed in the incubation mixture at that time to the expected thiol content after a 20-fold dilution.

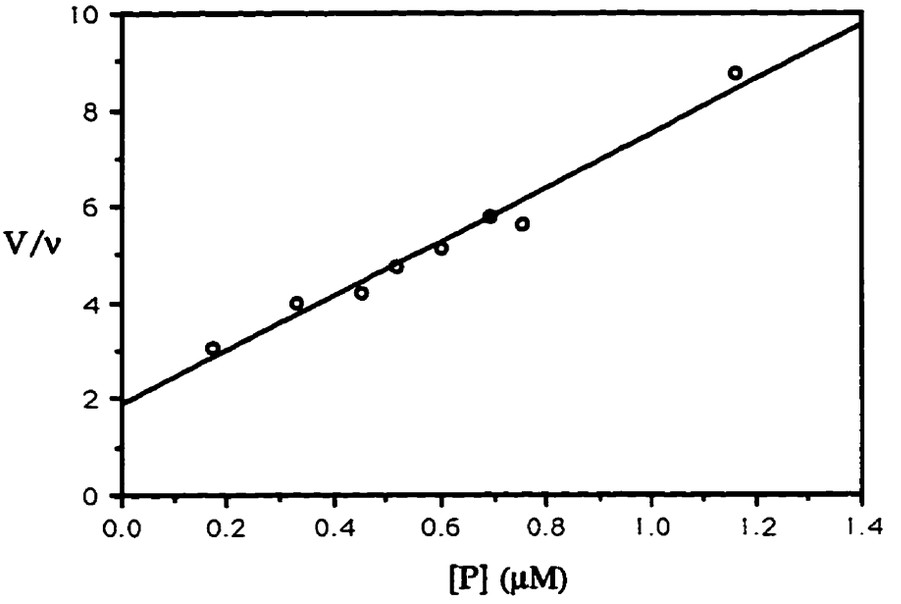

2.2.4 Oxidation of Thiol Inhibitor 35

The thiol **35** was observed to be surprisingly susceptible to oxidation by dissolved O_2. Cushman and coworkers conducted inhibition studies of tight-binding thiol inhibitor **36**, the homo-analogue of **35**, which required low concentrations of **36** to be dissolved in solution for long assay times of up to 1 hour.[147] During these assays, no precautions were taken to protect **36** in solution from oxidation, where **36**

concentrations ranged from 10 nM to 100 nM. This therefore suggests that thiol **36** may be more resistant to oxidation in solution as compared to **35**.

An investigation into the susceptibility of thiols **35** and **36** to oxidation was conducted. Thiol **36** was synthesized from the precursors benzylacrylic acid and thiolacetic acid (Scheme 41).[147] Thiols **35** and **36** were incubated in 10% EtOH (v/v) 25 mM Tris buffer at 25°C, while aliquots were withdrawn at various time intervals to test for thiol content using DTNB (Figure 41). Under these assay conditions, **35** was observed to be oxidized 6.7 times faster than **36**.

Scheme 41

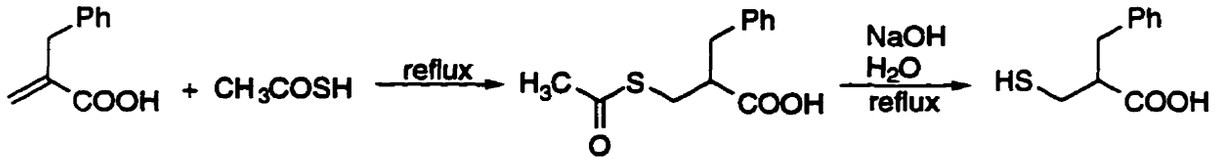

36

Furthermore, as shown in Figure 42 (lower curve), peptidase activity for CPA in the presence of **35** was associated with a biphasic progress curve. There is an initial strong inhibition of activity by **35**, which gradually weakens as **35** is oxidized to its disulfide **73**. The inhibitor **35** is added from a concentrated solution in ethanol where the ratio of thiol to dissolved O_2 is much higher. In a similar experiment, peptidase activity was monitored in the presence of **36** (326 nM), which revealed no loss of inhibitory activity over a 10 min period, in agreement with Cushman's results.[147] The susceptibility of **35** to oxidation, especially at lower concentrations, posed a problem for accurate measurement of the inhibition constant for **35**. This observation plus the resulting low K_i of 59 nM for **35** also led to the question of the potency the disulfide **73** as an inhibitor of CPA. It is suspected that during the study conducted by Vallee[97] on the inhibition of CPA by racemic **35**, the disulfide **73** may have been the inhibiting species studied rather than the thiol **35**. To verify this hypothesis, the inhibition of

CPA by authentic **73** was conducted in this laboratory, as discussed below in Section 2.2.5.

Figure 41: The loss of thiol content of thiols **35** (curve **B**) and **36** (curve **C**) while incubated in 25 mM Tris buffer, 0.5 M NaCl, pH 7.5, containing 10% EtOH (v/v), at 25°C. Curve **A** represents the oxidation of **35** in a O_2-free solution with the use of Ar. Thiol content was measured at 412 nm after the addition of 0.5 mL of 0.4 mM DTNB to 0.5 mL of incubation mixture. Rates for curves **B** and **C** were measured to be 67±4 nM/min and 10.0±0.3 mM/min respectively. Each point represents a single determination.

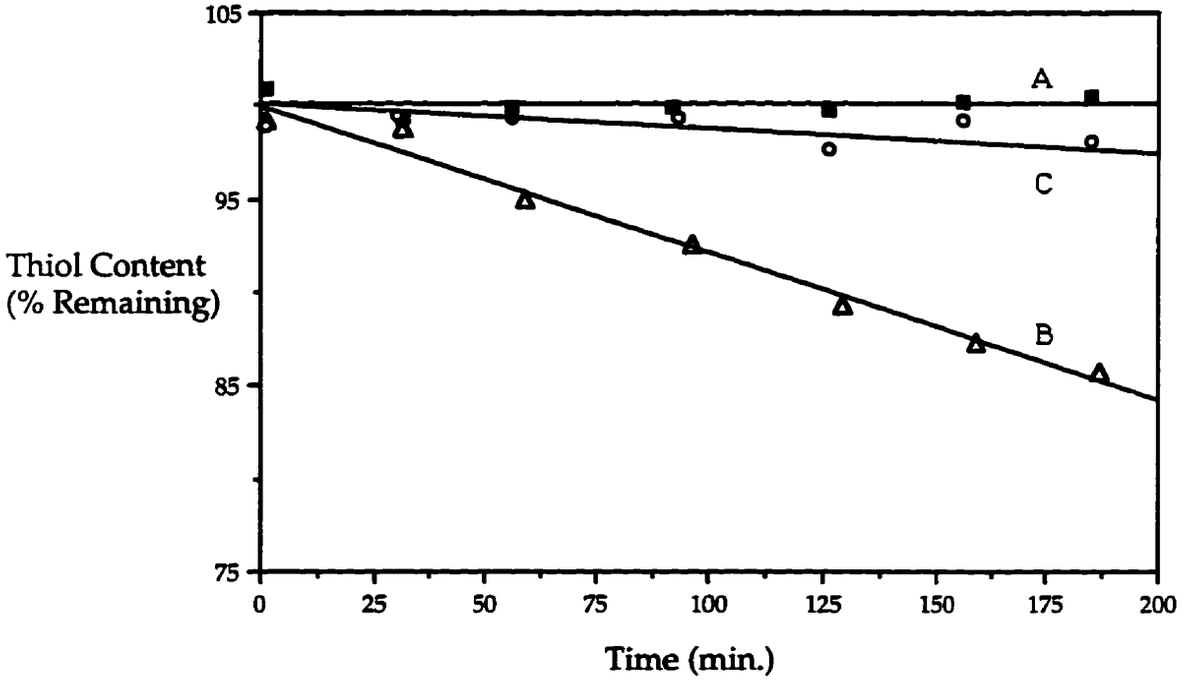

In the absence of additional experimental information concerning the oxidation of **35**, it is not possible to provide a detailed mechanistic rationalization for the strong susceptibility of **35** to air oxidation. It is worth noting, however, that the carboxylate group is closer to the thiol in **35** than it is in **36** which might lead to an acceleration in oxidation if the $-CO_2^-$ group can act as a intramolecular general base at some stage of

the oxidation process. Clearly, further experimentation will be necessary to establish a firm explanation of this phenomena.

Figure 42: HP (0.5 mM) hydrolysis by CPA (126 nM) at 265 nm in the presence of **35** (760 nM) in 25 mM Tris buffer, 0.5 M NaCl, pH 7.5, containing 3.5% EtOH (v/v), at 25°C. Lower curve involved immediate addition of **35** to buffer solution prior to assay. Upper curve involved a 5 min incubation of **35** in buffer solution prior to assay. Steady-state rates for the lower and upper curves were 2.1 μM/s and 2.0 μM/s. The control rate (absence of **35**) was 6.7 μM/s.

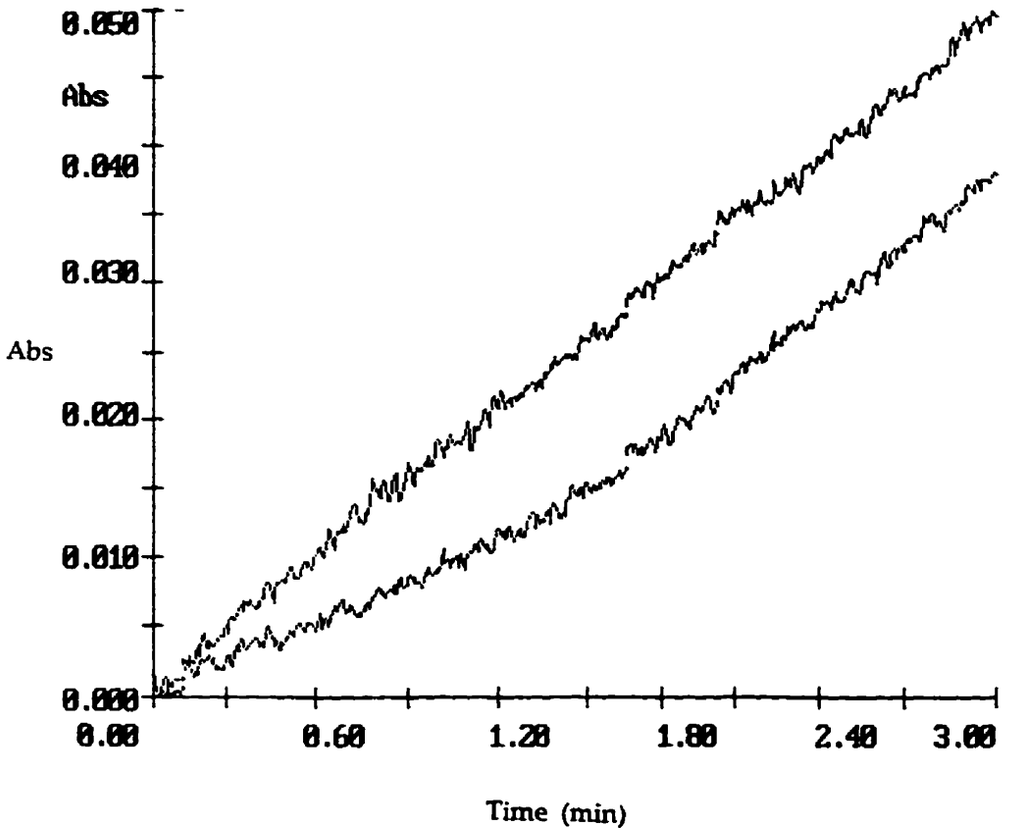

2.2.5 Inhibition of CPA by 73

Our observation that **35** was easily oxidized led us to believe that Vallee had in fact inadvertently measured the inhibition of CPA by the disulfide **73**. To investigate this possibility, the authentic disulfide **73** was produced in this laboratory and tested for its inhibitory potency against CPA.

The disulfide was produced by allowing a 140 μM solution of **35** in 25 mM Tris buffer, 0.5 M NaCl, pH 7.5, containing 10% EtOH (v/v), at 25°C, to incubate for 4 days to enhance full oxidation. The oxidation was monitored daily by testing for residual free thiol using DTNB. The product was characterized using ^{1}H-NMR and high resolution mass spectroscopy (HRMS). The inhibition of CPA peptidase activity by the disulfide was assayed using concentrations of **73** ranging from 0 μM to 6.52 μM, HP concentrations ranging from 0.25 mM to 1.3 mM, and with a E_o of 117 nM. As shown in Figure 44, the resulting double reciprocal plot reveals **73** as a fairly potent competitive inhibitor with a K_i of 3.5±0.5 μM.

The somewhat unexpected observation that the disulfide **73** was a moderately effective inhibitor of CPA peptidase activity caused us to consider briefly the possibility that inhibition by **73** might actually involve inhibition by **35** generated enzymatically from **73** as shown is Figure 43. This possibility was excluded, however, on the basis of several observations. The inhibitory potency of **73** was not altered by preincubation with CPA in an Argon atmosphere and no evidence for thiol generation in the presence of DTNB could be detected. Furthermore, the initial rate data could be fitted well to a reversible competitive inhibition model as shown by the Lineweaver-Burk plots in Figure 44.

Figure 43

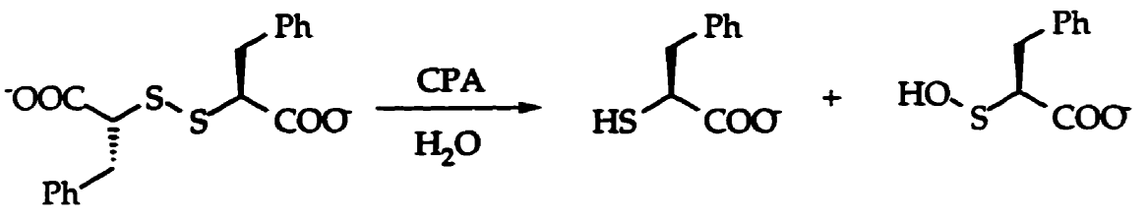

73 **35** **81**

Figure 44: Double reciprocal plot of inhibition of CPA peptidase activity in the presence of **73** in 25 mM Tris buffer, 0.5 M NaCl, pH 7.5, containing 3.5% EtOH (v/v), at 25°C. E_o=117 nM.

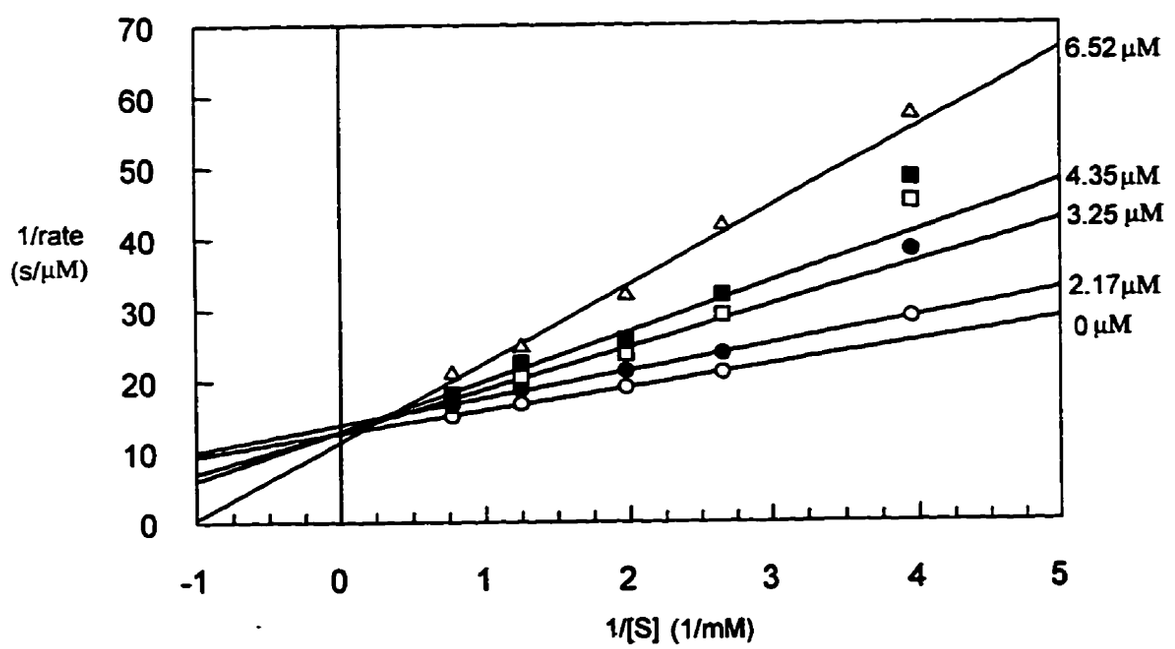

Each data point is the average of six or more separate determinations. Standard error bars are not shown. Standard errors for the data point averages were less than 4%.

The K_i value of 3.5 μM is comparable to the K_{iapp} value of 1.2 μM reported by Vallee.[97] If the thiol **35** was prepared in a fairly dilute solution (10 μM or less) prior to inhibition testing, it is likely, based on our experience in this laboratory, that full oxidation to the disulfide would have taken place in a matter of minutes. Vallee also studied the inhibition of CPA by other thiols under the same conditions.

The susceptibility of **35** to oxidation by dissolved O_2 raised questions regarding the techniques to be used for measuring the inhibition potency of **35**. As discussed in Section 2.2.3, argon was used to remove O_2 from solution. It was difficult, however, to ensure an O_2-free atmosphere during the mixing of aliquots of the O_2-free incubation with the DTNB solution used for measuring thiol content, and with the HP solution used for measuring peptidase activity. Partial oxidation during these analyses would lead to an inaccurate estimate of thiol content. As a result, the use of the radical scavenger glutathione to prevent disulfide formation was pursued as an alternative. The use of glutathione for this purpose is discussed below.

2.2.6 Effects of Glutathione on CPA Activity

The recognition that inhibition of CPA by the thiol **35** required some set of reaction conditions which would minimize the oxidation of **35** to form the disulfide **73** led to the examination of the use of glutathione (GSH, δ-Glu-Cys-Gly), as an antioxidant scavenger.[187] This possibility was an especially attractive alternative since the long term goal of this work involved extension of the inhibition strategy to therapeutically interesting enzymes which might be found in biological environments which are naturally rich in glutathione. Glutathione is an ubiquitous natural thiol which serves a variety of biological functions including the protection of proteins possessing free thiol groups from inactivation through disulfide formation. The

stoichiometry of disulfide formation through air oxidation is shown in equation 2.15 and that for glutathione mediated reactivation is shown in Figure 45.

Figure 45

$$2\,R\text{-}S\text{-}H + 1/2\,O_2 \rightleftharpoons R\text{-}S\text{-}S\text{-}R + H_2O \qquad (2.15)$$

$$R\text{-}S\text{-}S\text{-}R + G\text{-}S\text{-}H \rightleftharpoons R\text{-}S\text{-}H + G\text{-}S\text{-}S\text{-}R$$

$$G\text{-}S\text{-}S\text{-}R + G\text{-}S\text{-}H \rightleftharpoons G\text{-}S\text{-}S\text{-}G + R\text{-}S\text{-}H$$

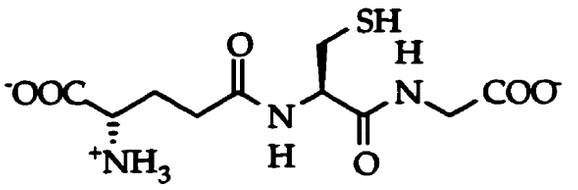

glutathione

The relatively high glutathione concentration in most cells and the maintenance of a GSH/GSSG ratio of about 100:1 through reduction by the NADPH/$NADP^+$ dependent flavoprotein glutathione reductase ensures that thiols are retained in a reduced state.

For this reason, it was felt that glutathione would be useful for preventing thiol oxidation. It was clear, however, that, since glutathione contains a mercapto group, it might act as a competitive inhibitor of CPA much like **35, 36** and other mercaptans. Before using glutathione in assays, its effect on CPA activity was studied.

The peptidase activity of CPA was monitored at varying concentrations of GSH to determine any inhibitory effects by this thiol (Figure 46). The inhibition, which was observed only at relatively high concentrations of glutathione (>1 mM) was unusual

kinetically. Typical competitive, uncompetitive and non-competitive modes of inhibition display a linear relationship between inhibitor concentration and the inverse of the initial rate. The Dixon plot for CPA inhibition by glutathione shows a dramatic decrease in activity as GSH concentration increases above 1 mM.

Figure 46: Dixon plot of CPA inhibition by GSH. Peptidase activity measured at 265 nm using 0.54 mM HP in 25 mM Tris buffer, 0.5 M NaCl, pH 7.5, containing 3.5% EtOH (v/v), at 25°C. E_o=120 nM

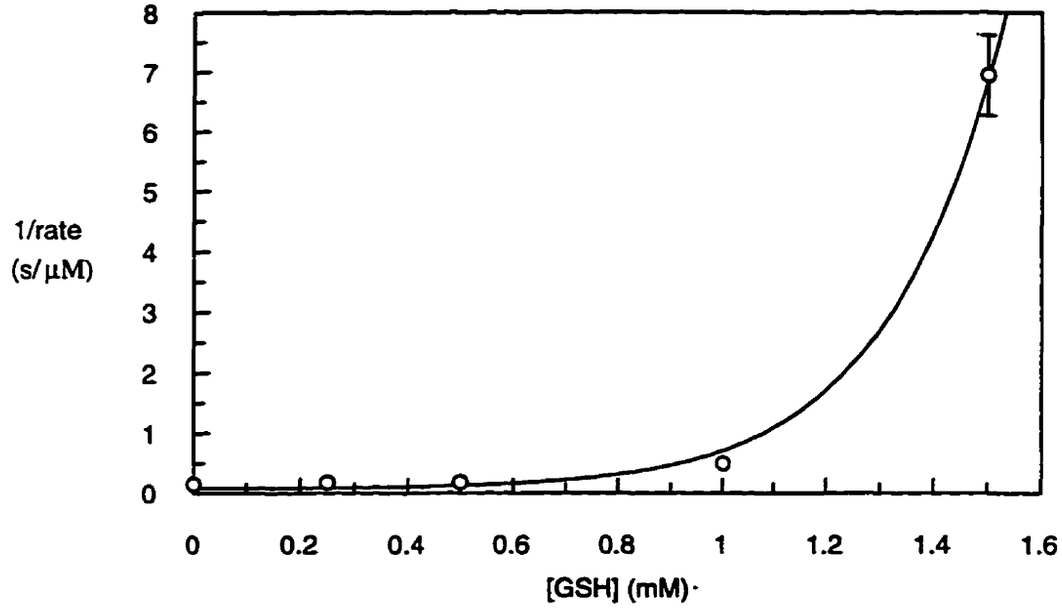

Each data point is the average of three or more separate determinations, shown with standard error bars. Error bars smaller than the symbols are not shown. For the graphical presentation, the data was fitted to a single exponential function.

A similar, apparently parabolic, relationship has been observed in this laboratory for the Dixon plot associated with the inhibition of CPA peptidase activity by the metal chelating agent *o*-phenanthroline (OP) (Figure 47), although the inhibition by OP required preincubation with the enzyme. Vallee and coworkers[95] have demonstrated that inhibition of CPA by OP is accompanied by removal of the catalytically essential

zinc ion from the active site. This observation is consistent with an inhibition mechanism in which two inhibitor molecules bind to the catalytic site, departing, eventually, as a bis-adduct with the metal ion, to leave behind a catalytically inactive apoenzyme (Scheme 42).

Figure 47: Dixon plot of CPA inhibition by 1,10-phenanthroline (OP). Peptidase activity measured at 265 nm using 0.5 mM HP in 25 mM Tris buffer, 0.5 M NaCl, pH 7.5, containing 3.5% EtOH (v/v), at 25°C. E_o=200 nM.

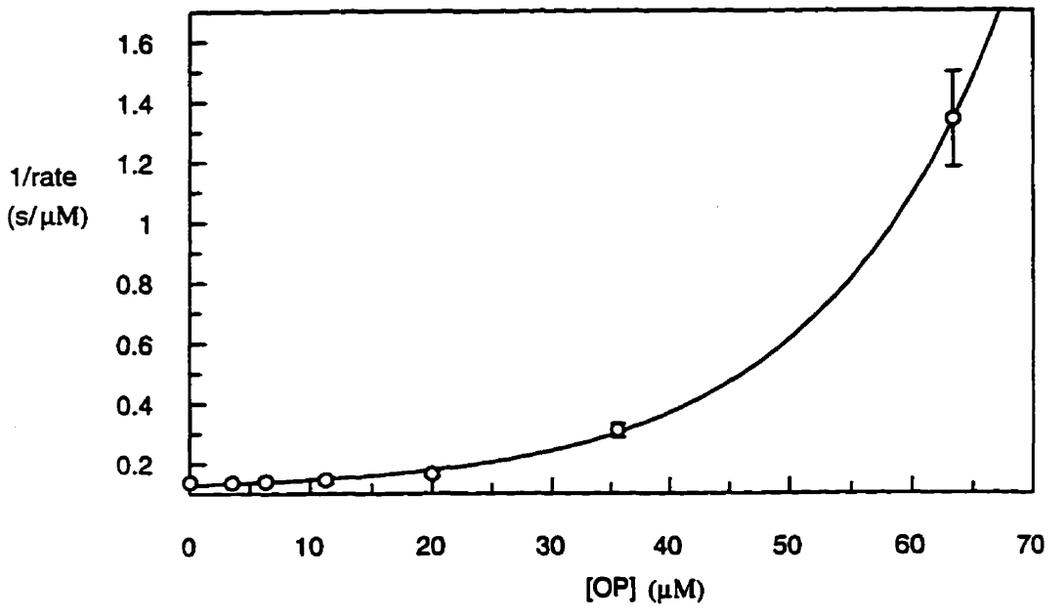

Each data point is the average of three or more separate determinations, shown with standard error bars. Error bars smaller than the symbols are not shown. For the graphical presentation, the data was fitted to a single exponential function.

Scheme 42

$$\text{E-M} \overset{\text{I}}{\rightleftharpoons} \text{E-M-I} \overset{\text{I}}{\rightleftharpoons} \underset{\text{I}}{\text{E-M-I}} \rightleftharpoons \text{E' + I-M-I}$$

Such dual binding by the inhibitor would explain the apparently parabolic relationship between $1/\upsilon_{app}$ and [I]. A similar inhibition mode for glutathione is feasible. Glutathione has been shown to bind Zn^{2+} as well as other metals which are free in solution,[188] but it must be noted that no experimental evidence regarding the removal of the metal ion by GSH from an active site is available.

In any event, it was clear that concentrations of GSH below 1 mM result in negligible inhibition of peptidase activity. For the present study of inhibition of CPA by the thiol **35**, a GSH concentration of 0.1 mM was chosen.

2.2.7 Inhibition of CPA by Free Thiol 35

Our initial analysis of **35** as an inhibitor of CPA in the presence of GSH revealed **35** to be a tight-binding inhibitor. The peptidase activity of CPA was greatly affected by **35** at concentrations equal to that of CPA. With both CPA and **35** at 113 nM, and HP and GSH at 0.5 mM and 0.1 mM respectively, the rate of HP hydrolysis was observed to be 35% of that observed in the absence of **35**. Peptidase activity was monitored at inhibitor concentrations of 0 nM, 56.5 nM, 87 nM and 113 nM (I_o/E_o of 0, 0.5, 0.75 and 1.0), with HP concentration varying 0.25 mM to 1.3 mM. As shown in Figure 48, the thiol **35** seems to inhibit in a competitive fashion. There is substantial inhibition at I_o concentrations equal to or less than E_o, suggesting that **35** is a tight-binding inhibitor. The simple fitting of initial rate data for such an inhibitor to the Michaelis-Menten relationship (2.16) cannot be used to accurately determine the inhibition constant K_i.[189] In such cases the assumption that the free inhibitor concentration [I] corresponds to the total inhibitor concentration $[I]_o$ which is made in the derivation of equation 2.16 is not valid.

$$v_A = \frac{E_o k_{cat}^A [A]}{[A] + K_m^A (1 + [I]/K_I)} \qquad (2.16)$$

Figure 48: Double reciprocal relationship between CPA peptidase activity and HP concentration in the presence of **35** in 25 mM Tris buffer, 0.5 M NaCl, pH 7.5, containing 3.5% EtOH (v/v), at 25°. E_o=113 nM.

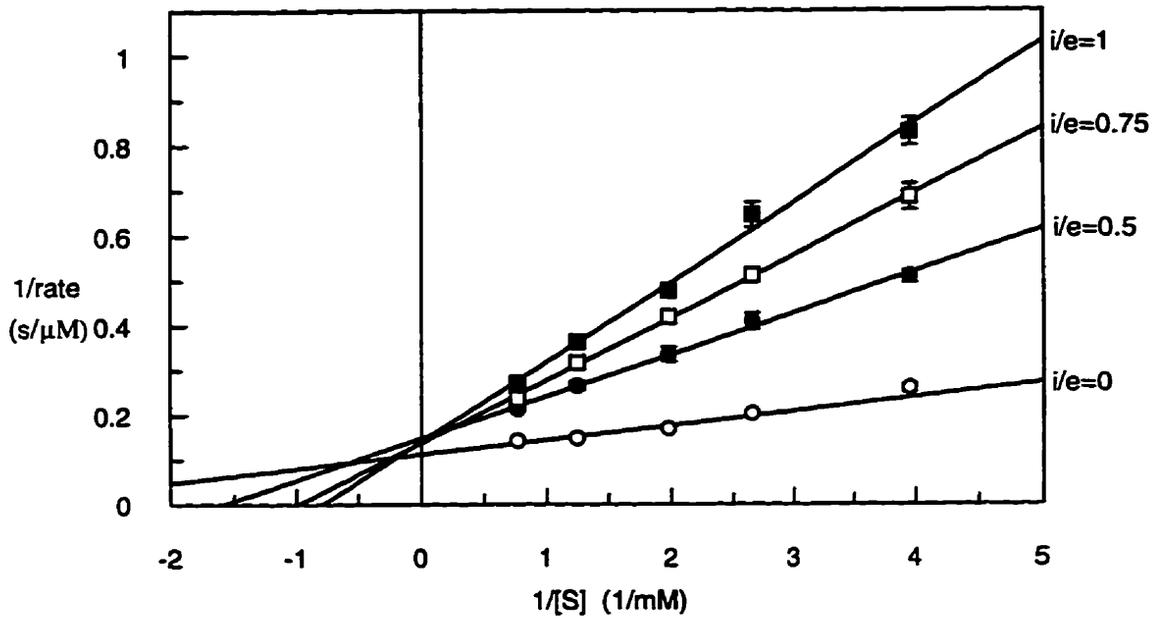

Each data point is the average of four or more separate determinations, shown with standard error bars. Error bars smaller than the symbols are not shown.

Cushman,[147] while studying the inhibition of tight-binding inhibitor **36**, overcame this problem by maintaining the relationship of $I_o >> E_o$ with an E_o of 1.4 nM and I_o ranging from 10 nM to 100 nM. The very low rates observed under these conditions were measured by allowing assays to run for up to 1 hr. In our studies, we made use of Dixon's graphical method[189] for which the relationship $I_o >> E_o$ is not a

requirement (see Appendix C for details on the Dixon graphical method). From this method, we determined a K_i of 12.6±1.0 nM for the thiol **35**. This value is close to the value of 7.8 nM which was reported for (S)-**36**[149], the homologue of **35**.

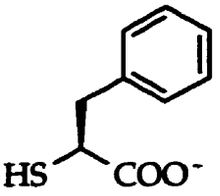

35

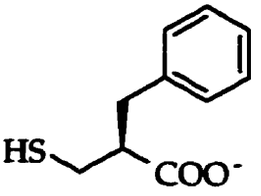

36

Our observation of **35** as a tight-binding inhibitor of CPA was surprising considering the structure of the other tight-metal-binding inhibitors of CPA (Figure 49). The tight-binding of phosphonate inhibitors **82** (CBZ-Ala-Ala^P-Phe), CBZ-Phe-Ala^P-Phe and CBZ-Phe-Val^P-Phe[76,141] to CPA have been studied using x-ray crystallography[36,69]. These inhibitors were observed to bind to CPA in the "closed" conformation with Tyr-248 in its "down" position. The phenyl groups are positioned deep into the S_1'-subsite. There is a salt bridge between Arg-145 and the carboxylate of the inhibitor and an important interaction between the active site Zn^{2+} and metal-binding phosphonate of the inhibitor. These interactions are similar to those proposed for the binding of substrates and other inhibitors as well.[40,64] X-ray crystallographic analysis has revealed that the inhibitor **83**[190], which incorporates metal binding sulfodiimine group, binds in a similar way.[68] The mercapto inhibitor **36** was expected to bind to the CPA active site in the same fashion.[147,150,151] This leads to the simple observation that **35** is unlike the other tight-binding inhibitors in that it incorporates a metal binding-site which is at a shorter distance from the carboxylate group. The competitive inhibition of CPA by thiol inhibitors is known to involve an important strong interaction between the active site Zn^{2+} and the sulfur atom of the inhibitor.[97,146] In order for the sulfur-Zn^{2+} interaction to occur for **35**, the rest of the

molecule could not bind in the same way in which the other tight-binding inhibitors bind. The carboxylate of **35** would be further from the Arg-145, and the phenyl group could not bind deep into the hydrophobic pocket of the S_1'-subsite.

Figure 49

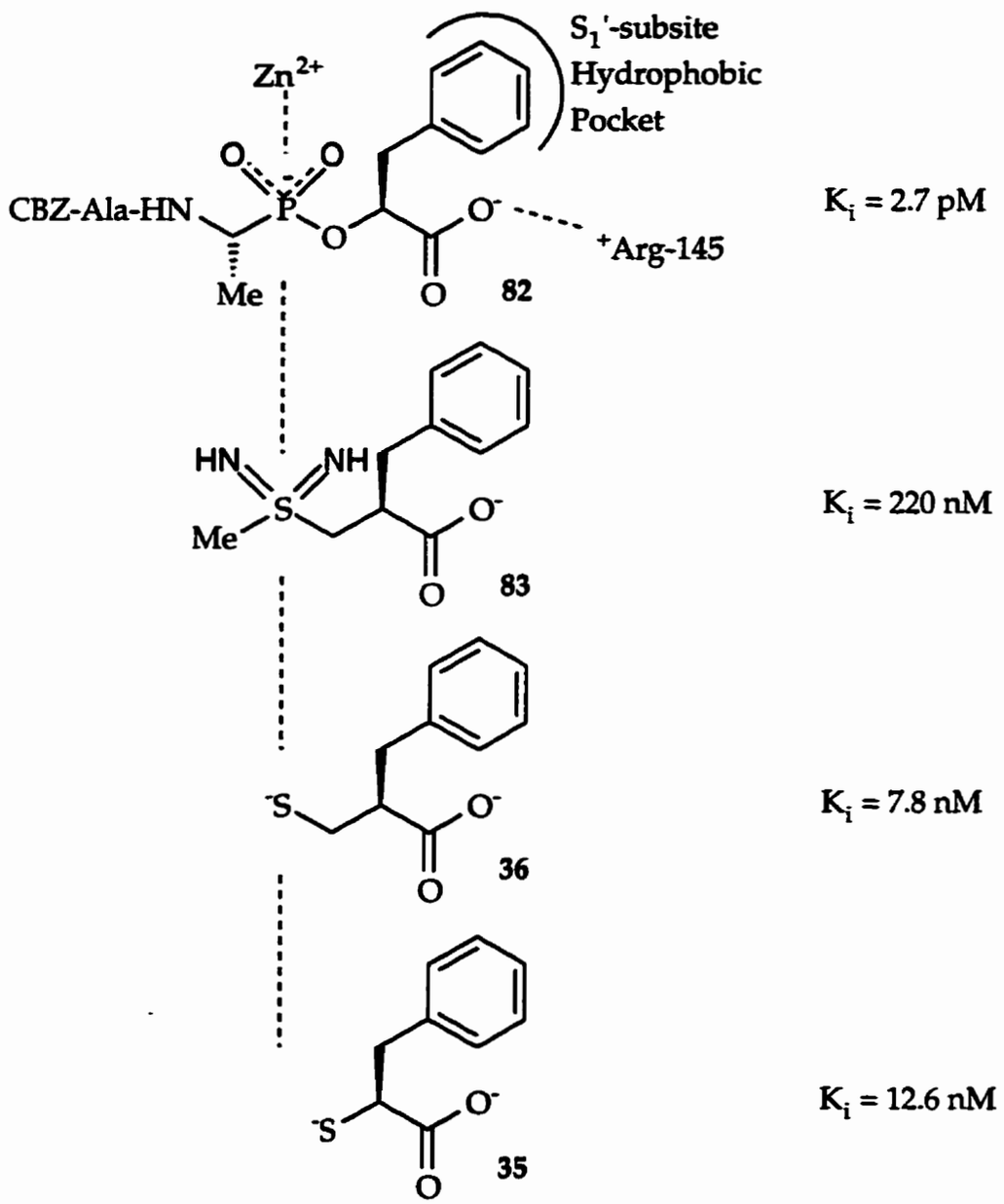

The discovery that the thiol **35** (K_i=12.6 nM) was actually comparable in potency to its homologue **36** (K_i=7.8 nM) was also surprising given the current thinking concerning the binding of **36** to the active site of CPA. The thiol **36** was designed by Ondetti and Cushman[147] based on the assumption that the distance between the metal binding center, the thiol in this case, and the carboxylate group should approximate that in the substrate or putative tetrahedral intermediate involved in the catalytic process. It was reasoned that such a spatial arrangement would allow for a tight complex between the metal ion and the thiol group while simultaneously retaining the favourable interaction of the benzyl side chain with the hydrophobic pocket of S_1' and the favourable electrostatic contact of the carboxylate group with Arg-145. The lower potency of the thiol **35** which was reported by Vallee and coworkers[97] was understandable in terms of this analysis since the shorter distance between the thiol, the hydrophobic side chain and the expected to result in a poorer interaction of both the side chain and the carboxylate group with the active site of CPA when the thiol was ligand to the zinc ion.

The inhibitor **84**, which inhibits the endopeptidase thermolysin with a K_i of 750 nM,[191] was observed using x-ray crystallography to bind to thermolysin through the expected Zn^{2+}-S interaction (Figure 50).[154] Thiol **84** also contains the methylene extension between the α-carbon and the thiol group which is present in **36**.

In order to gain some insight into a possible model for binding of **35** to CPA which would help to explain the unexpectedly high potency of this thiol inhibitor, an analysis of the available x-ray crystallography data for native CPA[24,28,29] and for CPA-bound to inhibitors[25,26,30,33,34,35,36,37,41,64,65,68,69,71,134,137,192] and to products[61,62] was conducted. As previously mentioned in Chapter 1, CPA has been found to exist in two main conformations. The open conformation is one in which the side chain of Tyr-248 is found in the "up" position, where the hydrophobic S_1' subsite pocket is

open for easy access to substrates or inhibitors. There is a water molecule bound to the active site zinc. The other conformation observed for CPA is one in which the enzyme is bound to inhibitors, substrates or products. In this conformation, the Tyr-248 side chain is oriented in a "down" position, where the hydrophobic S_1' subsite pocket is closed around the hydrophobic moiety of the complexed inhibitor, substrate or product.[40] The whole polypeptide region 247-249 has been observed to move 1 to 2 Å upon inhibitor binding. Other observed conformational changes involve Arg-145, Arg-127, and Glu-270, which move to adapt to and to participate in the binding of the inhibitor or substrate. In the CPA-inhibitor complexes the Zn^{2+} bound H_2O found in native CPA is observed to be displaced by the metal coordinating groups of the inhibitors.

Figure 50

Thermolysin

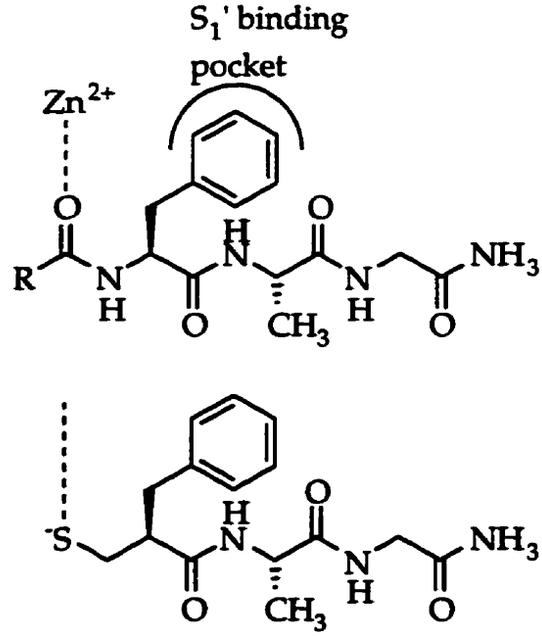

It was reasoned that, in order for **35** to bind tightly, there must be a Zn^{2+}-S interaction, an interaction between the carboxylate of **35** and a positively charged group in the active site, and finally, some hydrophobic interaction to stabilize the binding of the phenyl group. Using molecular modeling, **35** was modeled and docked into the active site which was in the "down" position.

First, a molecular model of the inhibitor **35** was constructed using the commercial molecular modeling software SYBYL™ (Tripos Associate Inc.), which incorporates the MAXIMIN2 force field for molecular mechanics-based energy minimization. This model was then docked manually into the active site as defined by the x-ray crystallographic coordinates for the complex of CPA with **83** (Brookhaven Protein Data Bank entry pdb1cps.ent).[8,190] The binding geometry of the inhibitor **83**, which was removed from the model for the purpose of this modeling exercise, was used as a guide to define a starting geometry for the energy minimization of the complex between **35** and CPA. Since the MAXIMIN2 force field does not incorporate force constants to describe a Zn^{2+}-S interaction, this interaction was defined by placing distance and angle constraints on the length of the Zn^{2+}-S bond and on the Zn^{2+}-S-C_α bond angle. The constraints chosen were based on the geometry typically found for Zn^{2+}-S interactions between the sulfur of cysteine residues and Zn^{2+} found in zinc fingers as studied by 2D NMR techniques[193]. (More details of this computational exercise are presented in Appendix D). Energy minimization of this complex was carried out using the Anneal function within SYBYL™ in which the "hot" region (the region to be subject to geometry optimization) included **35** and the active site residues of CPA.

A similar analysis was carried out for **36**, the homologue of **35**. As indicated in Figures 51 and 52, the model of the complex between CPA and **36** which emerged from this analysis exhibits strong contacts between the sulfur atom of **36** and the zinc ion of CPA, as well as between the carboxylate group of the inhibitor and the

guanidino group of Arg-145. In addition, the hydrophobic side chain of **36** is docked well into the hydrophobic pocket of the S_1' subsite.

In the case of the model constructed for the complex between **35** and CPA, strong interaction between the sulfur atom of the inhibitor and the zinc ion of the enzyme is achieved at the expense of the strong hydrophobic contact of the side chain with the S_1' subsite (see Figure 51 and 53). In particular, the para-carbon atom of the phenyl group of **35** is 2.1 Å further from the hydrophobic pocket than the same atom in the complex of **83** with CPA.

This modeling exercise reveals, however, that the active site of CPA may adapt to the structural differences between **35** and **36** in such a way as to affect the loss of binding energy which would be expected to accompany the diminished hydrophobic contact. In particular, the side chains of both Arg-145 and, most interestingly, Arg-127 are predicted to take up conformations modified so as to allow for strong contacts to the carboxylate group of **35**. It is reasonable to propose that the electrostatic and H-bonding contact between the carboxylate group of **35** and Arg-127, which is not present in the complex of **36** with CPA, may be responsible for the potency of this inhibitor.

Figure 51: Resulting CPA-36 and CPA-35 complex geometries after energy minimization. Distances are in Å.

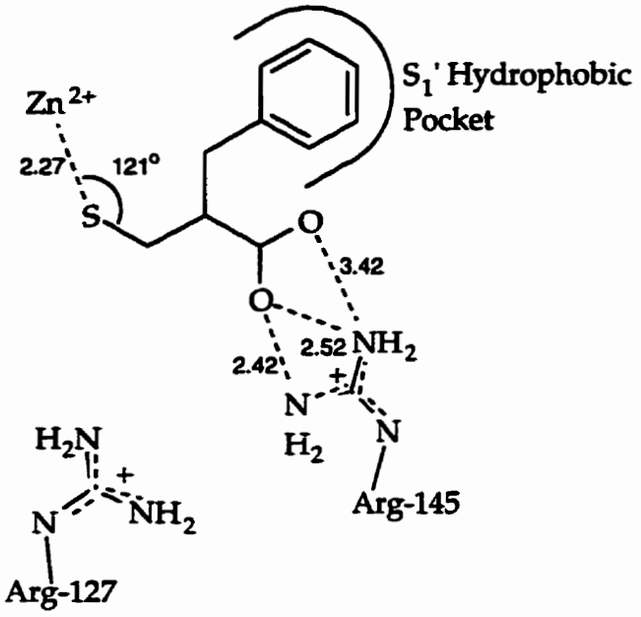

CPA-36

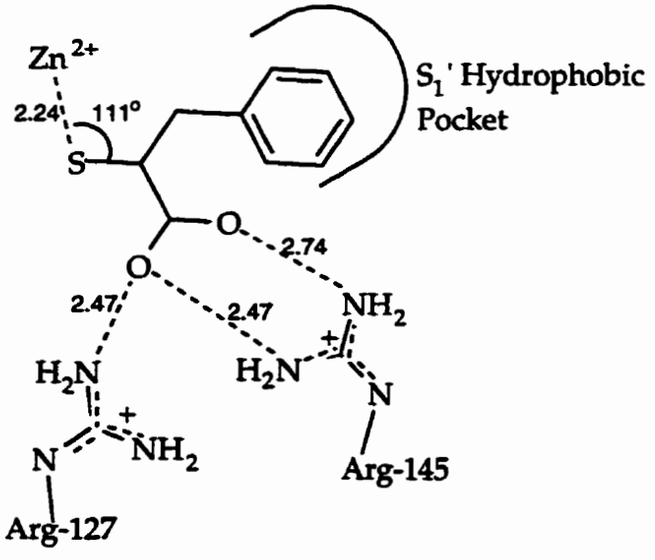

CPA-35

Figure 52: Predicted binding of 36 to CPA active site.

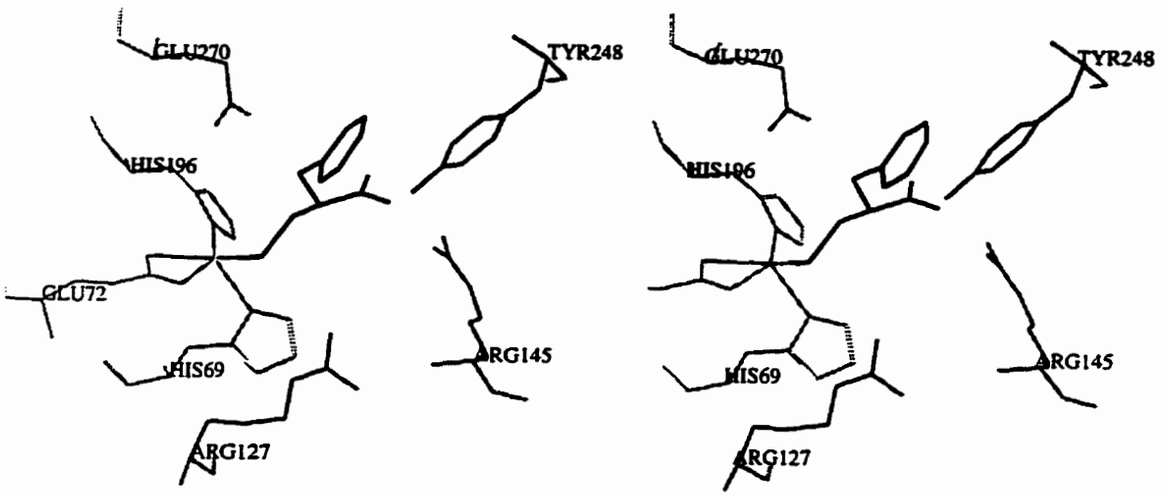

Figure 53: Predicted binding of 35 to CPA active site.

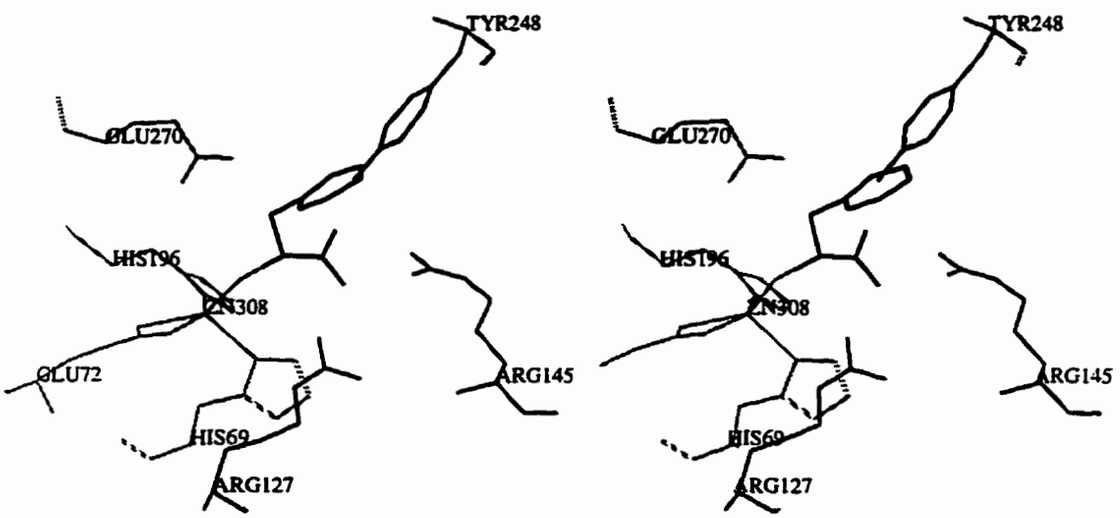

That the side chains of Arg-127 and Arg-145 do have some conformation flexibility is indicated by the observation that the crystal structures of the complexes of CPA with a variety of other inhibitors do exhibit some variations in the conformations of these essential active site residues.[33,36,64,65,68,69] This proposed binding mode for **35** differs substantially from that established by an x-ray crystallographic study for β-phenyllactate.[61] β-Phenyllactate, which is a much weaker inhibitor of CPA than is **35**, is found to bind to the active site with the side-chain of the inhibitor well within the hydrophobic pocket in the S_1' subsite and the carboxylate group in contact only with Arg-145. The interaction with the zinc ion is indirect, involving a hydrogen bond from the α-hydroxyl group of the inhibitor and a water molecule bound to the zinc ion as well as to Glu-270. While it might be argued that **35** could bind in an analogous fashion, this binding mode could not explain the much higher potency of **35** relative to L-β-phenyllactate. In fact, the poor H-bond acceptor properties of a thiol group would lead one to expect that the H-bond between **35** and a zinc-bound water molecule would be much weaker, rather than stronger, than observed with L-β-phenyllactate.

2.2.8 Mechanism-Based Inhibition of CPA by the Thioester Substrate Analogue (S)-50

Once (S)-**50** had been shown to be hydrolyzed by CPA and the free thiol product **35** had been demonstrated to be a tight-binding inhibitor, it was of great interest to follow up on the original goal of evaluating (S)-**50** as a mechanism-based inhibitor. Again, GSH was employed to protect the catalytically released free thiol **35** from oxidation. Initial experiments with and without GSH showed the advantageous effect of the presence of GSH on the inhibition of CPA by (S)-**50** (Figure 54). In the

absence of GSH, after 5.2 min on the progress curve, 4.3 μM of (S)-**50** was hydrolyzed giving 2.2 μM of the disulfide **73**. Under these experimental conditions, the presence of 2.2 μM **73** with a K_i of 3.5 μM would have an expected minor effect on the rate of (S)-**50** hydrolysis (calculated 10% decrease in rate). On the other hand, in the presence of GSH, strong inhibition by the thiol **35** is clearly evident with only 1.5 μM of the thioester having been hydrolyzed at time 5.2 min.

Figure 54: Hydrolysis of (S)-**50** (58.5 μM) by CPA (1.5 μM) in 0.1 mM GSH (**A**) and no GSH (**B**), in 25 mM Tris buffer, 0.5 M NaCl, pH 7.5, containing 3.5% EtOH (v/v), at 25°.

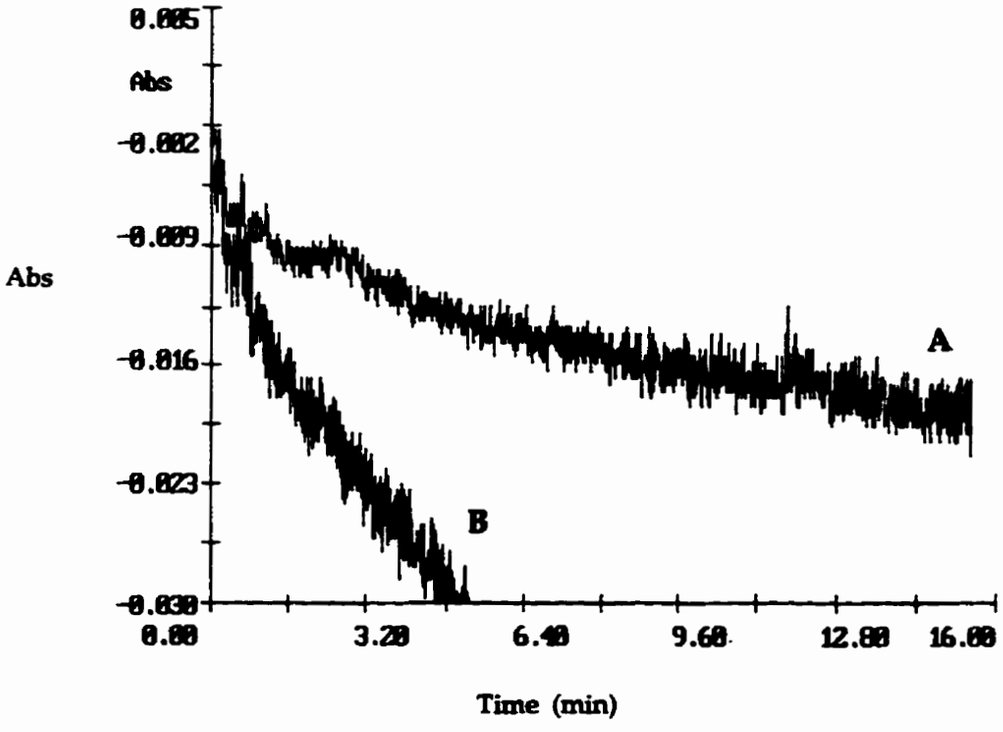

Attention was then turned to the study the potency of (S)-**50** as a mechanism-based inhibitor of CPA peptidase activity. The present investigation was modeled after the standard strategy for studying mechanism-based inhibition as defined by Silverman.[159] In these experiments, which are graphically outlined in Figure 55, CPA (137 nM) is incubated with (S)-**50** at I_o/E_o ratios of 0, 7 and 70, in 0.1 mM GSH, 25 mM Tris buffer, 0.5 M NaCl, pH 7.5, containing 3.5% EtOH (v/v), at 25°. Residual peptidase activity was determined by periodically withdrawing aliquots from the incubation mixtures and mixing with HP to monitor peptidase activity at 265 nm.

Figure 55

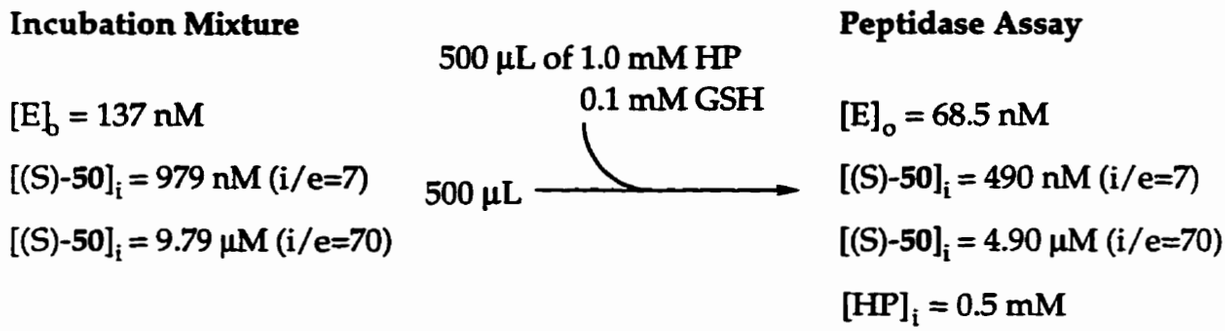

Figure 56: Inactivation of CPA by incubating with (S)-**50** in 0.1 mM GSH, 25 mM Tris buffer, 0.5 M NaCl, pH 7.5, containing 3.5% EtOH (v/v), at 25°. The incubation mixtures contain 137 nM CPA with concentrations of (S)-**50** of 0, 979 nM and 9.79 μM. Peptidase activity was determined at 265 nm at 25° after mixing 500 μL of the incubation mixture with 500 μL of 1.0 mM HP in 0.1 mM, 25 mM Tris buffer, 0.5 M NaCl, pH 7.5.

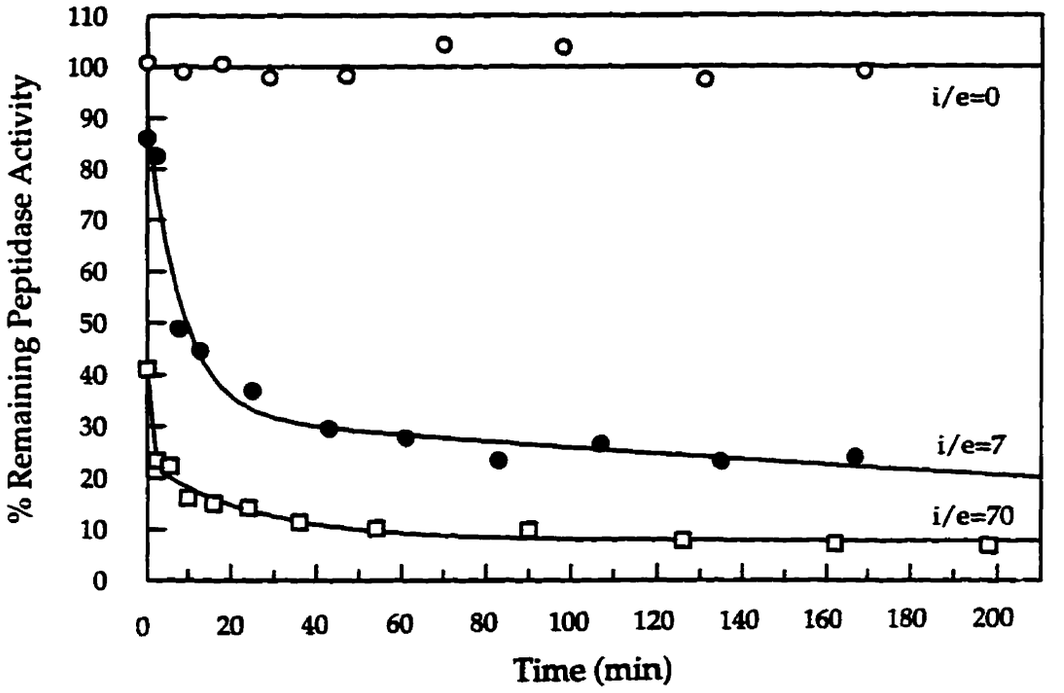

The data points for i/e=0 were fitted to linear regression to give the control curve. The solid traces through the data points for i/e=7 and i/e=70 correspond to double exponential functions fitted to the data using Grafit 3.01 and are presented for ease of visualization of the data only, since no kinetic model predicting a double exponential relationship has been established. The rates reported above are expressed as the percent residual activity of the expected rate from the control curve.

As shown in Figure 56, there is a dramatic loss in peptidase activity of CPA in the first 10 min of incubation, with a loss of 53% peptidase activity in the i/e=7 incubation and a loss of 84% peptidase activity in the i/e=70. After the first 10 min of incubation the rate of inactivation begins to slow down considerably, with the rate of inactivation becoming quite slow in the last 150 min of the incubations. The slow rate of inactivation following the initial 10 min of the incubations is undoubtedly a consequence of the concentration of **35** which inhibits further release of thiol by CPA catalyzed hydrolysis of (S)-**50**. From the inhibition of thioesterase activity, we would expect incomplete hydrolysis of the thioester substrate. In both cases of i/e=7 or i/e=70, complete hydrolysis of all (S)-**50** in solution did not occur during the time of this experiment. There is a difference between the observed peptidase activity and that expected if all of (S)-**50** had been completely hydrolyzed to **35**. In the case of i/e=70, with the [**35**] and [HP] at 4.9 μM and 0.5 mM respectively, and a K_m=0.31 mM, k_{cat}=85.7 s^{-1}, K_i(**35**)=12.6 nM and $[E]_o$=68.5 nM, the expected peptidase rate would be 23.0 nM/s. The actual peptidase rate was observed to be 295 nM/s. In the case of i/e=7, with the [**35**] at 490 nM, the expected peptidase rate would be 218 nM/s. The actual peptidase rate was observed to be 1030 nM/s.

UV spectroscopy was used to further support the conclusion that thioester hydrolysis was incomplete. After 170 min of incubation, the I_o/E_o=70 solution gave a total loss of absorbance of 0.016, whereas the expected loss of absorbance, based on the known $\Delta\varepsilon_{273}$, would be 0.068 if the hydrolysis of (S)-**50** was complete. As a result of the low absorption of the I_o/E_o=7 mixture, it was not possible to measure the loss of (S)-**50** in such experiments.

In both experiments, the last 150 min of the progress curves showed a very slow rate of decrease of peptidase activity even though (S)-**50** was not completely hydrolyzed. This can be explained by simple product inhibition by the already released **35**. In the case of the I_o/E_o=70 experiment, the rate of hydrolysis of HP in the

peptidase assay at the 198 min point was 295 nM/s. From this value we can estimate the amount of **35** in solution. The equation 2.13 represents the rate of HP (A) hydrolysis in the presence of the competitive substrate (S)-**50** (B) and the inhibitor **35** (P).

$$v_A = \frac{k_{cat}^{A} E_o [A]}{[A] + K_m^{A}\left(1 + \frac{[B]}{K_m^{B}} + \frac{[P]}{K_i^{P}}\right)} \qquad (2.13)$$

For this calculation, the inhibition of CPA activity by the competitive substrate (S)-**50** must be taken into consideration. As mentioned earlier, the overall loss of (S)-**50** concentration at this point was considered to be small, and the observed peptidase rate was more than 10 times greater than the peptidase rate expected for total (S)-**50** hydrolysis to **35**. The expression in equation 2.13 can rewritten so that [B] is represented by $[B]_o$-[P].

$$v_A = \frac{k_{cat}^{A} E_o [A]}{[A] + K_m^{A}\left(1 + \frac{[B]_o - [P]}{K_m^{B}} + \frac{[P]}{K_i^{P}}\right)} \qquad (2.17)$$

where

$[A]$ ($[HP]$) = 5×10^{-4} M
$[B]_o$ ($[(S)\text{-}50]$) = 4.90×10^{-6} M
$K_m^{A} = 3.12 \times 10^{-4}$ M
$k_{cat}^{A} = 85.7\ s^{-1}$
$K_m^{B} = 6.18 \times 10^{-5}$ M
$K_i^{P} = 1.26 \times 10^{-8}$ M
$[E]_o = 6.85 \times 10^{-8}$ M
v_A (observed rate) = 2.95×10^{-7} M/s

The [P] value (concentration of **35**) was calculated to be 368 nM (in the peptidase assay), whereas the concentration of **35** in the incubation mixture would be 736 nM. The [B] would therefore be 9.79 μM - 0.736 μM = 9.054 μM. Therefore, in the incubation mixture, we can calculate the expected rate of (S)-**50** hydrolysis:

$$\upsilon_B = \frac{k_{cat}^{\ B}\, E_o\, [B]}{[B] + K_m^{\ B}\left(1 + \frac{[P]}{K_i^{\ P}}\right)} \qquad (2.18)$$

where
$[P]$ ([**35**]) = 7.36×10^{-7} M
$[B]$ ([(S)-**50**]) = 9.07×10^{-6} M
$K_m^{\ B} = 6.18\times10^{-5}$ M
$k_{cat}^{\ B} = 1.53\times10^{-2}\ s^{-1}$
$K_i^{\ P} = 1.26\times10^{-8}$ M
$[E]_o = 1.37\times10^{-7}$ M

The expected rate of (S)-**50** hydrolysis was calculated to be 5.2 pM/s, which is 1.8% of the expected thioesterase activity in the absence of **35**.

A similar calculation was done for the last peptidase measurement for the i/e=7 incubation assay as well. At time=167 min, the peptidase rate was observed to be 1.03 μM/s. Using equation 2.17, the concentration of **35** in the incubation mixture was calculated to be 165 nM. At this [**35**], the concentration of unhydrolyzed thioester (S)-**50** was determined to be 814 nM, and the expected rate of thioester hydrolysis was calculated to be 1.96 pM/s (using equation 2.18). This rate is 6.72% of the expected rate if **35** was absent from the solution. In both cases, the i/e=70 and the i/e=7 incubations, the rates of release of **35** are expected to be very low during the tail end of the incubation experiments, especially relative to the rate of **35** release which is observed at the initial 10 min of the incubation. Slow rates of thioester hydrolysis past

the 50 min time during the incubations explain the slow rate of inactivation which are observed (Figure 56).

2.2.9 Summary and Conclusions

The observation that the thioester (S)-**50** is a potent time-dependent inhibitor for CPA demonstrates the validity of the type of mechanism-based metalloenzyme inhibitor defined in Section 2.0.1. In particular, (S)-**50** is a masked metal-binding inhibitor which is converted into a very potent reversible inhibitor capable of binding tightly to the active site metal ion in CPA upon CPA-catalyzed hydrolytic removal of the acyl group which masks the metal-binding thiol group.

In this laboratory, this process has been considered to be a form of mechanism-based inhibition. It is worth pointing out, however, that the inhibition of CPA by (S)-**50** does not fit the definition of mechanism-based inhibition which has been proposed by Silverman.[159] According to Silverman[159], the classical definition for "mechanism-based inactivation" is a process in which the target enzyme catalyzes the conversion of the "mechanism-based inhibitor" into a very reactive species which remains in the active site to inactivate the target enzyme. This inactivation may result from covalent modification of the active site or result from a tight reversible complex between the inactivator and the target enzyme. In the present study, it has been shown that the mechanism by which the thioester (S)-**50** inactivates CPA differs from this definition. As discussed at the end of Section 2.1.7, the activated species, which is the thiol **35** in this case, is actually a tight-binding reversible inhibitor which leaves the active site following thioester hydrolysis, and returns to bind in a high affinity reversible complex (EP_1'), as shown in Figure 57. This enzyme-product complex differs from the enzyme-product complexes which are formed during the mechanism of hydrolysis of (S)-**50**. As mentioned earlier, the dissociation of products during the hydrolysis of (S)-

50 and **51** is thought to involve a mechanism in which the conjugated base of the acid product is the last to leave the active site (Path A in Scheme 38c on pg 108), so that an (S)-**35**-CPA intermediate does not occur.

Figure 57

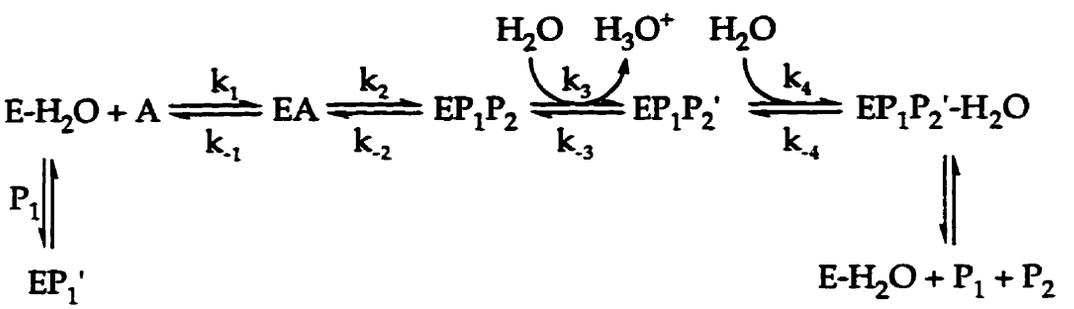

-where A is (S)-**50**
P_1 is **35**
P_2 is benzoate

As a consequence of the actual inhibition mechanism of (S)-**50**, we cannot classify the thioester as a "mechanism-based inactivator", by Silverman's definition. Silverman has argued further that an inhibitor which is enzyme activated but produces an inactivator which leaves the active site prior to inactivation, should be classified as a "metabolically activated inhibitor" and is more likely to be a non-specific inhibitor once activated, than are true "mechanism-based inhibitors". Silverman's analysis presupposes that activation leads to release of a reactive functionality not designed to possess specificity for the active site of the target enzyme. Such a characterization would not apply to (S)-**50** which releases **35** which in itself possesses structural features, in addition to the "reactive" site (the thiol group) which result in substantial specificity for the active site of the target enzyme. It is

suggested that a term such as "target enzyme activated inhibitor" might more accurately describe inhibitors such as (S)-**50**.

The conclusions arising from the pre-steady state and steady state kinetic analysis of the hydrolysis of the thioester (S)-**50** and the ester **51** described above, which are summarized in the kinetic mechanism shown in Figure 57 and in the molecular mechanism shown in Figure 38 (pg 106-108), can be employed to suggest possible strategies for improvement in the design of modified versions of the inhibitor (S)-**50**. Our data suggests that the carboxylate derived from the hydrolysis of the thioester is the second product to depart the active site. The thiol **35**, which is likely released prior to the carboxylate, then binds to the free enzyme which is generated upon carboxylate release. In this mechanism the thiol product does not achieve a strong interaction with the zinc ion during the catalytic cycle since the carboxylate is liganded to the metal during catalysis. We have argued also that this order of product release may arise in the case of (S)-**50** and **51** as a consequence of the steric properties of the benzoyl group which inhibits the hydration of the zinc-carboxylate product complex which must occur before release of the carboxylate product. This hypothesis is consistent with all of our data and also may explain the data of others who observed very similar kinetic parameters for the hydrolysis of esters of mandelate and β-phenyllactate which possess the same acyl group but different alcohol leaving groups (see pg 112).[53] If this hypothesis is correct, it is logical to argue that modification of (S)-**50** such that the acyl group is not as sterically bulky, may alter the order of product release such that the carboxylate may depart before the thiol. If this were achieved, the thiol would have the opportunity to form a tight complex with the active site zinc ion before being released into solution. Such a modified thioester would then fall within the definition of mechanism-based inhibitors presented by Silverman. Regardless of whether or not a reversal of the order of product release is achieved, it is clear that structural alterations of (S)-**50** to improve the rate of

hydrolysis, for example by making the rate of the actual hydrolytic step rather than the product release step more rapid, will improve the effectiveness of this inhibition strategy. A more readily hydrolyzed thioester would lead to a more rapid approach to complete enzyme inhibition. For example, the fact that N-benzoylphenylalanine and O-benzoylphenyllactate (**51**), which are amide and ester analogues of (S)-**50**, are both known to be much poorer substrates for CPA[7,17,64] than hippurylphenylalanine[182] (**85a**) or hippurylphenyllactate[14,185] (**85b**) suggests that the thioester **85c** should be a more effective target enzyme activated inhibitor for CPA.

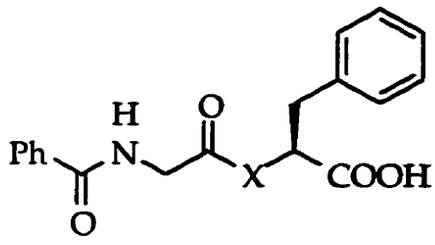

85a (X=NH)
85b (X=O)
85c (X=S)

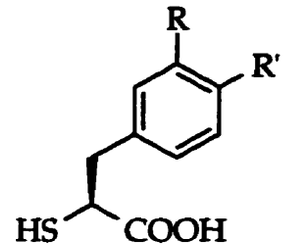

85d (R=OH, R'=H)
85e (R=OMe, R'=H)
85f (R=R'=Me)

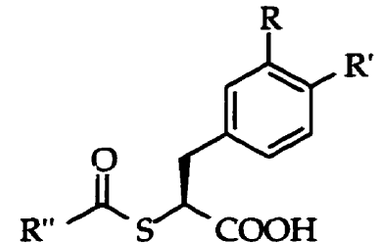

85g

In terms of possible improvements in the inhibitory potency of the thiol product of thioester hydrolysis, consideration of the observations made in this study concerning the likely binding made of the thiol **35** in the activity of CPA. In the model described in Section 2.2.7 for the binding of **35** to CPA, it was pointed out that the aromatic ring of **35** is only partially inserted into the S_1' subsite in the enzyme. Closer inspection of this model leads to the suggestion of structural alternations of **35** which might enhance the potency of this thiol inhibitor. For example, it is proposed that structures such as **85d** and **85e** where R=OH or OCH_3 respectively might be constructed. The hydroxyl or ether group of such compounds would be positioned, according to our model, such that an hydrogen bond could be formed with the side-

chain hydroxyl group of Thr-268 acting as a hydrogen bond donor in the S_1' subsite. Alternatively, methyl substituents in the *meta* and/or *para* positions (eg. **85f**) might result in greater favourable van der Waals contact with the relatively hydrophobic S_1' subsite amino acid residues.

The possibility that such alterations would have a deleterious effect on the behaviour of the corresponding thioesters, **85g**, would, however, need to be considered if such structural modifications are to be incorporated into a target enzyme activated inhibitor for CPA.

Although the directions for possible improvements in the inhibition strategy for CPA were relatively clear as defined above, attention in this project was turned to the related therapeutically important target enzyme, ACE.

Chapter 3:
Results and Discussion

3.1 Mechanism-Based Inhibition of Angiotensin Converting Enzyme by Thioester Substrate Analogues

Once the thioester substrate analogue model **50** had been proven to be an effective mechanism-based or target enzyme activated inhibitor for CPA, it was decided the strategy should be applied to a therapeutically important metalloprotease such as angiotensin converting enzyme (ACE). As mentioned in Section 1.5, ACE is an important pharmaceutical target and has been the subject of many inhibition studies as a consequence of its important role in blood pressure regulation.[90] Although a crystal structure has never been determined for ACE, its active site is considered to be structurally similar to that of CPA.[92,113] This Zn^{2+}-dipeptidyl carboxypeptidase cleaves dipeptides from the C-terminal end of peptides, including the natural peptides angiotensin I and bradykinin.[89] It was necessary that thioester substrate analogues contain the thioester linkage in the appropriate scissile position (Figure 58) in order to inhibit ACE in a fashion analogous to the inhibition of CPA by **50** described above. ACE was known to show no activity toward N-acyl-dipeptides, and low activity toward tripeptides with a free N-terminal amino group.[102] The N-acyl-tripeptides are known to be good substrates for ACE, and were thus judged to be appropriate structures to mimic (Figure 58).

As mentioned in Section 1.5, ACE exhibits a much broader substrate specificity than other metalloproteases.[99] In determining which residues would be best in the P_1, P_1' and P_2' positions, both the substrate specificity of the thioester-tripeptide analogue and the binding specificity of the free thiol dipeptide analogue must be taken into consideration.

Figure 58

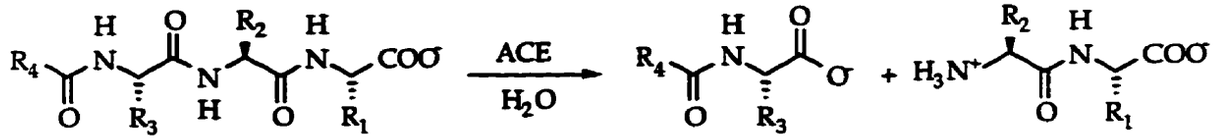

N-acyl-tripeptide

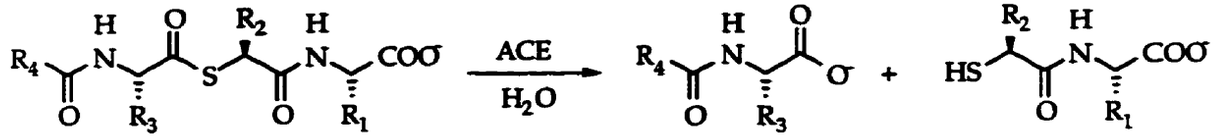

P_1 P_1' P_2'

Thioester-tripeptide analogue

Free thiol dipeptide analogue

As mentioned earlier in Chapter 2, in order for a thioester substrate analogue to act as a good mechanism-based inhibitor, the thioester substrate must be recognized as a substrate by the target enzyme so that the thioester linkage is hydrolyzed. Also, importantly, the thiol product produced during the hydrolysis must be a good inhibitor. In designing the thioester substrate, the P_1 residue is of concern only with respect to substrate specificity, because once hydrolysis of the thioester substrate has occurred, the P_1 residue is not part of the inhibiting free thiol product.

Rohrbach and coworkers[101] have conducted a detailed study of the effects of various residues on substrate binding (K_m) and substrate specificity (k_{cat}/K_m) for the P_1, P_1' and P_2' positions. Rohrbach et al. showed that a P_1 Phe was best for substrate specificity. They also demonstrated that Phe or Ala in either the P_1' or P_2' position were useful for both substrate binding and substrate specificity. A Pro residue in the P_2' position has been shown in the past to result in the tightest binding ACE inhibitors such as captopril.[99] It has also been shown, however, that tripeptides with Pro in the P_2' position are poor substrates.[101,103]

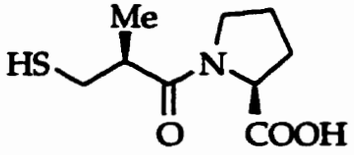

Captopril

From these considerations, the N-CBZ thioester substrate analogues **86** and **87** were designed (Figure 59) as potential target site activated inhibitors for ACE. Both possess the P_1 Phe residue and P_1' Ala residue. Groups such as carbobenzoxy (CBZ)[99,130], benzoyl[99,100,101,144], 2-furanacryloyl[102,106,194], and dansyl[109] have all been used as N-acyl groups for tripeptides which are good substrates for ACE.

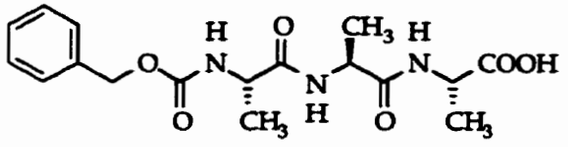

CBZ-Ala-Ala-Ala[130]
K_m=130 μM

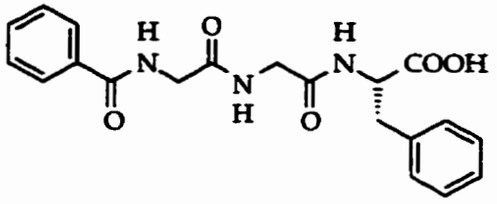

Bz-Gly-Gly-Phe[130]
K_m=2.5 μM
k_{cat}=620 s^{-1}

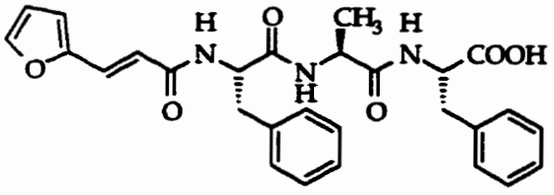

FA-Phe-Ala-Phe[106]
K_m=120 μM
k_{cat}=140 s^{-1}

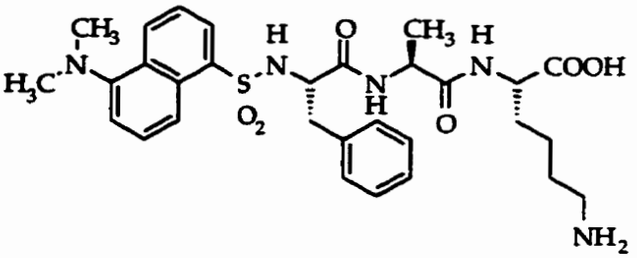

Dns-Phe-Ala-Lys[109]
k_{cat}/K_m=6.3x10^{-4} $M^{-1}s^{-1}$

Figure 59

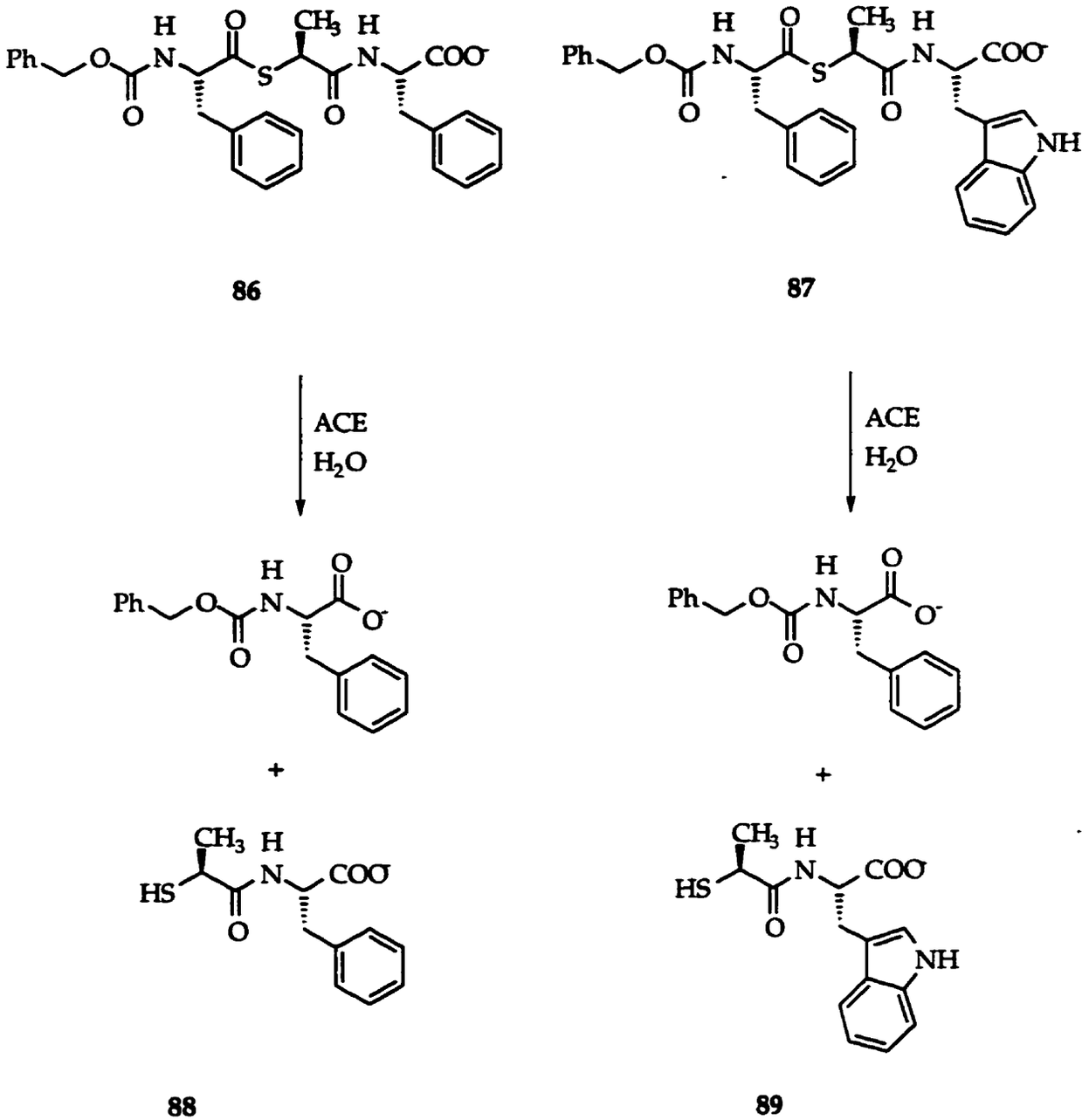

86 **87**

88 **89**

The hydrolysis of **86** by ACE was expected to result in CBZ-Phe and the free thiol **88**. Similarly, the hydrolysis of **87** by ACE was expected to result in CBZ-Phe and the free thiol **89**. Thiol **89** was previously shown to inhibit ACE with an IC_{50} of 80 nM.[153]

The synthesis of **86** is outlined in Scheme 43. The α-bromo acid **90** was synthesized from (R)-alanine with retention of configuration.[164] Thiobenzoate was reacted with **90** to give **91**, which was coupled with N-hydroxysuccinimide to give the activated ester **92**, which was then reacted with either L-phenylalanine or L-tryptophan to give **93** or **94** respectively. The thioester of **93** was hydrolyzed under basic conditions to generate the free thiol **88**, which was coupled with the mixed anhydride **95** to give **86**. The hydrolysis of the thioester bond of **94** followed by the coupling to CBZ-L-Phe to give **87** was not completed due to time restraints. But the evaluation of **94** as well as **93**, as inhibitors of ACE was conducted, as described later.

3.2 Inhibition of ACE by Free thiol 88

Since the free thiol **88** was expected to be the inhibiting species generated during the mechanism-based inhibition of ACE by **86**, the inhibitory potency of **88** against the peptidase activity of ACE was studied. For these ACE activity assays, ACE peptidase activity was monitored in 50 mM HEPES, 0.3 M NaCl, pH 7.5 at an activity concentration of 0.03 units/mL, using 2-furanacryloyl-L-phenylalanylglycylglycine (FAPGG) as a substrate.[102] ACE was purchased from Sigma as a lyophilized powder isolated from rabbit lung and purified as described by Cushman.[195] During these inhibition assays, DMSO at 5% (v/v) was used as a cosolvent to allow for solubilization of the inhibiting species studied. Under these conditions, the K_m for FAPGG hydrolysis was determined to be 0.44±0.03 mM.

Scheme 43

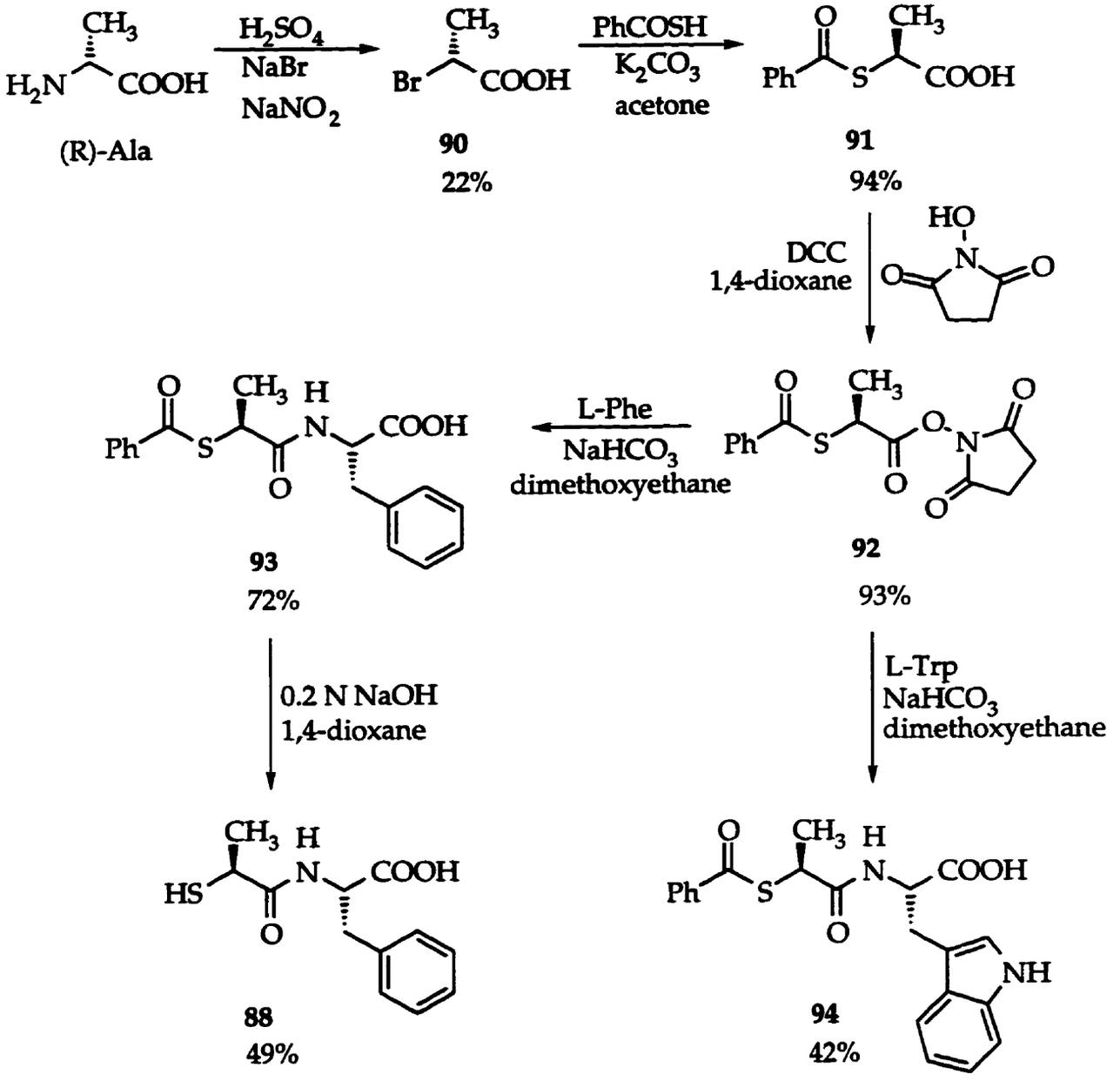
(R)-Ala
H2SO4
NaBr
NaNO2
90
22%
PhCOSH
K2CO3
acetone
91
94%
DCC
1,4-dioxane
92
93%
L-Phe
NaHCO3
dimethoxyethane
93
72%
0.2 N NaOH
1,4-dioxane
88
49%
L-Trp
NaHCO3
dimethoxyethane
94
42%

Scheme 43 (continue)

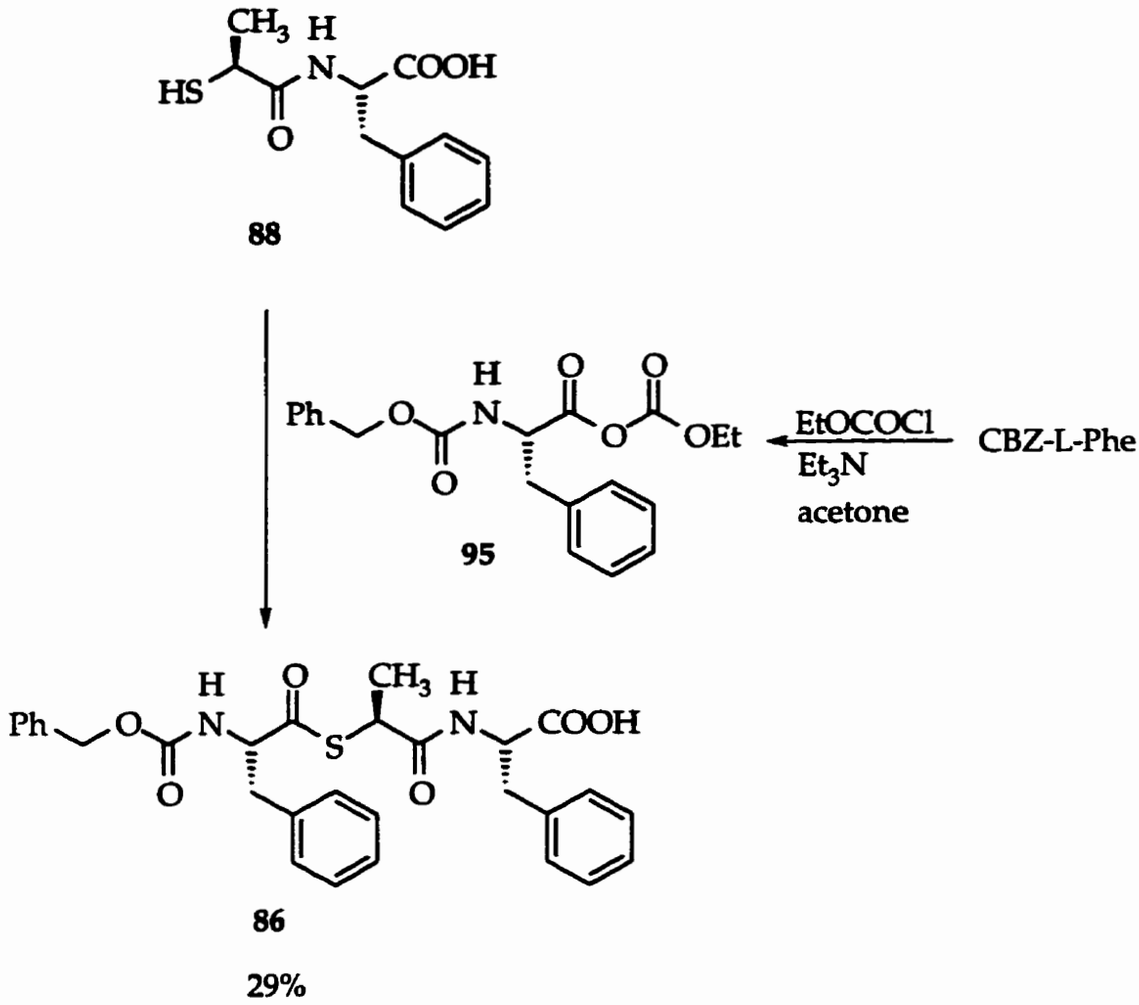

For studying the inhibition by **88**, ACE peptidase activity was monitored at 330 nm at a constant FAPGG concentration of 0.1 mM at 25°C, 5% DMSO (v/v), with concentrations of **88** being varied from 0 to 1.16 μM. The resulting inhibitor-activity relationship is shown in Figure 60. The IC_{50} value for the inhibition of ACE activity by **88** was measured to be 34.0±3.3 nM. An additional experiment was conducted in which peptidase activity was monitored at inhibitor concentrations of 0, 34 and 69 nM with FAPGG concentrations varying from 0.17 mM to 1.12 mM. The thiol **88** was

observed to inhibit the activity of ACE in a competitive fashion (see Appendix E.2). As discussed earlier, the structure of **88** was designed such that it should bind to the active site in a competitive fashion with respect to the substrate (Figure 61), similar to the expected binding fashion of captopril[152] to the S_1' and S_2' subsites of the ACE active site.

Figure 60: The IC_{50} curve inhibition of ACE peptidase activity by **88** in 50 mM HEPES, 0.3 M NaCl, pH 7.5, at 25°C, 5% DMSO (v/v). Peptidase activity was monitored at 330 nm using 0.1 mM FAPGG ($\Delta\varepsilon_{330}$ of 2480 $M^{-1}cm^{-1}$), with an ACE concentration of 0.03 units/mL.

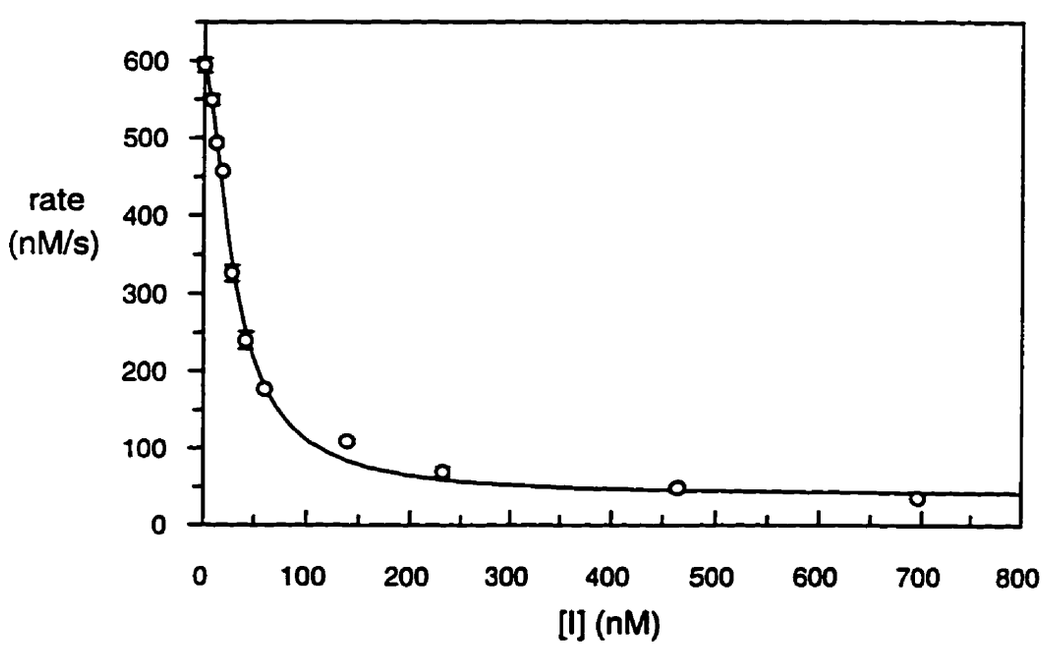

Each data point is the average of three or more separate determinations, shown with standard error bars. Error bars smaller than the symbols are not shown.

Unlike the CPA the situation observed with the thiol inhibitor **35**, the susceptibility of **88** to oxidation by dissolved O_2 under these experimental conditions was found to be negligible. As shown in Table 5, allowing the thiol **88** to incubate in

solution for 10 min prior to the addition of ACE, resulted in no change in activity. These results suggest that the **88** concentration is unchanged over the 10 min of incubation as a consequence of exposure to dissolved and atmospheric O_2. The alternative of this observation that the disulfide derived from **88** is comparable to the thiol in inhibitory potency is judged to be unlikely.

Table 5: Rate of the ACE-catalyzed hydrolysis of FAPGG (0.1 mM) in the presence or absence of **88** (27.8 nM).

[88]	[b] Rate of FAPGG hydrolysis
0	598±9 nM/s
27.8 nM (no incubation)	326±12 nM/s
27.8 nM (after 10 min incubation)	317±12 nM/s

[a] The thiol **88** was allowed to incubate in 5.26% DMSO (v/v), 50 mM HEPES, 0.3 M NaCl, pH 7.5 solution at 25° for 10 min prior to addition of ACE to initiate the measurement of peptidase activity. After the addition of enzyme, the DMSO content was 5% (v/v).
[b] The reported rates are the means of three separate determinations ± standard error.

As mentioned in Chapter 2, a similar result was observed for the free thiol **36** at low concentrations, whereas the free thiol **35** at a concentration of 326 nM was easily oxidized within 3 min. The stability of **88** towards oxidation therefore eliminated the need for the use of an argon atmosphere or glutathione to prevent significant disulfide formation from **88** during the inhibition experiments.

The IC_{50} value of 34.0±3.3 nM for **88** indicated the possibility of **88** being a tight-binding competitive inhibitor. As demonstrated with the inhibition of CPA by the free thiol **35**, however the K_i of the inhibitor can be determined from the IC_{50} curve (Dixon graphical method) if the inhibitor is competitive. From the studies of tight-binding thiol inhibitors of CPA (**36**[97] and **35**) and ACE (captopril[152]), it has been shown that these inhibitors, as expected, inhibit activity through a reversible competitive mode by binding to the active site with the aid of a strong Zn^{2+}-S

interaction. The IC_{50} curve was analyzed graphically to determine a K_i value. As described in Appendix C, **88** was determined to be a tight-binding inhibitor, with a K_i value of 15.2±0.4 nM. As also discussed in Appendix C, the $[E]_o$ for this analysis was calculated to be 30.9 nM (for 0.03 units/mL).

Figure 61

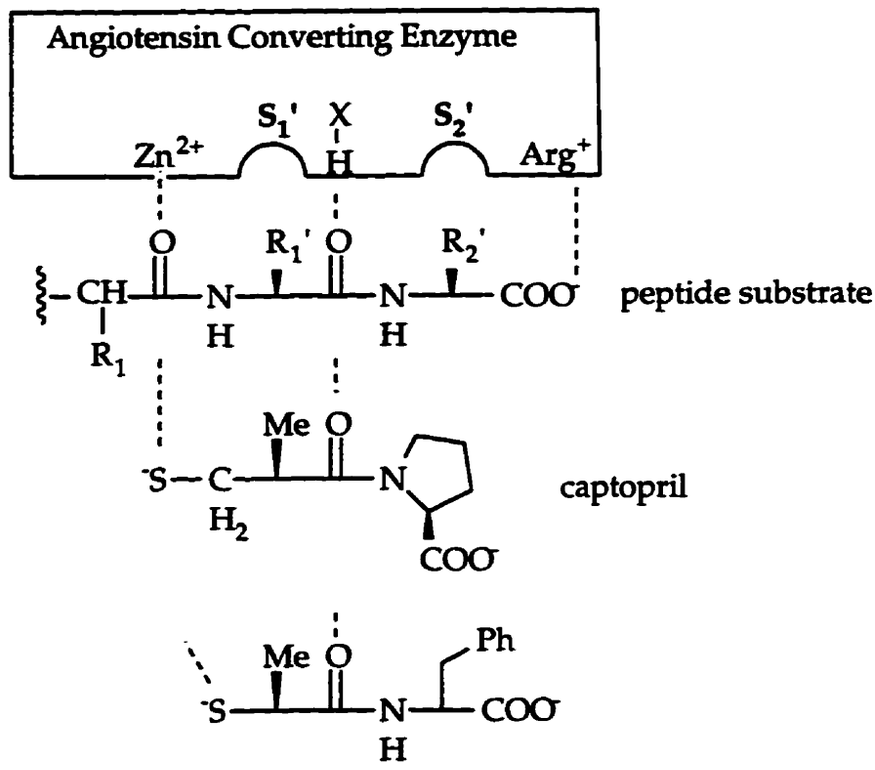

88

Once **88** was shown to be a potent inhibitor of ACE-catalyzed peptidase activity,[153] the next step was to evaluate the ability of our proposed thioester substrate analogues to act as mechanism-based inhibitors. As shown in Scheme 43, N-benzoyl-thioester-dipeptides **93** and **94** were produced as intermediates during the synthesis of the larger thioester substrate analogues. Even though N-acyl-dipeptides have not

been shown to be substrates of ACE,[102] it was of interest to investigate **93** and **94** as inhibitors of ACE activity since even low levels of hydrolytic activity should be sufficient to result in significant inhibition by the thiol product since **88** and **89** are potent inhibitors.

3.3 The Hydrolysis of 93 and 94 by ACE

The uv/visible spectra of **93** and **94** are shown in Figure 63. The UV spectrum was observed to be unchanged over a time period of 22 hours when **93** (84 μM) or **94** (84 μM) was incubated with 0.03 units/mL of ACE, indicating a lack of susceptibility to ACE-catalyzed hydrolysis. The absence of the free thiol hydrolysis product was also demonstrated by the addition of DTNB to the assay solutions after the 22 h incubations.

Figure 62

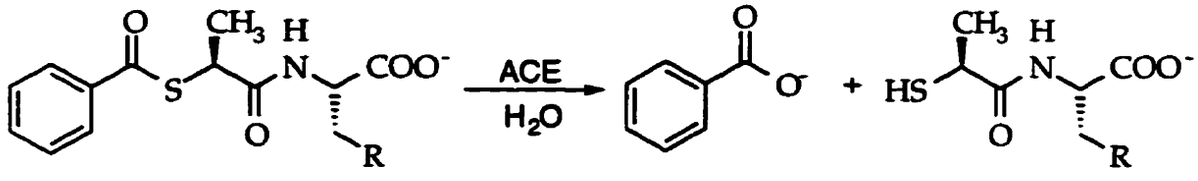

93: R=phenyl
94: R=indole

88: R=phenyl, IC_{50}=34 nM
89: R=indole, IC_{50}=80 nM[153]

Figure 63: Spectra of **93** (210 μM, upper spectrum) and **94** (84 μM, lower spectrum) in 50 mM HEPES, 0.3 M NaCl, pH 7.5, at 25°C, 5% DMSO (v/v).

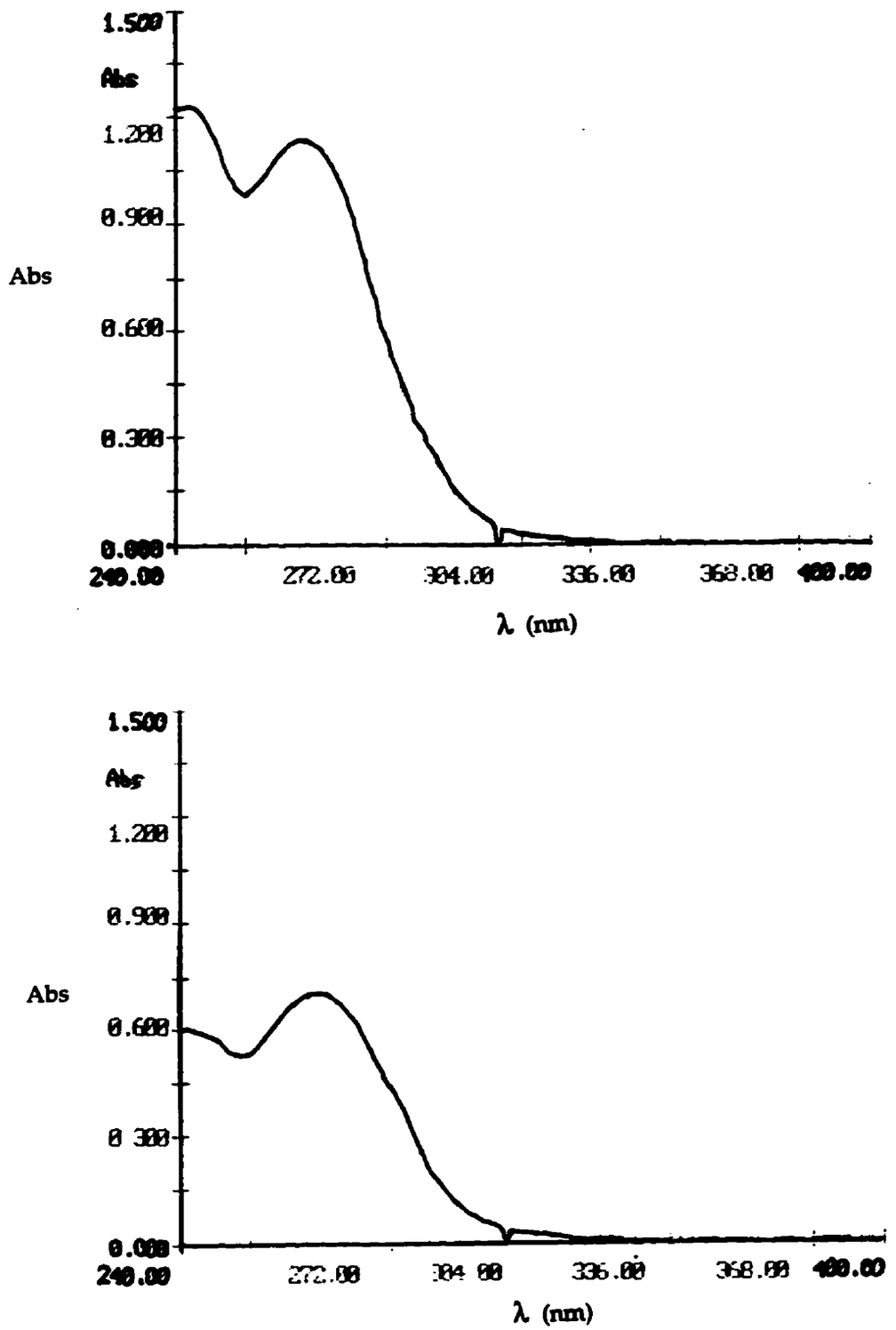

In another experiment, **93** (84 μM) was incubated with ACE (0.03 units/mL) in the presence of DTNB (0.1 mM), and the interaction was monitored at 412 nm to detect any generation of TNB due to thioester hydrolysis. No TNB was observed to be released over a 10 min period. It should be noted that in a separate experiment, DTNB was shown not to affect ACE peptidase activity at a DTNB concentration of 0.1 mM, even after DTNB had been incubated with ACE for 30 min. These results further establish that the N-benzoylthioester-dipeptides are inert toward ACE catalyzed hydrolysis.

The analysis of peptidase activity with FAPGG[102] (0.1 mM) at 330 nm ($\Delta\varepsilon_{330}$ of 2483 $M^{-1}cm^{-1}$) in the presence of **93** (84 μM) also showed that **93** caused no loss in the activity of ACE. The apparent lack of binding affinity between **93** and ACE may help explain the lack of susceptibility of the thioester bond towards hydrolysis. The presence of a benzoyl group in place of an appropriate amino acid residue in the P_1 position of the thioester substrate seems to prevent binding to the enzyme.

3.4 The Hydrolysis of 86 by ACE

The thioester tripeptide analogue **86** was then subjected to analysis as a mechanism-based inhibitor. The detection of the hydrolysis of **86** by ACE was of interest initially. As in the study of hydrolysis of (S)-**50** by CPA, monitoring of the hydrolysis of **86** by ACE was possible by the use of DTNB which reacts with any thiol product such as **88** (Figure 64). This reaction between DTNB and **88** would allow thioesterase activity to be measured without the product inhibition by **88**. The rate of thioester hydrolysis and therefore thiol release can be measured at 412 nm ($\Delta\varepsilon_{412}$ of 14,160 $M^{-1}cm^{-1}$).

Figure 64

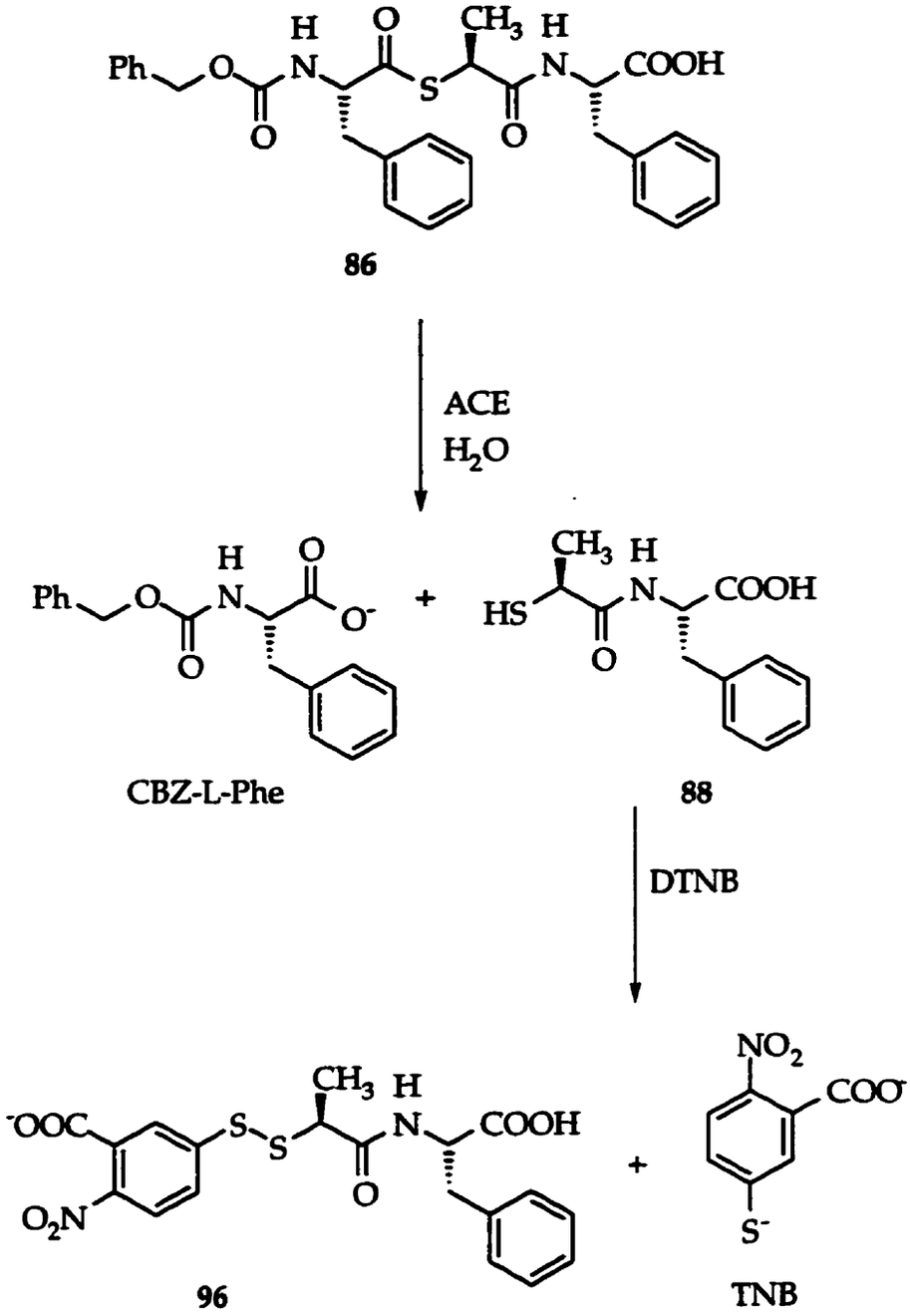

The hydrolysis of **86** by ACE was observed using this method. The concentration of **86** was varied from 2.5 μM to 100 μM, at constant concentrations of ACE (0.1 unit/mL) and DTNB (0.1 mM) in 50 mM HEPES, 0.3 M NaCl, pH 7.5, at 25°C, 5%

DMSO (v/v). The relationship between the concentration of **86** and the release of **88** (from hydrolysis of **86**), is shown in Figure 65. K_m and V values of 18.9±2.5 μM and 407.7±18.8 nM/min respectively were determined. As discussed in Appendix C, the concentration of ACE in 1 unit of the enzyme purchased from Sigma was estimated to be 1.03 nmoles. From this value, we estimated the $[E]_o$ during the assay to be 103 nM, therefore allowing us to estimate the k_{cat} to be approximately 3.96 min^{-1}.

Figure 65: The hydrolysis of **86** (2.5 μM to 100 μM) by ACE (0.1 unit/mL) in the presence of DTNB (0.1 mM) in 50 mM HEPES, 0.3 M NaCl, pH 7.5, at 25°C, 5% DMSO (v/v). The hydrolysis was measured as a function of TNB generation, monitored at 412 nm ($\Delta\varepsilon_{412}$ of 14160 $M^{-1}cm^{-1}$).

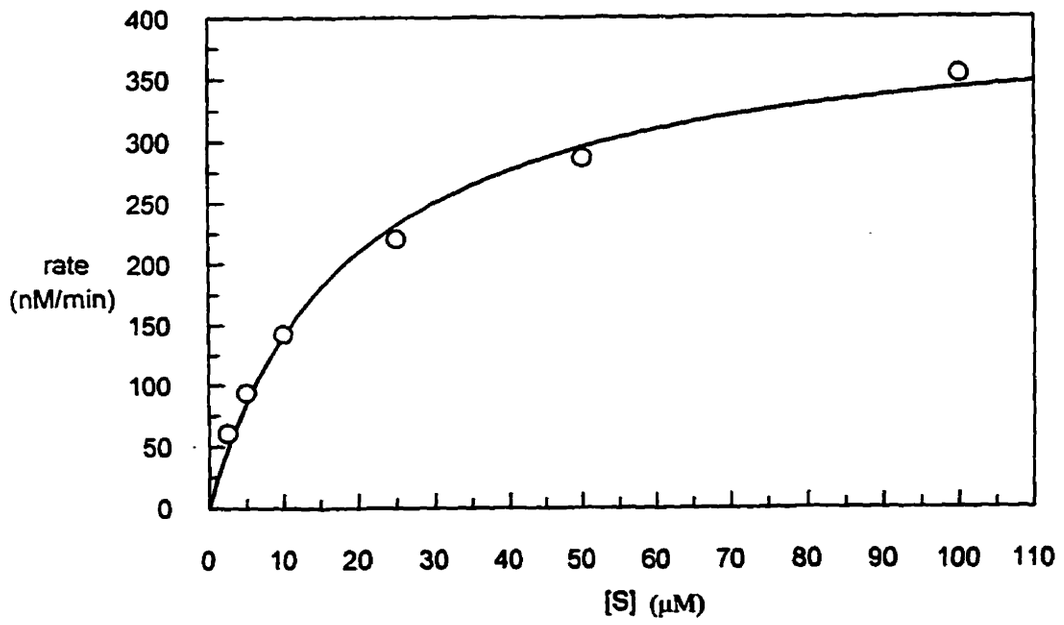

The hydrolysis of a structurally similar 2-furanacryloyl tripeptide substrate (**97**) has been studied by Riordan and coworkers.[106] Our thioester analogue **86** was observed to bind more than 6 times more tightly than **97**. On the other hand, **86** was observed to be hydrolyzed nearly 2000 times more slowly than **97**. This is not

surprising considering that ACE has been found to be relatively selective toward the hydrolysis of peptide bonds. For the hydrolysis of ester substrates (N-acyl-tripeptide analogues with an ester linkage in place of the scissile amide bond) by ACE, it was found that the ester substrates have K_m values very similar those of the corresponding amide substrates, but the k_{cat} values for ester substrate hydrolysis were found to be 5 to 33 times lower. To our knowledge this hydrolysis of **86** described above represents the first report of the hydrolysis of a thioester by ACE.

Although the ACE thioester substrate **86** was shown to be hydrolyzed slowly, it was still expected to act as an effective mechanism-based inhibitor of ACE as a consequence of the tight-binding qualities of the free thiol product **88**.

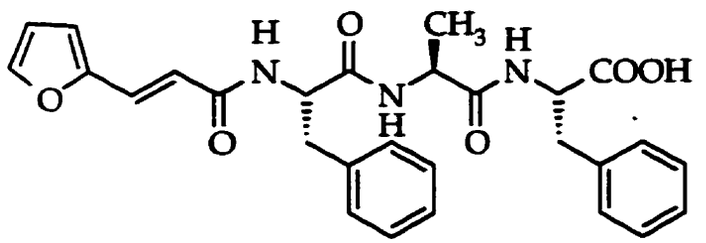

K_m=120 μM

k_{cat}=8400 min^{-1}

97 (FA-Phe-Ala-Phe)

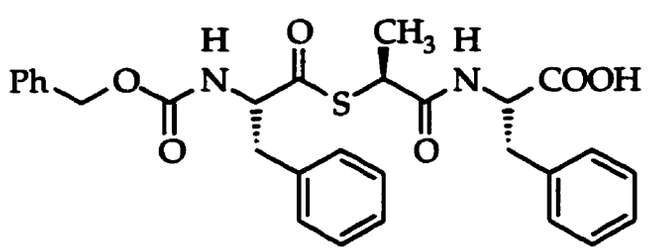

K_m=18.9 μM

k_{cat}=3.96 min^{-1}

86 (CBZ-Phe-(S)Ala-Phe)

3.5 Mechanism-Based Inhibition of ACE by the Thioester Substrate Analogue 86

The mechanism-based inhibition of ACE by **86** was studied using a method similar to that used for the mechanism-based inhibition of CPA by (S)-**50**. In this case there was no need for inclusion of glutathione because of the relative stability of **88** towards oxidation by O_2. In this experiment, ACE (0.033 units/mL) was incubated for over 160 min, with **86** at concentrations of 0, 50, 500 and 5000 nM in 50 mM HEPES, 0.3 M NaCl, pH 7.5, at 25°C, 5% DMSO (v/v). Residual peptidase activity was determined at different time intervals by withdrawing aliquots from the incubation mixtures and mixing with a solution of FAPGG and monitoring ACE peptidase activity at 330 nm ($\Delta\varepsilon_{330}$ of 2483 $M^{-1}cm^{-1}$). The control incubation assay showed no loss of ACE peptidase activity during the time of the experiment. A plot of the percent peptidase activity remaining as a function of time is shown in Figure 66, where the rate of deactivation increases with increasing concentration of thioester inhibitor.

In the case of the experiment employing **86** at a concentration of 50 nM, the decrease in ACE peptidase activity seems to stop at about the 100 min point of the incubation. On the other hand, in the case of the 500 nM and 5000 nM **86** incubation assays, the peptidase activity seems to be still decreasing slowly towards the 160 min point of the incubation. It would appear that all of the **86** in the 50 nM **86** incubation assay has been hydrolyzed by the 100 min point. From the results of the inhibition analysis of **88** against ACE, we can determine the expected peptidase activity of ACE if all of the **86** was hydrolyzed. From the IC_{50} curve from Figure 60, the expected peptidase activity in the presence of 50 nM **88** was determined to be 230 nM/s. The actual peptidase activity at time 100 min was observed to be 280 nM/s. This observation suggests that most of the thioester has been hydrolyzed.

Figure 66: Deactivation of ACE by incubating with **86** in 50 mM HEPES, 0.3 M NaCl, pH 7.5, at 25°C, 5% DMSO (v/v). The incubation mixtures contain 0.033 units/mL ACE with concentrations of **86** of 0, 50 nM, 500 nM and 5000 nM. Peptidase activity was determined at 330 nm at 25°C after mixing 900 mL of the incubation mixture with 100 mL of 1.0 mM FAPGG in 50 mM HEPES, 0.3 M NaCl, pH 7.5, at 25°C, 5% DMSO (v/v).

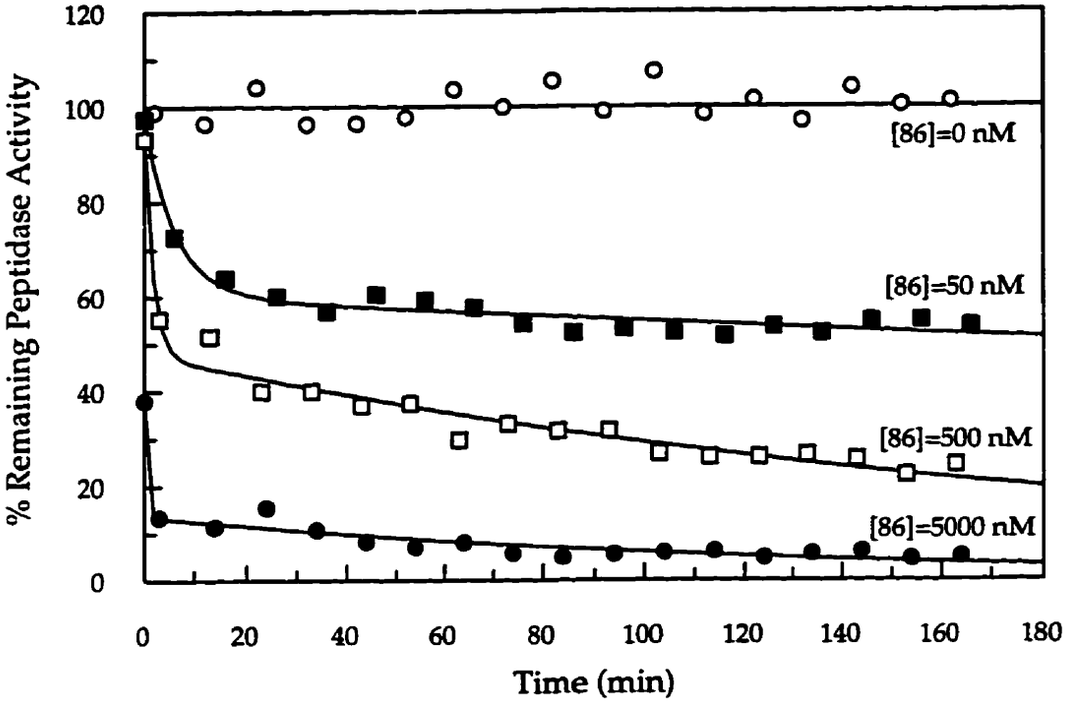

The data points for [86]=0 were fitted to linear regression to give the control curve. The solid traces through the data points for [86]=50, 500, 5000 nM correspond to double exponential functions fitted to the data using Grafit 3.01 and are presented for ease of visualization of the data only, since no kinetic model predicting a double exponential relationship has been established. The rates reported above are expressed as the percent residual activity of the expected rate from the control curve.

In the case of the 500 nM incubation assay, the expected peptidase activity was determined to be 36 nM/s if all of the **86** was hydrolyzed, and the actual peptidase activity was observed to be 138 nM/s. With the 5000 nM incubation assay, the expected peptidase activity was determined to be 8.5 nM/s if all of the **86** was hydrolyzed, and the actual peptidase activity was observed to be 28 nM/s. In both these cases, total hydrolysis of **86** seems to have not occurred by time 160 min. As in the case of the mechanism-based inhibition of CPA by (S)-**50**, total hydrolysis of the thioester substrate analogue by the target enzyme did not occur within the incubation period of the experiment as a result of strong inhibition of the thioester hydrolysis process by the thiol product. Although total deactivation was not observed, the thioester **86** was successfully shown to inhibit ACE activity in a mechanism-based manner. With a 5 μM concentration of **86** >95% inhibition was observed after approximately 90 minutes.

3.6 Concusion: The Use of Thioester substrate Analogues as Target Enzyme-Activated Inhibitors of CPA and ACE

In conclusion, substrate analogue **86**, which possesses a thioester linkage in place of the scissile amide bond, is an effective target enzyme activated inhibitor for ACE. In the cases of both CPA and ACE, greater than 90% inactivation occured after 60 minutes of incubating either enzyme with a target enzyme activated inhibitor ((S)-**50** and **86** respectively). During these inactivation experiments, less than 10 μM of the thioester inhibitor was required to obtain substantial inhibition within 60 minutes, with significantly little of that amount hydrolyzed during the experiment. When considering the therapeutic usefulness of this type of target enzyme activated inhibitor, a low percent of turnover of the thioester would be beneficial considering the possible side effects due to nonspecific inhibitor-enzyme which may occur when excess amounts of the free thiol inhibitor exist in a biological system. The low rate of

thioester hydrolysis by the target enzyme to release a potent tight-binding inhibitor at the location of the target enzyme will no doubt increase selective inhibition in a complex biological system.

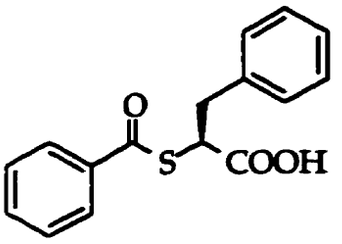

(S)-50

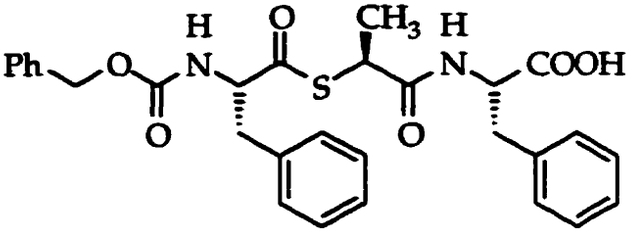

86

As mention earlier in Section 2.0.1, the recognition of the thioester substrate analogue as an efficient substrate is an important criterion for this mode of inhibition. A thioester substrate which would be more easily hydrolyzed by the target enzyme would therefore be expected to be a better target enzyme activated inhibitor. As a result, future work in this area should be directed towards the search for more easily hydrolyzable thioester substrates. The inhibition of other therapeutic targets such as matrix metalloproteases and enkephalinase may also be of interest. Matrix metalloproteases, including collogenases, gelatinases and stromelysins, are responsible for the breakdown of extracellular matrix (fibrillar collagens, prteoglycans, fibronectin and gelatin) during tissue morphogenesis, differentiation, and wound healing.[196,197] These zinc enzymes are thought to also aid in metastasis and tumor invasion through matrix degradation, allowing for the spread of cancer cells to other parts of the body. Enkephalinase (endopeptidase 24.11) plays a major role in the inactivation of endogenously released enkephalins at enkephalinergic synapses.[5] Enkephalins are opioid peptides which produce an analgesic effect when synaptically released. Inhibitors of enkephalinase have been found to prolong the analgesic effects, and have been invetigated for pain reducing responses.

Enkephalinase has also been found to be involved in blood pressure regulation, the modulation of smooth muscle contraction, and the immune system. The inhibition of matrix metalloproteases and enkephalinase using this strategy is also recommended.

Chapter 4:

The Inhibition of Carboxypeptidase A and Angiotensin Converting Enzyme by N-Acylhydrazones

N-Acylhydrazones (NAH's) **98**, have been studied as potential therapeutic agents in a number of pharmaceutical contexts. For example PIH, **99**, and related compounds have been shown to be potent chelators for Fe^{3+} and, as such, have been examined as potential medicinal agents for the treatment of iron overload in patients suffering from thalassemia with somewhat promising results.[198] Other reports indicate that NAH's can exhibit antimalarial properties,[199] as well as antibiotic and antifungal activities,[200] but the molecular mechanisms responsible for these biological activities have not been established. Of particular interest is the observation that the toxicity usually associated with non-specific metal binding agents is much less pronounced with the NAH's, some of which have been employed in clinical trials.

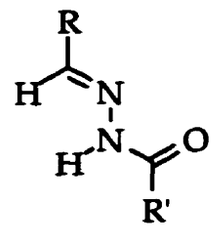

98

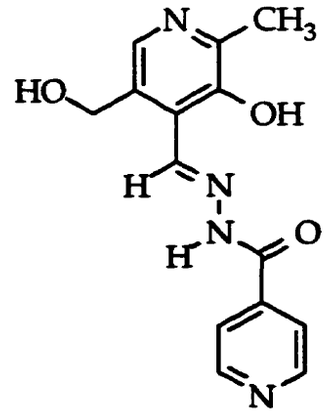

99

Recent studies in these laboratories have revealed that certain NAH's are specific inhibitors of both the RNA-dependent DNA polymerase and the RNase H activities of HIV-1 reverse transcriptase (RT).[201] Significant inhibition of viral

replication has been demonstrated in cells infected with HIV-1 and in cells infected with HIV-2.[202] RNases H from *E. coli* and from *Thermus thermophilus* are also susceptible to inhibition by NAH's but the structure activity relationship amongst the NAH's observed for inhibition of the bacterial enzymes differs significantly from that observed for the retroviral enzyme.[203] Inhibition of RNase H activity was found to be reversible upon dilution suggesting that removal of the catalytically essential metal ions from the active site was not involved in the inhibition process.

The possibility that NAH's might also be relatively non-toxic inhibitors of divalent metal ion dependent proteolytic enzymes prompted us to carry out preliminary experiments concerning the interaction of NAH's with CPA and ACE. In particular, the interaction of CPA with the NAH's shown in Figure 67 was studied with a view to determining if some degree of specificity might be attainable in the inhibition process. For comparison, the inhibition of CPA by *o*-phenanthroline (OP), a relatively non-specific inhibitor known to inhibit CPA by removal of the catalytically essential zinc ion from the active site for the enzyme,[195] was studied in parallel.

Figure 67

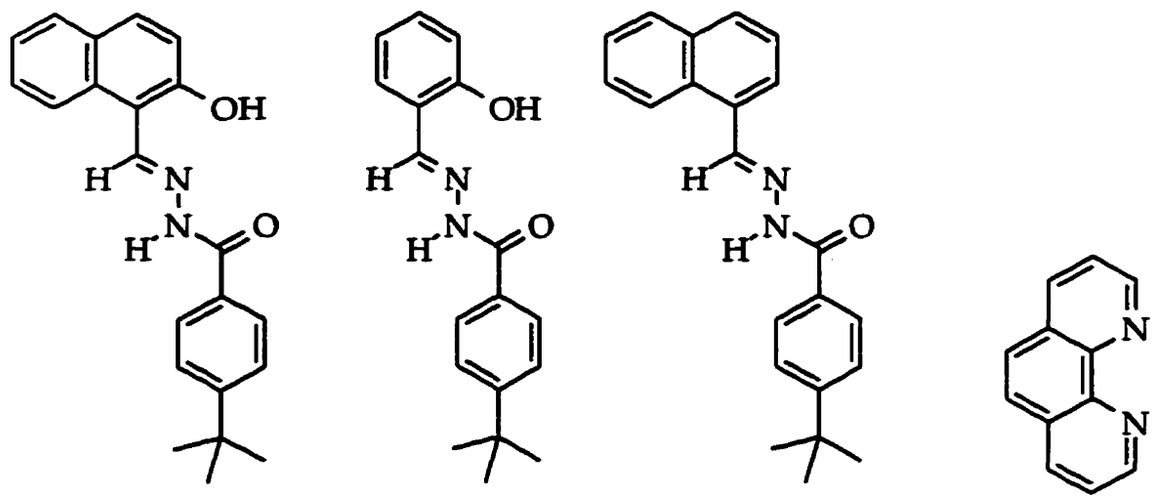

NAH306 **NAH206** **des-OH 306** **OP**

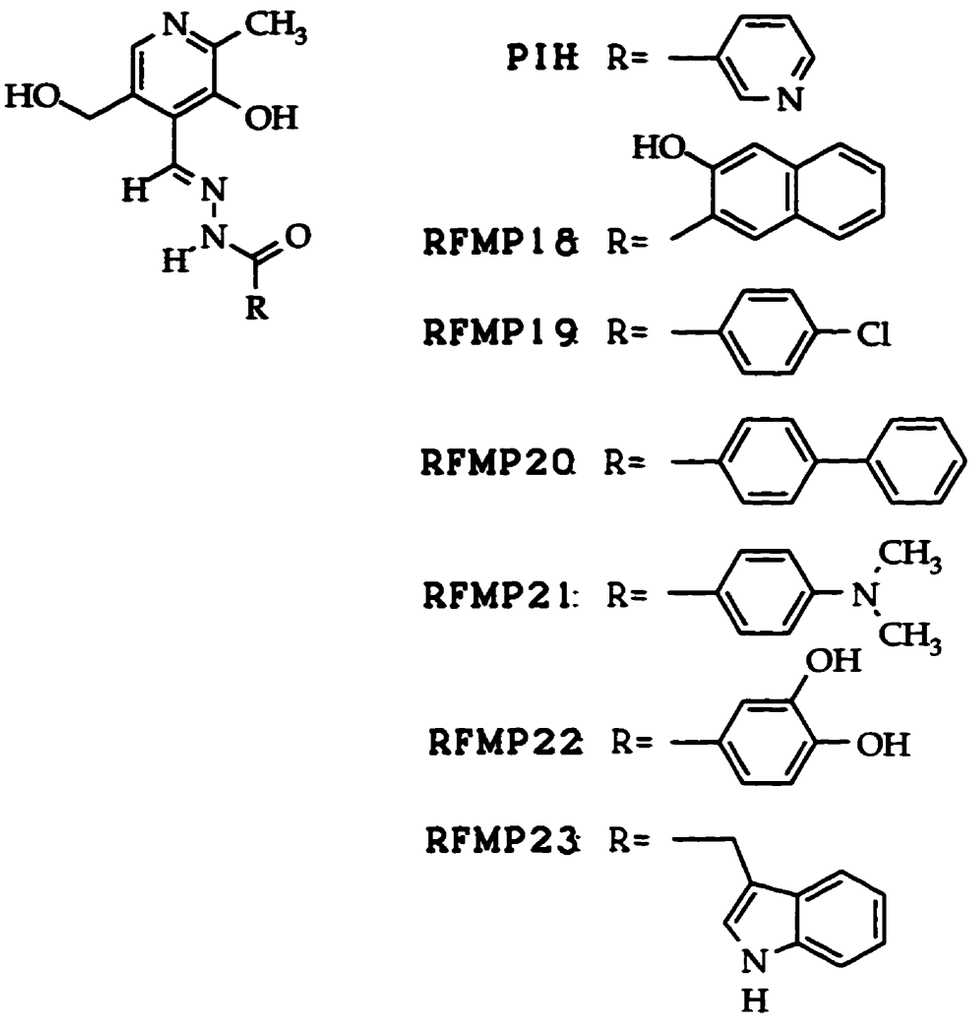

Inhibition of the proteolytic activity of CPA was studied by examining the influence of potential inhibitors at concentrations in the 0.2 to 64 μM range on the rate of CPA-catalyzed hydrolysis of hippurylphenylalanine as monitored by absorbance changes at 265 nm. Solubility problems with these inhibitors precluded the use of higher inhibitor concentrations during these assays. As shown in Table 6 below, the peptidase activity of CPA was found to be susceptible to inhibition by NAH's with NAH306 being the most potent of the NAH's studied, with an IC_{50} of 29 μM. That the inhibition process is associated with interactions of the inhibitors with the active site

metal ion is suggested by the observation that the des-hydroxy derivative of **NAH306**, which lacks one of the metal ion binding sites, is a very weak inhibitor. On the other hand the observation that **NAH206**, which is expected to have comparable metal ion affinity to that of **NAH306** since it possesses the same metal ion binding sites as does **NAH306** but lacks the benzenoid ring fused to the hydroxyl-bearing ring, suggests that interactions with structural features of the active site other than the metal ion play an important role in the inhibition of CPA by NAH's.

Table 6: Inhibition of CPA by **NAH306, NAH206** and **des-OH 306**. Peptidase activity was monitored at 265 nm using 0.5 mM HP in 25 mM Tris, 0.5 M NaCl, pH 7.5, containing 3.5% ethanol (v/v), at 25°C.

NAH	Inhibition
NAH306	IC_{50}=29 μM
NAH206	IC_{33}=63 μM*
des-OH 306	IC_{17}=63 μM*

* Solubility problems precluded the possibility of determining IC_{50} values for these compounds.

Analysis of the inhibition kinetic data for **NAH306** and **NAH206** by the Dixon plot method reveals linear relationships typical of simple reversible enzyme inhibition. These observations are in contrast to the non-linear Dixon plot observed for inhibition by *o*-phenanthroline which has been shown to inhibit CPA by removal of the essential metal ion from the enzyme active site.[95] The possibility that the apparently parabolic Dixon plot for *o*-phenanthroline inhibition results from binding of two molecules of *o*-phenanthroline, followed by departure of a metal complex incorporating the catalytic zinc ion and two molecules of the inhibitor has been outlined above in Section 2.2.6.

Figure 68: Dixon plot of the inhibition of CPA peptidase activity by **NAH306, NAH206** and **des-OH 306**. Peptidase activity was monitored at 265 nm using 0.5 mM HP in 25 mM Tris, 0.5 M NaCl, pH 7.5, containing 3.5% ethanol (v/v), at 25°C. $[E]_o$=200 nM.

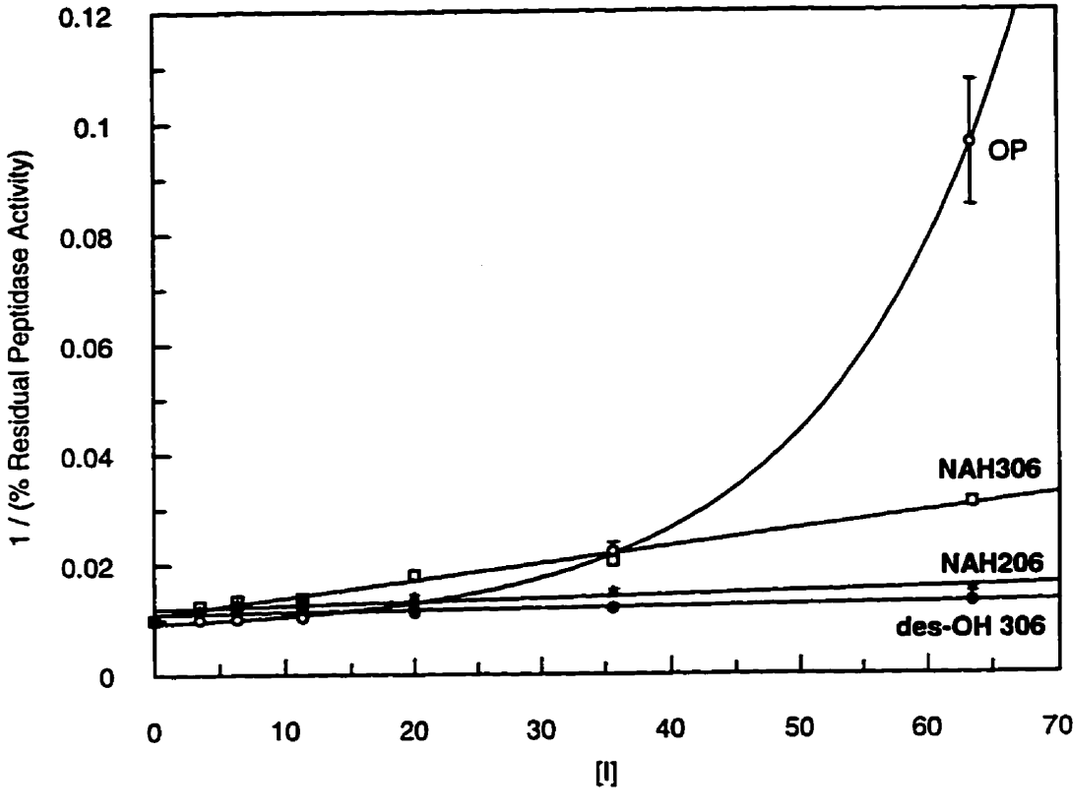

Each data point is the average of two or more separate determinations. Error bars are shown with data points with a standard error greater than 6%. For graphical presentation, the resulting data from analysis with OP was fitted to a single exponential function, and the resulting data from the analysis with **NAH306, NAH206** and des-OH **306** were fitted to linear regression.

Although **NAH306** is a relatively effective inhibitor for CPA it has been found to be a relatively poor inhibitor for ACE (Table 7) even though ACE has been shown to possess a substantially weaker affinity ($\log K_E$=8.6) for its catalytically essential zinc ion than does CPA ($\log K_E$=10.5).[95] These observations were consistent with the

suggestion that **NAH306** inhibits the activity of CPA through the formation of an enzyme-inhibitor complex, unlike *o*-phenanthroline which inactivates CPA[95] and ACE[144] by removal of the active site zinc ion. Some inhibition of ACE was observed with pyridoxyl NAH derivatives as indicated in Table 7, but the degree of inhibition was too small to warrant more detailed study.

Table 7: Inhibition of ACE by various NAH derivatives in 50 mM HEPES, 0.3 M NaCl, pH 7.5, containing 5% DMSO (v/v), 25°C, 0.03 units/mL ACE, using 0.1 mM FAPGG (λ=330 nm). NAH concentrations were 10 µM.

NAH	Concentration of NAH	[a] Observed % Residual Activity
NAH306	20 µM	no inhibition
PIH	10 µM	no inhibition
RFMP18	10 µM	no inhibition
RFMP19	10 µM	89.3±0.8%
RFMP20	10 µM	93.1±1.3%
RFMP21	10 µM	92.5±2.4%
RFMP22	10 µM	91.9±2.2%

[a] The inhibited activities are a percentage of the activity in the absence of inhibitor, reported as a mean of three separate determinations ± standard error.

To investigate further the mode by which **NAH306** inhibits CPA, more detailed inhibition experiments were conducted in which CPA peptidase activity was monitored at varying substrate concentrations and concentrations of **NAH306** at 0, 6.7 and 13.3 µM. The double-reciprocal plot shown in Figure 69 indicates that the inhibition is not simply competitive. This type of pattern of intersecting lines in the double reciprocal plots is consistent with the mixed inhibition model shown below in Scheme 44. In this kinetic mechanism the inhibitor can bind to the free enzyme with a

dissociation constant of K_i, thereby excluding S from the active site. The inhibitor can also bind to the ES complex with a different dissociation constant, K_i'. It can be shown that when $K_i' < K_i$ the common intersection point for the double reciprocal plots must be in the third quadrant, as found for inhibition of CPA by **NAH306**.[204]

Figure 69: Double-reciprocal plot of the inhibition of CPA peptidase activity by **NAH306** in 25 mM Tris, 0.5 M NaCl, pH 7.5, containing 3.5% ethanol (v/v), at 25°C. The enzyme concentration was constant at 132 nM, with HP concentrations being varied from 0.25 mM to 1.3 mM, and **NAH306** concentrations of 0 μM (○), 6.7 μM (●) and 13.3 μM (□).

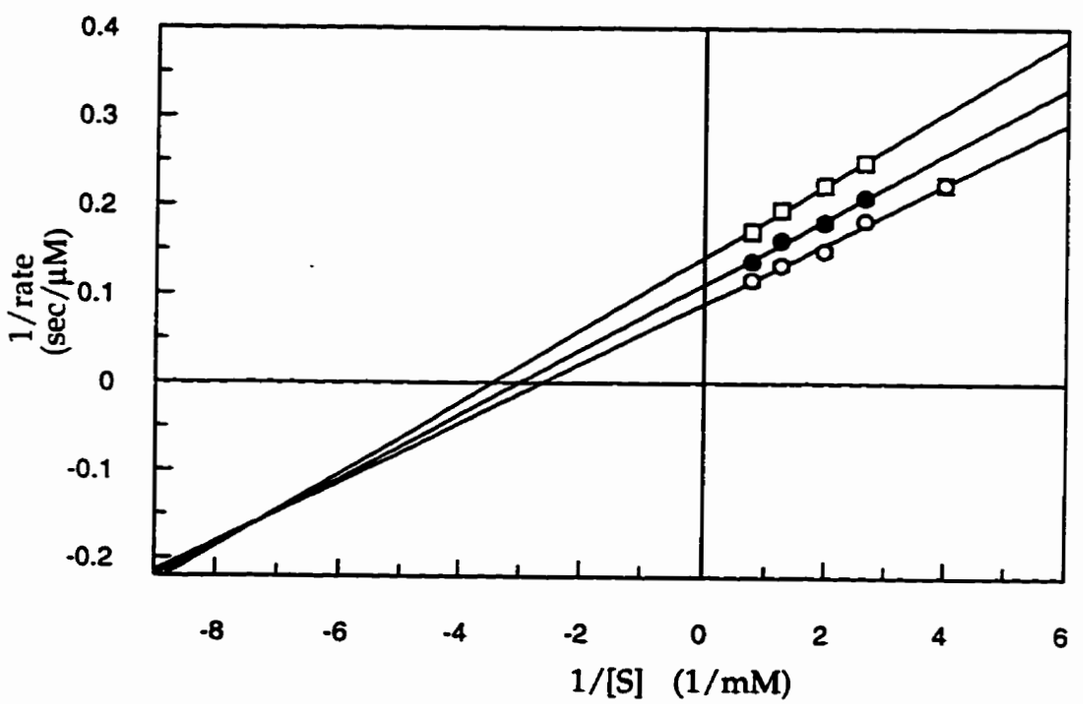

Each data point is the average of three or more separate determinations, shown with standard error bars. Error bars smaller than the symbols are not shown.

Scheme 44

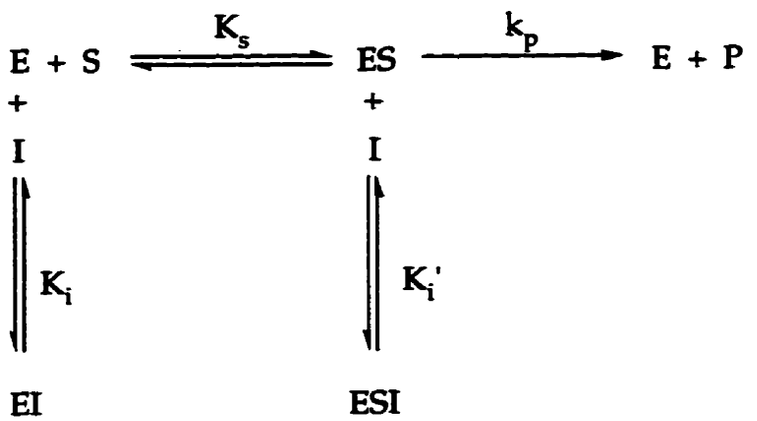

Scheme 45

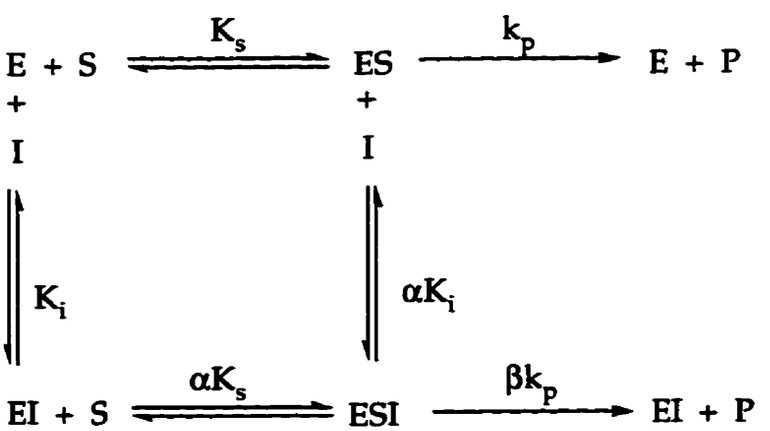

In this model, the inhibitor **NAH306** has two binding sites to the enzyme, a competitive inhibition site which might involve the S_1'-subsite (K_i), and an uncompetitive site which is available to **NAH306** after S binds to E to form the Michaelis-Menten complex (K_i'). Equation 4.1 represents the rate of HP hydrolysis with the suggested mechanistic mode shown in Scheme 44. It should be noted that an

alternative model in which the ESI complex is catalytically competent can also result in a qualitatively similar kinetic pattern.[204] That the mechanism of inhibition in this case is dead-end inhibition as shown in Scheme 44 is supported by the observation that the slope and intersection replots are linear rather than hyperbolic as predicted for the mechanism in Scheme 45 (see Appendix E.3).

$$v = \frac{V[S]}{K_s\left(1 + \frac{[I]}{K_i}\right) + [S]\left(1 + \frac{[I]}{K_i'}\right)} \qquad (4.1)$$

The experimental data shown in Figure 69 was fitted to equation 4.1 using non-linear regression to give K_s=0.36±0.04 mM, V=11.0±0.4 μM/s, K_i=47±16 μM and K_i'=28±3 μM. The K_i and K_i' values of 47 μM and 28 μM, respectively, suggest that the formation of the ESI complex is somewhat more favourable than the formation of the EI complex.

In order to help deduce a possible molecular mechanism consistent with this kinetic model of the inhibition process, molecular modeling studies of potential modes of binding of **NAH306** to E and ES were undertaken. This study employed an x-ray crystallographic structure of **NAH306** determined by Dr. N. J. Taylor, which is shown in Figure 70 as a stereoscopic framework representation. The initial qualitative conclusions which were reached in these studies made us suspect that the simple kinetic model outlined above might be inappropriate. For example, attempts to dock **NAH306** into the active site region with the amide bond of the inhibitor positioned as expected for the scissile amide linkage of a normal substrate revealed that the dimensions of the S_1-subsite were inadequate to accommodate the bulky *p*-t-butyl-benzoyl group. Furthermore, it was clear that, once the substrate HP was bound

productively in the active site, there was insufficient free volume remaining in the S_1 and S_2 subsites to allow for binding of a bulky inhibitor such as **NAH306.**

Figure 70

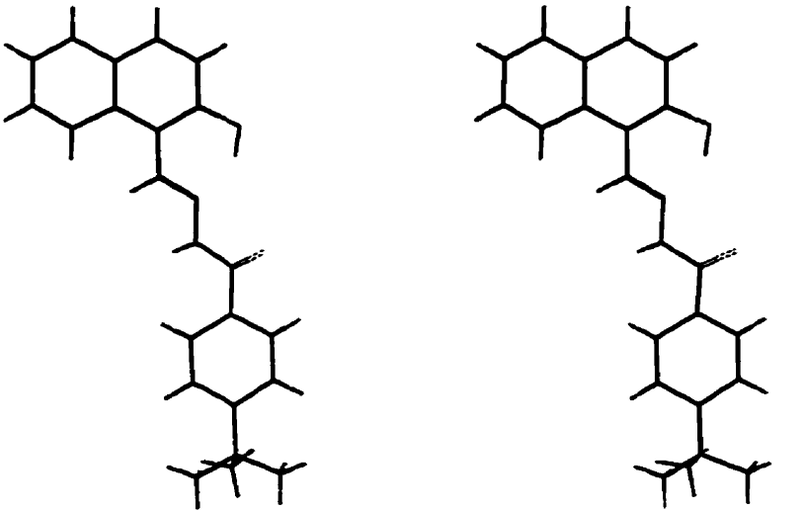

These observations led us to examine in detail the report of an alternative non-productive binding mode defined in x-ray crystallographic studies carried out by Lipscomb and coworkers.[40,192]

Lipscomb[192], found that the slow hydrolyzing substrate, N-benzoyl-phenylalanine, could bind to the enzyme-product complex CPA-Phe (Figure 71) such that the hydrolysis product, phenylalanine, occupies the S_1'-subsite, and the substrate, N-benzoyl-phenylalanine, occupies the S_1 and S_2-subsites.

Figure 71

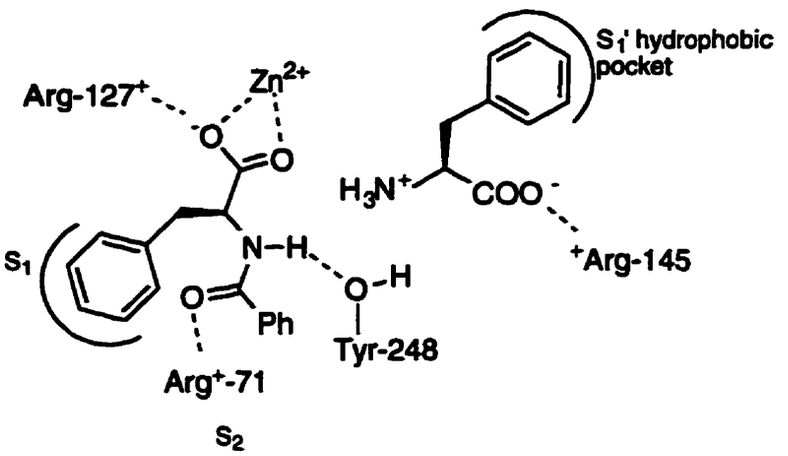

Since phenylalanine is also a hydrolysis product for HP, it occurred to us that **NAH306** might bind to span the S_1 and S_2 subsites in a manner similar to that observed for N-benzoyl-phenylalanine, shown schematically in Figure 71. With phenylalanine present in the S_1'-subsite, this would correspond to an enzyme-product-inhibitor ternary complex, whereas in the absence of phenylalanine such binding would yield an EI complex with insufficient space available to allow binding of the substrate. The appropriate kinetic model is shown below in Scheme 46.

Scheme 46

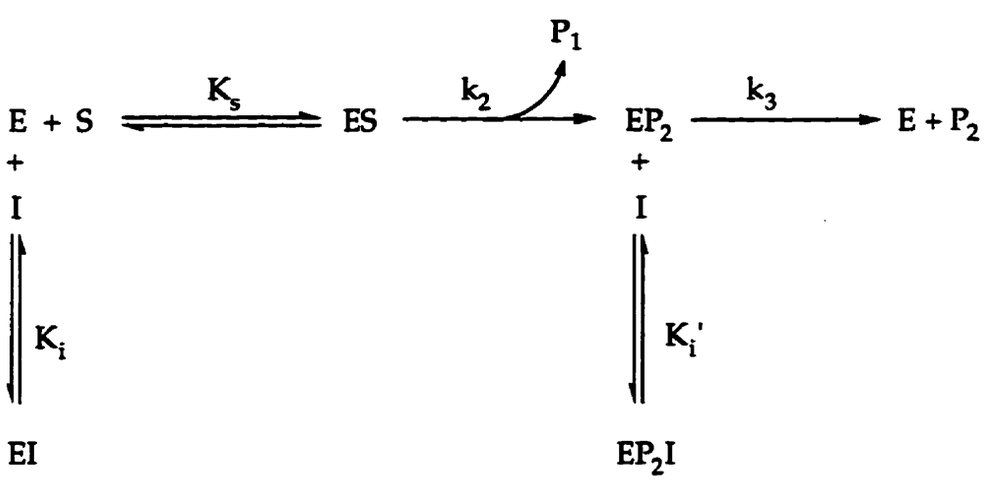

Derivation of the initial rate expression for such a system (Scheme 46) using the King-Altman method[205] reveals that the mathematical form of the expression is qualitatively indistinguishable from that predicted for the mixed inhibition model in Scheme 44. As shown in equation 4.2, the apparent K_i' is not a simple true dissociation constant but is also a function of the rate constants k_2 and k_3.

$$v = \frac{V[S]}{K_m\left(1+\frac{[I]}{K_i}\right) + [S]\left[1+\left(\frac{k_2}{k_3}\right)\left(\frac{[I]}{K_i'}\right)\right]} \qquad (4.2)$$

Using equation 4.2, the K_i was determined to be 47±16 μM, and the expression k_3K_i/k_2 was determined to be 28±3 μM. Since, for HP hydrolysis, k_2 is expected to be less than k_3, $K_i'=(K_i'_{app}k_2/k_3)$ is expected to be smaller than the measured $K_i'_{app}$.

Using Lipscomb's crystallographic study of the binding of N-benzoyl-phenylalanine to the phenylalanine-CPA complex[192] as a guide, the binding of **NAH306** to the phenylalanine-CPA complex was modeled. Since the full x-ray coordinates for this complex were not available, a model of the complex was constructed using the coordinates for the (Gly-Tyr)-CPA[25] complex and distance relationships reported for the ternary complex of interest[192] (see Appendix D for details). In this model, with phenylalanine complexed into the S_1'-subsite, the active site Zn^{2+}, and the S_1 and S_2-subsites are available for interaction with **NAH306**. In the case of the N-benzoyl-phenylalanine-CPA complex, shown in Figure 71, the phenyl group of the phenylalanine residue in N-benzoyl-phenylalanine occupies the S_1-subsite hydrophobic pocket which consists of Tyr-198, Ser-199, Leu-201, Ile-247, Tyr-248 and Phe-279. The carboxylate group of N-benzoyl-phenylalanine interacts electrostatically with the Zn^{2+} ion and Arg-127. Other interactions which were observed by Lipscomb are the hydrogen bonding of the N-benzoyl-phenylalanine

amide to Tyr-248 and Arg-71, and the edge to face interaction between the benzoyl ring and the ring of Tyr-248.

Attempts were then made to employ this model to predict a possible mode of binding of **NAH306** to CPA. It was found that direct interactions between the metal binding sites of **NAH306** and the active site zinc ion were strongly disfavoured as a result of steric interactions. As a result, it was decided that inclusion of a water molecule as the fourth zinc ligand would be necessary. The likelihood of the formation of such a hydrated enzyme product complex in the course of product release has been alluded to above in Chapter 2 (Section 2.1.7). It was also decided that the presence of the C=N bond in **NAH306** would lower the pK_a of the phenolic hydroxyl group sufficiently relative that of most phenols (pK_a=9-10), that a substantial proportion of **NAH306** would exist in the ionized form. Docking of this ionized version of **NAH306** into the S_1/S_2 region of CPA such as to minimize steric repulsions followed by a molecular mechanics energy minimization (as described in Appendix D) resulted in the model shown in Figure 72a, 72b and 73.

In the resulting energy minimized structure, **NAH306** is oriented such that the **B** ring of the naphthalene structure is placed into the hydrophobic pocket of the S_1-subsite formed by the side chains of Tyr-198 and Phe-279. Besides the hydrophobic interactions, this interaction is further stabilized by the edge-to-face orientation between the **B** ring of the naphthelene structure and the aromatic ring of Tyr-198. The rest of the **NAH306** structure lies in a cleft formed by the active site residues Arg-127, Arg-145, Tyr-248, Gly-155, Ala-156, Ser-157 and Thr-164. The phenyl ring of the t-butylbenzoyl structure lies within favourable van der Waals distance of the α-carbons of Gly-155 and Ala-156. The hydroxyl group of Thr-164 appears to interact with the π-electron cloud on the face of this phenyl group as well (distance of 3.68 Å between the Thr-164 OH and the center of the phenyl ring). One of the methyls of the t-butyl group is within van der Waals distance of the methylene group of Ser-157 (3.58 Å).

Figure 72a: (i) Energy minimized complex between CPA, phenylalanine and **NAH306.**

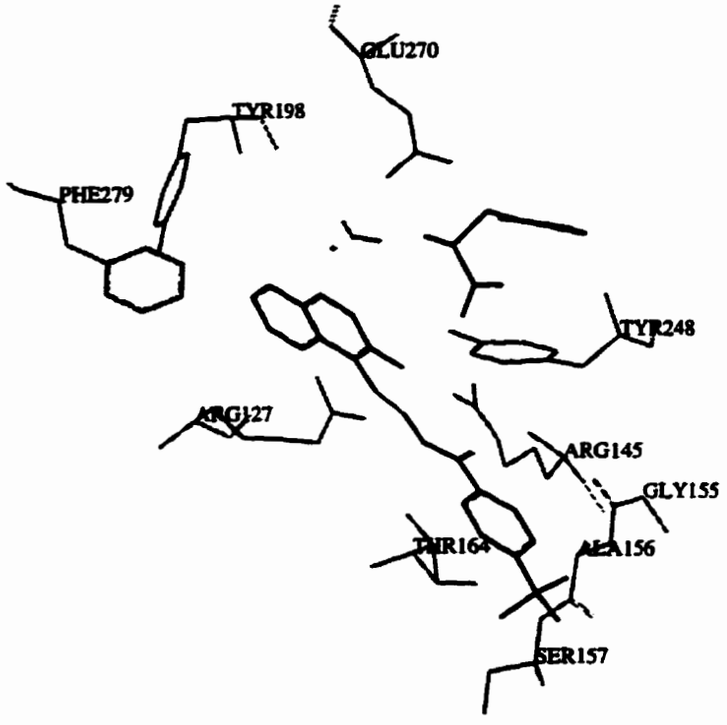

(ii) Stereoscopic view of (i).

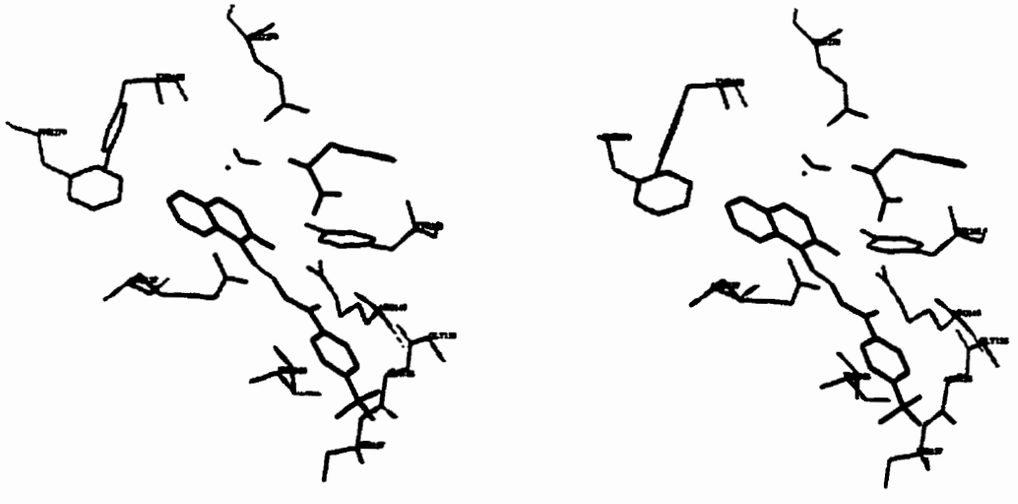

Figure 72b: (i) Energy minimized complex between CPA and **NAH306.**

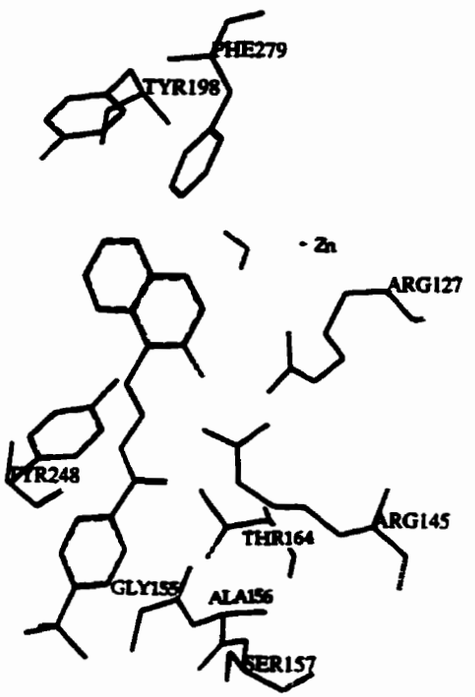

(ii) Stereoscopic view of (i).

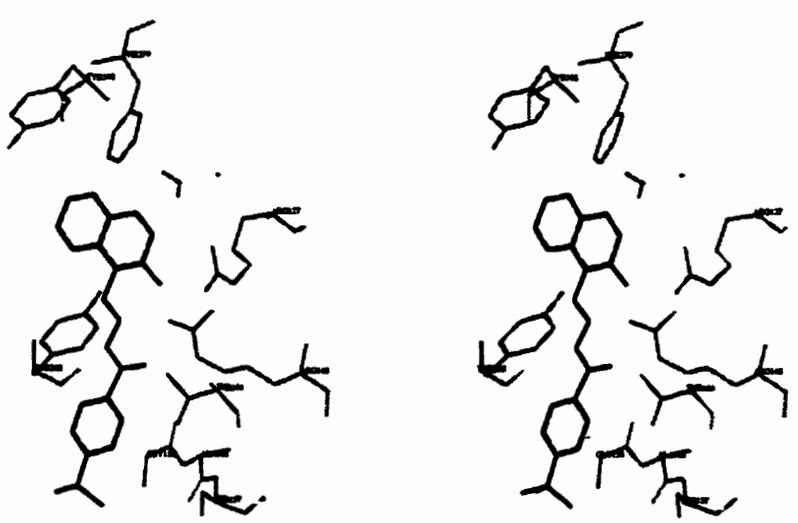

Figure 73: CPA active site interactions with phenylalanine and **NAH306** from the energy minimized CPA-Phe-**NAH306** complex. Distances in Å.

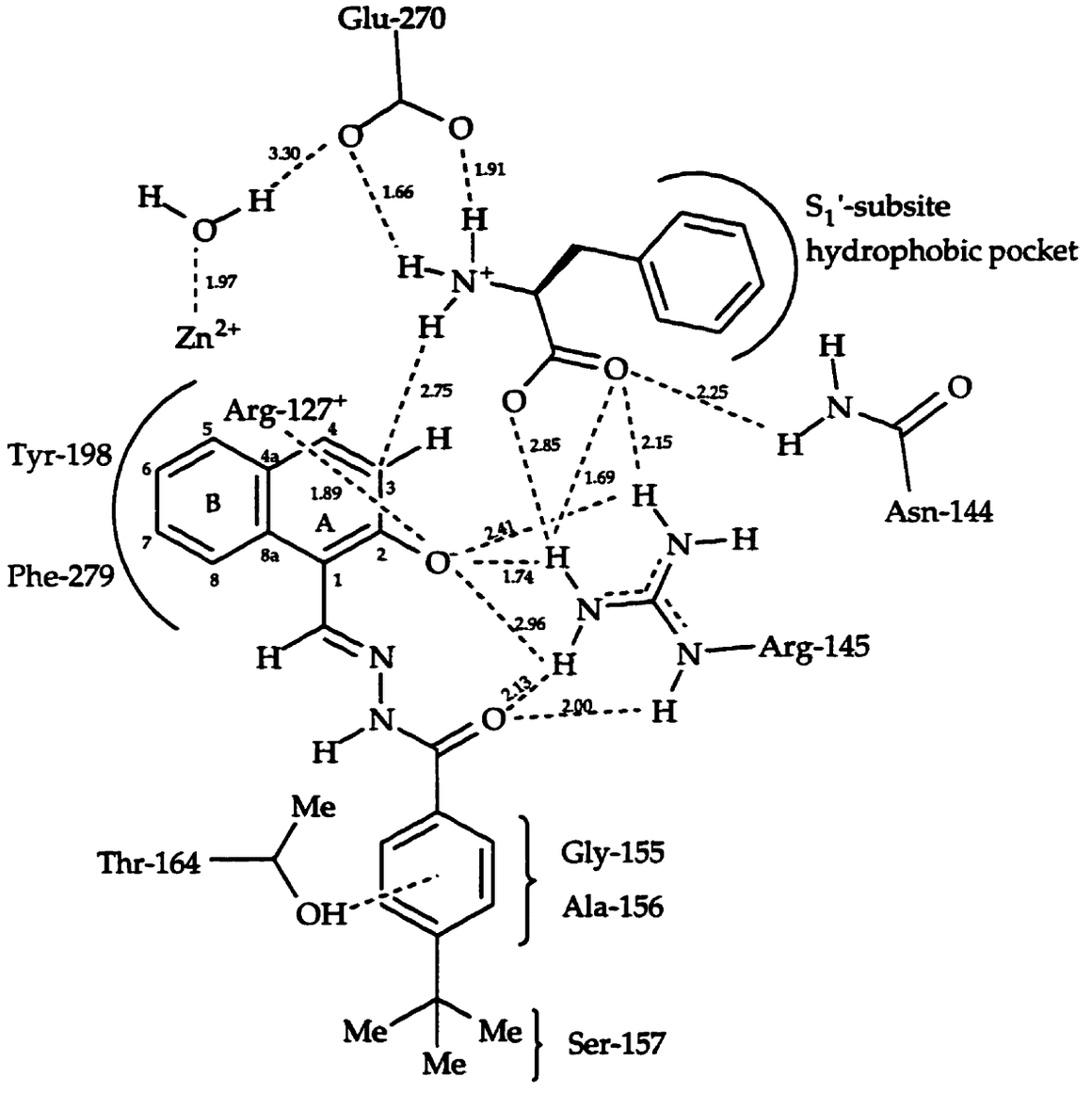

The ionized alcohol of **NAH306** interacts electrostatically with Arg-127 and Arg-145. The carbonyl oxygen of the amide group of **NAH306** is hydrogen bonded to Arg-145. The hydrogen of this amide appears not to be involved in any interactions with active site residues, since it points out from the active site in this model.

The phenylalanine component of the ternary complex is bound into the S_1'-subsite with the same interactions that are observed with the tyrosine substructure in the (Gly-Tyr)-CPA complex (Figure 71). There is an additional electrostatic interaction between the ammonium group of phenylalanine and the carboxylate of Glu-270. The Glu-270 also interacts with the zinc bound water molecule. The only interaction observed between phenylalanine product and **NAH306** is a 2.75 Å interaction between a hydrogen of the ammonium group and the C-3 carbon of the naphthalene ring. This interaction is considered to be electrostatically favourable because of the -0.175 charge at C-3 (determined using MOPAC calculations) and the positive charge on the ammonium group.

These proposed interactions in the ternary complex not only rationalize the affinity **NAH306** for CPA, but also may help explain the lack of binding ability of **NAH206** and **des-OH 306** to CPA.

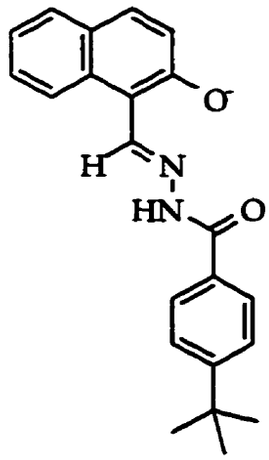

NAH306

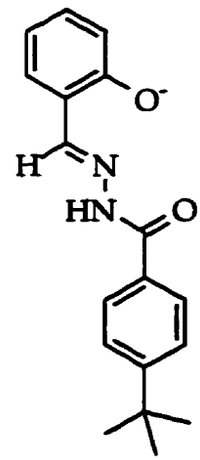

NAH206

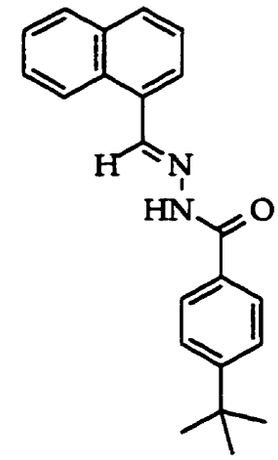

des-OH 306

As shown above in Table 6, **NAH206** and **des-OH 306** are much weaker inhibitors of CPA as compared to **NAH306**. The NAH **NAH206** lacks the extra phenyl ring found in the naphthalene structure of **NAH306** which interacts favourably with the hydrophobic pocket of the S_1-subsite. The NAH **des-OH 306** lacks the C-2 phenolate,

in the model in Figure 73, which is involved in important electrostatic interactions with the active site Arg-127 and Arg-145.

Another important observation concerning this hypothetical interaction between CPA and **NAH306** is that the hydrolysis product phenylalanine need not be bound to CPA in order for **NAH306** to bind to the S_1/S_2 subsites in this orientation. As previously mentioned, there appears to be some favourable interaction between the NH_3^+ group of phenylalanine and the π-electron rich C-3 carbon atom of **NAH306** in the ternary complex. Otherwise, the favourable interactions with S_1/S_2 subsites are very similar in the models of the ternary complex (CPA-**NAH306**-Phe) and the binary complex (CPA-**NAH306**). Thus, the binding of **NAH306** to free CPA may be qualitatively very similar to that suggested for the binding of **NAH306** with the CPA-Phe complex.

The modeling study undertaken for the binding of **NAH306** to CPA may also be used to design tighter binding NAH compounds. From close observations of this ternary complex, structural modifications to the inhibitor can be recommended that may result in more favourable interactions and subsequently tighter binding.

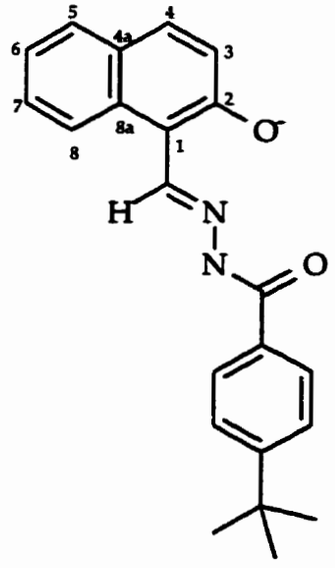

NAH306

The C_3 and C_4 of the naphthalene ring are situated in close proximity to the active site zinc, at 4.17 Å and 4.30 Å respectively. A substituent such as $-CH_2-OH$, $-CH_2-CO_2^-$ or $-CH_2-CO-NH_2$ at the C_3 and/or C_4 position might allow for a direct ligand interaction between such groups and the active site zinc. Also, a polar hydrogen bonding group at C_6 or C_7 may improve contact with the OH group of Tyr-198. Another possible modification which does not involve the naphthalene ring is the substitution of the t-butyl group with a hydrogen or methyl group. The suggested interactions between the t-butyl group of **NAH306** and the methylene group of the Ser-157 are not considered essential for the overall binding ability of **NAH306**, and a less hydrophobic group in this position might result in improved solubility which is, a common problem found with **NAH306** and other N-acylhydrazones.

Concusion: The Use of N-Acylhydrazones as Inhibitors of CPA and ACE

In conclusion, it has been shown that the N-acylhydrazone **NAH306** is a relatively specific inhibitor of CPA with no activity against ACE. Kinetic and molecular modeling studies suggest that **NAH306** binds to CPA without chelation or direct binding to the active site metal ion. Furthermore, the observed results are best explained by the assumption that **NAH306** binds to the S_1/S_2 subsites of CPA unlike normal substrates and known competitive inhibitors which interact strongly with the S_1' subsite and with the active site metal ion. Modeling studies further suggest a number of structural variations in the naphthalene ring of **NAH306** which might enhance the potency of this unusual inhibitor. Further studies to test such hypotheses are recommended.

Chapter 5: Experimental

5.1 Organic Synthesis

General Procedures

All reactions were conducted under an N_2 atmosphere unless otherwise stated. Acetone was dried by refluxing over calcium sulphate for several hours followed by distillation and storage over activated 4 Å molecular sieves (dried acetone was used within two days of preparation). Benzene was dried by refluxing over Na metal and benzophenone for several hours followed by distillation. Toluene was dried by refluxing over CaH_2 for several hours followed by distillation. N,N-Dimethylformamide (DMF) was dried by distillation from activated molecular sieves at reduced pressure and stored over activated 4 Å molecular sieves. Diethyl ether (ether) was dried by refluxing over Na metal and benzophenone for several hours followed by distillation. Methylene chloride (CH_2Cl_2) was dried by reflux over calcium hydride (CaH_2) for several hours, then followed by distillation. All dried solvents were stored over activated 4 Å molecular sieves.

Reactions were monitored by thin layer chromatography (TLC) using aluminum backed sheets precoated with silica gel (Merck) containing a fluorescent indicator. Purification by preparative TLC was conducted on precoated silica gel 60 F_{254} plates with 0.25 mm layer thickness (Merck). Purification by column chromatography was done using silica gel 60 mesh (70-230) (Merck). Silica plates and aluminum backed sheets were analyzed using a UV lamp (254 nm).

Melting points were determined using a Meltemp melting point apparatus and are reported uncorrected. IR spectra were recorded on an Bomem MB-100 FTIR instrument.

^{1}H-NMR spectra were obtained using either a Bruker AC-200 (200 MHz), AM-250 (250 MHz) or AMX-500 (500 MHz) instrument. The spectral parameters are listed in the following order: (frequency, solvent) chemical shift in ppm (multiplicity, coupling constant(s), number of protons, assignment).

^{13}C-NMR spectra were obtained using either Bruker AC-200 (50.3 MHz), AM-250 (62.9 MHz) or AMX-500 (125.8 MHz) instrument. The spectral parameters are listed in the following order: (frequency, solvent) chemical shift in ppm.

The solvents used to obtain NMR spectra were $CDCl_3$ (where tetramethylsilane (TMS) or $CHCl_3$ as an internal reference), DMSO-d_6 (DMSO-d_5 as an internal reference), benzene-d_6 (benzene-d_5 as an internal reference) and CD_2Cl_2 ($CDHCl_2$ as an internal reference).

Mass spectra were generally determined by eletron impact methods. Low and high resolution mass spectra were determined by Dr. R. Smith at the McMaster Regional Centre for Mass Spectrometry, McMaster University, Hamilton, Ontario, on a VG ZAB-E instrument. In some cases chemical ionization was conducted using ammonia gas as the bath gas to obtain results reported as M+18. Eletrospray (ES) and Fast Atom Bombardment High Resolution Mass Spectrometry (FAB-HRMS) were determined by Mr. Lorne Taylor in the Department of Chemistry, University of Waterloo. Electospray analysis was conducted using a VG Quatro II triple quadrupole Mass Spectrometer equipped with an Electrospray source. Results are reported as M+1. FAB analyses were conducted using a VG Analytical 7070E Spectrometer with results reported as $M+H^+$.

Combustion analyses (M-H-W Laboratories, Phoenix, Arizona) were used to determine C, H and N content.

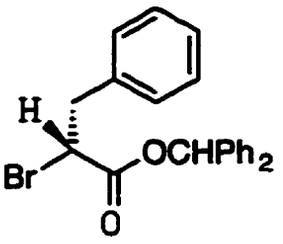

53

Benzhydryl (R)-2-bromo-3-phenylpropanoate (53). (R)-Phenylalanine (Aldrich, 25.00 g, 151 mmol) and NaBr (156 g, 1.516 mol) were dissolved in 2.5 M H_2SO_4 (600 mL) in a 1-L round-bottom flask and chilled to -5°C. Aqueous $NaNO_2$ (31.25 g, 453 mmol, dissolved in a minimum amount of water) was added drop-wise, and the mixture was stirred for 30 min at -5°C. The product was then extracted with $CHCl_3$ (150 mL), and the organic phase was washed with water, brine and dried over Na_2SO_4. The solvent was removed *in vacuo* leaving 2-bromo-3-phenylpropanoic acid (**52**), as a yellow oil (30.50 g), which was esterified without further purification. This method was similar to that of Prescott et al.[164] Diphenyldiazomethane (15.75 g, 81.1 mmol, prepared from benzophenone hydrazone (Aldrich) as discribed by Miller[166], was dissolved into 40 mL of dry benzene. A solution of **52** (18.90 g) in benzene (40 mL) was added drop-wise. The mixture was allowed to stir for 15 min and was then washed with 5% $NaHCO_3$, brine and dried over Na_2SO_4. The solvent was removed *in vacuo* leaving a pale yellow oil. The crude product was purified by column chromatography (1:12 EtOAc:Hexane) to give a hard pale yellow waxy product (17.1g, 46.1% yield from (R)-phenylalanine): R_f 0.37 (1:12 EtOAc:Hexane); IR (KBr): 1741 cm^{-1}; ^1H NMR (250 MHz, $CDCl_3$) δ 3.26 (dd, J = 14.1, 7.0 Hz, 1H, CH_2), 3.47 (dd, 1H, J = 14.1, 8.6 Hz, 1H, CH_2), 4.51 (dd, J = 7.0, 8.5 Hz, 1H, CH), 6.83 (s, 1H, O-C<u>H</u>Ph_2), 7.09-7.37 (m, 15H, Ar-H); ^{13}C NMR (50.3 MHz, $CDCl_3$) δ 41.2, 45.5, 78.6, 113.9, 127.1, 127.4, 128.1, 128.3,

128.6, 128.7, 128.8, 129.3, 136.6, 139.4, 168.4; HRMS calcd for $C_{22}H_{19}O_2{}^{79}Br$ 394.0569, found 394.0559; Anal. Calcd for $C_{22}H_{19}O_2Br$: C, 66.85; H, 4.78. Found: C, 66.91; H, 5.04.

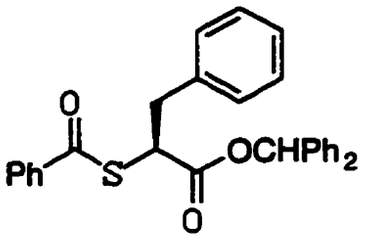

54

Benzhydryl (S)-2-(S-benzoylthio)-3-phenylpropanoate (54). Thiobenzoic acid (Aldrich, 1.30 mL, 11.0 mmol, dissolved in acetone (10 mL)) was added drop-wise to a solution of **53** (3.617 g, 9.15 mmol) in acetone (20 mL), and then stirred with K_2CO_3 (1.40 g, 10.13 mmol) for 30 min at rt. Diethyl ether (30 mL) and 5% $NaHCO_3$ (30 mL) were added and the organic phase was separated, washed with 5% $NaHCO_3$, brine and dried over Na_2SO_4. The solvent was removed *in vacuo* to give a waxy solid (2.363 g, 57% yield): R_f 0.24 (1:12 EtOAc:Hexane); IR (KBr) 1739, 1669 cm^{-1}; ^1H NMR (200 MHz, $CDCl_3$) δ 3.15 (dd, J = 13.9, 6.8 Hz, 1H, CH_2), 3.34 (dd, J = 14.0, 8.5 Hz, 1H, CH_2), 4.78 (dd, J = 6.8, 8.4 Hz, 1H, CH), 6.84 (s, 1H, O-C<u>H</u>Ph_2), 7.13-7.93 (m, 20H, Ar-H); ^{13}C NMR (50.3 MHz, $CDCl_3$) δ 38.1, 47.4, 78.1, 126.97, 127.06, 127.15, 127.39, 127.85, 127.91, 128.41, 128.48, 128.70, 129.19, 133.73, 139.53, 170.0; MS: m/z (CI, NH_3) 470 ($M+NH_4^+$); Anal. Calcd for $C_{29}H_{24}O_3S$: C, 76.96; H, 5.34. Found: C, 76.86; H, 5.38.

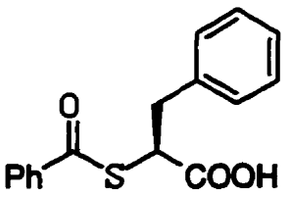

(S)-**50**

(S)-2-(S-Benzoylthio)-3-phenylpropanoic acid (50). Phenol (Baker Chemical Co., 1.20 g, 12.8 mmol) and **54** (2.00 g, 4.42 mmol) were dissolved in TFA (8.0 mL), and stirred for 30 min at rt. The solvent was removed *in vacuo* , and the crude product was dissolved in EtOAc (20 mL), and extracted with three aliquots of 5% $NaHCO_3$ (15 mL). The aqueous layer was washed with 30-60 pet. ether and acidified to pH 2 with 6 M HCl. The product was then extracted with CH_2Cl_2 and dried over Na_2SO_4 and $MgSO_4$. The solvent was removed *in vacuo* to leave a light yellow wax-like solid (1.110 g, 87.7% yield): R_f 0.41 (1:1 hexane:EtOAc containing 1.4% AcOH); IR (KBr) 1704, 1681 cm^{-1}; ^1H NMR (250 MHz, $CDCl_3$) δ 3.14 (dd, J = 14.1, 7.5 Hz, 1H, CH_2), 3.40 (dd, J = 14.1, 7.7 Hz, 1H, CH_2), 4.64 (dd, J = 7.5, 7.6 Hz, 1H, CH), 7.21-7.93 (m, 10H, Ar-H), 9.91 (br, 1H, COOH); ^{13}C NMR (50.3 MHz, $CDCl_3$) δ 37.6, 47.1, 127.3, 127.6, 128.7, 128.8, 129.3, 134.1, 136.1, 137.0, 176.4, 190.1; HRMS calcd for $C_{16}H_{14}O_3S$: 286.0664, found: 286.0654; Anal. Calcd for $C_{16}H_{14}O_3S$: C, 67.11; H, 4.93. Found: C, 66.90; H, 5.07.

(R)-2-(S-Benzoylthio)-3-phenylpropionic acid ((R)-**50**) was also synthesized, starting with (S)-phenylalanine and using the same synthetic route desribed for (S)-**50**. This thioester of (R)-**50** was originally synthesized for bioassays as an enantimer of (S)-**50**, but was used to help determine the enantiomeric purity of (S)-**50**, as described below.

Determination of the Enantiomeric Purity of 50

The enantiomeric purity was determined after reacting (S)-**50** and its enantiomer (R)-**50** with optically active α-(S)-methylbenzylamine to form chiral salts. The salts were produced by mixing equimolar amounts of (R) or (S)-**50** with α-(S)-methylbenzylamine in benzene-d_6 to give 8.6 mM solutions.

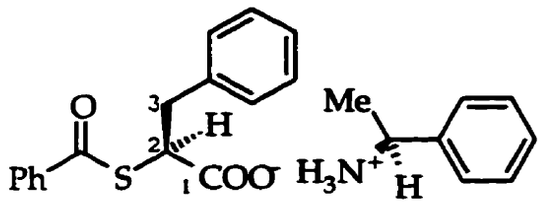

(S,S)-salt

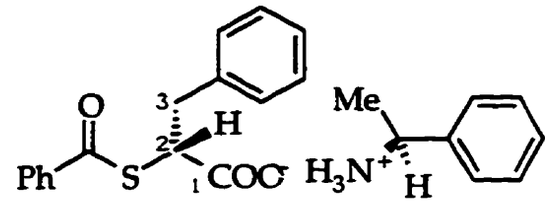

(R,S)-salt

55

The chiral salts were analyzed using ^{1}H-NMR at 500 MHz on a Bruker AMX-500. From analysis of each of the salts, as well as a 1:1 mixture of the salts, the chemical shifts were determined for the methyene and methine protons of the diastereomeric salts: (S,S)-salt, δ 3.20 (dd (A of ABX), J_{AB} = 13.5 Hz, J_{AX} = 7.5 Hz, 1H, CH_2), 3.44 (dd (B of ABX), J_{AB} = 13.6 Hz, J_{BX} = 7.3 Hz, 1H, CH_2), 4.78 (dd (X of ABX), J_{AX}=7.5 Hz, J_{BX}=7.3 Hz, 1H, CH); (R,S)-salt, δ 3.19 (dd (A of ABX), J_{AB} = 13.5 Hz, J_{AX} = 7.0 Hz, 1H, CH_2), 3.40 (dd (B of ABX), J_{AB} = 13.5 Hz, J_{BX} = 7.0 Hz, 1H, CH_2), 4.69 (dd (X of ABX), J_{AX}=7.0 Hz, J_{BX}=7.0 Hz, 1H, CH). The chemical shifts of the methine protons of the diasteroemeric salts of **50** were sufficiently well resolved to allow for accurate measurement of the ratio of diastereomers by electronic integration. From these measurements, the enantiomer purity of samples of (S)-**50** and (R)-**50** were estimated to be 90% **ee** and 94% **ee** respectively.

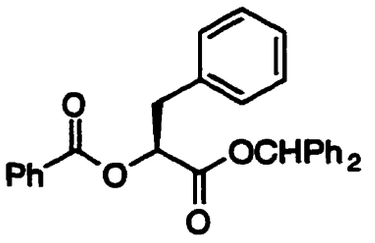

56

Benzhydryl O-(S)-2-benzoyl-3-phenyllactate (56). Sodium benzoate (Aldrich, 0.5539 g, 3.84 mmol) and **53** (0.760 g, 1.92 mmol) were dissolved in 10 mL of dry DMF and stirred for 6 h at rt. EtOAc (100 mL) was added and the mixture was washed four times with water (50 mL), then washed with brine and dried over Na_2SO_4. The crude product, obtained by removal of the solvent *in vacuo*, was purified using column chromatography (1:12 EtOAc:Hexane) to give a clear thick gum (0.233 g, 28% yield): R_f 0.33 (1:12 EtOAc:Hexane); IR (neat) 1755, 1728 cm^{-1}; ^1H NMR (200 MHz, $CDCl_3$) δ 3.24 (dd, 1H, CH_2), 3.33 (dd, 1H, CH_2), 5.61 (dd, 1H, CH), 6.91 (s, 1H, OC<u>H</u>Ph_2) 7.20-8.03 (m, 20H, Ar-H); ^{13}C NMR (50.3 MHz, $CDCl_3$) δ 37.3, 73.3, 77.9, 126.9, 127.3, 127.9, 128.0, 128.3, 128.4, 129.3, 129.7, 133.2, 135.6, 139.4, 165.7, 168.6; MS: m/z (CI, NH_3) 454 ($M+NH_4^+$); Anal. Calcd for $C_{29}H_{24}O_4$: C, 79.80; H, 5.54. Found: C, 80.00; H, 5.70.

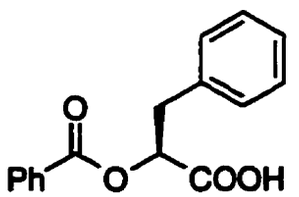

51

(S)-O-Benzoyl-3-phenyllactic acid (51). Phenol (Baker Chemical Co., 0.4377 g, 4.65 mmol) and **56** (0.198 g, 0.454 mmol) were dissolved in TFA (6.2 mL) and stirred for 30 min at rt. The solvent was removed *in vacuo* and the crude product was triturated twice with water (8 mL) to remove the majority of the phenol. The crude product was then dissolved in CH_2Cl_2, dried over Na_2SO_4 and $MgSO_4$, and the solvent was removed *in vacuo* to give a yellow oil (0.332 g). The product was further purified by preparative TLC (3:1 hexane:EtOAc containing 1.4% AcOH) to give a light yellow-orange solid (0.101 g, 83% yield): R_f 0.35 (3:1 hexane:EtOAc containing 1.4% AcOH); IR (neat) 1722 cm^{-1}; ^1H NMR (500 MHz, $CDCl_3$) δ 3.29 (dd, J=14.4, 8.5 Hz, 1H, CH_2), 3.35 (dd, J=14.4, 4.3 Hz, 1H, CH_2), 5.48 (dd, J=8.5, 4.3 Hz, 1H, CH), 7.24-8.02 (m, 10H, Ar-H); ^{13}C NMR (50.3 MHz, $CDCl_3$) δ 37.2, 73.0, 127.1, 128.4, 128.5, 129.0, 129.3, 129.8, 133.4, 135.7, 165.9, 175.3; MS: m/z (CI, NH_3) 288 ($M+NH_4^+$); Anal. Calcd for $C_{16}H_{14}O_4$: C, 71.10; H, 5.22. Found: C, 70.93; H, 5.07.

The enantiomeric purity of **51** was determined using a similar procedure for determining the enantiomeric purity of **50**, through the use of (R) and (S)-α-methylbenzylamine for chiral salt formation followed by ^1H-NMR (500 MHz) analysis. Two salt solutions were produced using equal amounts of **51** and α-(S)-methylbenzylamine or α-(R)-methylbenzylamine in $CDCl_3$ to give final concentration of 8.6 mM. The chemical shifts of the (S,R)-salt in the (S,R)-salt solution are important in that this complex is an enantiomer of the (R,S)-salt complex (therefore having the same chemical shifts), which is the enantiomeric impurity being measured in the (S,S)-

salt solution. The proper detection of the (R,S)-salt complex in the (S,S)-salt solution lead to an accurate measurement of enantiomeric purity for **51**.

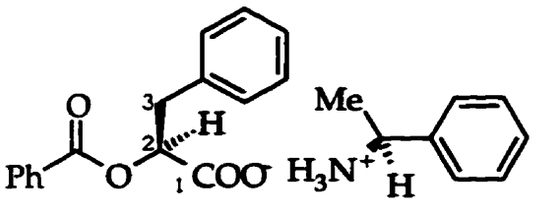

(S,S)-salt

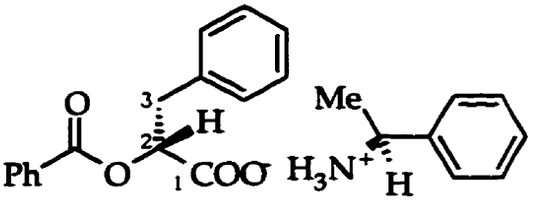

(R,S)-salt

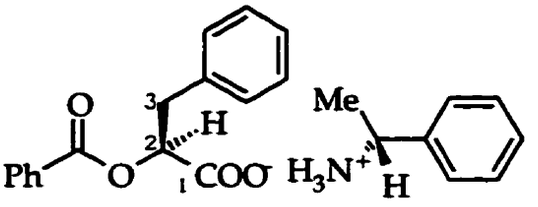

(S,R)-salt

^{1}H-NMR analysis of (S,S) and (S,R)-salt solutions revealed little separation of the chemical shifts of the methylene protons of the (S,S) and (S,R)-salts. The chemical shifts of the C-3 hydrogens, however, differed sufficiently to allow accurate integration measurements: (S,S)-salt, δ 5.17 (dd, J=3.6 Hz and 9.4 Hz); (S,R)-salt, δ 5.13 (dd, J=3.8 Hz and 9.5 Hz). In the case of the (S,S)-salt solution, the diastereomeric impurity (R,S) formed by reaction of the enantiomeric impurity (R)-**51** with α-(S)-methylbenzylamine was present to the extent of 23%. As a result, the enantiomeric excess (**ee**) was determined to be 54%.

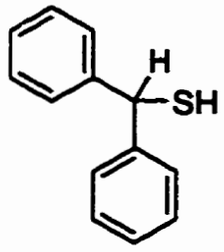

64

Diphenylmethanethiol (64). According to the method of Lawesson[177]; benzhydrol (Aldrich, 1.05 g, 5.70 mmol) and Lawesson's reagent (Aldrich, 1.27 g, 3.14 mmol) were heated in dry toluene at reflux (8.5 mL) for 30 min. The solution was cooled and the solvent was removed *in vacuo* . The yellow liquid crude product was purified twice using column chromatography (1:15 EtOAc:Hexane) to give a colourless liquid (0.696 g, yield 60%): R_f 0.66 (1:15 EtOAc:Hexane); IR (neat) 2561 cm^{-1} (S-H); ^1H NMR (200 MHz, $CDCl_3$) δ 2.26 (d, J = 5.5 Hz, 1H, S-H), 5.42 (d, J = 5.5 Hz, 1H, C-H), 7.17-7.45 (m, 10H, Ar-H).

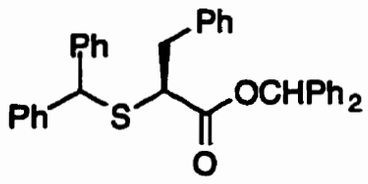

65

Benzhydryl (S)-2-(benzhydrylthio)-3-phenylpropanoate (65). A solution containing (R)-**53** (0.556 g, 1.41 mmol) and **64** (0.296 g, 1.48 mmol) were dissolved in dry acetone (11.5 mL) and the reaction was stirred with K_2CO_3 (0.314 g, 2.27 mmol) for 12.5 h at rt. EtOAc (15 mL) and 5% $NaHCO_3$ (5 mL) were added and the mixture was well agitated. The organic layer was dried over Na_2SO_4. Evaporation of the organic solvent and purification using column chromatography (1:15 EtOAc:Hexane) gave a clear gummy solid (0.6619 g, 92.4% yield): R_f 0.26 (1:15 EtOAc:Hexane); IR (neat) 1732 cm^{-1}; ^1H NMR (250 MHz, $CDCl_3$) δ 2.89 (dd, J = 13.9, 7.5 Hz, 1H, CH_2), 3.17 (dd, J = 13.9, 8.2 Hz, 1H, CH_2), 3.37 (apparent t, J = 7.8 Hz, 1H, CH), 5.12 (s, 1H, S-C<u>H</u>Ph_2), 6.88 (s, 1H, O-C<u>H</u>Ph_2), 6.97-7.34 (m, 25H, Ar-H); ^{13}C NMR (50.3 MHz, $CDCl_3$) δ 37.3, 48.4, 54.2, 77.5, 126.6, 126.8, 127.3, 127.3, 127.6, 127.7, 128.1, 128.3, 128.4, 128.5, 129.2, 137.6, 139.6, 139.8, 139.9, 140.3, 170.9; MS: m/z (CI, NH_3) 532 ($M+NH_4^+$); Anal. Calcd for $C_{35}H_{30}O_2S$: C, 81.68; H, 5.87. Found: C, 81.86; H, 5.80.

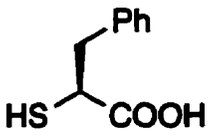

35

(S)-2-Mercapto-3-phenylpropanoic acid (35). A solution of **65** (0.2904 g, 564 μmol) and phenol (Baker Chemical Co., 1.24 g, 13.2 mmol) were dissolved in CH_2Cl_2 (5.4 mL) and TFA (5.4 mL) and the solution was stirred for 18 h at rt. The solvent was removed *in vacuo* , and the crude product was dissolved in EtOAc, and extracted with three aliquots of 5% $NaHCO_3$. The aqueous layer was washed with 30-60 pet. ether and acidified to pH 2 with 6 M HCl. The product was then extracted with CH_2Cl_2 and dried over Na_2SO_4 and $MgSO_4$. Further purification was effected using preparative TLC (2:1 hexane:EtOAc containing 1.4% AcOH) to produce **35** as a light yellow oily product (0.0283 g, 31% yield): R_f 0.47 (2:1 hexane:EtOAc containing 1.4% AcOH); IR (neat) 2562 cm^{-1}, 1713 cm^{-1}; ^1H NMR (250 MHz, CD_2Cl_2) δ 2.22 (d, J = 9.0 Hz, 1H, SH), 3.03 (dd, J= 14.0, 7.0 Hz, 1H, CH_2), 3.26 (dd, J=13.9, 8.2 Hz, 1H, CH_2), 3.64 (m, 1H, CH), 7.21-7.34 (m, 5H, Ar-H); ^{13}C NMR (50.3 MHz, CD_2Cl_2) δ 42.5, 43.2, 128.3, 129.8, 130.3, 137.9*, 176.9*; MS: m/z (CI, NH_3) 200 ($M+NH_4^+$); HRMS calcd for $C_9H_{10}O_2S$: 182.0402, found: 182.0409; Anal. Calcd for $C_9H_{10}O_2S$: C, 59.32; H, 5.53. Found: C, 59.50; H, 5.62.

* As a result of the low intensity of the ^{13}C NMR spectral signals, the values marked * were not detected directly. These chemical shift values were determined using a ^{13}C-^1H Heteronuclear Multiple Bond Correlation (HMBC) experiment on the AMX-500 in CD_2Cl_2.

Determination of the Enantiomeric Purity of 35

For the determination of enantiomeric purity of (S)-**35**, a parallel synthetic pathway was required to produce the methyl ester derivative of (S)-**35**, which was reacted with (S)-(+)-Mosher's chloride [(S)-(+)-α-methoxy-(trifluoromethyl)phenylacetyl chloride, **100**] to produce diastereomers which were analyzed using high field NMR to determine the diastereomeric ratio.

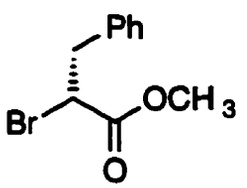

67

Methyl (R)-2-bromo-3-phenylpropanoate (67): Diazald (Aldrich, 5.0 g) was converted to diazomethane in ether solution using a Mini-Diazald kit (Aldrich). The diazomethane solution was added drop-wise to a chilled (-10°C) ether solution of (R)-**52** (3.27g, 0.0143 mol) until no more diazomethane was consumed as indicated by the persistance of the yellow colour. Acetic acid was added drop-wise to react with the slight excess of diazomethane. The solvent was removed *in vacuo*, leaving a crude yellow oil product, which was purified using column chromatography (1:19 EtOAc:Hexane) to give **67** as a pale yellow oil (1.90 g, 55% yield): R_f 0.46 (1:19 EtOAc:Hexane); IR (neat): 1741 cm^{-1}; ^1H NMR (250 MHz, $CDCl_3$) δ 3.24 (dd, J=14.1, 7.1Hz, 1H, CH_2), 3.46 (dd, J=14.2, 9.4Hz, 1H, CH_2) 3.73 (s, 3H, OCH_3), 4.40 (dd, J = 7.1, 8.3Hz, 1H, CH), 7.16-7.34 (m, 5H, Ar-H); MS: (ES) M+1=242.8 ($C_9H_{12}O_2{}^{79}Br$), M+1=244.8 ($C_9H_{12}O_2{}^{81}Br$).

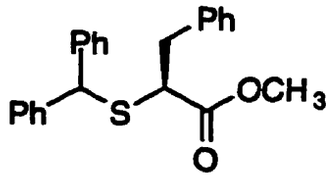

68

Methyl (S)-2-(benzhydrylthio)-3-phenylpropanoate (68): Compound **67** (1.19 g, 4.88 mmol) and diphenylmethane (**64**, 1.13 g, 5.62 mmol) were dissolved in acetone (17 mL) and the solution was stirred with K_2CO_3 (0.810 g, 5.86 mmol) for 12.5 h at rt. EtOAc and water were added and the mixture was shaken well. The organic layer was separated and dried over Na_2SO_4. The solvent was removed *in vacuo* and the product was purified using preparative TLC (1:15 EtOAc:Hexane) to yield **68** as a colourless oil (0.187 g, 97% yield): R_f 0.34 (1:15 EtOAc:Hexane); ^1H NMR (250 MHz, $CDCl_3$) δ 2.88 (dd, J = 13.9, 7.4Hz, 1H, CH_2), 3.15 (dd, J=13.8, 8.2Hz, 1H, CH_2), 3.32 (dd, J=7.4, 8.2 Hz, 1H, CH), 3.59 (s, 3H, OCH_3), 5.22 (s, 1H, S-C<u>H</u>Ph_2), 7.02-7.35 (m, 15H, Ar-H); MS: (ES) M+1=363.0.

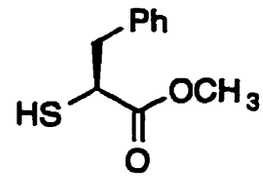

69

Methyl (S)-2-mercapto-3-phenylpropanoate (69): Compound **68** (0.1178 g, 325 mmol) and phenol (Baker Chemical Co., 0.699 g, 7.43 mmol) were dissolved in CH_2Cl_2 (3.2 mL) and TFA (3.2 mL) the mixture was stirred for 18 h at rt. The solvent was removed *in vacuo,* and the crude product was purified using preparative TLC (1:12 EtOAc:Hexane) to give **69** as a pale yellow oil (0.057g, 89% yield): R_f 0.46 (1:12 EtOAc:Hexane); ^1H NMR (250 MHz, $CDCl_3$) δ 2.15 (d, J=9.0 MHz, 1H, SH), 3.00 (dd, J=13.9, 7.1 Hz, 1H, CH_2), 3.24 (dd, J=13.9, 8.1 Hz, 1H, CH_2), 3.63 (m, 1H, CH), 3.66 (s, 3H, OCH_3), 7.17-7.33 (m, 5H, Ar-H); MS: (ES) M+1=196.8.

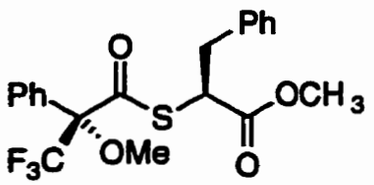

66

Methyl S-[(S)-α-methoxy-α-(trifluoromethyl)phenylacetoyl]-(S)-2-mercapto-3-phenylpropionate (66):

Compound **69** (0.022 g, 113 mmol) and (S)-(+)-Mosher's chloride (0.0324 g, 128 mmol) were dissolved in CH_2Cl_2 (2.5 mL). Et_3N (0.0073 g, 216 mmol) was added and the solution was stirred at rt for 10 min. The solvent was removed *in vacuo*. The crude product was dissolved in a mixture of EtOAc and water. The organic phase was separated and washed with water, brine, and dried over Na_2SO_4. The solvent was removed *in vacuo* leaving a white solid. As an aid to identifying ^{1}H-NMR signals from the diastereomer salts, a 1:1 mixture of diastereomeric esters was prepared in the same way, but using (R,S)-Mosher's chloride in place of (S)-Mosher's chloride. The product was a 1:1 mixture of **66** and **71**. MS: (ES) M+1=413.0.

(S)-(+)Mosher's chloride, (S)-(+)-α-methoxy-α-(trifluoromethyl) phenylacetyl chloride, was prepared from (R)-(+)-Mosher's acid using $SOCl_2$ (Aldrich).[178]

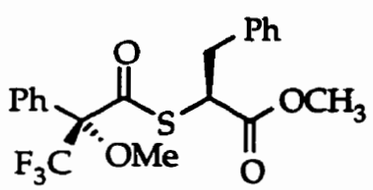

66
(S,S)

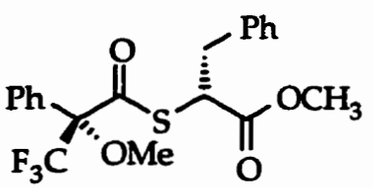

70a
(S,R)

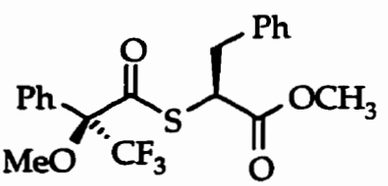

71
(R,S)

Enantiomeric Ratio Determination: The sample of thioester prepared using (S)-Mosher's chloride was analyzed by ^{1}H-NMR at 500 MHz in CD_2Cl_2 in order to estimate diastereomeric purity. The ^{1}H-NMR spectrum of the thioester prepared from (R,S)-Mosher's chloride served as a guide to assigning ^{1}H-NMR signals. From analysis of each of the 1:1 mixture of **66** and **71**, only the chemical shifts of the methoxy functionalities were adequately separated on the spectrum to be characterized: **66**, δ 3.43 (q, J=1.6 Hz, 3H, OCH_3), 3.65 (s, 3H, ester methyl); **71**, δ 3.51 (q, J=1.5 Hz, 3H, OCH_3), 3.70 (s, 3H, ester methyl). Integration analysis of the pure **66** sample revealed signals form the **70a** isomer are the same as those for **71**. Only the signals from the ester methyl were well separated from one another and from signals arising from other parts of the molecule, therefore the ratio of diastereomers was estimated by measuring their integrated intensities. The ratio was found to be 1:17.8, which indicates that 94.7% of the sample was the (S,S) diastereomer corresponding to an **ee** value of 89.3%.

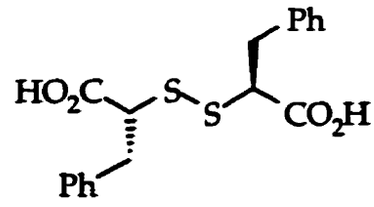

73

The disulfide **73** was synthesized by allowing a solution of **35** (140 mM) in Buffer A (see pg 223 for definition) to sit for 4 days allowing full oxidation. Residual thiol content was monitored by adding 500 μL of DTNB (1.0 mM in Buffer C (see pg 223 for definition)) to a 500 μL aliquot of the reaction solution, and absorbance measurement at 412 nm. The resulting mixture was acidified to pH 2 using 6 M HCl, then extracted three times with 10 mL of CH_2Cl_2. The combined organic extract was washed with brine (10 mL), dried over Na_2SO_4, filtered, and the solvent was removed *in vacuo* to leave a pale yellow oil (1.2 mg): R_f 0.42 (2:1 hexane:EtOAc containing 1.4% AcOH); ^1H NMR (250 MHz, CD_2Cl_2) δ 3.04 (dd, J=14.2, 7.4 Hz, 2H, CH_2), 3.23 (dd, J=14.2, 8.1 Hz, 2H, CH_2), 3.68 (dd, 2H, CH), 7.17-7.33 (m, 10H, Ar-H); HRMS calcd for $C_{18}H_{18}O_4S_2$: 362.0647, found: 362.0627.

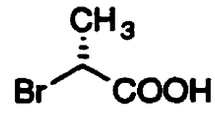

90

(R)-2-Bromo-3-phenylpropanoic acid (90). The method used to prepare **90** was similar to that of Prescott et al.[164] (R)-Alanine (Aldrich, 5.00 g, 56.1 mmol) and NaBr (57.5 g, 560 mmol) were dissolved in 2.5 M H_2SO_4 (220 mL) in a 500 mL round-bottom flask and the solution was chilled to -5°C in an ice-salt bath. An aqueous solution of $NaNO_2$ (11.61 g, 168 mmol, dissolved in minimum amount of water) was then added drop-wise and the mixture was stirred for 30 min at -5°C. The product was then extracted with $CHCl_3$, and the organic phase was separated, washed with water, brine and dried over Na_2SO_4. The solvent was removed *in vacuo* leaving a yellow oil product (1.846 g, 22% yield): ^1H NMR (250 MHz, $CDCl_3$) δ 1.86 (d, J= 7.0 Hz, 3H, CH_3), 4.41 (q, J=7.0 Hz, 1H, CH), 9.4 (b, 1H, COOH); ^{13}C NMR (50.3 MHz, $CDCl_3$) δ 21.3, 39.3, 176.3.

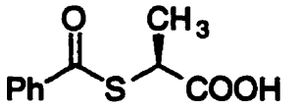

91

(S)-S-Benzoyl-2-mercaptopropanoic acid (91). Compound **90** (1.190 g, 7.71 mmol) and thiobenzoate (Aldrich, 1.426 g, 9.29 mmol) were dissoved in acetone (13 mL) and stirred with K_2CO_3 (1.066 g, 7.71 mmol) for 30 min at rt. Ethyl acetate and water were added and mixed well. The mixture was acidified to pH 2 with 6 M HCl. The organic phase was separated, washed with water, brine and then dried over Na_2SO_4. The solvent was removed *in vacuo* to give an orange oily product. The crude product was purified using column chromatography (4:1 hexane:EtOAc containing1.4% HOAc) to give **91** aa a light yellow wax (1.518 g, 94% yield): R_f 0.44 (4:1 hexane:EtOAc containing 1.4% HOAc); IR (KBr) 1708 cm^{-1}, 1669 cm^{-1}; ^1H NMR (200 MHz, CD_2Cl_2) δ 1.63 (d, J=7.3 Hz, 3H, CH_3), 4.42 (q, J=7.3 Hz, 1H, CH), 7.45-7.97 (m, 5H, Ar-H), 9.64 (b, 1H, COOH); ^{13}C NMR (50.3 MHz, CD_2Cl_2) δ 17.4, 41.1, 127.7, 129.1, 134.3, 136.5, 178.5, 190.7; FAB-HRMS calcd for $C_{10}H_{11}O_3S$ ($M+H^+$): 211.0429, found: 211.0430.

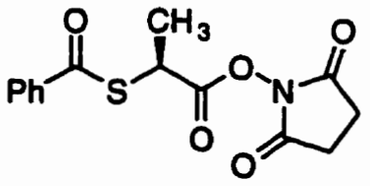

92

N-Hydroxysuccinimide ester of (S)-S-Benzoyl-2-mercaptopropanoic acid (92). 1,3-Dicyclohexylcarbodiimide (Aldrich, 1.391 g, 6.74 mmol), N-hydroxysuccinimide (Aldrich, 0.776 g, 6.74 mmol) and **91** (1.417 g, 6.74 mmol) were dissolved in 1,4-dioxane (280 mL) and stirred for 18 h at rt. The mixture was then filtered to remove 1,3-dicyclohexylurea (DCU), and the solvent was removed *in vacuo* to give **92** as a pale yellow oil (1.920 g, 93% yield): R_f 0.45 (1:1 EtOAc:Hexane); IR (neat) 1779 cm^{-1}, 1726 cm^{-1}, 1676 cm^{-1}; ^1H NMR (200 MHz, CD_2Cl_2) δ 1.74 (d, J=7.3 Hz, 3H, CH_3), 2.81 (s, 4H, CH_2), 4.71 (q, J=7.3 Hz, 1H, CH), 7.46-7.98 (m, 5H, Ar-H), 9.64 (b, 1H, COOH); ^{13}C NMR (50.3 MHz, CD_2Cl_2) δ 17.6, 26.0, 38.5, 127.8, 129.2, 134.5, 136.2, 168.6, 169.2, 189.3.

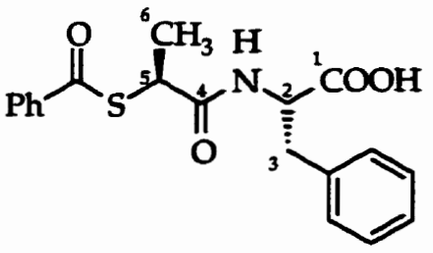

93

S-Benzoyl-(S)-2-mercaptopropanoyl-(S)-phenylalanine (93). L-Phenylalanine (Aldrich, 0.506 g, 3.06 mmol) and $NaHCO_3$ (0.514 g, 6.12 mmol) were dissolved in water (20 mL) and dimethoxyethane (20 mL). Compound **92** (0.627 g, 2.04 mmol, dissolved in 8 mL of dimethoxyethane) was then added and the solution was stirred for 3 h at rt. CH_2Cl_2 and 5% $NaHCO_3$ were added and crude product extracted into the aqueous phase. The aqueous phase was washed with CH_2Cl_2 and then acidified to pH 2 with 6 N HCl and extracted with EtOAc. The organic phase was separated, washed with 0.1 M HCl twice, then with brine and dried over Na_2SO_4. The solvent was removed *in vacuo* to give a pale yellow oil. The crude product was purified using preparative TLC (1:1 hexane:EtOAc containing 1.4% HOAc) to give a pale yellow wax (0.527 g, 73% yield): R_f 0.53 (1:1 hexane:EtOAc containing 1.4% HOAc); IR (KBr) 1742 cm^{-1}, 1726 cm^{-1}, 1655 cm^{-1}; ^1H NMR (200 MHz, CD_2Cl_2) δ 1.51 (d, J=7.3 Hz, 3H, CH_3), 3.08 (dd, J=14.1, 5.1 Hz, 1H, CH_2), 3.23 (dd, J=14.0, 7.1 Hz, 1H, CH_2), 4.30 (q, J=7.3 Hz, 1H, CH (C-5)), 4.87 (m, 1H, CH (C-2)), 6.89 (d, J=7.6 Hz, 1H, NH), 6.95-7.95 (m, 10H, Ar-H), 9.30 (b, 1H, COOH); ^{13}C NMR (50.3 MHz, CD_2Cl_2) δ 16.1, 37.5, 40.5, 53.8, 127.2, 127.8, 128.7, 129.1, 129.6, 134.5, 136.0, 136.4, 172.3, 176.7, 192.3; FAB-HRMS calcd for $C_{19}H_{20}NO_4S$ ($M+H^+$) 358.1113, found 358.1117.

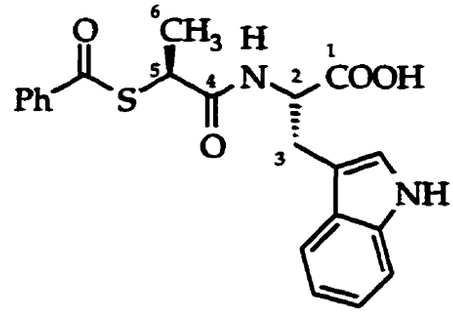

94

S-Benzoyl-(S)-2-mercaptopropanoyl-(S)-tryptophan (94). L-Tryptophan (Aldrich, 0.146 g, 0.717 mmol) and $NaHCO_3$ (0.121 g, 1.43 mmol) were dissolved in water (5 mL) and dimethoxyethane (5 mL). Compound **92** (0.147 g, 0.478 mmol) was dissolved in dimethoxyethane (2 mL) then added to the above solution and stirred for 3 h at rt. CH_2Cl_2 and 5% $NaHCO_3$ were added and the crude was product extracted into the aqueous phase. The aqueous phase was washed with CH_2Cl_2 and then acidified to pH 2 with 6 M HCl and extracted with EtOAc. The organic phase was separated, washed with 0.1 M HCl twice, then with brine, then dried over Na_2SO_4. The solvent was removed *in vacuo* to give a pale orange oil. The crude product was purified using preparative TLC (1:1 hexane:EtOAc containing 1.4% HOAc) to give **94** as a light yellow powder (0.0791 g, 42% yield): IR (KBr) 1739, 1654,1639 cm^{-1}; ^1H NMR (200 MHz, CD_2Cl_2) δ 1.51 (d, J=7.0 Hz, 3H, CH_3), 3.04 (dd, J=8.4, 14.8 Hz, 1H, CH_2), 3.18 (dd, J=5.1, 14.8 Hz, 1H, CH_2), 4.41 (q, J=7.0 Hz, 1H, CH (C-5)), 4.45 (m, 1H, CH (C-2)), 6.90-7.89 (m, 11H), 8.54 (d, J=7.7 Hz, 1H), 10.84 (s, 1H, COOH); FAB-HRMS calcd for $C_{21}H_{21}N_2O_4S$ ($M+H^+$) 397.1222, found 397.1219.

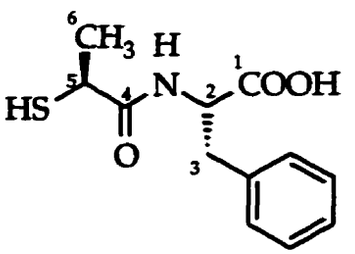

88

(S)-2-mercaptopropanoyl-(S)-phenylalanine (88): To a solution of **93** (0.2089 g, 0.585 mmol) in 1,4-dioxane (1.25 mL) was added an aqueous solution of 0.2 M NaOH (14.6 mL) and the mixture was stirred under Ar for 25 min at rt. The mixture then acidified to pH 2 with 6 M HCl and extracted with EtOAc twice, washed with water twice, then brine once and dried over Na_2SO_4. The solvent was removed *in vacuo* and the crude product was purified using preparative TLC (1:1 hexane:EtOAc containing 1.4% HOAc) to give a pale yellow crystalline product (0.062 g, 44% yield): R_f 0.43 (1:1 hexane:EtOAc containing 1.4% HOAc); IR (KBr) 1711, 1655 cm^{-1}; ^1H NMR (250 MHz, CD_2Cl_2) δ 1.51 (d, J=7.1 Hz, 3H, CH_3), 2.04 (d, 1 H, J=8.3 Hz, 1H, SH), 3.12 (dd, J=14.0, 6.7 Hz, 1H, CH_2), 3.27 (dd, J=14.0, 5.5 Hz, 1H, CH_2), 3.42 (m, 1H, CH (C-5)), 4.80 (m, 1H, CH (C-2)), 6.81 (d, J=7.4 Hz, 1H, NH), 7.20-7.36 (m, 10H, Ar-H), 9.58 (b, 1H, COOH); ^{13}C NMR (50.3 MHz, CD_2Cl_2) δ 22.0, 37.5, 38.1, 53.8, 127.6, 128.9, 129.8, 136.1, 174.1, 174.6; MS: HRMS calcd for $C_{12}H_{15}NO_3S$: 253.0773, found: 253.0762; Anal. Calcd for $C_{12}H_{15}NO_3S$: C, 56.90; H, 5.97; N, 5.53. Found: C, 57.16; H, 6.08; N, 5.34.

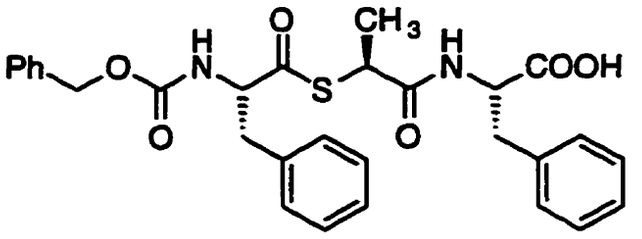

86

CBZ-Phe-(S)Ala-Phe (86): N-(Carbobenzyloxy)-L-phenylalanine (Aldrich, 0.0592 g, 198 mmol) was dissolved into dry acetone (2.0 mL) and cooled to 0°C. Triethylamine (0.0200 g, 198 mmol) and ethylchloroformate (0.0215 g, 198 mmol) were then added and the mixture was stirred for 5 min at 0°C. The mixture was then cooled to -20°C in a CCl_4-dry ice bath and **88** (0.0477 g, 198 mmol, dissolved in dry acetone(2.0 mL)) containing triethylamine (0.0200 g, 198 mmol), was added. The mixture was stirred for 30 min at -20°C, then 30 min at rt. EtOAc (5 mL) and water (1 mL) were then added. The mixture was acidified to pH 2 with 6 M HCl, and organic phase was separated, washed with 0.1 M HCl, brine and dried over Na_2SO_4. The solvent was removed *in vacuo* to give a yellow oily crude product. The crude product was purified using preparative TLC (1:1 hexane:EtOAc containing 1.4% HOAc) to give **86** as a pale yellow wax (0.0306 g, 29.0% yield): R_f 0.31 (1:1 hexane:EtOAc containing 1.4% HOAc); IR (KBr) 1665, 1696, 1710 cm^{-1}; ^1H NMR (500 MHz, CD_2Cl_2) δ 1.38 (d, J=7.3 Hz, 1H, CH_3), 2.97 (dd, J=14.3, 8.1 Hz, 1H, CH_2), 3.08 (dd, J=14.1, 6.9 Hz, 1H, CH_2), 3.13 (dd, J=14.2, 4.7 Hz, 1H, CH_2), 3.20 (dd, J=14.1 , 5.6 Hz, 1H, CH_2), 3.99 (q, J=7.3 Hz, 1H, CH), 4.62 (m, 1H CH), 4.73 (m, 1H, CH), 5.08 (s, 2H, CH_2 of CBZ group), 5.17 (d, J=8.5 Hz, 1H, NH), 6.59 (d, J=6.3 Hz, 1H, NH), 7.14-7.36 (m, 15H, Ar-H); ^{13}C NMR (50.3 MHz, CD_2Cl_2) δ 18.9, 36.5, 41.8, 53.7, 62.5, 65.6, 96.8, 126.4, 126.5, 127.3, 127.7, 128.15, 128.22, 128.28, 129.3, 137.2, 155.6, 170.4, 172.5, 200.4; FAB-HRMS calcd for $C_{29}H_{30}N_2O_6S$ 534.1824 ($M+H^+$), found 534.1826.

5.2 Biochemical Materials and Methods

All buffers were prepared using distilled deionized water. For CPA assays, Tris (Tris(hydroxymethyl)aminomethane) from Sigma was used with 0.5 M NaCl. The buffer was titrated to pH 7.5 using 6 M HCl and a Corning pH meter-115. For ACE assays, the sodium salt of HEPES (N-[2-hydroxylethyl]piperazine-N'-[2-ethanesulfonic acid]) from Sigma was used, with 0.3 M NaCl. HEPES buffer was titrated to a pH of 7.5 using 6 M HCl.

Carboxypeptidase A_α (CPA, EC 3.4.17.1), purified from bovine pancreas, was purchased from Sigma as an aqueous suspension of crystalline enzyme with toluene added.[206] The enzyme was prepared for activity measurements by mixing the suspension with Tris buffer at least one hour prior to use in enzyme assays. Enzyme concentration was determined using absorbance at 280 nm, where ε_{280} is 6.42×10^4 $M^{-1}cm^{-1}$.[97]

Angiotensin converting enzyme (ACE, EC 3.4.15.1) was purchased from Sigma as a lyophilized powder from rabbit lung, purified by Sigma by the method of Cushman.[195] The quantities of enzyme present in this commercial preparation is expressed in units, where one unit is defined as that quantity of enzyme preparation which will produce 1.0 μmole of hippuric acid from hippuryl-His-Leu per min in 50 mM HEPES and 0.3 M NaCl at pH 8.3 at 37°C.[195] ACE was prepared for assays by dissolving the powder (5 units) into 5 mL of 50 mM HEPES, 0.3 M NaCl, pH 7.5 buffer (Buffer E), giving a concentration of 1 unit per mL of solution. Such a solution has been reported to be stable at 5°C for months by Cushman.[195]

A Varian DMS-200 uv/visible spectrophotometer was used to carry out spectrophotometric enzyme assays and to record uv/visible spectra. PC Control DMS SCAN v1.0 (Softcom Ltd.) software was used on a Tatung 286 computer to measure

initial rates on progress curves and to analyze recorded spectra. Quartz cuvettes with a 1.0 cm pathlengths and 1 mL or 3 mL volume were employed.

The evaluation of kinetic data was carried out with the aid of various software packages on a DX2-66 486 computer. Grafit 3.01 (Erithacus Software Ltd.) was used to produce Lineweaver-Burk plots, determine the kinetic constants K_m and V using non-linear regression, and determine IC_{50} constants using the equation developed by Halfman[207]:

$$y = \frac{a}{1 + \left(\frac{x}{i}\right)^s}$$

-where y is enzyme activity, a is maximum activity (no inhibition), x is inhibitor concentration, i is the concentration of inhibitor which decreases the enzymatic activity to 50% of that of a control lacking the inhibitor (IC_{50}), and s is the slope factor. Grafit 3.01 was also used to determine parameters for other unique kinetic equations which are dicussed below. The software package EZ-FIT® (Perrella Scientific Inc.) was used to determine inhibition constants for competitive inhibitors. All kinetic software packages used employ the Marquardt-Levenberg non-linear regression analysis method,[208] with the standard errors of kinetic parameters being calculated by the matrix inversion method. Kinetic parameters which are determined from non-linear and linear regression analysis are quoted with ± standard errors. Other experimental values (rates, π, etc.) which were expressed as a mean of more than one determination are quoted with ± standard errors (unless otherwise stated). Standard error is defined as:

$$\text{standard error} = \frac{\sigma}{\sqrt{n}}$$

- where σ is the standard deviation, which is defined as:

$$\sigma = \left[\frac{1}{n-1} \sum_{i=1}^{n} (x_i - \bar{x})^2 \right]^{\frac{1}{2}}$$

$\bar{x}$ is the mean of the data

n is the number of data points

The buffer solutions used during kinetic experiments were as follows: (i) for the CPA assays: "Buffer A" represents 25 mM Tris, 0.5 M NaCl, pH 7.5 containing 10% ethanol (v/v); "Buffer B" represents 25 mM Tris, 0.5 M NaCl, pH 7.5 containing 3.5% ethanol (v/v); "Buffer C" represents 25 mM Tris, 0.5 M NaCl, pH 7.5 containing no ethanol; (ii) for ACE assays; "Buffer D" represents 50 mM HEPES, 0.3 M NaCl, pH 7.5 containing 5% DMSO (v/v); "Buffer E" represents 50 mM HEPES, 0.3 M NaCl, pH 7.5 containing no DMSO. All assays, with CPA or ACE, were conducted at 25°C, unless otherwise stated.

Peptidase activity of CPA was measured using hippuryl-L-phenylalanine (HP, Sigma) as substrate with monitoring at 265 nm.[182] The HP concentrations used in these assays ranged from 0.25 mM to 1.3 mM. The $\Delta\mathcal{E}_{265}$ for hydrolysis of HP to hippuric acid and L-Phe was 137.7 $M^{-1}cm^{-1}$, with an observed K_m and k_{cat} of 0.31±0.04 mM and 85.7±3.0 s^{-1} respectively in Buffer B.

ACE peptidase activity was measured using 2-furanacryloyl-L-phenylalanylglycylglycine (FAPGG) from Sigma as substrate.[102] The hydrolysis of FAPGG to produce 2-furanacryloyl-L-phenylalanine and glycylglycine was monitored by measuring absorbance decrease at 330, 335, 340, 348 or 350 nm depending on the substrate concentration range as described on pg 242.

Thioester (S)-50 as a Substrate of CPA

The hydrolysis of (S)-**50** by CPA was monitored by measuring the diminution of absorbance at 273 nm. The extinction coefficient at 273 nm for (S)-**50** (ε_{273}=8740±32 $M^{-1}cm^{-1}$) was determined using a 4.56 μM solution of the thioester in Buffer A. The ε_{273} value for benzoate in Buffer A was determined to be 476±1 $M^{-1}cm^{-1}$ using a 917 μM solution of the authentic acid. A 283.9 μM solution of the thiol **35** in Buffer A was employed for determination of ε_{273}=1405±7 $M^{-1}cm^{-1}$. A solution of the disulfide **73** was prepared by allowing a 283.9 μM solution of **35** to incubate at 25°C for 4 days to ensure complete oxidation. The resulting solution of **73** gave an ε_{273} value of 3030±11 $M^{-1}cm^{-1}$. All ε_{273} value determinations were conducted in duplicate or triplicate. From these observed ε_{273} values, the expected $\Delta\varepsilon_{273}$ value for the hydrolysis of (S)-**50** into benzoic acid and the thiol **35** was calculated as 6860 $M^{-1}cm^{-1}$, and the expected $\Delta\varepsilon_{273}$ value for the hydrolysis of (S)-**50** into benzoic acid and the disulfide **73** was predicted to be 6750 $M^{-1}cm^{-1}$.

The actual observed $\Delta\varepsilon_{273}$ value for (S)-**50** hydrolysis was determined by allowing 10 mL solutions of 8.78×10^{-5} M (S)-**50** in Buffer A to be fully hydrolyzed by CPA (456 nM). Full hydrolysis was observed after the solution was incubated for 30 h, at which point no further spectral changes were detected. A $\Delta\varepsilon_{273}$ value of 6930±25 $M^{-1}cm^{-1}$ was determined by performing the experiment in quadruplicate. The resulting solution contained CPA, benzoate and the expected disulfide **73**.

A CPA concentration of 1.0 μM to 1.5 μM was found to be most convenient for these assays. At this concentration thioesterase activity is easily measured, and $[E]_o$ is much lower than the lowest (S)-**50** concentration (6.4 μM) employed. The use of ethanol as a cosolvent was required to prevent precipitation of the substrate ((S)-**50**) at higher concentrations.

The $\Delta\varepsilon_{273}$ value of 6930 $M^{-1}cm^{-1}$ was utilized for the analysis of all hydrolysis studies of (S)-**50**.

Identification of the Products of CPA-Catalyzed Hydrolysis of (S)-50

A solution of (S)-**50** (73 μM) and CPA (1.5 μM) was incubated for 24 h in Buffer A to generate a product mixture (2 mL). An aliquot (800 μL) of this mixture was withdrawn and mixed with 200 μL of 0.53 mM DTNB (5,5'-dithiobis-(2-nitrobenzoic acid). Analysis of thiol content was carried out by measurement of absorbance at 412 nm.

In a similar experiment, a 100 mL solution of CPA (2.6 μM) and (S)-**50** (160 μM) was allowed to incubate for 24 h. The resulting mixture was acidified to pH 2 using 6 M HCl and then extracted three times with 10 mL of CH_2Cl_2. The organic phase was washed with brine (10 mL), dried over Na_2SO_4, filtered, and the solvent removed *in vacuo* to leave a pale yellow oil (1.5 mg). The product was subjected to both TLC and HRMS analysis.

The thin layer chromatography properties of the reaction products on silical gel were compared with these of authentic benzoic acid, the disulfide **73** and the thioester (S)-**50** using 2:1 hexane:EtOAc containing 1.4% acetic acid as an eluant. The product exhibited two spots with R_f values of 0.42 and 0.63, which corresponded closely to the spots observed with **73** and benzoic acid respectively. The thioester (S)-**50** was not observed in the extracted product. The synthesis of authentic **73** is discussed later.

HRMS analysis of the extracted product resulted in the identification of a peak at 362.0644 (Calc. for $C_{18}H_{18}O_4S_2$: 362.0647) consistant with the presence of **73** at 122.0381 (Calc. for $C_7H_6O_2$: 122.0368) consistent with the presence of benzoic acid.

Pre-Steady State and Steady State Analysis of the CPA-Catalyzed Hydrolysis of (S)-50 in Buffer A

The CPA-catalyzed hydrolysis of (S)-**50** (6.4 μM to 257 μM) was monitored in Buffer A at 273 nm. For the pre-steady state analysis, 100 μL of CPA solution in Buffer C (15 μM) was added to 900 μL of (S)-**50** in 25 mM Tris, 0.5 M NaCl, pH 7.5, containing sufficient ethanol to yield a final ethanol concentration of 10% (v/v). The enzyme solution was added and mixed quickly with a glass stir rod, and the recording of the progress curve was started as soon as possible. The time elapsed between enzyme addition and the start of recording of the progress curve was about 3 to 5 s. The initial rate was measured from the initial linear portion of the progress curve. The results reported are the averages of at least four individual determinations. For the steady state analysis of the hydrolysis of (S)-**50**, the rate was estimated by measuring the slope of the second linear portion of the progress curve which followed the burst phase. The results were fitted to the Michaelis-Menten equation ($\Delta\varepsilon_{273}$ of 6930 $M^{-1}cm^{-1}$) using Grafit 3.01.

Analysis of Thiol Release During CPA-Catalyzed Hydrolysis of (S)-50 Using DTNB

CPA (100 μL in Buffer C) was added to a solution (900 μL) containing (S)-**50** and DTNB in sufficient ethanol to achieve a final ethanol concentration of 10% (v/v). The final concentrations achieved were 1.5 μM CPA, 0.1 mM DTNB, and concentrations of (S)-**50** of 9.6 μM, 34.5 μM or 178 μM, in Buffer A. TNB production in the reaction between **35** and DTNB was monitored at 412 nm assuming that $\Delta\varepsilon_{412}$ for this reaction is 14160 $M^{-1}cm^{-1}$.[179] Control experiments in which (S)-**50** was omitted or CPA was excluded were carried out to ensure that TNB generation resulted solely from the reaction with the hydrolysis product.

Hydrolysis of (S)-50 at Various DTNB Concentrations: The rate of TNB generation was observed at 412 nm at varying concentrations of DTNB (0.62 mM to 9.9 mM) at a constant concentration of CPA (3.2 μM) and (S)-**50** (168 μM) in Buffer A. CPA (15 μM in Buffer C) was added to start the assay. Assays were performed in triplicate or quadruplicate. The results are plotted in Figure 31. The maximum TNB production was observed at 4.9 mM DTNB.

Hydrolysis of (S)-50 in 4.9 mM DTNB: The hydrolysis of (S)-**50** at varying concentrations (13.4 μM to 168 μM) was observed at a constant CPA (3.0 μM) and DTNB (4.9 mM) concentrations in Buffer A at 412 nm. The results, which are plotted in Figure 32, were analyzed using Grafit 3.01 to yield K_m and V which are reported in Section 2.1.5.

Inhibition of CPA Peptidase Activity by DTNB: The inhibition of CPA peptidase activity by DTNB was studied using varying concentrations of DTNB (0, 50 μM, 150 μM) and hippuryl-L-phenylalanine (0.16 mM to 1.12 mM) at a constant CPA concentration of 121 nM in Buffer A. The results are shown in Lineweaver-Burk format in Figure 32. The data (using averages of three or more separate determinations) was analyzed by EZ-FIT® to determine the K_i which is reported in Section 2.1.5.

The Use of Bromothymol Blue for Detecting Proton Release

The ε values for bromothymol blue (BTB) and the sodium salt form (NaBTB) where determined at 420 nm and 615 nm. A solution of bromothymol blue (127 μM) was prepared in freshly boiled distilled water. The extinction coefficients for BTB were found to be ε_{420} of 2140 $M^{-1}cm^{-1}$ and ε_{615} of 0 $M^{-1}cm^{-1}$. Sufficient 0.01 M KOH was added to completely deprotonate BTB to give a final concentration of 124 μM in a solution containing 10% EtOH (v/v). The extinction coefficients for NaBTB were found to be ε_{420} of 1780 $M^{-1}cm^{-1}$ and ε_{615} of 38500 $M^{-1}cm^{-1}$. These values give a $\Delta\varepsilon_{420}$ of 369 $M^{-1}cm^{-1}$ and $\Delta\varepsilon_{615}$ of 38500 $M^{-1}cm^{-1}$ for the deprotonation of BTB or protonation of NaBTB. Based on these results, the wavelength of 615 nm was chosen to be the ideal wavelength to observe changes of NaBTB concentration.

A stock solution of BTB/NaBTB was prepared by dissolving bromothymol blue and NaCl into freshly boiled distilled water, followed by titration of the solution to a pH of 7.5 using 0.1 M NaOH. The final [BTB+NaBTB]=181 μM and [NaCl]=0.625 M.

A control experiment was conducted to test the accuracy of the BTB/NaBTB buffer for detecting changes in proton concentration. A 30 μM solution of benzoic acid was prepared in freshly boiled distilled water. Aliquots of the benzoic acid solution were added to the solution of BTB/NaBTB of 145 μM containing 10% ethanol (v/v). The changes in absorbance at 615 nm corresponded accurately with the expected changes for the introduction of H^+ to solution.

Substrate Hydrolysis Detected using Bromothymol Blue Buffer: For the analysis of substrate hydrolysis, the substrate, such as (S)-**50**, was predissolved in ethanol and added to the stock BTB/NaBTB solution. The addition of substrate changed the

colour and pH of the BTB/NaBTB mixture because of the introduction of H^+. This was corrected by titrating each mixture to a pH of 7.5 using 0.1 M NaOH to generate the substrate/BTB/NaBTB solutions. Activity was then monitored at 615 nm after 100 μL of CPA (15 μM in 0.5 M NaCl in freshly boiled distilled water) was added to 900 μL of the substrate/BTB/NaBTB solution. Final concentrations were [BTB+NaBTB]=145 μM, [NaCl]=0.55 M, $[E]_o$=1.35 μM, and [(S)-**50**] ranging from 10 μM to 26 μM, ethanol 10% (v/v). The starting absorbance of 1.95 indicates that the actual concentrations for BTB and NaBTB are 94.4 μM and 50.6 μM respectively.

Control experiments were conducted, in which a solution of (S)-**50** (10 μM) in BTB/NaBTB containing 10% ethanol (v/v) showed no change at 615 nm when incubated in the absence of CPA.

The Hydrolysis of Bz-(S)-OPhe (51) by CPA

For the hydrolysis of Bz-(S)-OPhe (**51**), preliminary spectral studies of **51** and its hydrolysis products β-phenyllactate and benzoic acid showed that hydrolysis is best monitored at 280 nm, with a $\Delta\varepsilon_{280}$ of -394 $M^{-1}cm^{-1}$.

The hydrolysis of **51** was also examined in a solution containing 3.5% ethanol (v/v). Using the method as previously mentioned, the sodium salt of **51** was prepared. The kinetic parameters K_m and k_{cat} were determined using substrate concentrations 72, 128, 283, 424 and 640 μM, with a constant $[E]_o$=1.5 μM.

As discussed earlier in Section 2.0.2, the ester **51** was shown to possess an ee of 54%. Therefore, the sample of **51** used contained 77% of the S-configuration, and 23% of the R-configuration. Since only the S-configuration is assumed to be active with respect to CPA catalysis, the actual active concentration is therefore 77% of the total concentration. The $\Delta\varepsilon_{280}$ can be recalculated to be -512 $M^{-1}cm^{-1}$. The K_m and k_{cat} calculated on the basis of this $\Delta\varepsilon_{280}$ are reported in Section 2.1.7.

The hydrolysis of **51** was also monitored in Buffer A at two substrate concentrations (50 μM and 160 μM) at constant $[E]_o$=1.44 μM. The observed initial rates are reported in Section 2.1.7.

Studying the Hydrolysis of 51 Using Bromothymol Blue: The hydrolysis of **51** was studied using the same procedure employed for the analysis of hydrolysis of (S)-**51** using bromothymol blue. The CPA concentration was 1.44 μM. Two concentrations of **51** were used, 50 μM (38.5 μM of (S)-enantiomer) and 160 μM (123.3 μM of (S)-enantiomer), to yield the results shown in Table 4.

The Hydrolysis of Bz-Gly-(R,S)-OPhe (76) by CPA

The hydrolysis of **76** by CPA was monitored in Buffer A. The ester **76** was purchased from Sigma in the sodium salt form. The hydrolysis of **76** was measured using solutions of **76** (0.23, 0.45, 0.68, 0.90 and 1.19 μM) at a constant $[E]_o$=20 nM in Buffer A. The activity was recorded using a wavelength of 265 nm ($\Delta\varepsilon_{265}$=118 $M^{-1}cm^{-1}$). The kinetic parameters K_m and k_{cat} were determined using Grafit 3.01 and are reported in Section 2.1.7.

Proton Release During Hydrolysis of Bz-Gly-(R,S)-OPhe Using Bromothymol Blue Buffer: The hydrolysis of **76** was studied using a procedure similar to that employed in the analysis of hydrolysis of (S)-**50** using bromothymol blue. Two concentrations of **76** were used, 0.20 and 1.01 mM. The rate of hydrolysis of **76** by CPA was observed to be much faster than those of (S)-**50** and **51**. As a result, a lower enzyme concentration ($[E]_o$=7.2 nM) was employed to avoid exceeding the capacity of the buffer during the assay.

The measured initial rates were corrected for the concentration of active enantiomer present and are reported in Section 2.1.7.

Pre-Steady State Kinetic Analysis

The π values, as defined in Section 2.1.4, were determined graphically using the back-extrapolation procedure. The progress curves in which π values were measured contained the pre-steady state burst as well as some portion of the linear steady state.

The Pre-Steady State Burst for (S)-50 Hydrolysis Monitored at 273 nm: The π values were measured from the progress curves where [(S)-**50**]=70.6 μM in Buffer A at $[E]_o$=1.5 μM. The reported π value is an average of three determinations.

The Burst for (S)-50 Hydrolysis Monitored Using Bromothymol Blue (615nm): The π values were measured from the progress curves of reactions in which the concentrations of (S)-**50** were 11 or 16 μM, in the BTB/NaBTB buffer solution described above ($[E]_o$=1.49 μM). Using the graphical method described above, the π values are the averages of four determinations.

The Effect of Ethanol Content on CPA-Catalyzed Hydrolysis of Hippuryl-L-Phenylalanine

The hydrolysis of HP was monitored in 25 mM Tris, 0.5 M NaCl, pH 7.5 at 25°C buffer containing 0%, 2.5%, 5% or 10% ethanol (v/v), at substrate concentrations of 0.44 mM and 1.76 mM. The assays were conducted in quadruplicate at a wavelength of 265 nm. From the observed rates at each ethanol concentration, the data were fitted

to the Michaelis-Menten equation to derive approximate K_m and k_{cat} values (using Grafit 3.01).

The CPA-catalyzed hydrolysis of HP was monitored in Buffer B with HP concentrations ranging from 0.25 mM to 1.3 mM. The parameters K_m and k_{cat} were found to be 0.31±0.04 mM and 85.7±3.0 s^{-1} respectively (determined using Grafit 3.01).

The Hydrolysis of (S)-50 by CPA in Buffer B: Using an assay procedure similar to that used to study the hydrolysis of (S)-**50** in Buffer A, the CPA-catalyzed hydrolysis of (S)-**50** was also monitored in Buffer B. In this case, the initial burst was too rapid to allow for accurate measurement of pre-steady state kinetic parameters. It appeared that much of the burst occured during the manual mixing of enzyme and reactants which took an estimate 3 to 5 s. The steady state rates were measured using (S)-**50** concentrations ranging from 20.9 μM to 207 μM, at a constant $[E]_o$=1.34 μM. The resulting substrate concentration-rate relationship is shown in Appendix E.1.

The Hydrolysis of (S)-50 by CPA in the Absence of Ethanol: As a result of solubility problems in the absence of an organic cosolvent, the most concentrated solution of (S)-**50** prepared was 55.6 μM. The hydrolysis of (S)-**50** (50 μM) was monitored at 273 nm after mixing 100 μL of CPA (11. 5 μM) to with 900 μL of (S)-**50** (55.6 μM) solution in Buffer C. The time course plot was observed to be biphasic but the time scale of the burst was shorter than in experiments employing ethanol as cosolvent making accurate estimates of π impossible.

Analysis of (S)-50 as a Competitive Inhibitor of CPA

The CPA-catalyzed hydrolysis of HP was monitored in the presence of (S)-**50**. The hydrolysis of the peptide HP is normally monitored at 265 nm ($\Delta\varepsilon_{265}$=137.7

$M^{-1}cm^{-1}$). Since the hydrolysis of (S)-**50** can also be detected at this wavelength, the possibility of significant spectral changes at 265 nm due to hydrolysis of (S)-**50**, interfering with the determination of spectral changes resulting from HP hydrolysis, had to be addressed. In the presence of competing substrate B, the rate of catalysis (υ_A) for substrate A can be expressed as:[186]

$$\upsilon_A = \frac{[E]_o \, k_{cat}{}^A [A]}{[A] + K_m{}^A(1 + [B]/K_m{}^B)} \qquad (5.1)$$

The rate of catalysis for substrate B can be expressed as:

$$\upsilon_B = \frac{[E]_o \, k_{cat}{}^B [B]}{[B] + K_m{}^B(1 + [A]/K_m{}^A)} \qquad (5.2)$$

By dividing $K_m{}^A$ into equation 5.1, and dividing $K_m{}^B$ into equation 5.2, the resulting equations possess the same denominators:

$$\upsilon_A = \frac{(k_{cat}{}^A/K_m{}^A)[E]_o \, [A]}{[A]/K_m{}^A + 1 + [B]/K_m{}^B} \qquad (5.3)$$

$$\upsilon_B = \frac{(k_{cat}{}^B/K_m{}^B)[E]_o \, [B]}{[A]/K_m{}^A + 1 + [B]/K_m{}^B} \qquad (5.4)$$

By dividing equation 5.4 into 5.3, we get the ratio of the rate of reaction:

$$\frac{\upsilon_A}{\upsilon_B} = \frac{(k_{cat}/K_m)_A[A]}{(k_{cat}/K_m)_B[B]} \qquad (2.10)$$

From equation 2.10, and the fact that $\Delta A=(\Delta\varepsilon)(\Delta conc.)$, leads to equation 2.11:

$$\frac{\Delta A_A}{\Delta A_B} = \frac{(k_{cat}/K_m)_A[A]\Delta\varepsilon_A}{(k_{cat}/K_m)_B[B]\Delta\varepsilon_B} \qquad (2.11)$$

The situation where spectral changes from hydrolysis of (S)-**50** would be expected to interfere most with the spectral changes from hydrolysis of HP would be at the highest [(S)-**50**] and lowest [HP]. In the present study, those concentrations were 132 μM and 160 μM for [(S)-**50**] and [HP], respectively. The K_m, k_{cat} and $\Delta\varepsilon_{273}$ for steady state hydrolysis of (S)-**50** in Buffer B are 61.8 μM, 1.53×10^{-2} s^{-1} and 5070 $M^{-1}cm^{-1}$ respectively. The K_m, k_{cat} and $\Delta\varepsilon_{265}$ for HP hydrolysis under the same conditions are 310 μM, 85.7 s^{-1} and 137.7 $M^{-1}cm^{-1}$ respectively. Using these kinetic parameters and equation 2.11, it was determined that spectral changes from HP hydrolysis at 265 nm should be 35 or more times greater than those from the hydrolysis of (S)-**50**. As a result it was judged that the spectral changes from the hydrolysis of (S)-**50** could be ignored in interfering the results of the competing substrate assays.

The peptidase activity of CPA in the presence of (S)-**50** was measured after adding 50 μL of CPA (1.25 μM in Buffer C) to 300 μL of 0, 95 or 440 μM of (S)-**50** (in Buffer C containing 11.7% ethanol (v/v)) and allowing this mixture to incubate for 1 to 2 min. The HP solution (650 μL in Buffer C) was then added so that the final ethanol content was 3.5% (v/v) (Buffer B). The final HP concentrations ranged 0.16 mM to 1.6 mM whereas the final (S)-**50** concentrations were 0, 28.4 and 132 μM, and a

constant final $[E]_o$=62.3 nM. The data was analyzed by EZ-FIT® to determine the K_m^B which was reported in Section 2.2.2.

The Hydrolysis of (S)-50 in a O_2-Free Environment: Measurement of Thiol Release and Residual Peptidase Activity

As outlined briefly in Scheme 40, CPA (1.26 μM) and (S)-**50** (2.40 μM) are incubated in a large test tube in a total volume of 18 mL. The buffer was degassed under vacuum and argon was bubbled through the solution prior to use. During the experiment, a stream of Argon gas was passed over the reaction solution to maintain an O_2-free atmosphere. A control solution which lacked (S)-**50** was also studied. In both the reaction and control experiments Buffer B was employed and the solutions were incubated for 4 h at 25°C. During the incubation, aliquots were withdrawn and tested for both peptidase activity and thiol content.

CPA-catalyzed peptidase activities was measured by adding 50 μL aliquots of either the "control" or "reaction" mixture to 950 μL of HP solution (0.992 mM in Buffer B). The reported residual peptidase activities in the presence of (S)-**50** ("reaction") were determined as a percent of the activities in the absence of (S)-**50** ("control").

Thiol content was measured by mixing 500 μL of either the "control" or "reaction" mixture with 500 μL of DTNB solution (0.4 mM in Buffer C), and observing TNB generation at 412 nm. As shown in Figure 74, the reaction between DTNB and **35** present in solution is not spontaneous. Also, after the majority of **35** was reacted with DTNB, there was a remaining slow but constant increase in absorbance from the reaction between DTNB and additional **35** which is generated from further hydrolysis of (S)-**50** which occurs during course of the DTNB analysis experiment. This was explained by the fact that after an aliquot of the "reaction" mixture is withdrawn, it contains a mixture of CPA, (S)-**50** and **35**. The majority of the thioesterase activity is

inhibited by the presence of **35**. Once DTNB is added to the solution, any **35** present reacts with DTNB producing disulfide **72** (Figure 25). The CPA which is now not inhibited by **35**, catalyzes the hydrolysis (S)-**50** at a faster rate subsequently generating more **35**, and at a constant rate. The concentration of **35** prior to the addition of DTNB was estimated by back-extrapolating the constant rate to time zero, as shown in Figure 74. The results were plotted in Figure 39.

Figure 74: The reaction between DTNB and **35** at 412 nm.

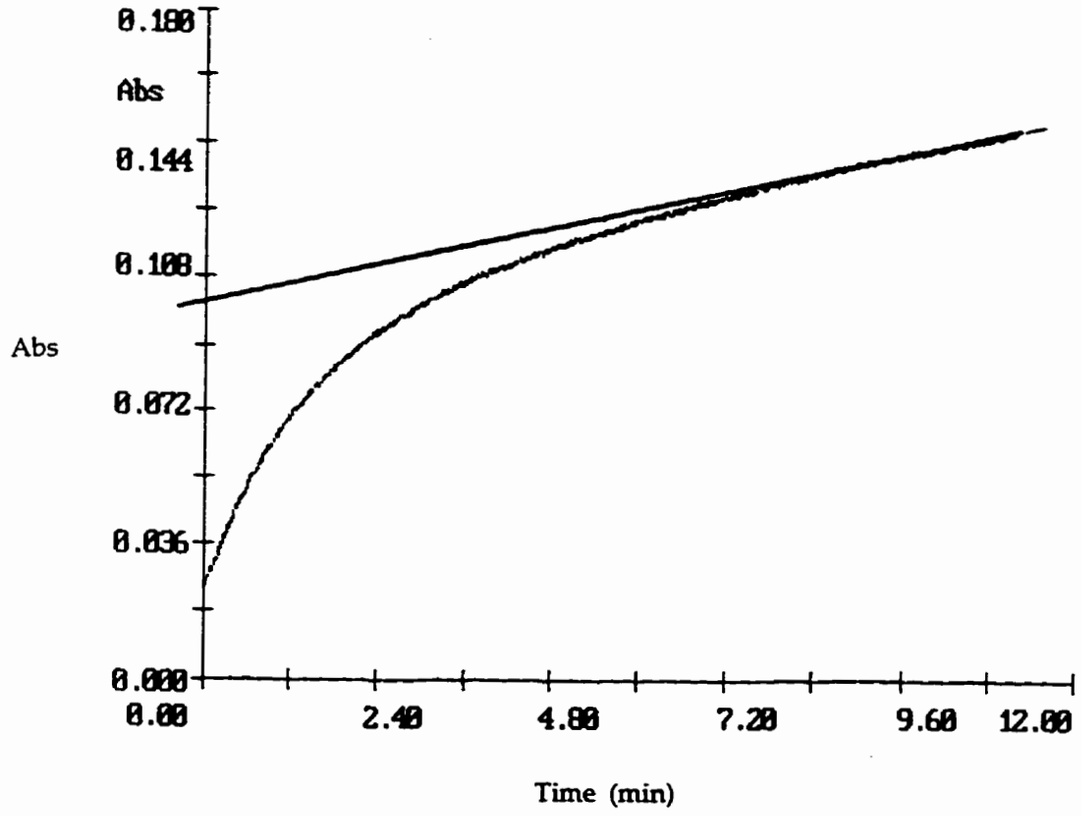

As discussed in Section 2.2.3, these results were used to estimate a K_i for the binding of **35** to CPA using equation 2.14.

$$\frac{V}{\upsilon_A} = \frac{K_m{}^A}{K_i{}^P[A]}[P] + \frac{K_m{}^A}{[A]}\left(1 + \frac{[B]}{K_m{}^B}\right) + 1 \qquad (2.14)$$

If V/υ_A is plotted against [P], the slope will equal $K_m{}^A/K_i{}^P[P]$. At each measured υ_A, the [P] is derived from the thiol versus time plot in Figure 39. The resulting slope from the resulting linear regression was 5.60×10^6(±6.8%) M^{-1}. $K_i{}^P$ was determined from the slope obtained by linear regression analysis of the data using the known concentration of HP and the known K_m for HP ($K_m{}^A$=0.31 mM). From the slope, $K_i{}^P$ was calculated to be 59.5±8.7 nM. The y-intercept is represented by:

$$b = \frac{K_m{}^A}{[A]}\left(1 + \frac{[B]}{K_m{}^B}\right) + 1 \qquad (5.5)$$

Oxidation of 35 and 36 in Buffer A

Solutions of **35** and **36** (95 µM in Buffer A) were prepared and allowed to incubate in an open flask at ambient temperature. Aliquots (500 µL) were withdrawn periodically and mixed with 500 µL of DTNB (1.0 mM), followed by absorbance measurement at 412 nm to determine thiol content (ε_{412} of 14160 $M^{-1}cm^{-1}$). A control solution which contained **35** (95 µM) was also prepared, using a degassed buffer solution, and incubated under an Ar atmosphere. The results are displayed graphically in Figure 41.

Inhibition of CPA Peptidase Activity by 35

A stock solution of **35** was prepared in ethanol at a concentration of 1.9 mM. The stability of this stock solution was tested by adding 25 μL to 100 μL of DTNB (1.0 mM) and 875 μL of Buffer C every 30 min over 3.5 h to test thiol content. The thiol content was found to be unchanged over this time range.

To a cuvette containing 925 μL of HP (0.55 mM) and 15 μL of ethanol, 20 μL of the freshly prepared stock solution of **35** (76 μM) was added, followed by 40 μL of CPA (3.15 μM). The reaction components were mixed quickly and peptidase activity recorded. The final concentrations were $[E]_o$=126 nM, [**35**]=760 nM and [HP]=0.5 mM, in Buffer B. In a similar assay, **35** (1.58 μM) was incubated in the buffer solution for 5 min prior to addition of CPA and recording of the progress curve. The 5 min preincubation in the oxidation of **35** to **73**. A control assay was also conducted as well, in the absence of **35** and **73**.

Inhibition of CPA Peptidase Activity by 36: The thiol **36** was tested as an inhibitor of CPA activity using experiments similar to those used to study inhibition by **35**. A solution of HP (0.5 mM), CPA (178 nM) and **36** (0.33 μM) was monitored at 265 nm in quadruplicate experiments to give a peptidase activity of 0.41±0.07 μM/s. In a parallel experiment, **36** (0.34 μM) was incubated in the buffer solution for 10 min prior to addition of CPA, the peptidase activity was observed to be 0.44±0.03 μM/s.

The Inhibition of CPA by Glutathione

The peptidase activity of CPA at [HP]=0.54 mM and $[E]_o$=120 nM was monitored in the presence of 0, 0.25, 0.5, 1.0 and 1.5 mM glutathione (GSH), in Buffer

B. The assay involved to addition of 40 μL of CPA solution (2.93 μM in Buffer C) to a 960 μL solution of HP and GSH. This experiment was repeated using HP concentrations of 0.27 mM and 0.37 mM. The results are displayed in Figure 46.

The Inhibition of CPA by *o*-Phenanthroline

This method used was similar to that reported by Vallee.[95] CPA (200 nM) was incubated with *o*-phenanthroline (OP) at varying OP concentrations of 0.2 μM to 63 μM, in Buffer B for 1.5 h at 5°C. The total volume of each incubation mixture was 3.0 mL. The CPA peptidase activity was measured after adding 100 μL of HP solution (5 mM in Buffer B) to 900 μL aliquots of the incubation mixtures, followed by analysis of peptidase activity. The peptidase activity analyses were done at 25°C in triplicate for each OP concentration. The data obtained is displayed graphically in Figure 47.

The Inhibition of CPA by 35 in the Presence of GSH

(i) Determination of Inhibition Type: To prevent oxidation of **35** in the stock solution during the experiment, the stock solution was prepared with 5 mM GSH (in Buffer C containing 15% EtOH (v/v)) with **35** concentrations of 0, 2.82, 4.35 and 5.65 μM. CPA-catalyzed peptidase activity was monitored after adding 40 μL of CPA solution (2.83 μM) to a mixture of 940 μL of HP solution (varying from 0.27 mM to 1.39 mM, in Buffer C containing 3.4% EtOH (v/v)) and 20 μL of stock **35** solution. The final HP concentrations were 0.25, 0.38, 0.51, 0.80 and 1.3 mM, and the final concentrations of **35** were 0, 56.5, 87 and 113 nM, in Buffer B, at a constant $[E]_o$=113 nM and [GSH]=0.1 mM. The data was analyzed graphically in the form of Lineweaver-Burk plots (see Figure 48).

(ii) Determination of K_i: The Dixon graphical method[189] was used to determine the K_i of **35**, as outlined in Appendix C. This method requires an IC_{50} curve for inhibition of CPA by **35**. The stock **35** solution in this experiment contained **35** (17.5 μM) and GSH (5 mM) in Buffer C containing 15% EtOH (v/v). CPA peptidase activity was monitored after 40 μL of CPA (2.94 μM) was added to 940 μL of HP (0.54 mM), and 20 μL of stock solution of **35** containing GSH (5 mM) solution. The final HP, GSH and CPA concentrations were 0.5, 0.1 and 117 nM respectively, in Buffer B. The concentrations of **35** were varied from 0 nM to 350 nM.

The Inhibition of CPA by Disulfide 73

(a) Reversible Inhibition: The inhibition of CPA by **73** was studied by monitoring the CPA-catalyzed hydrolysis of HP (0.25 mM to 1.3 mM), at inhibitor concentrations of 0, 2.17, 3.25, 4.35 and 6.52 μM in Buffer B, where $[E]_o$=117 nM. The competitive K_i value was determined using EZ-FIT®.

(b) Preincubation Experiments:

1. A 3.9 mL solution of **73** (327 μM) and CPA (1.5 μM) in 30% EtOH (v/v), 25 mM Tris buffer, 0.5 M NaCl, pH 7.5, was incubated at 25°C for 30 min under argon gas to remove O_2. Aliquots (50 μL) were withdrawn from the incubation mixture every 6 min and tested for peptidase activity by adding 950 μL of 1.1 mM HP (in 2.11% EtOH (v/v), 25 mM Tris buffer, 0.5 M NaCl, pH 7.5, 25°C) and monitoring peptidase activity at 265 nm. No loss of peptidase activity was observed over the 30 min incubation.

2. A solution (1.0 L) of **73** (437 μM), DTNB (0.1 mM) and CPA (7.5 μM) in 10% EtOH (v/v), 25 mM Tris buffer, 0.5 M NaCl, pH 7.5, 25°C was monitored at 412 nm

for 10 min at 412 nm. No release of **35**, which would be expected to react with DTNB to generate TNB observable at 412 nm (ε_{412} of 14160 $M^{-1}cm^{-1}$), could be detected.

Hydrolysis of (S)-50 by CPA in the Presence of Glutathione

The hydrolysis of (S)-**50** was monitored at 273 nm in Buffer A in the presence and in the absence of GSH (0.1 mM). This assay was conducted with concentrations of (S)-**50** of 29.7 μM and 58.5 μM. The enzyme component (200 μL of 7.59 μM CPA in Buffer C) was added and mixed in quickly before the start of the recording of the progress curve. The progress curves for these two experiments are presented in Figure 54.

Mechanism-Based Inhibition of CPA by the Thioester Substrate Analogue (S)-50

Solutions of CPA in Buffer B (137 nM) containing the thioester (S)-**50** (0, 979 nM and 9.79 μM) were incubated. The total volume was 10 mL. Aliquots (500 μL) were withdrawn periodically from the incubation mixtures and mixed with 500 μL of HP (1.0 mM in Buffer B) to yield solutions which were 68.6 nM in CPA and 0.50 mM in HP. The peptidase activity was monitored at 265 nm. The inhibitor to enzyme ratios (i/e) for the 0, 979 nM and 9.79 μM (S)-**50** mixtures were 0, 7 and 70 respectively. The peptidase activity at time zero was measured after adding 36 μL of CPA (1.9 μM) to 964 μL of (S)-**50** (0, 508 nM or 5.08 μM), HP (0.52 mM) and GSH (0.104 mM) in Buffer B. The data is presented graphically in Figure 56 as a percent residual peptidase activity of the observed activity for the control incubation (where [(S)-**50**]=0).

The absorbance observed for the incubation mixture after 170 min was measured to be 0.070, in the case of the i/e=70 experiment. In the case of the i/e=7

incubation, an absorbance reading was not possible due to the low concentrations of the species in solution.

The Determination of $\Delta\varepsilon$ Values and K_m the ACE-Catalyzed Hydrolysis of FAPGG

The ACE substrate FAPGG[102,194] was used to study ACE peptidase activity. This substrate has been suggested by Holmquist et al.[102] to be analyzed most conveniently at wavelengths between 328 nm and 354 nm. Larger ε values from substrate absorbance as well as large $\Delta\varepsilon$ from substrate hydrolysis are observed at lower wavelengths. As a result of the strong absorbance at 328 nm by FAPGG, higher wavelengths are required to study FAPGG hydrolysis at substrate concentrations higher than 0.1 mM.

Under our experimental conditions (Buffer D), the ε and $\Delta\varepsilon$ were determined for wavelengths 330, 335, 340, 345, 348 and 350 nm. FAPGG (16.0 mg) was dissolved in HEPES buffer (40 mL) to produce the stock solution (1.00 mM). The absorbance of FAPGG at various wavelengths was measured at a concentration of 100 μM. As expected, the absorbance by ACE (0.003 units/mL) at the wavelengths listed above was found to be zero. The substrate FAPGG (0.1 mM) and ACE (0.003 units/mL) were incubated allowing for complete hydrolysis of FAPGG, and the absorbances of the hydrolysis products were measured. From these absorbances, $\Delta\varepsilon$ values were determined. The resting ε and $\Delta\varepsilon$ values which were determined are reported below in Table 8.

Table 8: Extinction coefficient values and $\Delta\varepsilon$ values for FAPGG and FAPGG hydrolysis.

Wavelength (nm)	ε of FAPGG Absorbance ($M^{-1}cm^{-1}$)	$\Delta\varepsilon$ of FAPGG Hydrolysis ($M^{-1}cm^{-1}$)
330	9570	-2480
335	5620	-1630
340	2910	-1160
345	1310	-560
348	750	-354
350	520	-254

The $\Delta\varepsilon_{330}$ of -2480 $M^{-1}cm^{-1}$ at 330 nm observed under our conditions compares well to a $\Delta\varepsilon_{328}$ value of -2300 $M^{-1}cm^{-1}$ observed by Holmquist et al.[102] in 50 mM Tris, 0.3 M NaCl, pH 7.5.

The hydrolysis of FAPGG by ACE was then studied at varying FAPGG concentration (0.1 to 2.2 mM) at a constant ACE concentration of 0.03 units/ml in Buffer D. The measurement of peptidase activity at [FAPGG]=0.1 mM was conducted at 330 nm, [FAPGG]=0.2 mM was conducted at 335 nm, [FAPGG]=0.4 mM was conducted at 340 nm, [FAPGG]=0.56 and 0.8 mM was conducted at 345 nm, [FAPGG]=1.12 mM was conducted at 348 nm, and [FAPGG]=2.2 mM was conducted at 350 nm. The kinetic parameters K_m and V were determined to be 0.44±0.03 mM and 3050±60 nM/s respectively by fitting the data to the Michaelis-Menten equation using Grafit 3.01.

Inhibition of ACE by 88

(i) IC_{50} Analysis: The peptidase activity of ACE (0.03 units/mL) was monitored using FAPGG (0.1 mM) at 330 nm in Buffer D. The inhibitor **88** was added to the assay mixture from a stock solution (0.927 mM) in DMSO. Recording of the progress curve was started after 100 µL of the ACE stock (in Buffer E) solution was added to the FAPGG-inhibitor solution. The assays were done in triplicate or quadruplicate. An IC_{50} value of 34.0±3.3 nM was determined from this analysis using Grafit 3.01. The Dixon graphical analysis of the IC_{50} curve is shown in Appendix C.

For a solution of ACE containing **88** at a concentration of 27.8 nM, the peptidase rate was measured to be 326±12 nM/s. In a parallel assay, in which **88** (30.9 nM) was allowed to incubate in solution for 10 min prior to the addition of ACE (final **88** concentration of 27.8 nM), the peptidase rate was measured to be 317±12 nM/s.

(ii) Determination of Inhibition Type: A stock solution of 10.3 µM **88** in DMSO was prepared as a source of inhibition for this assay. The ACE-catalyzed hydrolysis of FAPGG was monitored at FAPGG concentrations of 0.17 mM (λ=335 nm), 0.273 mM (λ=340 nm), 0.438 mM (λ=345 nm), 0.70 mM (λ=345 nm), and 1.12 mM (λ=348 nm), in the presence of **88** (0, 34 and 69 nM) in Buffer D (5% DMSO (v/v)), at 25°C. The assay was started after 100 µL of 0.3 unit/mL ACE (in Buffer E) was added to a 900 µL solution of FAPGG and inhibitor (or no inhibitor). The final ACE content was 0.03 unit/mL. The resulting Lineweaver-Burk plot is shown in Appendix E.2.

The Hydrolysis of 93 and 94 by ACE

(a) A solution containing **93** (84 µM) and ACE (0.03 units/mL) was incubated in Buffer D for 22 h. The total volume of the incubation mixture was 1 mL. The

absorbances at 270 nm and 242 nm were monitored to detect any change which might indicate hydrolysis of the thioester. A similar incubation was done using **94**, but monitoring was carried out at 270 nm only. In both cases, the absorbance was unchanged over the 22 h incubation period. The addition of 200 μL of DTNB (0.5 mM) to the assay mixture containing **93** after the 22 h incubation gave no absorbance at 412 nm (ε_{412} of 14160$M^{-1}cm^{-1}$ for TNB).

(b) In another experiment, **93** (84 μM) was incubated with ACE (0.03 units/mL) in the presence of DTNB (0.1 mM), in Buffer D. The generation of TNB due to thioester hydrolysis was monitored at 412 nm. No TNB was observed to be released over a 10 min period.

(c) The hydrolysis of FAPGG (0.1 mM) at 330 nm by ACE (0.03 units/mL) was monitored in the presence and absence of **93** (84 μM) in Buffer D. No differences in peptidase rates were observed.

Influence of DTNB on the Peptidase Activity of ACE

The hydrolysis of FAPGG (0.1 mM) by ACE (0.03 units/mL) was monitored at 330 nm in the presence and absence of DTNB (0.1 mM) in Buffer D. No difference in peptidase rates was observed. Also allowing DTNB (0.1 mM) to incubate with ACE (0.032 units/mL) for 30 min prior to the addition of FAPGG to give final concentrations of DTNB, ACE and FAPGG of 0.093 mM, 0.03 units/mL and 0.1 mM, respectively, gave no difference in peptidase activity as compared to the control experiment in which no DTNB was present.

The ACE-Catalyzed Hydrolysis of 86 in the Presence of DTNB

The hydrolysis of **86** by ACE (0.1 unit/mL) was monitored through the generation of TNB at 412 nm from the reaction between the hydrolysis product **88** and DTNB (0.1 mM), in Buffer D. The concentration of **86** was varied from 2.5 μM to 100 μM. The parameters K_m and V were determined by fitting the data to the Michaelis-Menten equation using Grafit 3.01.

A control experiment was conducted in which **86** (100 μM) was allowed to incubate in the presence of DTNB (0.1 mM), in Buffer D. No TNB generation was observed over a 10 min period.

Mechanism-Based Inhibition of ACE by the Thioester Substrate Analogue 86

The thioester analogue **86**, at concentrations of 0, 50, 500 and 5000 nM, was incubated with ACE (0.033 units/mL) for over 160 min in Buffer D. The total volume was 16.2 mL. Aliquots (900 μL) were withdrawn every 10 min from the incubation mixtures and mixed with 100 μL of 1.0 mM FAPGG solution. The peptidase activity was measured at 330 nm with a final [ACE]=0.03 units/mL and [FAPGG]=0.1 mM. The actual $[E]_o$ was estimated to be 32.1 nM (0.033 units/mL). Therefore, the i/e values for the 50 nM, 500 nM and 5000 nM the solution of **86** mixtures would be 1.6, 16 and 160 respectively. The peptidase activity at time zero was determined by adding 100 μL of ACE (0.3 units/mL) to 900 μL of **86** (50, 500 or 5000 nM) and FAPGG (0.11 mM) in Buffer D, and monitored absorbance change at 330 nm. The data are displayed graphically in Figure 66 as a percent residual peptidase activity of the observed activity for the control incubation ([**86**]=0). The control incubation assay showed no loss of ACE peptidase activity during the time of the experiment.

Inhibition of CPA by NAH306, NAH206 and des-OH 306

The N-acylhydrazones **NAH306, NAH206, PIH, RFMP18, RFMP19, RFMP20, RFMP21** and **RFMP22** were provided by Dr. M. A. Parniak of the Lady Davis Institute for Medical Research. The N-acylhydrazone **des-OH 306** was prepared in this laboratory by E. H. Rydberg and R. S. Fletcher.

This method used here is similar to that used to study the inhibition of CPA by *o*-phenanthroline, which was previously mentioned in this Experimental Chapter. CPA (200 nM) was incubated with **NAH306, NAH206** or **des-OH 306** at varying concentrations in the range 0.2 μM to 63 μM, in Buffer B for 1.5 h at 5°C. The total volume of each incubation mixture was 3.0 mL. The CPA peptidase activity was measured after adding 100 μL of HP (5 mM in Buffer B) to 900 μL aliquots of the incubation mixtures, followed by analysis of peptidase activity. The peptidase activity was monitored at 25°C in triplicate for each inhibitor concentration. The data obtained was employed to determine IC_{50} for **NAH306**. For **NAH206** and **des-OH 306**, FOR WHICH 50% inhibition could not be achieved, IC_{33} and IC_{17} values respectively were calculated using Grafit 3.01.

Inhibition of ACE by NAH306, PIH, RFMP18, RFMP19, RFMP20, RFMP21 and RFMP22

The peptidase activity of ACE (0.03 units/mL) was monitored at 330 nm in buffer D, with either **NAH306, PIH, RFMP18, RFMP19, RFMP20, RFMP21** or **RFMP22** (11.1 μM) for 1 h at 5°C. Peptidase activity was monitored at 25°C after mixing 100 μL of FAPGG (1.0 mM in Buffer D) with 900 μL of each of the incubation

mixtures. Each assay was carried out in triplicate. The results are presented in Table 7.

Detailed Study of CPA Inhibition by NAH306

The inhibition of CPA by **NAH306** was studied by monitoring the CPA-catalyzed hydrolysis of HP (0.25 mM to 1.3 mM), at **NAH306** concentrations of 0, 6.66 and 13.3 μM in Buffer B, where $[E]_o$=132 nM. The data are presented graphically in Lineweaver-Burk format in Figure 69. The resulting data were also fitted to the equations 4.1 and 4.2 of Chapter 4 using Grafit 3.01.

The data obtained from this experiment were also used to produce a slope versus inhibitor concentration (m vs. [I]) replot. The slopes were determined by fitting the data at each inhibitor concentration to the Lineweaver-Burk relationship. The m vs. [I] replot is graphically presented in Appendix E.3, and fitted to a straight line by linear regression.

Appendix A:

Derivation of the Burst Kinetcs Equation 2.3

The equation 2.3 was derived for the kinetic mechanism in Scheme 32 using a method similar to the one Bender used to derive burst kinetics for α-chymotrypsin.[181]

$$\pi = E_o\left(\frac{k_2}{k_2 + k_{-2} + k_3}\right)\left(\frac{1}{1 + K_m/S_o}\right) \qquad (2.3)$$

$$\underset{\mathbf{E}\quad\mathbf{S}}{E + S} \underset{k_{-1}}{\overset{k_1}{\rightleftharpoons}} \underset{\mathbf{x}}{ES_1} \underset{k_{-2}}{\overset{k_2}{\rightleftharpoons}} \underset{\mathbf{y}}{EP_1P_2} \xrightarrow{k_3} \underset{\mathbf{p}}{E + P_1 + P_2}$$

For the following derivation, it is assumed that the total substrate concentration is much greater than the total enzyme concentration ($S_o >> E_o$), that the free substrate concentration equal to the total substrate concentration ($S \equiv S_o$), and k_{-1} is much greater than k_2 ($k_{-1} >> k_2$). The following rate relationships can be stated:

$$\frac{dx}{dt} = k_1ES + k_{-2}y - (k_{-1} + k_2)x \qquad (A\text{-}1)$$

$$\frac{dy}{dt} = k_2x - (k_{-2} + k_3)y \qquad (A\text{-}2)$$

$$\frac{dp}{dt} = k_3y \qquad (A\text{-}3)$$

Since the total enzyme concentration is a sum of all enzyme species;

$$E_o = E + x + y \tag{A-4}$$

and;

$$K_s = \frac{k_{-1}}{k_1} = \frac{ES_o}{x} \tag{A-5}$$

$$E = \frac{xK_s}{S_o} \tag{A-6}$$

Therefore;

$$E_o = \frac{xK_s}{S_o} + x + y = x\left(1 + \frac{K_s}{S_o}\right) + y \tag{A-7}$$

and;

$$x = \frac{E_o - y}{1 + K_s/S_o} \tag{A-8}$$

Equation A-2 can be rewritten as;

$$\frac{dy}{dt} = k_2\left(\frac{E_o - y}{1 + K_s/S_o}\right) - (k_{-2} + k_3)y$$

$$= \frac{k_2E_o}{1 + K_s/S_o} - \frac{k_2y}{1 + K_s/S_o} - (k_{-2} + k_3)y$$

$$= \underbrace{\frac{k_2 E_o}{1 + K_s/S_o}}_{a} - y \underbrace{\left(\frac{k_2}{1 + K_s/S_o} + k_{-2} + k_3 \right)}_{b} \qquad \text{(A-9)}$$

Therefore;

$$\frac{dy}{dt} = a - by$$

$$\frac{dy}{a - by} = dt$$

Which integrates to;

$$y = a/b\,(1 - e^{bt}) \qquad \text{(A-10)}$$

Equation A-3 can be rewritten as $dp = k_3 y dt$, which, upon integration, gives;

$$p = k_3 yt + K$$

At time zero (t=0), p=0, and therefore K=0 and $p = k_3 yt$. During the spectral analysis of the burst for (S)-50 hydrolysis, the observed change in absorbance is equal to the sum of the enzyme-product(s) complex (y) and free hydrolyzed products (p) (assuming that p and y have the same extinction coefficients, as discussed earlier on pg 79);

$$y + p = a/b\,(1 - e^{-bt}) + k_3 yt = [a/b\,(1 - e^{-bt})]\,(1 + k_3 t)$$

$$= a/b - (a/b)e^{bt} + \frac{k_3 a}{b}(1 - e^{-bt})t$$

$$= a/b + \frac{k_3 at}{b} - (a/b)e^{-bt} - \frac{k_3 at}{b}e^{-bt}$$

$$y + p = (a/b)(1 + k_3 t) - (a/b)(1 + k_3 t)e^{-bt} \qquad \text{(A-11)}$$

If we solve for a/b;

$$a/b = \frac{\frac{k_2 E_o}{1 + K_s/S_o}}{\frac{k_2}{1 + K_s/S_o} + k_{-2} + k_3} = \frac{k_2 E_o}{k_2 + (k_{-2} + k_3)(1 + K_s/S_o)}$$

$$= \frac{k_2 E_o S_o}{S_o(k_2 + k_{-2} + k_3) + K_s(k_{-2} + k_3)}$$

$$= \frac{\frac{k_2}{(k_2 + k_{-2} + k_3)} E_o S_o}{S_o + K_s \frac{(k_{-2} + k_3)}{(k_2 + k_{-2} + k_3)}} \qquad \text{(A-12)}$$

For the experimentally observed progress curve, as time (t) approaches infinity, the e^{-bt} term in equation A-11 become negligible, and the linear portion of the observed progress curve is represented by;

$$y + p = (a/b)(1 + k_3 t) \qquad \text{(A-13)}$$

From the observed burst on the progress curve, the back extrapolation of the linear portion of the curve to time zero gives us the value of a/b, which is defined as π.

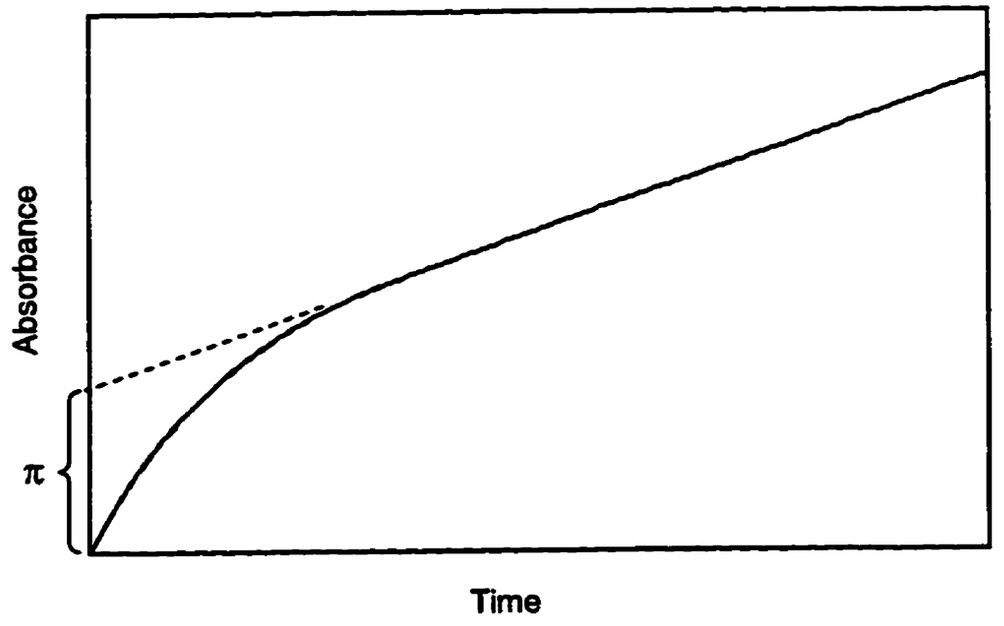

Therefore at t=0;

$$y + p = \pi = a/b = E_o\left[\frac{k_2}{k_2 + k_{-2} + k_3 + K_s\dfrac{(k_{-2} + k_3)}{S_o}}\right]$$

Since the K_m for this kinetic model is represented by;

$$K_m = K_s\,(k_{-2} + k_3) \,/\, (k_2 + k_{-2} + k_3)$$

The π can then be rewritten as;

$$\pi = E_o\left[\frac{k_2}{(k_2 + k_{-2} + k_3)(1 + K_m/S_o)}\right] \qquad \text{(A-14)}$$

The expression for K_m can rewritten as;

$$K_m = \frac{K_s}{\frac{k_2}{k_{-2} + k_3} + 1}$$

therefore;

$$\frac{k_2}{k_{-2} + k_3} = \left(\frac{K_s}{K_m} - 1\right) \qquad \text{(A-15)}$$

Equation A-14 can be rewritten to isolate the term $k_2/(k_{-2} + k_3)$:

$$\pi = E_o\left(\frac{k_2}{k_2 + k_{-2} + k_3}\right)\left(\frac{1}{1 + K_m/S_o}\right)$$

$$= E_o\left(\frac{\frac{k_2}{k_{-2} + k_3}}{\frac{k_2}{k_{-2} + k_3} + 1}\right)\left(\frac{1}{1 + K_m/S_o}\right) \qquad \text{(A-16)}$$

Now substituting the $k_2/(k_{-2} + k_3)$ term from equation A-15 into equation A-16;

$$\pi = E_o\left(\frac{\frac{K_s}{K_m} - 1}{\frac{K_s}{K_m}}\right)\left(\frac{1}{1 + K_m/S_o}\right) = E_o\left(\frac{1 - K_m/K_s}{1 + K_m/S_o}\right) \qquad \text{(A-17)}$$

With known K_m, K_s and E_o values, the expected π can be calculated for a given substrate concentration.

Appendix B:

The Effect of Stray Light on the Bromothymol Blue Assay

The presence of stray light has been known to cause errors in absorbance measurements when measuring at high absorbances, as the relationship between the observed absorbance and Beer's law breakdown.[209] Better quality instruments are less effected by stray due to lower stray light values. The stray light value (I_s) for the DMS-200 uv/vis spectrophotometer, the spectrophotometer used in our studies, was reported to be less than 0.02% (at 220 nm) by the manufacturer (Varian).

The absorbance is defined as;

$$A = \log\left(\frac{I_o}{I}\right)$$

The stray light interferes with the measurement by adding to both the reference and sample light intensities;

$$A_{obs} = \log\left(\frac{I_r + I_s}{I + I_s}\right)$$

$$\xrightarrow{I_o + I_s} \textbf{Sample Cell} \xrightarrow{I + I_s} \textbf{Sample Detector}$$

$$\xrightarrow{I_o + I_s} \textbf{Reference Cell} \xrightarrow{I_r + I_s} \textbf{Sample Detector}$$

During the bromothymol blue experiments in Sections 2.1.5 and 2.1.6 the starting absorbance was measured to be A=1.95. If we assume this to be the true absorbance (A_{true}), the effect of stray light can be determined. The reference cell

contains a control bromothymol blue solution with A=1.95 as well. If the maximum error due to stray light is assumed (0.02%);

$$I_s = 0.0002I_o$$

$$A_{true} = 1.95, \text{ therefore } I_{true} = 0.011I_o$$

$$I_r + I_s = 0.011I_o + 0.0002I_o = 0.0112I_o$$

$$I + I_s = 0.011I_o + 0.0002I_o = 0.0112I_o$$

Therefore, $A_{obs}=0$

During the bromothymol blue assay, the absorbance in the sample cell is monitored over a time period of 1.5 minutes, where the ΔA_{obs} was observed to be -0.110 or less. In the case of an assay where the progress curve is monitored with a $\Delta A_{obs}=-0.110$, where the sample cell A_{obs} has dropped from 1.95 to 1.84;

$$A_{obs} = \log\left(\frac{I_r + I_s}{I + I_s}\right) = -0.110$$

$$\frac{I_r + I_s}{I + I_s} = 0.776$$

The absorbance in the reference cell remains at 1.95, therefore $I_r=0.011I_o$. Since $I_s=0.0002I_o$,

$$\frac{0.0112I_o}{I + 0.0002I_o} = 0.776$$

$$I = 0.01463$$

From I=0.01463, the true absorbance (A_{true}) is 1.835. Comparing this value to the A_{obs} of 1.840, the effects of stray light under these experimental conditions using this instrument are judged to be negligible.

Appendix C:

Dixon Graphical Method of Determining Inhibition Constant for Tight-Binding Inhibitor

In many cases, the observation of any enzymatic activity in the presence of a tight-binding inhibitor will only occur at very low inhibitor concentrations. When the concentration of an inhibitor is not much greater than that of the enzyme, the Michaelis-Menten competitive inhibition relationship can no longer apply. This is because the free inhibitor concentration [I] cannot be represented by the total inhibitor concentration I_o unless I_o is much greater than E_o (ie. [I]>>[EI]).

$$v_A = \frac{E_o k_{cat}^{A}[A]}{[A] + K_m^{A}(1 + [I]/K_i)} \qquad (2.16)$$

The Dixon graphical method[189] overcomes this problem and allows the K_i to be determined for an inhibition scenario where a significant fraction of the inhibitor species exists in the EI complex. The enzyme is represented by three forms in the presence of a competitive inhibitor I:

$$[E]_o = [E] + [ES] + [EI] \qquad (C\text{-}1)$$

The velocity of catalysis gives the relationship:

$$[ES] = \frac{\upsilon}{k_{cat}} \qquad (C\text{-}2)$$

Since K_m = [E][S]/[ES], and combined with equation C-2, we can express the [E] species as:

$$[E] = \frac{K_m \upsilon}{k_{cat} [S]} \qquad \text{(C-3)}$$

After substituting in for [E], [ES] and $[E]_o$, where $[E]_o = V/k_{cat}$ we rewrite C-1 as:

$$\frac{V}{k_{cat}} = \frac{K_m \upsilon}{k_{cat} [S]} + \frac{\upsilon}{k_{cat}} + [EI] \qquad \text{(C-4)}$$

From equation C-4, [EI] can be expressed as:

$$[EI] = \frac{V}{k_{cat}} - \frac{K_m \upsilon}{k_{cat} [S]} - \frac{\upsilon}{k_{cat}} = \frac{1}{k_{cat}} \left[V - \upsilon \left(1 + \frac{K_m}{[S]} \right) \right] \qquad \text{(C-5)}$$

The inhibition constant K_i is represented by:

$$K_i = \frac{[E] [I]}{[EI]} = \frac{[E] ([I]_o - [EI])}{[EI]} = [E] \left(\frac{[I]_o}{[EI]} - 1 \right) \qquad \text{(C-6)}$$

Substituting in [E] from C-3 into C-6:

$$K_i = \frac{K_m \upsilon}{k_{cat} [S]} \left(\frac{[I]_o}{[EI]} - 1 \right) = \frac{K_m \upsilon [I]_o}{k_{cat} [S] [EI]} - \frac{K_m \upsilon}{k_{cat} [S]} \qquad \text{(C-7)}$$

Equation C-7 can be rearranged into:

$$\frac{[I]_o}{k_{cat}\,[EI]} = \frac{K_i\,[S]}{K_m\,\upsilon} + \frac{1}{k_{cat}} \qquad \text{(C-8)}$$

Now substituting the expression for [EI] from equation C-5 into equation C-8 gives:

$$\frac{[I]_o}{V - \upsilon\left(1 + \frac{K_m}{[S]}\right)} = \frac{K_i\,[S]}{K_m\,\upsilon} + \frac{1}{k_{cat}} \qquad \text{(C-9)}$$

In the absence of inhibitor, υ_o is given by:

$$\upsilon_o = \frac{[S]\,V}{[S] + K_m} = \frac{V}{\left(1 + \frac{K_m}{[S]}\right)} \qquad \text{(C-10)}$$

The υ_i term can represent some fraction of the υ_o term on a υ vs. [I] plot, where n is the fraction number (n=1, 2, 3, etc.):

$$\upsilon_i = \frac{\upsilon_o}{n} = \frac{V}{n\left(1 + \frac{K_m}{[S]}\right)} \qquad \text{(C-11)}$$

Now if the equation for υ_i (C-11) is substituted in for υ in the left handed side of C-9, and υ_o/n is substituted for υ in right side of C-9, we get:

$$\frac{n\,[I]_o}{(n-1)\,V} = \frac{n\,K_i\,[S]}{K_m\,\upsilon_o} + \frac{1}{k_{cat}} \qquad \text{(C-12)}$$

On the υ vs. [I] plot, a line drawn from υ_o through υ_i intersects at the inhibitor value of $[I]_n$, where $[I]_2$ for $\upsilon_i=\upsilon_o/2$, $[I]_3$ for $\upsilon_i=\upsilon_o/2$, etc..

Figure 75

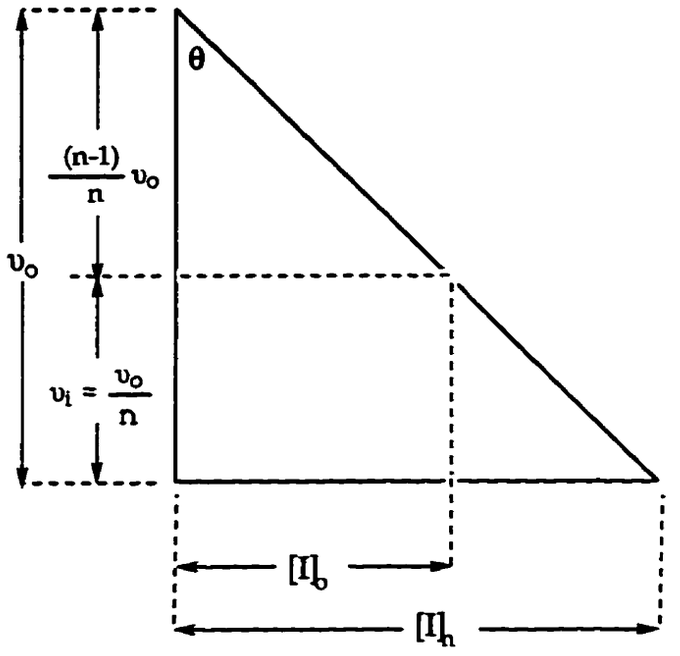

From the geometry of this plot:

$$\frac{[I]_n}{\upsilon_o} = \frac{n[I]_o}{(n-1)\upsilon_o} \qquad \text{(C-13)}$$

And therefore:

$$[I]_o = \frac{(n-1)}{n}[I]_n \qquad \text{(C-14)}$$

Now substituting for $[I]_n$ in equation C-12:

$$[I]_n = nK_i \frac{[S]\,V}{K_m\,\upsilon_o} + \frac{V}{k_{cat}} \qquad \text{(C-15)}$$

Since $V/\upsilon_o=(1+K_m/[S])$ and $V/k_{cat}=[E]_o$, equation C-15 can be rewritten as :

$$[I]_n = nK_i\left(1 + \frac{[S]}{K_m}\right) + [E]_o \qquad \text{(C-16)}$$

When lines are drawn from υ_o through υ_i on the υ vs. [I] plot at $[I]_n$ values of n=1,2,..., the distances between the [I] interceptions are equal to K_{iapp}. K_{iapp} is related to K_i as given:

$$K_{iapp} = K_i\left(1 + \frac{[S]}{K_m}\right) \qquad \text{(C-17)}$$

Inhibition of CPA by 35:

For the inhibition of CPA by **35**, a υ vs. [I] plot was made at $[E]_o$ and [HP] values of 117 nM and 0.5 mM respectively, in 25 mM Tris buffer, 0.5 M NaCl, pH 7.5 containing 3.5% EtOH (v/v), at 25°C. The **35** concentration was varied from 0 nM to 350 nM, resulting in the υ vs. [I] plot shown in Figure 76. The distances measured between the $[I]_2$, $[I]_3$,..., $[I]_6$ values were measured to be 32.9 nM, 34.2 nM, 32.9 nM and 31.3 nM, with a mean value of 32.8 nM and a standard error of 0.6 nM. With the use of equation C-17 and the values of 0.5 mM and 0.31±0.04mM for [S] and K_m respectively, the K_i for the inhibition of CPA by **35** was calculated to be 12.6±1.0 nM.

The Dixon graphical method can also be used to determine the amount of enzyme for a tight-binding inhibition situation. In the case of n=0, the $[I]_n$ in equation C-16 would then equal $[E]_o$, where $[I]_n=[I]_2-2(K_{iapp})$ at n=0. In our case, using this method $[E]_o$ was determined to be 118 nM, which was very close to the actual $[E]_o$ of 117 nM determined by absorption spectroscopy[97]. If [I]>>[EI], the n=0 line would coincide with the vertical axis.

Figure 76

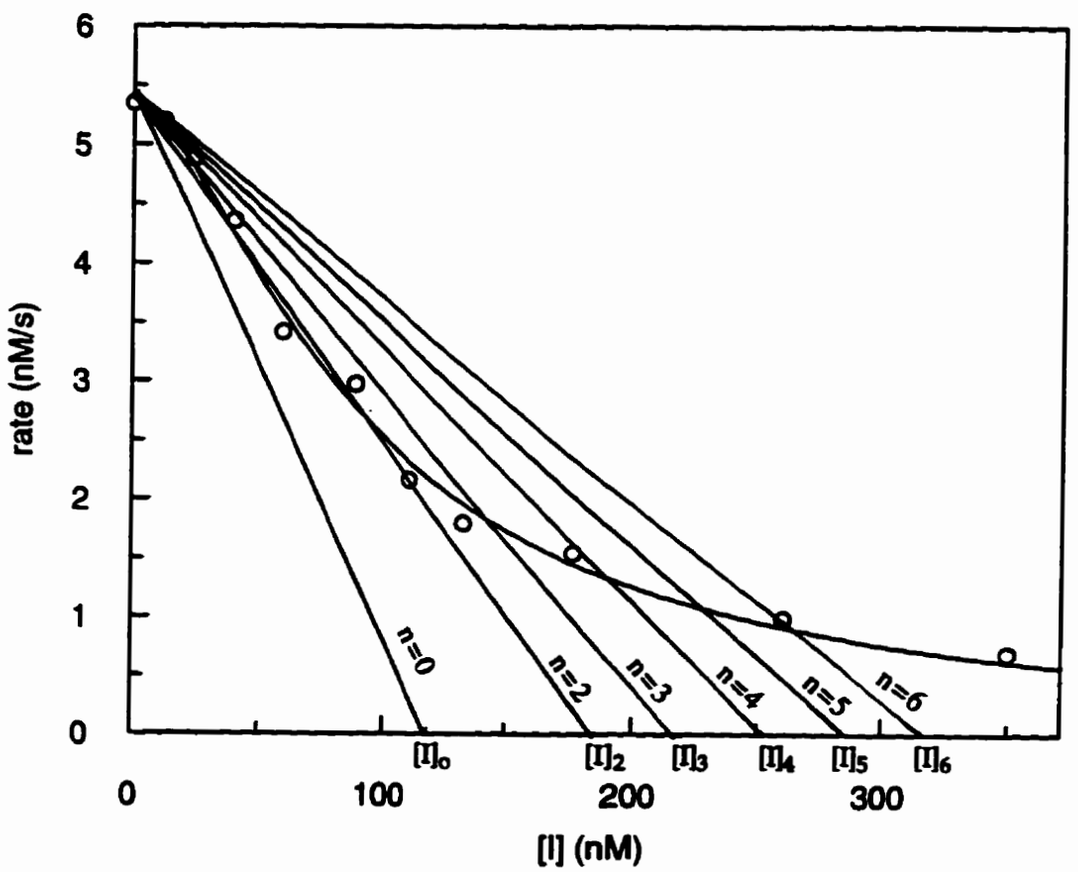

Inhibition of ACE by 88:

For the inhibition of ACE by **88**, a υ vs. [I] plot was made at a [S] value of 0.1 mM FAPGG in 50 mM HEPES buffer, 0.3 M NaCl, pH 7.5, containing 5% DMSO (v/v), at 25°C. The **88** concentration was varied from 0 to 1.16 mM, resulting in the υ vs. [I] plot shown in Figure 77. The distances measured between the $[I]_2$, $[I]_3$,..., $[I]_6$ values were measured to be 19.4 nM, 19.1 nM, 18.4 nM and 17.7 nM, with a mean value of 18.7 nM and a standard error of 0.4 nM. With the K_m=0.44±0.03 mM for ACE-catalyzed hydrolysis of FAPGG (determined previously in Section 3.2) and the [S]=0.1 mM, equation C-17 was used to determine a K_i of 15.2±0.4 nM for the inhibition of ACE by **88**.

As shown in Figure 77, the $[E]_o$ value was also calculated by determining the [I] at n=0. Using this method, $[E]_o$ was determined to be 30.9 nM. Since the assays were conducted at a volume of 1.0 mL, at 0.03 units/mL, the number of nmoles per unit enzyme can be calculated to be 1.03 nmoles.

Figure 77

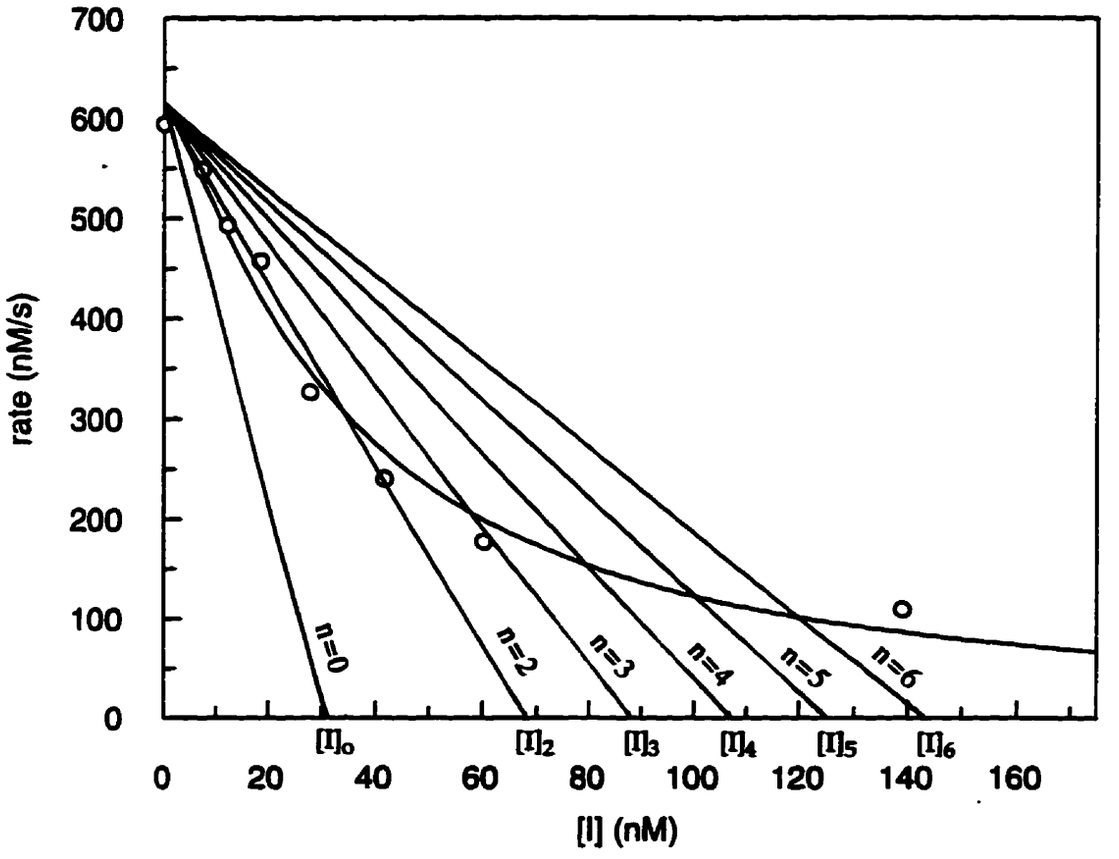
700
600
500
400
300
200
100
0
rate (nM/s)
n=0
n=2
n=3
n=4
n=5
n=6
[I]o
[I]2
[I]3
[I]4
[I]5
[I]6
0
20
40
60
80
100
120
140
160
[I] (nM)

Appendix D:

The Use of Molecular Modeling to Study Enzyme-Inhibitor Binding

The molecular modeling package Sybyl® from Tripos Association Inc. was used on the SGI 4D25TG and Indigo2 R4400 XZ graphics work station for all molecular modeling studies.

Anneal is a version of the geometry optimization algorithm MAXIMIN2 with Sybyl which was designed to allow for energy minimization of larger molecules such as proteins. There are three distinct regions of the protein that are manipulated differently during the minimization. The "hot region", which consists of protein residues which are energy minimized through conformational and geometrical changes. The "interesting region" is a static region of the protein that surrounds the "hot region", which is not subject to geometry changes during the minimization but is used for energy calculation purposes. In other words, the "interesting region" influences the geometry of the "hot region". The third region includes the areas of the protein that are not considered "hot" or "interesting". This region is held static and is ignored during the minimization.

During the minimizations using Anneal, the "hot" region, unless otherwise stated, included the active site bound inhibitor, Arg 127, Arg-145, Glu-270 and Tyr 248 of the S_1' subsite, Leu-203, Ala-250, Gly-252, Gly-253, Ile-255 and Thr-268 of the S_1' subsite hydrophobic pocket, Tyr-198, Phe-279 and Arg-71 of the S_1 subsite, and Asp-142, Ala-143, Asn-144, Glu-163, Ser-199, Leu-201, Leu-202, Gly-207, Ser-242, Ile-244, Ile-247, Gln-249, Ser-254 and Asp-256 which are other residues close to the active site. All protein residues within 13 Å of the "hot" region were designated as the "interesting" region. The active site Zn^{2+} and its ligands Glu-72, His-69 and His-196

were included in the "interesting" region and not "hot" region. Charges were calculated for all the atoms of the inhibitor-protein complex using the Gasteiger-Huckel method.[210] The active site Zn^{2+} was assigned a change of +2. The Tripos force field (MAXIMIN2) parameters were used during the minimization.

Protein coordinates used in this minimization were downloaded from the Brookhaven Protein Data Bank. In particular, entries pdb1cps.ent, which corresponds to the complex of CPA with **83**, and pdb3cpa.ent, which corresponds to the complex of CPA with Gly-Tyr, were employed.

Binding of 35 and 36 to CPA

For the binding of **35** or **36** to the CPA active site, a Zn^{2+}-S interaction was modeled into the complex. The Tripos force field did not include parameters that allow for minimization of the Zn^{2+}-S interaction. As a result distance and angle constraints were placed on the length of the Zn^{2+}-S bond and the Zn^{2+}-S-C_α angle. The restraints were based on the geometry found for Zn^{2+}-S interactions between cysteine residues and Zn^{2+} found in zinc fingers using 2D NMR.[193] From the zinc finger structures, Zn^{2+}-S interactions were found to range from 2.03 Å to 2.29 Å with an average of 2.22 Å, and the Zn^{2+}-S-C_α angle ranged from 106.0° to 126.8° with an average of 111.3°.[193] From the crystal structure of thermolysin with a substrate-analogue mercaptan **101** complexed into the thermolysin active site involving a Zn^{2+}-S interaction, the Zn^{2+}-S bond length was observed to be 1.9 Å and the Zn^{2+}-S-C_α was observed to be 124.9°.[154]

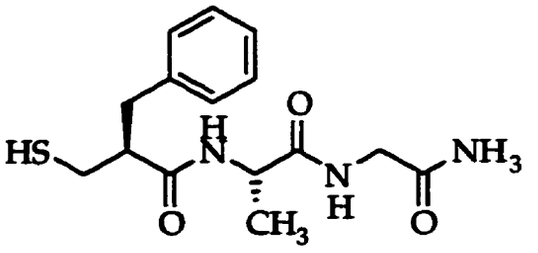

101

These ranges of Zn^{2+}-S interaction geometries were used as the expectable ranges for the Zn^{2+}-S interaction during the computational minimization experiments. Distance and angle constraints for the Zn^{2+}-S interaction were used during the minimizations for this purpose. During the energy minimization, the constraints are represented by the energy terms (in kcal/mol):

$$E_{ang\_c}=(1/2)k^a(\theta-\theta°)^2$$

$$E_{dist\_c}=(1/2)k^d(d-d°)^2$$

where $\theta°$ is the requested angle, d° is the requested distances, and k^a and k^d are the force constants. For both the minimization of the **35**-CPA and **36**-CPA complexes, the $\theta°$ and d° were set to 111° and 2.22 Å respectively. The parameter k^d was set to 400. Smaller k^d values allowed the Zn^{2+}-S bond length to be greater than 2.30 Å (the upper expectable limit for the bond length) in the minimized **35**-CPA structure. The k^a was set to 0.02. Lower k^a values caused little change in the Zn^{2+}-S-C_α angle of the minimized **35**-CPA structure.

During the energy minimization process using Anneal, minimization was continued until the change in energy between iterations was less than 0.005 kcal/mol.

Modeling of the Proposed NAH306-Phe-CPA Ternary Complex

The ternary (N-benzoyl-phenylalanine)-Phe-CPA complex determined by Lipscomb[192] was used as a guide for modeling the proposed ternary **NAH306**-Phe-CPA complex. Since the x-ray coordinates for Lipcomb's structure were not available from the Brookhaven Protein Data Bank, this complex was modeled using Sybyl and the geometric description offered by Lipscomb in this publication[192]. The following aspects of Lipscomb's description of this structure guided this modeling exercise:

- phenylalanine bound in the S_1'-subsite through expected the carboxylate-Arg-145 interaction and hydrophobic pocket interactions (Figure 71 of Chapter 5).
- N-benzoyl-phenylalanine bound is to the S_1/S_2-subsite region (Figure 71 of Chapter 5):
    - the carboxylate oxygens of N-benzoyl-phenylalanine are coordinated to the active site Zn^{2+} at distances of 2.7 and 2.2 Å, with the latter oxygen 3.3 Å away from Arg-127
    - the carboxylate carbon is 3.3 Å from the amino group of the phenylalanine bound in the S_1'-subsite
    - the amide carbonyl is 2.9 Å from Arg-71
    - the amide hydrogen donates a hydrogen bond to the Tyr-248 OH group (3.1 Å)
    - the phenyl group of the P_1 side chain is bound in the S_1 subsite hydrophobic pocket (Tyr-198, Ser-199, Leu-201, Ile-247 and Tyr-248), with a favourable edge-to-face interaction between the P_1 side chain phenyl group and the Tyr-198 phenyl group
    - the phenyl ring of the benzoyl group interacts in a similar edge-to-face interaction with the phenyl group of Tyr-248

Using the above interactions as a guide a molecule of N-benzoyl-phenylalanine and a molecule of phenylalanine were docked into the active site of CPA (crystal structure from (Gly-Tyr)-CPA complex (pdb3cpa.ent)[25] with the Gly-Tyr dipeptide removed).

This complex was geometrically minimized using Anneal using rigid distance constraints based on Lipscomb's observation of the actual (N-benzoyl-phenylalanine)-Phe-CPA ternary complex. During this minimization the "hot region" contained N-benzoyl-phenylalanine, Phe, Arg-71, Arg-127, Arg-145, Tyr-198, Ser-199, Leu-201, Ile-247, Tyr-248, Glu-270 and Phe-279. The geometric minimization was continued until the change in energy between iterations was less than 0.01 kcal/mol. The resulting structure is shown in Figure 78.

The constructed (N-benzoyl-phenylalanine)-Phe-CPA ternary complex was now used as a guide to model the hypothetical **NAH306**-Phe-CPA ternary complex. The N-benzoyl-phenylalanine was removed and replaced with a model of **NAH306** based on the x-ray crystallographic coordinates for **NAH306** but with the phenolic group ionized. The charges for **NAH306** were assigned using MOPAC-AM1 calculations. This complex was subject to Anneal minimization, which was continued until the change in energy between iterations was less than 0.001 kcal/mol. As mentioned in Section 2.2.7, x-ray crystallographic analysis of **NAH306** has shown the structure to be relatively planar. During minimization, no torsion angle constraints were needed to maintain the relatively planar geometry of **NAH306**.

Figure 78: (i) Energy minimized complex between CPA, phenylalanine and N-benzoyl-phenylalanine.

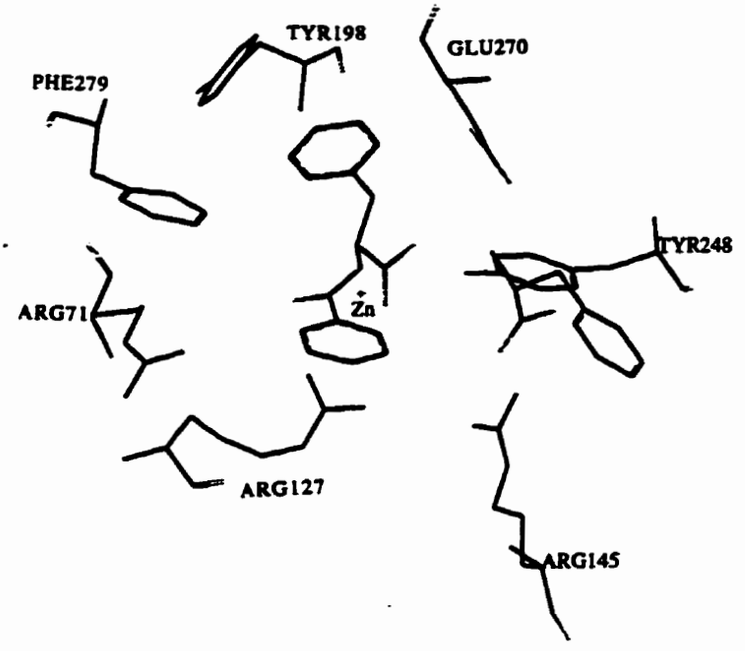

(ii) Stereoscopic view of (i).

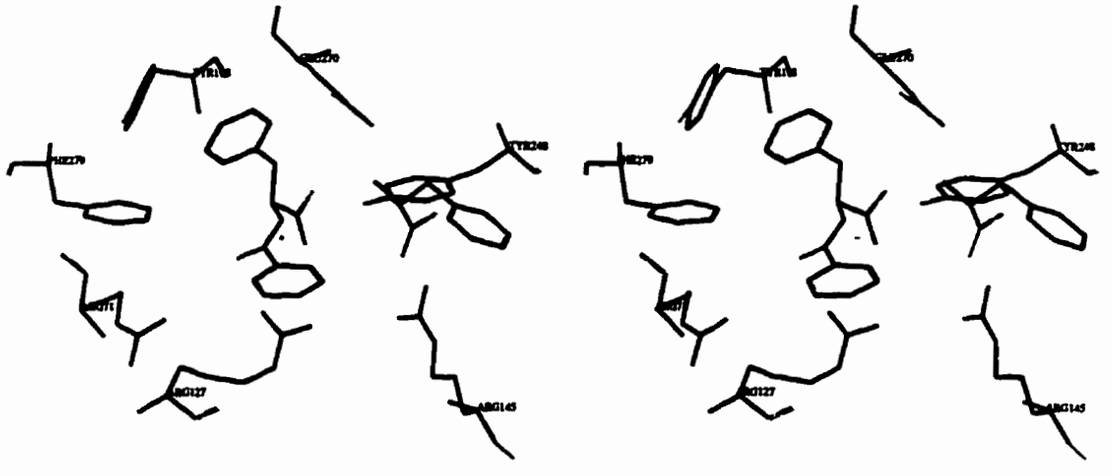

Appendix E.1:

Relationship between (S)-50 concentration and steady state rate in Buffer B.

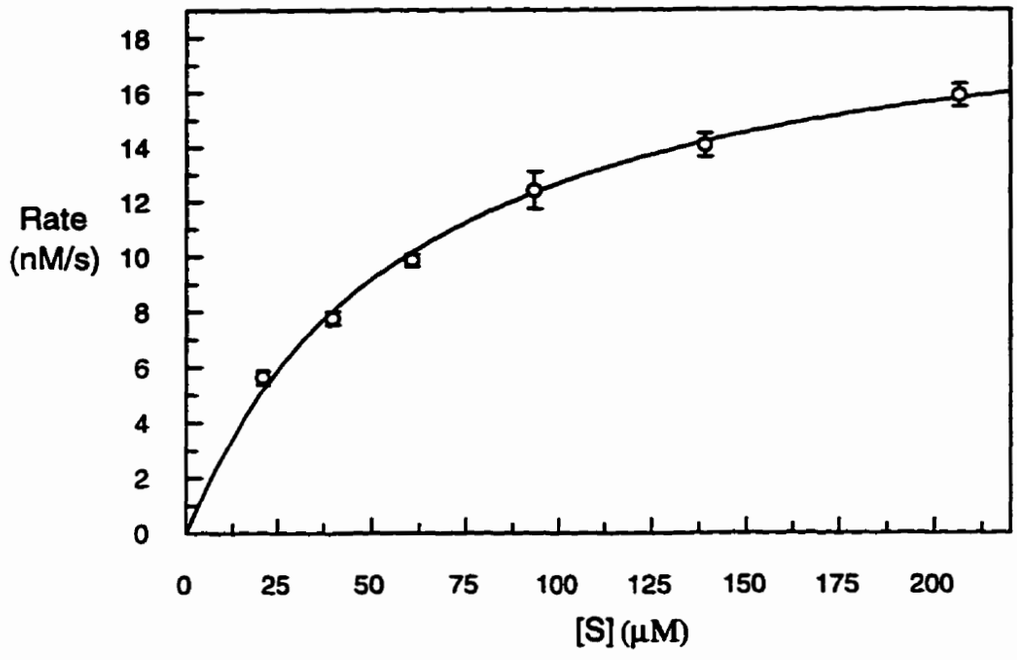

Each data point is the average of seven or more separate determinations, shown with standard error bars. Error bars smaller than the symbols are not shown. For the mathimatical determination of kinetic parameters, all determinations and not the means were included in the calculations.

Appendix E.2:

Double reciprocal relationship between ACE peptidase activity and FAPGG concentration in the presence of **88** in 50 mM HEPES, 0.3 M NaCl, pH of 7.5, containing 5% DMSO (v/v), at 25°C. The ACE concentration was 0.03 unit/mL.

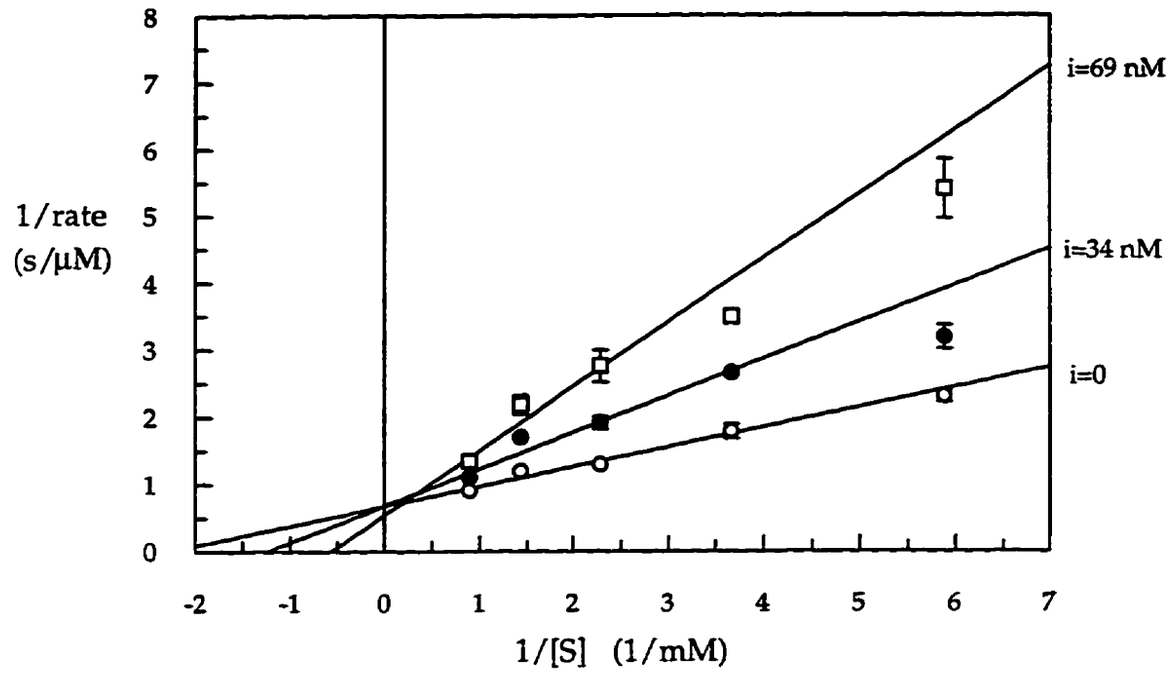

Each data point is the average of three or more separate determinations, shown with standard error bars. Error bars smaller than the symbols are not shown. The curves shown above are the result of the data being fitted to the Michaelis-Menten relationship.

Appendix E.3:

Slope versus inhibitor concentration replot for **NAH306** inhibition of CPA. Slope in units of s^{-1} and inhibitor concentration in units in mM.

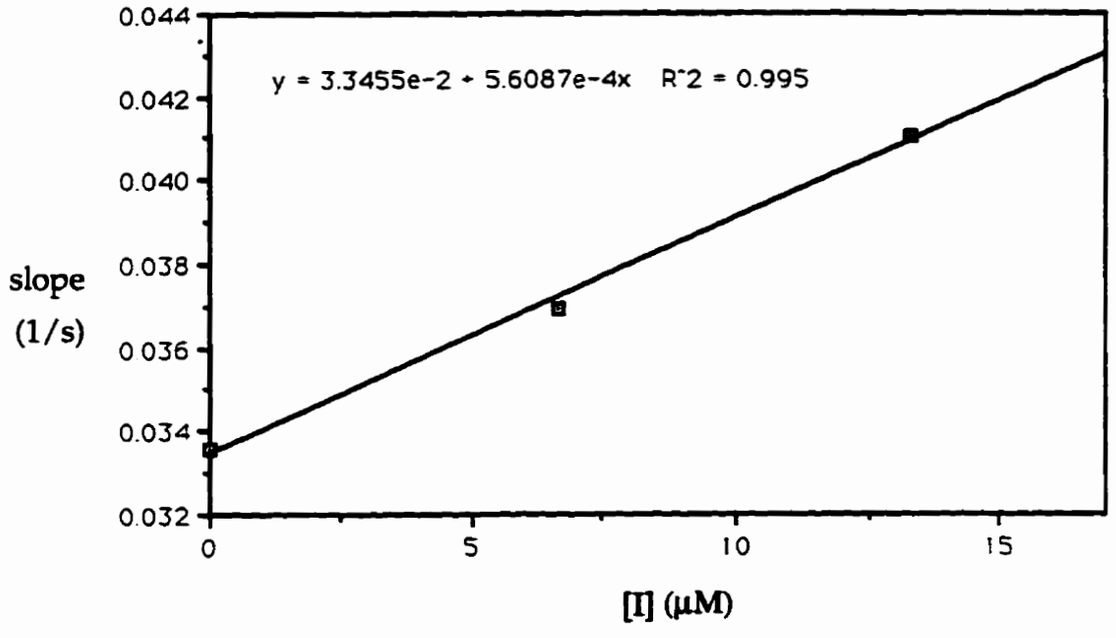

References

1. Ehlers, M. R. W.; Riordan, J. F. *Hypertension: Pathophysiology, Diagnosis, and Management* **1990**, Raven Press, Ltd., N.Y., Chapter 76.
2. Kim, H.; Lipscomb, W. N. *Adv. Enzymol.* **1994**, *68*, 153-213.
3. Springman, E. B.; Angleton, E. L.; Birkedal-Hanssen, H. *Proc. Natl. Acad. Sci. (U.S.A.)* **1990**, *87*, 364-368.
4. Van Wart, H. E.; Birkedal-Hanssen, H. *Proc. Natl. Acad. Sci. (U.S.A.)* **1990**, *87*, 5578-5582.
5. Vijayaraghavan, J.; Kim, Y.-A.; Jackson, D.; Orlowski, D.; Hersh, L.B. *Biochemistry*, **1990**, *29*, 8052-8056, and references within.
6. Vallee, B. L. *Zinc Enzymes* **1986**, ed. Bertini, I.; Luchinat, C.; Maret, W.; Zeppezauer, Birkhauser Boston Inc., pp 1-10.
7. Hofmann, K; Bergmann, M. *J. Biol. Chem.* **1940**, *134*, 225-235.
8. Snoke, J. E.; Schwart, G. W.; Neurath, H. *J. Biol. Chem.* **1948**, *175*, 7.
9. Bergmann, M.; Fruton, J. S. *J. Biol. Chem.* **1937**, *117*, 189.
10. Abramowitz, N.; Schechter, I.; Berger, A. *Biochem. Biophys. Res. Commun.* **1967**, *29*, 862-867.
11. Whitaker, J. R.; Menger, F.; Bender, M. L. *Biochemistry* **1966**, *5*, 386-392.
12. Auld, D. S.; Holmquist, B. *Biochemistry* **1974**, *13*, 4355-4361.
13. Bunting, J. W.; Murphy, J.; Myers, C. D.; Cross, G. C. *Can. J. Chem.* **1974**, *52*, 2648-2659.
14. Bunting, J. W.; Kabir, S. H. *J. Am. Chem. Soc.*, **1977**, *99*, 2775-2780.
15. Smith, E. L. *J. Biol. Chem.* **1948**, *175*, 39-47.

16. Kaiser, E. T.; Carson, F. W. *J. Am. Chem. Soc.*, **1964**, *86*, 2922-2926.

17. Grobelny, D.; Goli, U. B.; Galardy, R. E. *Biochemistry* **1985**, *24*, 7612-7617.

18. Snoke, J. E.; Neurath, H. *J. Biol. Chem.* **1949**, *181*, 789-790.

19. Fones, W. S.; Lee, M. *J. Biol. Chem.* **1953**, *201*, 847-856.

20. Kaiser, E. T.; Chan, T.; Suh, J. *Adv. Expt. Med. Biol.* **1974**, *48*, 59-80.

21. Campbell, P.; Nashed, N. T. *J. Am. Chem. Soc.*, **1982**, *104*, 5221-5226.

22. Bartlett, P. A.; Spear, K. L.; Jacobsen, N. E. *Biochemistry* **1982**, *21*, 1608-1611.

23. Suh, J.; Kaiser, E. T. *Biochem. Biophys. Res. Commun.* **1975**, *64*, 863-869.

24. Lipscomb, W. N. *Accts. Chem. Res.* **1970**, *3*, 81-89.

25. Rees, D. C.; Lipscomb, W. N. *Proc. Natl. Acad. Sci. (U.S.A.)* **1983**, *80*, 7151-7154.

26. Rees, D. C.; Lipscomb, W. N. *Proc. Natl. Acad. Sci. (U.S.A.)* **1981**, *78*, 5455-5459.

27. Rees, D. C.; Lewis, M.; Honzatko, R. B.; Lipscomb, W. N. *Proc. Natl. Acad. Sci. (U.S.A.)* **1981**, *78*, 3408-3412.

28. Lipscomb, W. N. *Tetrahedron* **1974**, *30*, 1725-1732.

29. Rees, D. C.; Lewis, M.; Lipscomb, W. N. *J. Mol. Biol.* **1983**, *168*, 367-387.

30. Lipscomb, W. N. *Proc. Natl. Acad. Sci. (U.S.A.)* **1980**, *77*, 3875-3878.

31. Coleman, J. E.; Vallee, B. L. *J. Biol. Chem.* **1960**, *235*, 390.

32. Coleman, J. E.; Vallee, B. L. *J. Biol. Chem.* **1961**, *236*, 2244.

33. Christianson, D. W.; Lipscomb, W. N. *Proc. Natl. Acad. Sci. (U.S.A.)* **1986**, *83*, 7568-7572.

34. Christianson, D. H.; Kuo, L. C.; Lipscomb, W. N. *J. Am. Chem. Soc.*, **1985**, *107*, 8281-8283.

35. Christianson, D. W.; Lipscomb, W. N. *Proc. Natl. Acad. Sci. (U.S.A.)* **1985**, *82*, 6840-6844.

36. Kim, H.; Lipscomb, W. N. *Biochemistry* **1991**, *30*, 8171-8180.

37. Christianson, D. H.; Lipscomb, W. N. *J. Am. Chem. Soc.*, **1986**, *108*, 4998-5003.

38. Nakagawa, S.; Umeyama, H. *J. Am. Chem. Soc.*, **1978**, *100*, 7716-7725.

39. Schepartz, A.; Breslow, R. *J. Am. Chem. Soc.*, **1987**, *109*, 1814-1826.

40. Christianson, D. W.; Lipscomb, W. N. *Accts. Chem. Res.* **1989**, *22*, 62-69.

41. Rees, D. C.; Lipscomb, W. N. *J. Mol. Biol.* **1982**, *160*, 475-498.

42. Hilvert, D.; Gardell, S. J.; Rutter, W. J.; Kaiser, E. T. *J. Am. Chem. Soc.*, **1986**, *108*, 5298-5304.

43. Gardell, S. J.; Craik, C. S.; Hilvert, D.; Urdea, M. S.; Rutter, W. J. *Nature* **1985**, *317*, 551-555.

44. Makinen, M. W.; Yamamura, K.; Kaiser, E. T. *Proc. Natl. Acad. Sci. (U.S.A.)* **1976**, *73*, 3882-3886.

45. Makinen, M. W.; Kuo, L. C.; Dymowski, J. J.; Jaffer, S. *J. Biol. Chem.* **1979**, *254*, 365-366.

46. Sander, M. E.; Witzel, H. *Biochem. Biophys. Res. Commun.* **1985**, *132*, 681-687.

47. Breslow, R.; McClure, D. E. *J. Am. Chem. Soc.*, **1976**, *98*, 259-261.

48. Breslow, R.; Wernick, D. L. *Proc. Natl. Acad. Sci. (U.S.A.)* **1977**, *74*, 1303-1307.

49. Makinen, M. W.; Fukuyama, J. M.; Kuo, L. C. *J. Am. Chem. Soc.*, **1982**, *104*, 2667-2669.

50. Suh, J.; Cho, W.; Chung, S. *J. Am. Chem. Soc.*, **1985**, *107*, 4530-4535.

51. Kuo, L. C.; Makinen, M. W. *J. Am. Chem. Soc.*, **1985**, *107*, 5255.

52. Suh, J.; Park, T. H.; Hwang, B. K. *J. Am. Chem. Soc.*, **1992**, *114*, 5141-5146.

53. Suh, J.; Hong, S.; Chung, S. *J. Biol. Chem.* **1986**, *261*, 7112-7114.

54. Hoffman, S. J.; Chu, S. S.-T.; Lee, H.; Kaiser, E. T. *J. Am. Chem. Soc.*, **1983**, *105*, 6971.

55. Britt, B. M.; Peticolas, W. L. *J. Am. Chem. Soc.*, **1992**, *114*, 5295-5303.

56. Auld, D. S.; Galdes, A.; Geoghegan, K. F.; Holmquist, B.; Mortinelli, R. A.; Vallee, B. L. *Proc. Natl. Acad. Sci. (U.S.A.)* **1984**, *81*, 5041-5045.

57. Galdes, A.; Auld, D. S.; Vallee, B. L. *Biochemistry* **1986**, *25*, 646-651.

58. Geoghegan, K. F.; Galdes, A.; Hanson, G.; Holmquist, B.; Auld, D. S.; Vallee, B. L. *Biochemistry* **1986**, *25*, 4669-4674.

59. Geoghegan, K. F.; Galdes, A.; Mortinelli, R. A.; Holmquist, B.; Auld, D. S.; Vallee, B. L. *Biochemistry* **1983**, *22*, 2255-2262.

60. Byers, L. D.; Wolfenden, R. *Biochemistry* **1973**, *12*, 2070-2078.

61. Teplyakov, A.; Wilson, K.; Orioli, P.; Mangani, S. *Acta Cryst.* **1993**, *D49*, 534-540.

62. Mangani, S.; Orioli, P. *Inorg. Chem.* **1992**, *31*, 365-368.

63. Gelb, M. H.; Svaren, J. P.; Abeles, R. H. *Biochemistry* **1985**, *24*, 1813-1817.

64. Christianson, D. W.; David, P. R.; Lipscomb, W. N. *Proc. Natl. Acad. Sci. (U.S.A.)* **1987**, *84*, 1512-1515.

65. Shoham, G.; Christianson, D. W.; Oren, D. A. *Proc. Natl. Acad. Sci. (U.S.A.)* **1988**, *85*, 684-688.

66. Galardy, R. E.; Kortylewicz, Z. P. *Biochemistry* **1985**, *24*, 7607-7612.

67. Galardy, R. E.; Kortylewicz, Z. P. *Biochemistry* **1984**, *23*, 2083-2087.

68. Cappalonga, A. M.; Alexander, R. S.; Christianson, D. W. *J. Biol. Chem.* **1992**, *267*, 19192-19197.

69. Kim, H.; Lipscomb, W. N. *Biochemistry* **1990**, *29*, 5546-5555.

70. Christianson, D. W.; Lipscomb, W. N. *J. Am. Chem. Soc.*, **1986**, *108*, 545-546.

71. Christianson, D. W.; Lipscomb, W. N. *J. Am. Chem. Soc.*, **1988**, *110*, 5560-5565.

72. Gelb, M. H.; Svaren, J. P.; Abeles, R. H. *Biochemistry* **1985**, *24*, 1813-1817.

73. Teater, C.; Grobelny, D.; Galardy, G. E. *Biochem. Biophys. Res. Commun.* **1988**, *153*, 773-778.

74. Phillips, M. A.; Fletterick, R.; Rutter, W. J. *J. Biol. Chem.* **1990**, *265*, 20692- 20698.

75. Kim, H.; Lipscomb, W. N. *Biochemistry* **1990**, *29*, 5546-5555.

76. Hanson, J. E.; Kaplan, A. P.; Bartlett, P. A. *Biochemistry* **1989**, *28*, 6294-6305.

77. Holden, H. M.; Tronurd, D. E.; Monzingo, A. F.; Weaver, L. H.; Matthews, B. W. *Biochemistry* **1987**, *26*, 8542-8553.

78. Tronrud, D. E.; Monzingo, A. F.; Matthews, B. W. *Eur. J. Biochem.* **1986**, *157*, 261-268.

79. Matthews, B. W. *Accts. Chem. Res.* **1988**, *21*, 333-340.

80. Bartlett, P. A.; Marlowe, C. K. *Biochemistry* **1987**, *26*, 8553-8561.

81. Phillips, M. A.; Kaplan, A. P.; Rutter, W. J.; Bartlett, P. A. *Biochemistry* **1992**, *31*, 959-963.

82. Bartlett, P. A.; Marlowe, C. K. *Biochemistry* **1983**, *22*, 4618-4624.

83. Lipscomb, W. N.; Sträter, N. *Chem. Rev.* **1996**, *96*, 2375-2433.

84. Groves, J. T.; Chambers Jr., R. R. *J. Am. Chem. Soc.*, **1984**, *106*, 630-638. Groves, J. T.; Olson, J. R. *Inorg. Chem.* **1985**, *24*, 2715-2717.

85. Groves, J. T.; Baron, L. A. *J. Am. Chem. Soc.*, **1989**, *111*, 5442-5448.

86. Mock, W. L.; Tsay, J. *J. Biol. Chem.* **1988**, *263*, 8635-8641.

87. Holmes, M. A.; Matthews, B. W. *Biochemistry* **1981**, *20*, 6912-6920.

88. Skeggs, L. T.; Marsh, W. H.; Kahn, J. R.; Shumway, N. P. *J. Exp. Med.* **1954**, *99*, 275.

89. Yang, H. Y. T.; Erdos, E. G.; Levin, Y. *Biochim. Biophys. Acta* **1970**, *241*, 374-376.

90. Peach, M. J. *Physiol. Rev.* **1977**, *57*, 313. For a detailed review of the Kallikrein-Kinin system, see Colman, R.W.; Schmaier, A.H.; Wong, P.Y. *Biochemical Regulation of Blood Pressure* , **1981**, ed. Soffer, R.L., Wiley, N.Y., pp 321-355.

91. Ryan, J. W.; Smith, U.; Niemeyer *Science* **1972**, *176*, 64-66.

92. Bunning, P.; Riordan, J. F. *J. Inorg. Biochem.* **1985**, *24*, 183-198.

93. Kleeman, S. G.; Keung, W. M.; Riordan, J. F. *J. Inorg. Biochem.* **1986**, *26*, 93-106.

94. Cushman, D. W.; Cheung, H. S. *Biochim. Biophys. Acta* **1971**, *250*, 261-265.

95. Coombs, T. L.; Felber, J.; Vallee, B. L. *Biochemistry* **1962**, *1*, 899-905.

96. Bicknell, R.; Holmquist, B.; Lee, F. S.; Martin, M. T.; Riordan, J. F. *Biochemistry* **1987**, *26*, 7291-7297.

97. Holmquist, B.; Vallee, B. L. *Proc. Natl. Acad. Sci. (U.S.A.)* **1979**, *76*, 6216-6220.

98. Bertini, I.; Donaire, A.; Messori, L.; Mortatal, J. *Inorg. Chem.* **1990**, *29*, 202-205.

99. Cushman, D. W.; Ondetti, M. A. *Progress in Med. Chem.* **1980**, ed. Ellis, G. P.; West, G. B. pp 41-104.

100. Keung, W.-M.; Holmquist, B.; Riordan, J. F. *Biochem. Biophys. Res. Commun.* **1980**, *96*, 506-513.

101. Rohrbach, M. S.; Williams Jr., E. B.; Rolstad, R. A. *J. Biol. Chem.* **1981**, *256*, 225-230.

102. Holmquist, B.; Bunning, P.; Riordan, J. F. *Anat. Biochemistry* **1979**, *95*, 540.

103. Cheung, H.-S.; Wang, F.-L.; Ondetti, M. A.; Sabo, E. F.; Cushman, D. W. *J. Biol. Chem.* **1980**, *255*, 401-407.

104. Ryan, J. W.; Chung, A.; Martin, L. C.; Ryan, U. S. *Tissue and Cell* **1978**, *10*, 555-562.

105. Dorer, F. E.; Kahn, J. R.; Lentz, K. E.; Levine, M.; Skeggs, L. T. *Biochim. Biophys. Acta* **1976**, *429*, 220-228.

106. Shapiro, R.; Holmquist, B.; Riordan, J. F. *Biochemistry* **1983**, *22*, 3850-3857.

107. Shapiro, R.; Riordan, J. F. *Biochemistry* **1984**, *23*, 5234-5240.

108. Bunning, P.; Riordan, J. F. *Biochemistry* **1983**, *22*, 110-116.

109. Harper, J. W.; Shapiro, R.; Riordan, J. F. *Biochemistry* **1987**, *26*, 1284-1288.

110. Bunning, P.; Riordan, J. F. *Biochemistry* **1987**, *26*, 3374-3377, and references within.

111. Bunning, P.; Holmquist, B.; Riordan, J. F. *Biochem. Biophys. Res. Commun.* **1978**, *83*, 1446-1449, and references within.

112. Harris, R. B.; Wilson, I. B. *J. Biol. Chem.* **1982**, *257*, 811-815.

113. Harris, R. B.; Wilson, I. B. *J. Biol. Chem.* **1983**, *258*, 1357-1362.

114. Harris, R. B.; Ohlsson, J. T.; Wilson, I. B. *Arch. Biochem. Biophys.* **1981**, *206*, 105-112.

115. Patchett, A. A. *Nature* **1980**, *288*, 280-283.

116. Reynolds, C. H. *Biochemical Pharm.* **1984**, *33*, 1273-1276.

117. Galardy, R. E.; Kontoyiannidou-Ostrem, V.; Kortylewicz, Z. P. *Biochemistry* **1983**, *22*, 1990-1995.

118. Shapiro, R.; Riordan, J. F. *Biochemistry* **1983**, *22*, 5315-5321.

119. Ethlers, M. R. W.; Kirsch *Biochemistry* **1988**, *27*, 5538-5544.

120. Lifshitz, R. L.; Levitzki, A. *Biochemistry* **1976**, *15*, 1987-1993.

121. Yang, J. J.; Artis, D. R.; Van Wart, H. E. *Biochemistry* **1994**, *33*, 6516-6523.

122. Williams, A. C.; Auld, D. S. *Biochemistry* **1986**, *25*, 94-100.

123. Williams, A. C.; Auld, D. S. *Fed. Proc.* **1991**, *41*, 743.

124. Tanaka, Y.; Grapses, I.; Dakoji, S.; Cho, Y. J.; Mobashery, S. *J. Am. Chem. Soc.*, **1994**, *116*, 7475-7480.

125. Kim, D. H.; Kim, K. B. *J. Am. Chem. Soc.*, **1991**, *113*, 3200-3202.

126. Kim, D. H.; Chung, S. J. *Bioorg. and Med. Chem. Lett.* **1995**, *5*, 1667-1672.

127. Yun, M.; Park, C.; Kim, S.; Nam, D.; Kim, S. C.; Kim, D. H. *J. Am. Chem. Soc.*, **1992**, *114*, 2281-2282.

128. Breckenridge, R. J.; Suckling, C. J. *Tetrahedron* **1986**, *42*, 5665-5677.

129. Ner, S. K.; Suckling, C. J.; Bell, A. R.; Wrigglesworth, R. *J. Chem. Soc., Chem. Commun.* **1987**, 480-482

130. Oshima, G.; NaGasawa *J. Biochem.* **1979**, *86*, 1719-1724.

131. Cheung, H. S.; Cushman, D. W. *Biochim. Biophys. Acta* **1973**, *293*, 451-463.

132. Almquist, R. G.; Crase, J.; Jennings-White, C.; Meyer, R. F.; Hoefle, M. L.; Smith, R. D.; Essenburg, A. D.; Kaplan, H. R. *J. Med. Chem.* **1982**, *25*, 1292- 1299.

133. Sugimoto, T.; Kaiser, E. T. *J. Am. Chem. Soc.*, **1979**, *101*, 3946-3951.

134. Rees, D. C.; Honzatko, R. B.; Lipscomb, W. N. *Proc. Natl. Acad. Sci. (U.S.A.)* **1980**, *77*, 3288-3291.

135. Byers, L. D.; Wolfenden, R. *J. Biol. Chem.* **1972**, *247*, 606-608.

136. Palmer, A. R.; Ellis, P. D.; Wolfenden, R. *Biochemistry* **1982**, *21*, 5056-5059.

137. Carloni, P.; Orioli, P. *J. Mol. Biol.* **1992**, *223*, 573-578.

138. Patchett, A. A. *J. Clin. Pharmacol.* **1984**, *18*, 201S-207S.

139. Shiparo, R.; Riordan, J. F. *Biochemistry* **1984**, *23*, 5225-5233.

140. Morgan, B. P.; Holland, D. R.; Matthews, B. W.; Bartlett, P. A. *J. Am. Chem. Soc.*, **1994**, *116*, 3251-3260.

141. Kaplan, A. P.; Bartlett, P. A. *Biochemistry* **1991**, *30*, 8165-8170.

142. Jacobsen, N. E.; Bartlett, P. A. *J. Am. Chem. Soc.*, **1981**, *103*, 654-657.

143. Kam, C.; Nishino, N.; Powers, J. C. *Biochemistry* **1979**, *18*, 3032-3038.

144. Cushman, D. W.; Cheung, H. S. *Biochem. Pharm.* **1971**, *20*, 1637-1648.

145. Martinelli, R. A.; Hanson, G. R.; Thompson, J. S.; Holmquist, B.; Pilbrow, J. R.; Auld, D. S.; Vallee, B. L. *Biochemistry* **1989**, *28*, 2251-2258.

146. Gettins, P. *J. Biol. Chem.* **1986**, *261*, 15513-15518.

147. Ondetti, M. A.; Condon, M. E.; Reid, J.; Sabo, E. F.; Cheung, H. S. *Biochemistry* **1979**, *18*, 1427-1430.

148. Suh, J.; Lee, S. H.; Uh, J. Y. *Bioorg. Med. Chem. Lett.* **1995**, *5*, 585-588.

149. Kim, D. H.; Kim, Y. J. *Bioorg. Med. Chem. Lett.* **1993**, *3*, 2681-2684.

150. Kim, D. H.; Kim, K. B. *Bioorg. Med. Chem. Lett.* **1991**, *1*, 323-326.

151. Kim, D. H.; Shin, Y. S.; Kim, K. B. *Bioorg. Med. Chem. Lett.* **1991**, *1*, 317-322.

152. Cushman, D. W.; Cheung, H. S.; Sabo, E. F.; Ondetti, M. A. *Biochemistry* **1977**, *16*, 5484-5491.

153. Funae, Y.; Komori, T.; Sasaki, D.; Yamamoto, K. *Jap. J. Pharmacol.* **1978**, *28*, 923.

154. Monzino, A. F.; Matthews, B. W. *Biochemistry* **1982**, *21*, 3390-3394.

155. Lippi, A. *Biochemical Pharm.* **1993**, *45*, 1358-1362.

156. Pfuetzner, R. A.; Chan, W. W.-C.; *J. Biol. Chem.* **1982**, *263*, 4056-4058.

157. Parfey, P. S.; Clement, M.; Vanderburg, M. J.; Wright, P. *Br. Med. J.* **1980**, *281*, 194.

158. Patey, G.; DeLa Baume, S.; Schwartz *Science* **1981**, *212*, 1153.

159. Silverman, R. B. *Mechanism-Based Enzyme Inactivation: Chemistry and Enzymology* **1988**, CRC Press, Vol 1, pp 3-30.

160. Chakravarty, P. K.; Frafft, G. A.; Katzenellenbogen, J. A. *J. Biol. Chem.* **1982**, *257*, 610.

161. Daniels, S. B.; Cooney, E.; Sofia, M. J.; Chakravarty, P. K.; Katzenellenbogen, J. A. *J. Biol. Chem.* **1983**, *258*, 15046.

162. Daniels, S. B.; Katzenellenbogen, J. A. *Biochemistry* **1986**, *25*, 1436.

163. MacKinnon, G. R. *Design of Inhibitors For beta-Lactamase and Carboxypeptidase-A* **1987**, Ph.D. Thesis, University of Waterloo.

164. Prescott, D. J. *J. Biol. Chem.* **1968**, *243*, 1551-1557.

165. Brewster, P.; Hiron, F.; Ingold, C. K.; Rao, D. S. *Nature* **1950**, *166*, 179.

166. Miller, J. B. *J. Org. Chem.* **1958**, *24*, 560-561.

167. (a) Saxton, B.; Meier, H. F. *J. Am. Chem. Soc.*, **1934**, *56*, 1918. (b) Hipkin, J.; Satchell, D. P. N. *Tetrahedron* **1965**, *21*, 835.

168. Professor J. Lajoie, Dept. of Chemistry, University of Waterloo, Waterloo, Canada.

169. Rovazzoni, C.; Valerio, R. *Ann. Chim. (Rome)* **1962**, *52*, 305.

170. Janssen, M. J. in *Chemistry of Carboxylic Acids and Esters* **1969**, ed. Patai, Interscience-Publishers, pp 705-764.

171. Bodansky, M.; Klauser, Y. S.; Ondetti, M. A. in *Peptide Synthesis* **1979**, John Wiley and Sons Inc.

172. Bunton, C. A.; Ng, P; Sepulved, L. *J. Org. Chem.* **1974**, *39*, 1130.

173. O'Connor, G. L.; Nace, H. R. *J. Am. Chem. Soc.*, **1953**, *75*, 2118.

174. Greene, T. W.; Wuts, P. G. M. *Protective Groups in Organic Synthesis* **1991,** Wiley and Sons Inc., p 109.

175. Felix, A. M. *J. Org. Chem.* **1974,** *39,* 1427.

176. Photaki, I; Taylor-Papadimitriou, J.; Sakarellos, C.; Mazarakis, P.; Zervas, L. *J. Chem. Soc. (C)* **1970,** 2683.

177. Nishio, T. *J. Chem. Soc., Chem. Commun.* **1989,** 205.

178. Dale, J. A.; Dull, D. L.; Mosher. H. S. *J. Org. Chem.* **1969,** *34,* 2543.

179. Riddles, P. W.; Blakely, R. L.; Zerner, B. *Anal. Biochem.* **1979,** *94,* 75-81.

180. Galdes, A.; Auld, D. S.; Vallee, B. L. *Biochemistry* **1983,** *22,* 1888-1893.

181. Bender, M. L.; Kezdy, F. J; Wedler, F. C. *J. Chem. Ed.* **1967,** *44,* 84-90.

182. Folk, J. E.; Schirmer, E. W. *J. Biol. Chem.* **1963,** *238,* 3884-3895.

183. Clark; Lubs *J. Wash. Acad. Sci.* **1915,** *5,* 609.

184. Kaiser, E. T.; Kaiser, B. L. *Accts. Chem. Res.* **1972,** *5,* 219-224, and references within.

185. McClure, W. O.; Neurath, H.; Walsh, K. A. *Biochemistry* **1964,** *3,* 1897-1901.

186. Cornish-Bowden, A.; Wharton, C.W. *Enzyme Kinetics* , **1980,** IRL Press, Washington D.C., pp 41-43.

187. Mannervik, B.; Carlberg, I; Larson, K. in *Glutathione, Part A* **1989,** ed.Dolphin, D.; Poulson, R.; Avramovic, O., John Wiley and Sons, pp 475-516.

188. Rabenstein, D. L. in *Glutathione, Part A* **1989,** ed.Dolphin, D.; Poulson, R.; Avramovic, O., John Wiley and Sons, pp 147-186.

189. Dixon, M. *Biochem. J.* **1972,** *129,* 197-202.

190. Mock, W. L.; Zhang, J. Z. *J. Biol. Chem.* **1991,** *266,* 6393-6400.

191. Nishino, N.; Powers, J. C. *Biochemistry* **1979,** *18,* 4340.

192. Christianson, D. W.; Lipscomb, W. N. *J. Am. Chem. Soc.*, **1987,** *109,* 5536-5538.

193. Kochoyan, M.; Havel, T. F.; Nguyen, D. T.; Dahl, C. E.; Keutmann, H. T.; Weiss, M. A. *Biochemistry* **1991,** *30,* 3371-3386.

194. Bunning, P.; Holmquist, B.; Riordan, J. F. *Biochemistry* **1983**, *22*, 103-110.

195. Cushman, D. W.; Cheung, H. S. *Biochem. Pharm.* **1971**, *20*, 1637-1648.

196. Birkedal-Hansen, H.; Moore, W. G.; Bodden, M. K.; Windsor, L. J.; Birkedal-Hansen, B.; DeCarlo, A.; Engler, J. A. *Crit. Rev. Oral. Biol. Med.* **1993**, *4*, 197-250.

197. Browner, M. F.; Smith, W. W.; Castelhano, A. L. *Biochemistry* **1995**, *34*, 6602-6610.

198. Baker, E.; Richardson, D.; Grass, S.; Ponka, P. *Hepatal.* **1992**, *15*, 492-501.

199. Scheibel, L. W.; Adler, A. *Mol. Pharmacol.* **1980**, *18*, 320-325.

200. Dimmock, J. R.; Baker, G. B.; Taylor, W. G. *Can. J. Pharm. Sci.* **1972**, *7*, 100.

201. Borkow, G.; Fletcher, R.S.; Arion, D.; Dmitrienko, G. I.; Parniak, M. A. *19th Int. Congress Chemother., Montreal* **1995**

202. Personal communication from J. Balzarini, Rega Institute for Medical Research, Leuver, Belgium

203. Spenser, P. C.; Fletcher, R. S.; Dmitrienko, G. I.; Parniak, M. A. *78th Canadian Society for Chemistry Conference and Exhibition*, Guelph, ON, May 1996, Abstract # 1039.

204. Segel, I. H. *Enzyme Kinetics* **1993**, John Wiley and Sons, pp 170-178.

205. King, E. L.; Altman, C. J. *J. Phys. Chem.* **1956**, *60*, 1375.

206. Cox, D.; Bovard, F. C.; Bargetzi, J.; Walsh, K.; Neurath, H. *Biochemistry* **1964**, *3*, 44-47.

207. Halfman, C. J. *Meth. Enzymol.* **1981**, *74*, 481-508.

208. Marquardt, D. *Ind. Appl. Math.* **1963**, *11*, 431.

209. Cook, R. B.; Jankow, R. *J. Chem. Ed.* **1972**, *49*, 405-408.

210. Gasteiger, J.; Marsili, M. *Organ. Magn. Reson.* **1981**, *15*, 353-360.